EXPLORING THE POTENTIAL SIGNALLING INTERPLAY BETWEEN WNK-SPAK/OSR1 KINASES AND THE β2-ADRENERGIC RECEPTOR

By

Abdulrahman Elzwawi

A thesis submitted to the University of Birmingham
For the degree of

Doctor of Philosophy

School of Pharmacy
College of Medical and Dental Sciences
University of Birmingham
Birmingham
B15 2TT

September 2018

Abstract

WNK, SPAK and OSR1 kinases are three serine/threonine protein kinases that regulate the function of cation chloride co-transporters (CCC). Such function has implicated these kinases in the regulation of electrolyte balance and hence blood pressure. This was confirmed by the discovery that genetic mutations in WNK kinases cause an inherited form of hypertension knowns as Gordon's syndrome. At the molecular level, WNK kinases become activated under osmotic stress leading to phosphorylation of SPAK and OSR1 kinases, which are their physiological substrates. Consequently, SPAK and OSR1 kinases phosphorylate CCCs and therefore switches on or off the transport of electrolytes inside and outside cells. To date, the only physiological substrates of SPAK and OSR1 reported are ion co-transporters. Aiming to identify novel substrates of SPAK and OSR1 kinases, we discovered that the human β2-adrenergic receptors (β2AR) contains an RFxV tetrapeptide, a unique peptide sequence of SPAK and OSR1 substrates. Thus, in this work, we focused on studying the possible interaction between the β2AR and SPAK /OSR1 kinases, and the role of such interaction on the function of this receptor.

Using peptide pulldown assays, we showed that the β2AR-derived RFHV peptide binds endogenous SPAK and OSR1. Additionally, the binding of overexpressed SPAK and OSR1 kinases to overexpressed β2AR in HEK293 cells was competed out by titration of the RFQV peptide. Notably, SPAK and OSR1 binding to the β2AR was inhibited by mutating the β2AR-RFHV motif to AFHV or by single point mutations in SPAK and OSR1 *C*-terminal domains, the site that binds the RFxV tetrapeptides. Critically, the binding of the β2AR to SPAK and OSR1 kinases was confirmed using the pulldown assays of over-expressed proteins. Using in vitro kinase assays, OSR1 was able to phosphorylate the human β2AR and this phosphorylation

was significantly reduced when the mutant β2AR-R239A was used or SPAK and OSR1 kinase inhibitors were used. Stimulation of the β2AR in cells by the agonist isoproterenol did not induce WNK-mediated SPAK and OSR1 activation.

Overall, our results confirm a novel interaction between the human β2AR and SPAK and OSR1 kinases. Given, the central role the β2AR plays in many human diseases such as blood pressure, heart failure, asthma and COPD, our findings provide a link between the electrolyte balance regulation by SPAK and OSR1 kinases to these β2AR-involving diseases.

Acknowledgments

I want to express my gratitude to my supervisor, Dr Youcef Mehellou for giving me this opportunity to work in his academic lab at Pharmacy school, University of Birmingham. I would like to thank him for his support, guidance and patience. I am very grateful for all the experiences that I have learnt during my PhD journey. Also, I would like to thank my co-supervisor Prof. Nick Barnes for his supervision, guidance and giving me an opportunity to work in his lab. I am also thank Dr Gillian for her technical and precise advices and teaching. Special thanks to Dr Hashemi Kaderi for his help, invaluable advice and notes. Many thanks to my colleagues Mubarak Alameri, Mohammed Alhanied and Huseimi for their help and support.

Finally, and the most importantly, I take this opportunity to thank other people who supported me a lot during my study. To thank my wife ‘Samar’ for her patience, infinity support, and taking care of our son ‘Tamim’. I would like to say sorry for the pressure that we had because of the study, and for all late nights and early mornings. To my relatives who supported me by their overseas prays which without all of these I would not reach where I am now.

TABLE OF CONTENTS

List of Figures and Tables

List of Figures and Tables in the Appendix

List of abbreviations

Å	Angstrom.
Ab	Antibodies.
AC	Adenylate cyclase.
ACE	Angiotensin-converting enzyme.
AFC	Alveolar fluid clearance.
Ang2	Angiotensin 2.
Asp	Aspartic acid.
ATP	Adenosine triphosphate.
β2AR	β2-adrenergic receptor.
BP	Blood pressure.
Ca	Calcium.
cAMP	Cyclic adenosine monophosphate.
CCC	Cation-chloride co-transporters.
CD	Collecting duct.
CFTR	Cystic fibrosis transmembrane conductor regulator.
Cl	Chloride.
CLC	Chloride channels.
Cz	Carazolol.
DCT	Distal convoluted tubules.
DMSO	Dimethyl sulfoxide.
ECL	Extracellular loop.
eNaC	Epithelial Na-channels.
GCK	germinal centre kinase
Glu	Glutamate.
GPCRs	G-protein coupled receptors.
HLB	Hypotonic low chloride buffer.
HPT	Hypertension.
hr.	hour.
IB	Immunoblotting.
IC_{50}	The concentration that give half of maximum inhibitory effect.

ICL	Intracellular loop.
IF	Immunofluorescence.
IP	Immunoprecipitation.
Iso	Isoproterenol.
K	Potassium.
kD	Kilo Dalton.
Leu	Leucine.
M	Molar.
MAPK	mitogen-activated protein kinase.
Min	Minute.
MO25	Mouse protein 25.
Na	Sodium.
NCC	Na/Cl co-transporter.
NKCC1	Na/K/Cl co-transporter-1.
NKCC2	Na/K/Cl co-transporter-2.
OSR1	oxidative stress responsive kinase 1.
PEI	Polyethylenimine.
PHA2	Pseudohypoaldosteronism type 2.
PKA	Protein kinase A.
PKs	Protein kinases.
pmol	Picomolar.
Pro	Propranolol.
ROMK1	renal outer medulla potassium1.
Ser	Serine.
SH3	Src homology domains 3
SPAK	STE20-SPS-related proline/alanine rich kinase.
STE20	Sterile20
TAL	Thick ascending limb.
St	STOCK1S-50699.
Thr	Threonine.
Vas	Vasopressin
WNK	With-no-Lysine (K)
Y2H	Yeast two hybrid.

Chapter 1 : Introduction.

WNK-SPAK/OSR1 signalling pathway and hypertension.

Hypertension (HPT) is a health condition defined by rise the blood pressure (BP) above 140/90 mmHg. The ethnicity plays vital role in prevalence of HPT, South Asian and Afro-Caribbean are the most affected groups in the UK while white populations showed less prevalence (Khan and Beevers, 2005). HPT is a considerable problem in public health as it affects a billion people globally (Murthy et al., 2017). Although if it is managed properly, the health damage caused by HPT could be minimal, it is the case where HPT is not well managed where major health issues arise Indeed, poorly managed HPT leads to other complications such as renal failure, heart failure and stroke, with this latter alone causing a worldwide 9.4 million deaths annually. Despite the continuous educational health campaigns about the dangers of HPT, the number of individuals suffering from HPT is constantly rising due to the sharp increase of causative factors such as lack of exercise, increased fatty food consumption and obesity (O'Shaughnessy and Karet, 2006).

The adjustment of the BP is a complex multifactorial process, which is affected by genetic predisposition, stress, quality of food and eating habits (O'Shaughnessy and Karet, 2006). Although lifestyle modulation could be adopted to manage HPT for a significant number of hypertensive patients, a combination of various antihypertensive drugs is often needed to achieve substantial reduction in BP. The currently used antihypertensive medications include furosemide (a loop diuretics) or thiazide in combination with either atenolol (beta-blocker) or Doxazosin (alpha-blocker) have been commonly prescribed (Richardson and Alessi, 2008). Moreover, a

class of drugs known as angiotensin converting enzyme (ACE) inhibitors, e.g. Ramipril, or angiotensin 2 receptor antagonists e.g. Losartan are also used (**Table 1.1**). Like other medications, these antihypertensive agents are associated with various side effects and their used in combinations, especially if they are prescribed for long term for patients with chronic cardiovascular diseases that could be led to the development of drug resistance (O'Shaughnessy and Karet, 2006, Richardson and Alessi, 2008).

Class	***Example***
1. Targeting renin-angiotensin system:	
Angiotensin-converting enzyme inhibitors	Captopril, ramipril and lisinopril.
Angiotensin receptor antagonists	Candesartan, losartan and valsartan.
Direct renin antagonists	Aliskiren.
2. Adrenoceptor antagonists:	
β-blockers	Atenolol, metoprolol and propranolol
α-blockers	Doxazosin, labetalol, phentolamine and phenoxybenzamine
3. Calcium channel blockers:	
Phenylalkamines	Verapamil
Dihydropyridines	Amlodipine, nifedipine and nimodipine.
Benzodiazepines	Diltiazem.
4. Diuretics	
Thiazides	Hydrochlorothiazide and Bendroflumethiazide.
Loop	Furosemide and Bumetanide
5. Potassium sparing/ aldosterone antagonists	
Ganglion block	Trimetaphan
Centrally acting agents	Clonidine and methyldopa.
Vasodilators	Hydralazine and minoxidil.

Table 1.1: Classification and examples of antihypertensive drugs. *Table adapted from (Jackson and Bellamy, 2015).*

According to Guyton's theory, HPT is driven by the inability of kidneys to excrete of excess salt in to urine (Guyton, 1991). Thus, since the early 1990s, there has been a great focus on the physiology and movement of electrolytes a cross the membrane of renal cells, which are tightly controlled by ions channels and co-transporters (Richardson and Alessi, 2008). These transmembrane carriers are electroneutral cation chloride co-transporters (CCC), which are a group of secondary active trans-membrane carrier proteins. They passively transport ions in and out of the cells by utilizing the electrochemical gradient that is generated from primary active transport of sodium (Na)/ potassium (K) *ATPase* pump (Alessi et al., 2014). Therefore, CCC can be divided into two categories; Na-mediated chloride (Cl) influx co-transporter such as Na/Cl co-transporter (NCC) and Na/K/Cl co-transporters (NKCC1 and NKCC2) and K-induced Cl efflux through K-Cl co-transporters (KCC) (Alessi et al., 2014).

NKCC1, NKCC2 and NCC belong to the solute carrier (*SLC12A*) family which are the molecular target of loop and thiazide diuretics that are used to modulate BP (Gamba, 2005). These co-transporters have critical roles in the regulation of cell volume and cellular protection from osmotic stress. In term of their role in regulating electrolytes balance, they control Na and Cl reabsorption at loop of Henle's and distal convoluted tubules (DCT) of renal nephrons, also they regulate Na/Cl levels in arterial smooth muscles leading to the direct modulation of calcium (Ca^{2+}) and smooth muscle contractility (Flatman, 2007). Although at the molecular level, the function of the *SLC12A* family of solute carriers is known to be regulated by post-translational phosphorylation, the distinct signalling pathway and the kinases that mediate this are not completely understood (Lytle and Forbush, 1996). Among of the key discoveries in this area was that by Wilson et al 2001 who reported that genetic mutations in the

with-no-lysine-kinases 1 and 4 (WNK1 and WNK4) caused an inherited form of HPT known as Gordon's Syndrome (Wilson et al., 2001).

1.1 WNK kinases:

The notion of protein phosphorylation as a regulatory mechanism of protein function began in last century when Krebs and Fischer found that glycogen phosphatase was dynamically regulated by reversible phosphorylation (Krebs et al., 1959). This pioneering study was the ground for discovering of the superfamily of human protein kinases (PKs). To date, more than 500 kinases have been identified and these are encoded by the largest genomic set called the human 'kinome'. A plethora of metabolic and biochemical reactions in eukaryotes are mediated by these enzymes, especially those that are related to the intracellular protein's communications (signaling transduction). Such phosphorylation mediated signal transduction is critical for cell growth and differentiation, cellular homeostasis, cell cycle and rearrangement of cytoskeleton. Therefore, PKs became of a major interest in the deep genetic analysis of the human kinome (Manning et al., 2002, Taylor et al., 2012).

PKs are categorised in to seven main groups as illustrated in (**Figure 1.1A**). They share a catalytic domain which consists of around 300 residues and the functional active site, adenosine triphosphate (ATP) binding site, which is formed by less than 10 conserved sequences (Hanks et al., 1988, Plowman et al., 1999). Within the ATP-binding site, one of the main amino acids that is crucial for the kinase function is a lysine (Lys) residue, which is primarily located near to amino-terminus (*N*-terminus) in subdomain 2 (β3 strand) of the most kinases (**Figure 1.2**). Among those kinases is protein kinase A (PKA), in which *N*-terminal Lys72 is vital in binding to and orientation of ATP, which it catalyses the kinase-mediated phosphorylation reaction.

Given the importance of this residue in ATP binding, it is unsurprising to find that mutations of this highly conserved Lys residue abolishes the catalytic activity of the protein kinase (Xu et al., 2000).

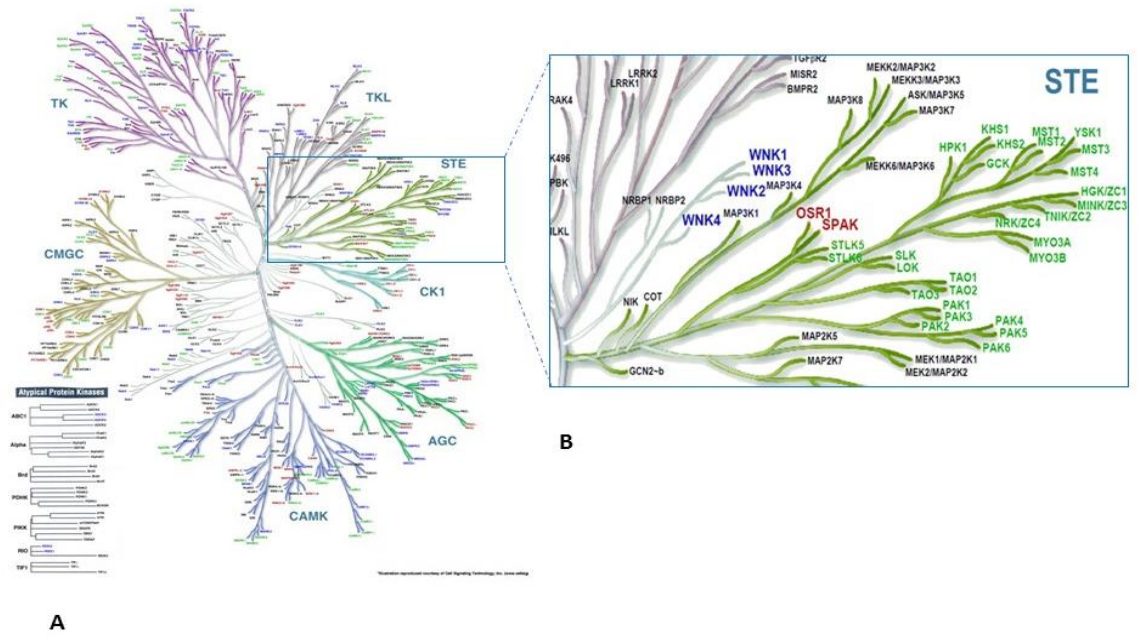

Figure 1.1: Human kinome tree showing families and subfamilies of protein kinases*. A) Kinome Render tree showing human protein kinases were organised in seven main groups. WNK kinases are highlighted and magnified. B) Zoomed section to show the close proximity of evolutionary WNKs (blue) to the STE serine/threonine kinase group, which includes SPAK (SPS-related proline-alanine rich protein kinase) and OSR1 (oxidative stress responsive 1) kinases in (red). Figure adapted from (Murthy et al., 2017).*

In 2000, a comprehensive study conducted by the Cobb laboratory, which was intended for detection of new members of mitogen-activated protein kinase (MAPK) in rat brain by polymerase chain reaction (PCR), resulted in the identification of the cDNA of a novel serine/threonine protein kinase named as WNK1. This kinase is composed of 2,126 amino acids and had a molecular weight of 230 kilo Daltons (kD) (Xu et al., 2000). Unlike the majority of protein kinases, WNK1 has unique structural feature, as it lacks the standard functioning Lys residue in β3 strand, which is critical for ATP binding. Interestingly, in WNK1 the catalytic lysine residue is replaced with cysteine

250 (Cys250) within the ATP binding pocket. The Lys residue (Lys233) in WNK1 is located in subdomain 1 (β2 strand), which is uncommon for protein kinases. This unusual structural feature gave rise to with no lysine (K), WNK kinases name (Murthy et al., 2017).

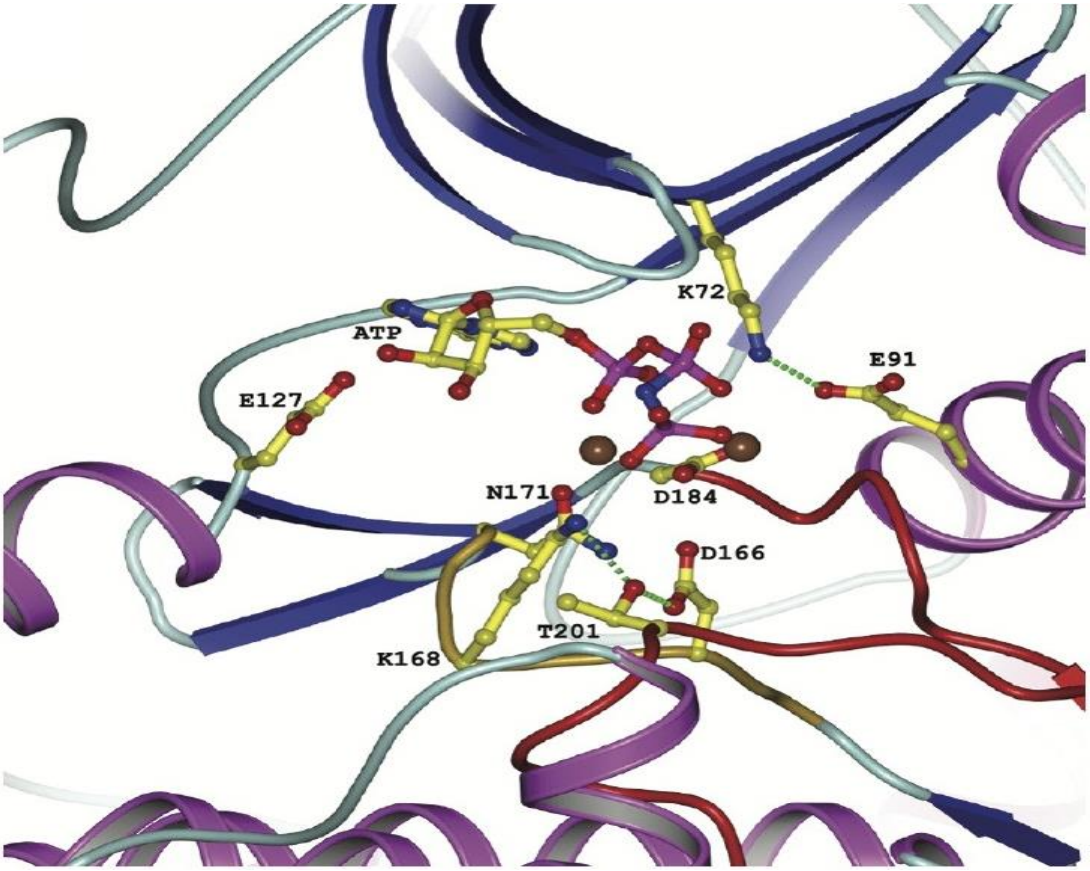

Figure 1.2: The active site of protein kinase A. Stereo diagram illustrates the active site of PKA. *Residues involved in ATP binding are shown in balls and sticks. The interactions between Lys72 and Glu91 and the hydrogen bonds between Thr201 and Lys168 and Asp166 are displayed in green dotted lines. Figure adapted from (Min et al., 2004).*

A year after WNK1 discovery, the successful isolation and characterisation of four paralogs of human WNK kinases was achieved, these were named WNK2, WNK3 and WNK4. Interestingly, all of these WNK isoforms were devoid of the Lys in β3 strand

similar to what was found with WNK1 (Verissimo and Jordan, 2001). Despite the displacement of catalytic Lys233 residue to β2 strand, WNK kinases are constitutively active, could auto-phosphorylate and form homo- and hetero-WNK complexes (Lenertz et al., 2005, Xu et al., 2002). As mentioned above, although mutation of catalytic Lys residue results in an inactive kinase, reversing the Cys250 residue that is in the ATP-active site in β3 strand in to Lys, and Lys233 in β2 strand to glycine (Gly) does not restore the activity of WNK1 (Xu et al., 2002). Therefore, WNK kinases have been classified in a distinct branch of serine/threonine protein kinases subfamily, which is located between the tyrosine kinase like proteins and sterile 20 (STE20) kinases in the human kinome tree (**Figure 1.1B**) (Verissimo and Jordan, 2001).

1.1.1 The key features of WNK kinases

WNK kinases are ancient enzymes, they have been identified in all mammals and multiple cellular organisms including nematodes such as *Caenorhabditis elegans,* where a single WNK was identified (McCormick and Ellison, 2011). WNKs are also found in plants such e.g. in *Arabiodpsis thaliana* where at least nine WNK homologous were reported (Nakamichi et al., 2002). Additionally, they are found in fungus like as *Phycomces*. However, they are absent in mono-cellular organisms such as yeast and bacteria except *Giardia lamblia* and *Chlamydomonas* (McCormick and Ellison, 2011). Interestingly, all WNK homologous either in mammals or invertebrates regulate the activity of NKCCs and NCCs though intermediate kinases e.g. SPAK and OSR1 or their orthologs respectively. This emphasis the vital role of WNK kinases in the physiology and development of diseases (Rodan and Jenny, 2017).

1.1.1.1 Topology of WNK kinase:

The first crystal structure of WNK1 was that of an inactive rat WNK1(194-483) mutant where serine-283 was mutated to alanine (Min et al., 2004). Although the general topology of WNK1 was similar to other serine/threonine protein kinases, *N*-terminus of WNK1 contains six rolled up β-sheets instead of five. While WNK1 carboxyl-terminus (*C*-terminus) possesses standard structure with absence the extension of the catalytic domain. The unique feature of WNK1 is that, in the β3 strand, Cys250 occupies the usual catalytic Lys in other kinases, but the side chain of this Cys residue is away from the ATP-binding site, thereby it is unlikely to be participated in catalytic reaction (Min et al., 2004).

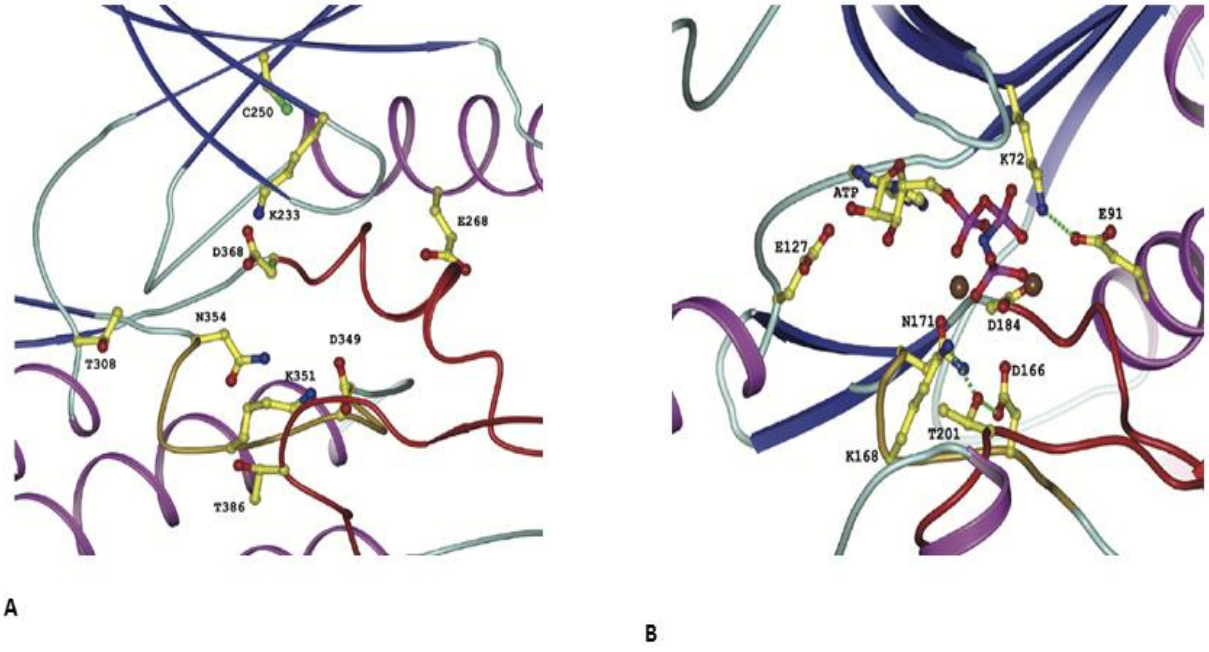

Figure 1.3: The WNK1 active site versus the PKA active site. *Ribbon illustration of the active site of the WNK1 kinase in comparison to usual kinase active site, PKA in this case. (A) WNK1 T-loop in red. Seven residues that are involved in the catalysis process are illustrated in ball and stick. Lys233 is 13 Angstrom (Å) away from glutamate residue 268 (Glu268). (B) The active site of PKA with ATP molecule in its binding pocket. Both ionic pairing between Lys72 and Glu91 and the hydrogen bonds between threonine 201 (Thr201), Lys168 and the aspartic acid 166 (Asp166) are demonstrated in green dotted lines. However, these interactions are absent in WNK1. Figure was adapted from (Min et al., 2004).*

Interestingly, the side chain of Lys233 in the β2 strand extended to the active site, generating a large cavity behind the active site. This allows Lys233 to adapt a particular rearrangement and ability to bind to ATP (**Figure 1.3**). Furthermore, in the ATP binding pocket there is a glutamate residue e.g. Glu127 of PKA that is critically involved in the binding with ATP, however it is completely absent in WNK1, indicating that WNK1 differently interact with ATP (Min et al., 2004). Remarkably, mutation of Lys233 inhibited the enzymatic activity of WNK1 protein, which is confirming that the catalytic Lys is in β2 strand (Xu et al., 2000).

The activation loop (T-loop) of WNK1 is made up by a wedge consisting of a double-turn helix 3_{10}-helix termed as 3_{10}-L_{12} helix (**Figure 1.4**), reaches the active site, where hydrophobic interactions take place between Leu369 and Leu374 residues of 3_{10}-L_{12} helix and Phe265 and Leu272 residues of helix C (Min et al., 2004). The other striking characteristic of WNK1 is that it possesses a glutamate-268 (Glu268) in helix C. This residue usually participates in ionic interaction with Lys at the catalytic domain in other protein kinases, but in WNK1 it interacts with arginine Arg348 instead. Also, Glu268 forms a hydrogen bond with Thr373 of activation loop (T- loop). The Glu268 protein mutated version of WNK kinases could not be expressed in *Escherichia coli* suggesting that this residue could be important in stabilizing the WNK protein (McCormick and Ellison, 2011, Min et al., 2004).

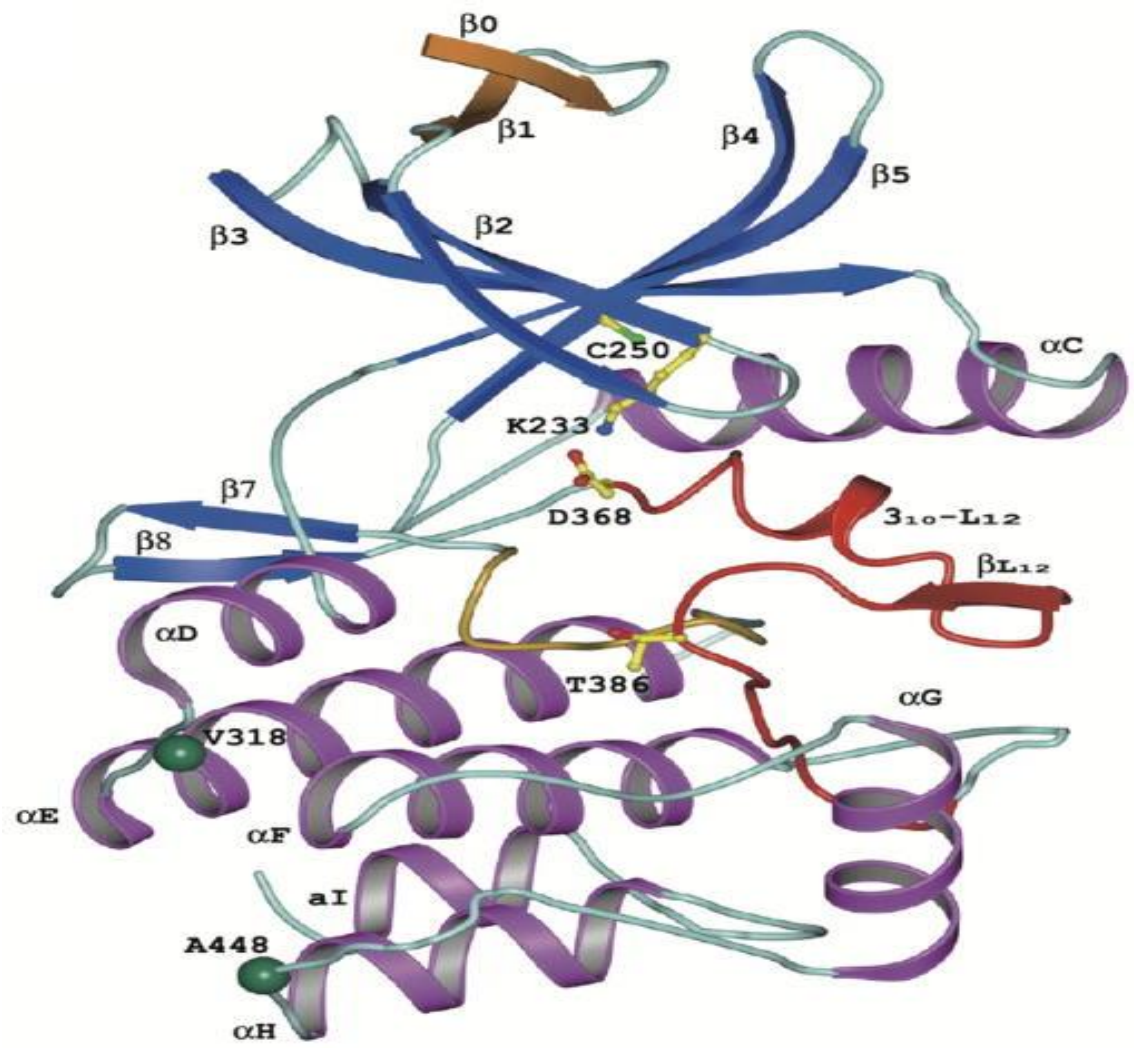

Figure 1.4: Structural topology of WNK1*. Crystal structure of rat WNK1-S283A showing the conserved β strands (blue), α helices (magenta) and the extra N-terminal β strand (gold). The (red) is the activation loop and (yellow) the catalytic loop. The atypical placement of Lys233 in β2 strand provides the catalytic side chain. Cys250 occupies the β3 strand in place of the catalytic lysine residue in other protein kinases (Min et al., 2004).*

1.1.1.2 The structural domain of WNK isoforms:

The human WNK family share ~ 85% sequence similarity of their *N*-terminal kinase domain. They are relatively large enzymes with amino acid sequences ranging from 1,243 (WNK4) to 2,382 (WNK1). Therefore, they exhibit extended molecular weight of 135-250 kD (McCormick et al., 2011, Richardson and Alessi, 2008). Although, WNK kinases have four prominent conserved regions, the analysis of their protein sequences revealed that their *C*-terminal region varies in length and are less conserved across the four isoforms, while their *N*-terminus kinase domain is well maintained (Rodan and Jenny, 2017).

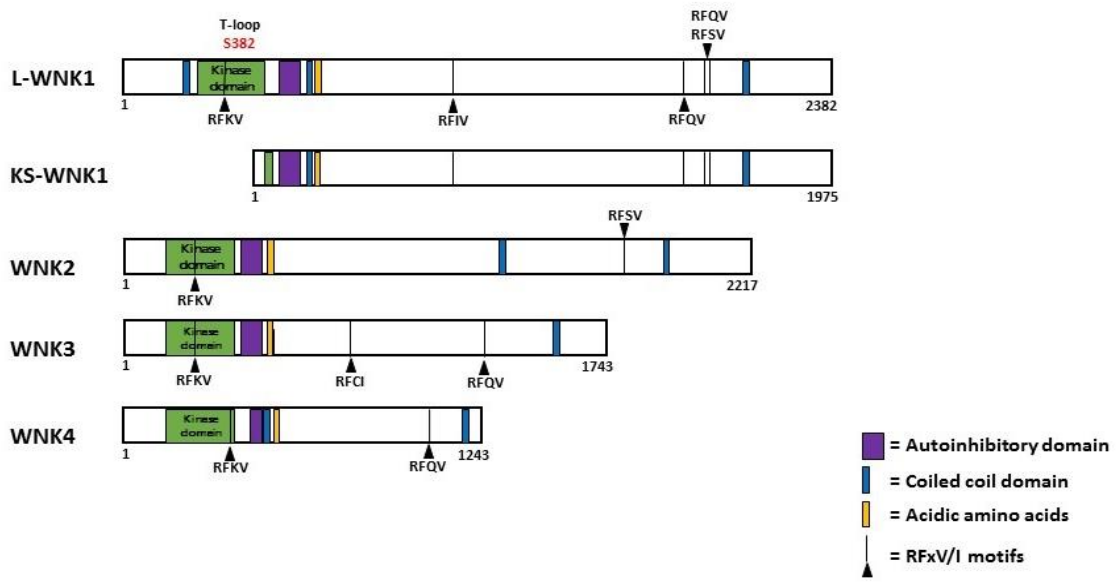

Figure 1.5: Structural domains of the human WNK isoforms. *A schematic diagram of the domain structures of the four human WNK isoforms showing the N-terminal kinase domain (green), the autoinhibitory domain (purple), the putative coiled coil domain (blue), and the conserved Ser382 (red). (RFxV/I) The site of the SPAK/OSR1 binding domains on WNK kinases are labelled. KS-WNK1: kidney specific-WNK1 (Richardson and Alessi, 2008).*

A. The WNK kinase domain:

As acronym of WNK kinases, with no lysine kinases, indicates that these enzymes have unusual serine/threonine catalytic domain, which is highly conserved in all of the four human WNK isoforms (Cope et al., 2005). This active site contains an atypical residue, Lys233 that occupies β2 strand instead of β3 strand (**Figure 1.4**). The kinase domain of WNK1 is located at the *N*-terminus between amino acids 221 - 479 and includes the conserved serine-382 (Ser382) whose phosphorylation is required for full WNK1 activation (**Figure 1.5**). WNK1 kinases with mutations in this Ser residue are catalytically inactive (McCormick and Ellison, 2011, Zagórska et al., 2007).

B. The autoinhibitory domain and autophosphorylation:

WNK kinases possess a preserved autoinhibitory domain. It is located outside the *N*-terminus of the kinase domain, between residues 515 and 569 of WNK1 at *C*-terminus of the kinase region (**Figure 1.5**). This autoinhibitory domain plays a vital role in suppression the activity of WNK kinases through intramolecular interaction with the kinase domain. The activation of WNK kinases leads to the release of the kinase domain from inhibitory site. Additionally, the autoinhibitory region is capable to supress the activity of other WNK homologous, a phenomenon known as ‘cross inhibition’ (Lenertz et al., 2005, Xu et al., 2002). Interestingly, mutation of two residues within the autoinhibitory region, namely Phe524 and Phe526, resulted in a loss of the inhibitory effect of the autoinhibitory region and a constitutively active WNK1 was generated (Lenertz et al., 2005, Richardson and Alessi, 2008, Xu et al., 2002).

Interestingly, the activity of WNK kinases is also regulated by trans-autophosphorylation (Xu et al., 2002), where WNKs autophosphorylate each other in

their T-loop, leading to a rapid and sufficient activation of WNK isoform. This process may be used by cells to handle rapidly osmotic stress (Richardson and Alessi, 2008). It has been reported, at least *in vitro* that Ser382 of WNK1 could be directly phosphorylated either intrinsic ability of WNK1 or by other WNK isoforms such as WNK2 or WNK3 but not WNK4 (Thastrup et al., 2012).

C. WNK kinases coiled coil motifs:

Structurally, WNK kinase also contain one to three coiled coil domain (CCD) (**Figure 1.5**) (Richardson and Alessi, 2008). These share a unique feature where the first and fourth residues are hydrophobic while the fifth and the seventh residues are primarily polar (McCormick and Ellison, 2011). The main role of CCD is to mediate protein-protein interactions between WNKs or other protein partners. To date these have been studies extensively in the formation of WNK homo- or hetero-dimerization or tetramer complex formation, as confirmed by co-immunoprecipitation and mutational analysis studies (Lenertz et al., 2005, Thastrup et al., 2012).

D. Proline-rich segments:

WNK kinases contain an unusually large number of proline residues, which make up proline rich region, which are known as the (PxxP) domains. Akin to the CCD, these PxxP domains are also involved in mediating the binding of WNK kinases to their protein partners (Richardson and Alessi, 2008). For instance, the PxxP stretch interacts with Src homology domains 3 (SH3), the most common structural feature used by proteins to mediate protein-protein interactions (He et al., 2007). The SH3-binding sequences play vital roles in several cell processes such as immune response, cell proliferation and protein regulation (McCormick and Ellison, 2011). For example,

He et al reported that such PxxP-SH3 interaction was important for WNK1 and WNK4 regulation of renal outer medulla potassium1 (ROMK1) (He et al., 2007). In particular, WNK1 and WNK4 were shown to internalize ROMK1 through endocytosis, a process mediated by the activation of the intersectin that possesses SH3 motif (He et al., 2007). This PxxP mediated interactions are also relevant for human diseases, since the WNK4 Pseudohypoaldosteronism type 2 (PHA2) causing mutations, E562K, D564A and Q565E were found to induce the elevation of ROMK1 endocytosis, as a result of increased the interaction between WNK4 and intersectin (He et al., 2007). Notably, these mutations are located within the conserved acidic motif, which is adjacent to PxxP motif (McCormick et al., 2011).

Beyond the PxxP motifs, WNK kinases possess two to five RFxV/I motifs, which are distributed throughout the protein kinase (Richardson and Alessi, 2008, Vitari et al., 2006). These sequences significantly contributed to the interactions between WNK kinases and their substrates, namely STE20-SPS-related proline/alanine rich kinase (SPAK) and oxidative stress responsive kinase 1 (OSR1) (**Figure1.5**), which are the effector substrates of osmotic stress (McCormick and Ellison, 2011)

1.1.1.3 The tissue expression of WNK proteins:

The human WNK proteins have different levels of tissue expression even though their mRNAs are widely expressed (Xu et al., 2000). WNK1 is the most abundant of the four human WNK isoforms. It is present in all tissues with higher expression in gonads, kidneys, heart, lungs and voluntary muscles (O'Reilly et al., 2003). Interestingly, in renal tissues, two isoforms of WNK1 have been detected; a full length WNK1 (L-WNK1), which is ubiquitously expressed, and a truncated WNK1 , which is appeared to be exclusive to the kidney hence denoted , kidney-specific WNK1

(KS-WNK1) (Delaloy et al., 2003). Unlike L-WNK1, KS-WNK1 was characterised by the absence of kinase domain (**Figure 1.5**) and is thought to be involved in regulating the kinase activity of L-WNK1 in renal cells (Subramanya et al., 2006).

WNK2 exists mainly in colon, small gut and brain, though it has also been detected in skeletal muscle and heart thought with lower expression levels (Moniz et al., 2008, Verissimo and Jordan, 2001). WNK3 is highly expressed in pituitary gland and through the brain mainly in the basal ganglia, hippocampus and frontal lobe of cerebral cortex while it appears to be of low levels in the lung, kidneys, liver, spleen and pancreas. Moreover, it is of very low levels in fetal organs including placenta, heart, thymus, and brain (Holden et al., 2004). The expression of WNK4 is strangely restricted to the secretory epithelium, e.g. pancreas, bile ducts, colon, skin, prostate and epididymis and it is significantly expressed in kidney especially in distal convoluted tubules (DCT) and collecting ducts (CD) (Kahle et al., 2004, Verissimo and Jordan, 2001).

1.1.2 Cellular regulation of WNK kinases:

1.1.2.1 Activation of WNKs and cellular osmolarity:

After the discovery of WNK kinases, numerous endeavours in animals and cell lines have been performed to explore the roles of these enzymes in health and disease conditions, and to identify how these enzymes are regulated as well as the conditions that activate them (Richardson and Alessi, 2008). Different conditions and signalling stimuli have been tested e.g. serum, insulin like growth factor-1 (IGF1), tumour necrotic factor (TNFα), phorbol ester, and phosphatase enzyme inhibitors to examine their effect on WNK kinases especially their activation (Zagórska et al., 2007). Although these conditions were successful in manipulating other signalling cascades,

however they failed to activate WNK1 (Zagórska et al., 2007). Interestingly, WNK1 was only reproducibly activated by osmotic stress, either in hyperosmotic condition (NaCl, KCl or sorbitol) (Lenertz et al., 2005, Zagórska et al., 2007) or in hypotonic low Cl stress (Moriguchi et al., 2005, Richardson et al., 2008). In order to avoid irreversible cell damage, the cells responded quickly and thus the activation of WNK1 was fast and was detected in less than a minute (min) with 0.5 molar (M) sorbitol and 5 min with exposure to hypotonic low Cl stress (Lenertz et al., 2005, Moriguchi et al., 2005, Zagórska et al., 2007).

In fact, osmotic stress activated WNK1 by triggering its phosphorylation on multiple Ser and Thr residues (Lenertz et al., 2005). Investigating WNK1 fragments by phosphopeptide screening, resulted in the detection of several phosphorylated serine/threonine residues, two serine, Ser15 and Ser167, proximal to WNK1 kinase domain, and Ser382 in catalytic kinase domain at T- loop. Moreover *C*-terminal domain phosphorylated residues such Ser1261, Thr1848, Ser2012, Ser2029, Ser2032 and Ser2372 were also identified. Surprisingly, apart from Ser15 , all of the mentioned residues were only conserved in rat and mouse WNK1 while Ser382 was conserved cross all human WNK homologous (Zagórska et al., 2007). This supported the notion that phosphorylation of this residue is essential for activating WNK kinases (**Figure 1.5**). Indeed, mutation of this residue to alanine (Ala) inhibited the WNK kinase, even if cells were exposed to osmotic stress, whereas mutation of Ser382 to glutamine (Glu) not only increased the kinase phosphorylation activity but also prevented its further stimulation by sorbitol (Zagórska et al., 2007)

1.1.2.2 WNKs activity and intracellular chloride:

Chloride (Cl) is one of many electrolytes that play a vital role in cell physiology (Piala et al., 2014). It participates primarily in the regulation of cell volume, BP, controlling membrane excitability and nerve conduction (Piala et al., 2014). Cl levels are strictly adjusted in cells, and its intracellular concentration is almost maintained within 30 – 60 mM (Russell, 2000, Salomonsson et al., 1991). It is well established that members of the cation chloride co-transporters (CCC) group regulate the cellular levels of Cl, by moving Cl in and out the cells. Examples include, NKCC1, NKCC2, NCC and KCC, which are all controlled by post-translational phosphorylation. The activity of these co-transporters has been shown to be regulated by WNK kinases (Richardson et al., 2008, Richardson et al., 2011). The mechanism by which WNK kinases sense intracellular Cl concentration [Cl] leading to its activation and subsequent phosphorylation of CCC is still not entirely defined (Alessi et al., 2014). Although the binding of Cl to proteins is poorly unclear, studying chloride channels (CLC) family gave clues as to how Cl binds to proteins. There was a large thought that the Cl binding is mainly mediated through hydrophobic pairings and interactions with amide backbone (Dutzler et al., 2002).

Moreover, other Cl-binding sites have been observed in angiotensin converting enzyme (ACE), serotonin transporter and in α-amylase, suggesting that chloride ions bind to proteins e.g. with WNK1, may be more common than previously thought (Pokhrel et al., 2011, Tavoulari et al., 2011, Tzakos et al., 2003). Interestingly, in 2014 a study by Cobb and Goldsmith groups hypothesised that a protein kinase located upstream to CCC serve as a Cl sensor (Piala et al., 2014). They demonstrated that WNK1 is the protein kinase, and it was crystalized in presence of Cl (Piala et al., 2014). Impressively, it was noticed that Cl directly bound to the WNK active site and formed

hydrogen bonds with the amide backbone of two leucine residues (Leu369) and (Leu371), which they generate a Cl-binding pocket. Additionally, the Cl also formed hydrophobic interactions with Phe283 of β3 strand, Leu299 of β4 strand and with Leu369 of Asp368-Leu369-Gly370 sequences (DLG-motif) (**Figure 1.6**) (Piala et al., 2014). This interaction prevented WNK1 autophosphorylation. In fact, the study indicated that Cl inhibited WNK1 activity with IC_{50} about 20 mM (Piala et al., 2014).

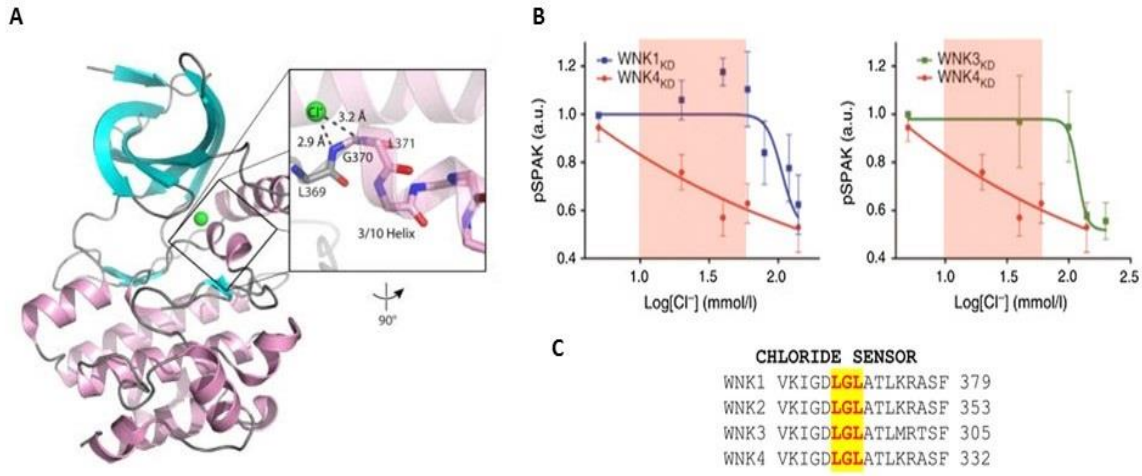

Figure 1.6: The crystal structure of WNK1 with chloride. *A) Cartoon diagram of WNK1, PDB ID: 3FPQ. α-helices (pink), β sheets (cyan), and loops (grey). In the magnified square, the position of the Cl (green ball) and distance of the hydrogen bonds between the Cl and amide backbones of Gly370 and Lys371. B) Graph of in vitro kinase assay illustrating the relationship of SPAK phosphorylation by WNK1, WNK3 and WNK4 and Cl concentration. WNK4 appeared to be the most sensitive WNK isoform to Cl concentration within the physiological range (pink). C) Sequence alignment of the human WNK1, WNK2, WNK3 and WNK4 showing conserved putative Cl binding site (Leu369, Gly370, Leu371), LGL motif (highlighted in yellow). Figures adapted from (Murthy et al., 2017, Piala et al., 2014).*

Mechanistically, this suggesting that when [Cl] was reduced by osmotic perturbation, the WNK1 bound Cl dissociates from the kinase active site, thereby leading to its activation (Alessi et al., 2014).

In another report, it was shown that all WNK homologous have a Cl-binding site (**Figure 1.6 C**), though they responded differently to [Cl]. Among the four human WNK kinase isoforms, WNK4 is the most sensitive to the [Cl], it is inhibited by the chloride ion within the physiological range in cells of renal DCT (**Figure 1.6B**). Furthermore, mutations in the Cl-binding site of WNK4 made it constitutively active, and resulted in the activation of NCC (Terker et al., 2016). Additionally, a study carried out in *Xenopus* oocytes showed that NCC was inhibited by WNK4 at physiological levels of Cl, a phenomenon that was reversed by low Cl condition (Bazúa-Valenti et al., 2015). Also, it was shown that mutation of Leu322 in WNK4 to Phe, which is equivalent to Leu369 in WNK1 (Cl-binding site), resulted in a persistent activation and autophosphorylation of WNK4 that led to increased NCC activity even if [Cl] was of normal concentrations (Bazúa-Valenti et al., 2015). Additionally, the stimulatory effect of WNK4-L322F on NCC was inhibited by introducing mutations either in active site D321A or D321K-K186D or in autophosphorylation residue S335A (Bazúa-Valenti et al., 2015).

1.1.2.3 Upstream regulation of WNK kinases:

The WNK kinase activity could be intracellular regulated by different mechanisms; 1) the alteration of cellular tonicity, which directly affects their kinase activity, and 2) the adjustment of the WNKs cellular abundance, by overexpression or increase degradation, which plays an important role in development of diseases, for instance PHA2 (Uchida et al., 2014). PHA2 is an infrequent autosomal dominant syndrome, featuring HPT, hyperkalaemia, metabolic acidosis and hyperchloremia (Wilson et al., 2001). It also known as familial hyperkaliaemic hypertension (FHH) or Gordon's syndrome (Cope et al., 2005, Gordon, 1986). The disease is caused by mutations in WNK1 and WNK4 genes (Richardson and Alessi, 2008). WNK1- causing

mutations are primarily deletions in intron1, likely to result with overexpression of WNK1 without alteration in protein sequence (Dbouk et al., 2016). As for WNK4 mutations, there are gene missense mutations, which are translated into protein point mutation that lead to an inhibition of WNK4 protein degradation (Murthy et al., 2017). Together, WNK1 and WNK4 mutations account for approximately 13 % of PHA2 patients (Dbouk et al., 2016).

In 2012, mutations in two genes termed cullin 3 (CUL3) and kelch-like 3 (KLHL3) were found to cause PHA2, a link that was subsequently shown to involve the WNK-signalling pathway (Boyden et al., 2012, Louis-Dit-Picard et al., 2012). CUL3 is a scaffolding protein that belongs to the cullin family proteins, which is composed of seven members (Uchida et al., 2014). These are relatively large proteins, 80 – 100 kD, that are involved in the central nucleation of ubiquitin E3-ligase subunits and in delivering of targeted proteins for degradation (Ferdaus and McCormick, 2016, Murthy et al., 2017). The most key step in protein ubiquitination is the final stage, in which the targeted protein is ubiquitinated by assembled E3-ligase, a process preceded by the activation of the E1 and conjugation of the E2 enzymes (Genschik et al., 2013, Hershko and Ciechanover, 1998).

KLHL3 belongs to of bric-a-brac/tramtrack/ broad complex (BTB) protein family (Dhanoa et al., 2013, Murthy et al., 2017). It contains single BTB motif, and five to six kelch domains (Uchida et al., 2014). KLHL3 interacts with CUL3 and WNKs via BTB and kelch segments respectively (Sohara and Uchida, 2016, Uchida et al., 2014). Thus, the substrate (WNK) is connected to CUL3-RING-E3 ubiquitin-ligase complex through KLHL3 (Murthy et al., 2017). It is now established that both WNK1 and WNK4 bind the kelch domain of KLHL3 via the acidic segment, which is situated near to the autoinhibitory domain and it is conserved in all WNK isoforms (Ohta et al., 2013,

Wakabayashi et al., 2013). Ubiquitination of WNK kinases is mediated by this cascade to their proteosomal degradation, which ultimately manifested in decreased WNK abundance and signalling.

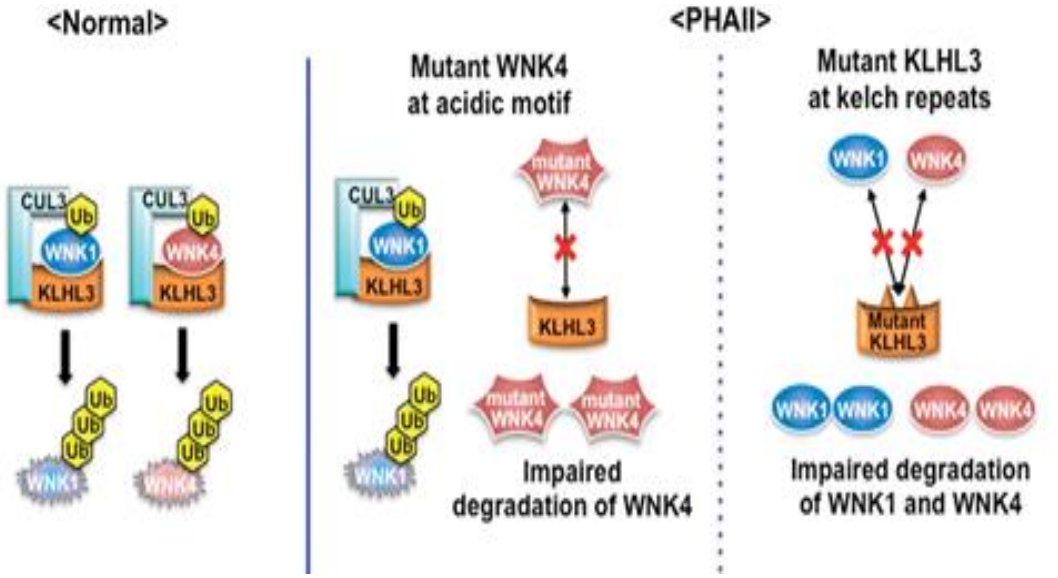

Figure 1.7: Molecular pathogenesis of the PHA2 syndrome. *Diagram showing the mechanism of regulating WNK kinases by KLHL3 and CUL3 E3 ubiquitin ligases. WNK1 and WNK4 total levels are tightly maintained in physiological state (left). Mutations in WNK4 or KLHL3 cause interruption of their interaction with KLHL3 and CUL3 leading to the inhibition of the ubiquitination and degradation of WNK1 and WNK4 and subsequently their accumulation. Figure adapted from (Sohara and Uchida, 2016).*

The above mechanism provided a compelling explanation of how WNK1 and WNK4 mutations causing PHA2. Interestingly, five of six mutations of WNK4 in PHA2, have been identified in the acidic region, which inhibited the binding of WNK4 to KLHL3 and led to defective degradation and subsequent WNK4 protein accumulation (**Figure 1.7**). As mentioned above, WNK1 mutations are deletions and these, result in an increase of protein transcription (Golbang et al., 2005, Gong et al., 2008). Furthermore, two further independent reports demonstrated that both WNK1 and WNK4 were substrates of KLHL3 and they were ubiquitinated by the CUL3-RING E3

ubiquitin ligase (Shibata et al., 2013, Wu and Peng, 2013). Lastly, to establish the *in vivo* roles of WNK mutations, elevated phosphorylation and activation of NCC had been observed because of overexpression of L-WNK1 and WNK4 accumulations in the kidneys of transgenic mice model with $WNK1^{+/FHH}$ or $WNK4\text{-}D461^{A/+}$ that exhibited PHA2-like phenotype (Vidal-Petiot et al., 2013, Wakabayashi et al., 2013).

Genes	***Type of Mutation***	***Effect***	***References***
WNK1	Intron 1 deletion	↑ L-WNK1	(Vidal-Petiot et al., 2013)
WNK4	Missense in acidic motif E562K, D564A, Q565E	↑ L-WNK4	(Vidal-Petiot et al., 2013)
	WNK4-$D561^{A/+}$ (mouse)	↑ L-WNK4	(Wakabayashi et al., 2013)
KLHL3	Missense in Kelch domain Q309R, A340V, R348Q, L387P, S410L, S432N, A494T, R528H/C, N529K.	↑ L-WNK1 ↑ L-WNK4 ↑ L-WNK3	(Boyden et al., 2012, Louis-Dit-Picard et al., 2012, Ohta et al., 2013, Shibata et al., 2013, Wakabayashi et al., 2013)
	Missense in BTB or BACK regions A77E, M78V, E85A, C164F.	↑ L-WNK1 ↑ L-WNK4 ↑ L-WNK3	
CUL3	Deletion in Exon 9 $CUL3^{\Delta 403\text{-}459}$	↓ KLHL3 ↑L-WNK1 ↑ L-WNK4 ↑ L-WNK3	(Boyden et al., 2012, McCormick et al., 2014, Ohta et al., 2013)

Table 1.2: Genetic mutations in PHA2 syndrome and their effects on the expression of WNK isoforms. *↑ indicates increased expression, ↓ indicates decreased expression. Both reduction of KLHL3 levels and elevation of WNKs expression rise BP via increasing renal Na reabsorption. Table adapted from (Murthy et al., 2017).*

Furthermore, mutations in CUL3 and KLHL3 prevent either the assembly of ubiquitination RING-CUL3 or block their binding WNK isoforms. For instance, in an extensive study by the Alessi group, out of the substrate binding site thirteen PHA2 causing mutations in KLHL3, eight occurred within the substrate binding site, kelch motif, and inhibiting significantly the interaction with WNK1 and the other five mutations interfered with KLHL3 binding with CUL3 (Ohta et al., 2013). These results

have been validated in mice carrying KLHL3 or CUL3 mutations where elevated of both WNK1 and WNK4 proteins and increased activity of NCC were noted (**Table 1.2**). In summary, these findings confirmed that mutations in CUL3 and KLHL3 lead to elevated protein levels of WNK kinases as a sequence of the inability of these mutated E3 ubiquitin ligases to degrade WNKs (Murthy et al., 2017).

1.2 SPAK/OSR1 kinases

Given the direct genetic link between WNK kinases, the regulation of BP and hence human HPT, identifying the WNK kinases physiological substrates became very important in dissecting the mechanism by which WNK kinases regulated BP. Although initial studies made a connection between WNK kinases and CCC, these studies showed that these ion-co-transporters are not the direct substrates of WNK kinases, despite early studies showing WNK1 was able to directly phosphorylate KCC2 and KCC3 in their *C*-terminal region, precisely (Thr906 and Thr991) respectively (Alessi et al., 2014). In 2002, a pulldown assay and yeast two hybrid (Y2H) analysis, aimed at identifying substrates of the sterile20 (STE20)-related proline/alanine rich kinase (SPAK) and oxidative stress responsive 1 kinase (OSR1), resulted in NKCC1, NKCC2 and KCC3 as possible substrates (Piechotta et al., 2002). Three years later, the link between SPAK/OSR1 and WNK kinases was established, when two research groups showed that SPAK/OSR1 were direct physiological substrates of WNK kinases (Moriguchi et al., 2005, Vitari et al., 2005).

1.2.1 The discovery of SPAK/OSR1:

SPAK and OSR1 are two serine/threonine kinases that belong to the germinal centre kinase (GCK-VI) family of protein kinases, which itself is a subfamily of a large

family of protein kinases named Ste20-related (Ste20) (**Figure 1.1B**). This family of protein kinases is conserved in both the animal and plant kingdoms (Gagnon and Delpire, 2012). The mammalian Ste20 contains about thirty enzymes, which are organised based on the localisation of their catalytic domain into two main categories; 1) *C*-terminal position as in p21 activated kinases (PAKs) and 2) *N*-terminal side as in GCKs. Each group is subsequently subdivided according to their structure and function (**Figure 1.8**). Moreover, PAKs are characterised by a conserved regulatory region at their *N*-termini (Boyce and Andrianopoulos, 2011). PAKs are involved in cell motility, tumour invasion and modulation of cytoskeleton (Hoffman and Cerione, 2000). In addition to their *N*-terminal kinase domain, the *C*-termini of GCKs varies in sequences and is composed of motifs that participate in protein-protein interaction (Dan et al., 2001). These kinases have roles in cell migration, proliferation, apoptosis, and osmotic shock responses (Dan et al., 2001).

SPAK was firstly identified by immunoblotting (IB) and PCR analysis in rat brain (Ushiro et al., 1998). It showed molecular weight 60-64 kD, it has an *N*-terminal kinase domain preceded by proline-rich *N*-terminal domain (Johnston et al., 2000). The OSR1 gene was detected in chromosome 3 by genetic mapping of the human genome (Tamari et al., 1999). The protein is 527 amino acids in length, with *N*-terminal kinase domain and interestingly it was found to play a role in oxidative stress (Tamari et al., 1999). Notably, unlike SPAK, OSR1 does not have a proline-rich *N*-terminal region (Chen et al., 2004). Sequence alignment of human SPAK and OSR1 demonstrated that they have 68 % overall sequence identity and about 89 % homology in their kinase domains (Chen et al., 2004). Unlike WNK kinases, the orthology of SPAK and OSR1 indicated that OSR1 was recognised in protist, plant and in the animal kingdom, through worms to human (Gagnon and Delpire, 2012). However, there was no

evidence of SPAK in monocellular organisms or even plants, which makes it exclusive to vertebrates (Gagnon and Delpire, 2012).

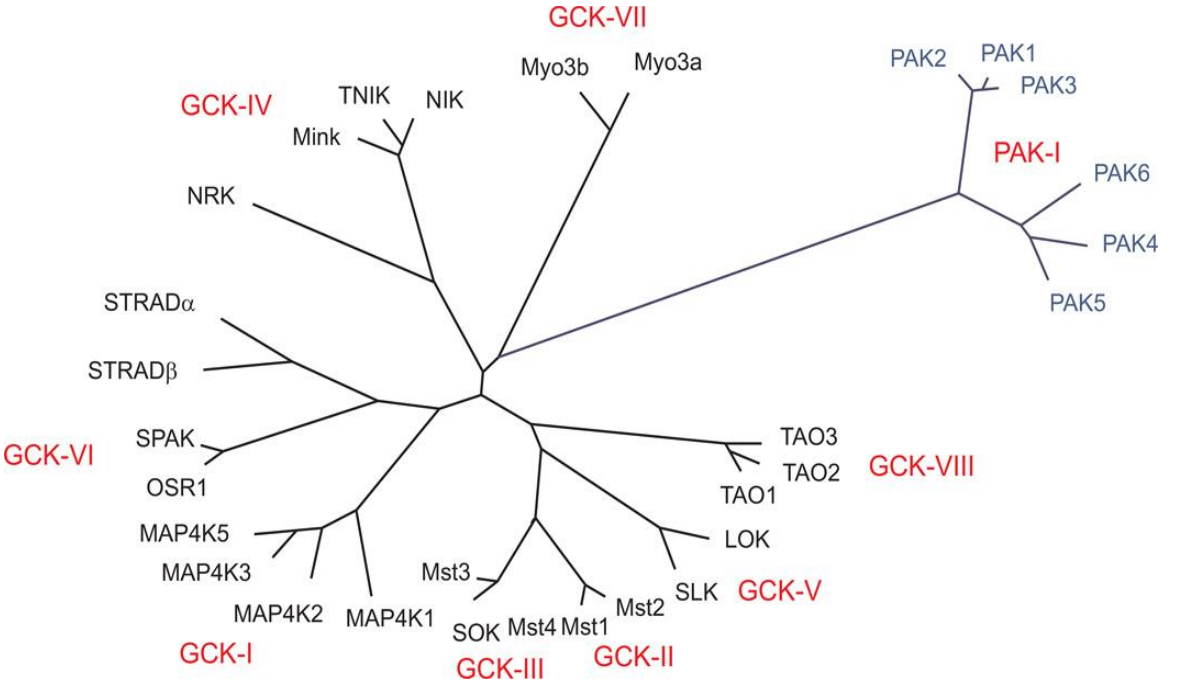

Figure 1.8: Classification of mammalian Ste20-protein kinase family. *The tree illustrates all Ste20-protein kinases arranged in nine subfamilies. SPAK and OSR1 located in GCK-VI between STRAD and MAP4K kinases. Figure adapted from (Gagnon and Delpire, 2012).*

1.2.2 Tissue expression and cellular localisation of SPAK/OSR1:

Initially, primary searches that employed Northern blotting for detection of SPAK/OSR1 mRNAs indicated that these kinases have variable expression in mouse organs (Delpire and Gagnon, 2008). OSR1 is highly transcribed in cardiac tissue, liver, skeletal muscles and colon, and to lesser extent in small intestine, kidney, brain, pancreas, spleen, testis, ovary and thymus (Piechotta et al., 2003, Tamari et al., 1999). SPAK protein and mRNA distribution overlapped largely with OSR1 distribution and was abundant in salivary glands, brain, adrenal glands, testis, and pancreas, and to a lesser extent in spleen, heart, kidneys, lungs, ovary, uterus, thymus and skeletal muscles (Delpire and Gagnon, 2008, Johnston et al., 2000).

The determination of tissue SPAK and OSR1 protein levels showed variation in expression between the two kinases. SPAK and OSR1 are highly homological proteins, so the generation of a kinase-specific antibodies (Ab) with high specificity was challenging (Delpire and Gagnon, 2008). A 74 amino acids domain in their *C*-terminal domains with very low conservation (approximately 9 %) was used to generate specific Ab against SPAK and OSR1 (Piechotta et al., 2003). The first polyclonal anti-SPAK Ab was developed in 2000 by Harrison group who showed that mouse tissues such as pancreas, testis, brain, spleen and liver had high levels of SPAK while it was less in the lung and kidneys (Johnston et al., 2000). The OSR1 protein was shown to be expressed in the spleen, heart, liver, lung, small and large intestine whereas the kidneys and stomach had low expression and it was not detected in the thymus (Chen et al., 2004).

Immunoblotting (IB) studies revealed that three SPAK analogous exist in the kidneys; 1) full length SPAK (FL-SPAK), which is ubiquitously expressed, 2) SPAK-2 is also ubiquitously expressed but lacks the *N*-terminal proline rich region, and a part

of catalytic domain, and 3) kidney specific SPAK (KS-SPAK) which was only expressed in the kidneys (Murthy et al., 2017). OSR1, however, appeared as single species (i.e.OSR1 exists as a single band in Western blot analysis) and truncated- or kidney-specific analogues have not been reported (Rafiqi et al., 2010).

Immunofluorescent (IF) and IB analysis of renal segments was performed, and these demonstrated that the FL-SPAK was prominent in thick ascending limb (TAL) of Henle and DCT, whereas SPAK2 and KS-SPAK were found in renal medulla, which is composed of only TAL (McCormick et al., 2011). However, OSR1 expression was predominantly in TAL and to a lesser extent in the DCT (Lin et al., 2011, Yang et al., 2010). Additionally, immunohistological investigations showed that SPAK and OSR1 are mostly cytoplasmic enzymes (Ushiro et al., 1998). In the kidneys, SPAK/OSR1 were shown to have an apical and basolateral distribution at cellular levels (Gagnon and Delpire, 2012). This suggested that SPAK and OSR1 are primarily co-localised with NCC and NKCC2 respectively (McCormick et al., 2011).

Similar observations were made in immunohistological studies in nerve samples, where SPAK was detected in the apical apart of cytoplasm in cells of choroidal plexus (Gagnon and Delpire, 2012) . Interestingly, this apical translocation was completely lost in choroidal epithelium of homozygote NKCC1 knockout mice (Gagnon and Delpire, 2012, Piechotta et al., 2003). This indicated that the co-localisation of SPAK was a strategy for targeting NKCC1, because NKCC1 is considered to be a physiological substrate of SPAK. Moreover, both SPAK and NKCC1 were found to be highly expressed in the sciatic nerve and were less expressed in the white and grey matter of spinal cord (Gagnon and Delpire, 2012). Notably, OSR1 also existed in neurons but in much less quantity (Piechotta et al., 2003).

1.2.3 Structure of SPAK/OSR1:

Among the GCK subfamily of protein kinases SPAK/OSR1 have been extensively studied, due to their disease relevance, primarily through their ability to regulate the activity of *SLC*12A family in ion homeostasis (Gagnon and Delpire, 2012).

1.2.3.1 Domain structure of SPAK/OSR1:

Like other Ste20 kinases, the structural parts of these proteins revealed that they share a highly conserved *N*-terminal kinase domain and a regulatory region at their *C*-termini. Interestingly, SPAK harbours a unique extension at *N*-terminus prior to catalytic region, which composed of proline/alanine residues, known as PAPA box, a feature that is absent in OSR1 (**Figure 1.9**). Several biochemical studies showed that removing the PAPA box from SPAK does not disturb its kinase activity, and the precise function of this segment yet to be established (Delpire and Gagnon, 2008).

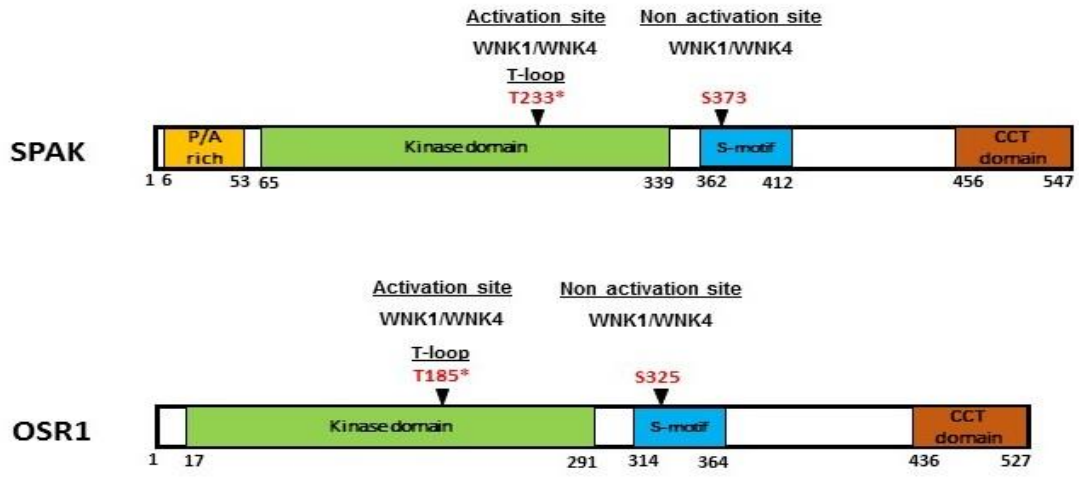

Figure 1.9: Structural domains of human SPAK and OSR1. *Schematic diagram of SPAK and OSR1 kinases showing the key structural domains. SPAK contains a unique proline/alanine (P/A) rich segment. * indicates the catalytic threonine (T) residues on SPAK and OSR1 kinase. T233, T185, S373 and S325 are WNK phosphorylation sites. The conserved C-terminal (CCT) domains mediate the binding to RFxV/I-possessing proteins (Richardson and Alessi, 2008).*

The kinase domain is situated between residues 17-291 of OSR1 and 65-339 of SPAK (**Figure 1.9**). The kinase domains encompass key threonine residues, Thr185 for OSR1 and Thr233 for SPAK, which are phosphorylated by upstream WNK kinases (Richardson and Alessi, 2008). Mutagenesis analysis illustrated that the only phosphorylation of OSR1 at Thr185 and SPAK at Thr233 by WNK1 or WNK4 was essential for their activation, as mutations of these residues to alanine abolished their kinase activity (Vitari et al., 2005, Zagórska et al., 2007). Additionally, the replacement of these threonine residues by glutamic acid, resulted in constitutively active kinases independent of WNK phosphorylation (Vitari et al., 2005).

SPAK/OSR1 have two conserved regulatory sections; 1) a serine rich domain, (termed the S-motif) in which WNK kinases also phosphorylate this segment at Ser373 in SPAK and Ser325 in OSR1, and 2) a highly conserved 92 amino acid *C*-terminal domains called (the CCT domain) (**Figure 1.9**). This latter domain is highly significant, as it acts as the docking site in the interaction of SPAK/OSR1 with Arg-Phe-Xaa-Val/Iso (RFxV/I) motifs, from the upstream activators, WNKs (**Figure 1.5**), and the downstream substrates, e.g. NKCC co-transporters (Piechotta et al., 2002). In addition to these large domains, SPAK and OSR1 kinase have small region of propinquity, termed the PF1 domain, a typical feature of GCK-VI members. PF1 is located immediately after the kinase domain. Moreover, although SPAK is largely a cytoplasmic protein, SPAK has a short sequence that is known for protein location to the nucleus (RAKKVRR) (Johnston et al., 2000). Finally, both kinases have a site for caspase cleavage, which it shares with other Ste20 kinases such as the MST1 kinases (Chen et al., 2004, Johnston et al., 2000).

1.2.3.2 The topology of SPAK/OSR1:

The crystal structures of SPAK/OSR1 co-crystallised with nonhydrolyzable ATP revealed that they were similar in configuration (Taylor et al., 2015). Both kinases do possess a canonical bi-lobal fold, with small *N*-terminus made up of β1 to β5, and a larger *C*-terminus, (**Figure 1.10 A**) which is composed primarily α-helices C to α F and β-sheets (β6 - β8) (Gagnon and Delpire, 2012, Taylor et al., 2015). The OSR1 conserved catalytic Lys, Lys46, is located in the last part of β3 strand, which is the ATP binding site. Additionally, the conserved magnesium (Mg) binding motif, composed of Asp, Phe and Gly (DFG), was found to be located between β8 strand and α-helix AL (Gagnon and Delpire, 2012). Interestingly, the most distinctive feature of OSR1 structures, is the exchange of T-loops (activation loops) between symmetric linked dimers, a phenomenon termed domain swapping (**Figure 1.10 B and C**) (Lee et al., 2009, Villa et al., 2008). The swapped part encompasses the αEF helix and P+1 loop, which it includes the essential Thr residues, e.g. (OSR1 Thr185 and SPAK Thr233), indicating that the vital role of domain swapping in dimers formation and kinase activation by trans-phosphorylation mechanism (Gagnon and Delpire, 2012, Villa et al., 2008). In addition, SPAK was also found to form dimers by the same mechanism, and this may suggest the role of dimerization in the multistep activation mechanisms of both kinases (Taylor et al., 2015).

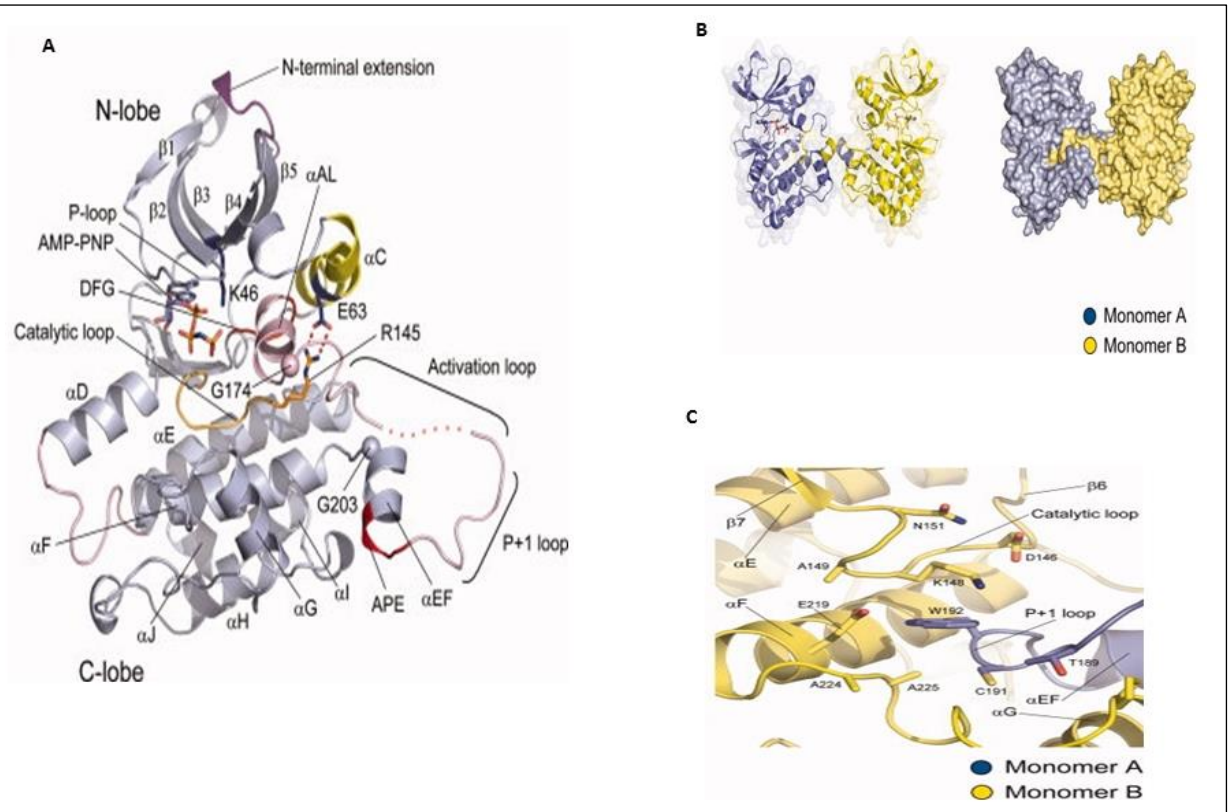

Figure 1.10: Crystal structure of the domain-swapped OSR1. *(A) Monomeric structure of OSR1 kinase domain showing N-terminal and C-terminal lobes as well as the disordered activation loop in dotted line. (B) Illustration of the domain swapped segment in the dimer formation, one OSR1 monomer shown in blue and the other monomer is in yellow. (C) The interface of the domain swapped in OSR1, showing the interaction of E219 from αF and W192 residue from P+1 loop of the other monomer. Figure adapted from (Lee et al., 2009).*

1.2.3.3 Role of CCT domain in SPAK/OSR1-protein interactions:

After the discovery of SPAK and OSR1 being the upstream regulators of NKCCs, decoding such interaction at molecular level was pursued (Piechotta et al., 2002). Delpire and Ganon performed a genome wide screening of nine residues containing the WNK RFxV/I motif, where (x) represented any amino acids, in the mouse proteomic data base. This led to identification of 131 proteins contained SPAK and OSR1 binding motifs. Interestingly, WNK1 and WNK4 were also identified as possible binders to SPAK and OSR1, as they have RFxV motifs (Delpire and Gagnon, 2007). Also, various screening were performed by yeast 2 hybridisation (Y2H) and immunoprecipitation (IP) from mouse tissues and cells, and these showed that SPAK and OSR1 kinases bind to WNK1, WNK4 and NKCC1, NKCC2 and NCC, and that binding was mediated by direct interaction of RFxV tetrapeptide into the CCT domain of SPAK and OSR1(Alessi et al., 2014).

Although the four WNK isoforms have more than one RFxV domains (**Figure 1.5**), it remains unclear whether these multiple RFxV motifs in the same WNK kinase facilitate their binding to multiple SPAK and OSR1 simultaneously (Anselmo et al., 2006, Moriguchi et al., 2005, Richardson and Alessi, 2008). Intriguingly, Y2H analysis using the SPAK-CCT domain, led to the identification of several possible protein partners such as the tumour necrosis factor (TNF), otoferlin, heat shock protein 105 (HSP105), gelsolin and the apoptosis associated tyrosine kinase (AATYK) (Piechotta et al., 2003). Admittedly, to date none of these possible SPAK binders has been extensively validated.

In order to understand the binding of the WNK RFxV peptide to the CCT domains, the co-crystal structure of the human WNK4 RFQV with the OSR1 CCT domain was solved (Villa et al., 2007). This structure revealed that the CCT domain

was arranged in a unique fold, called SPAK/OSR1 *C*-terminus (SPOC) fold that forms a long groove (Villa et al., 2007). Within this fold, there was a negatively charged fragment known as primary pocket, which serves as a docking site of the WNK4 RFQV peptide. Apart from glutamine (Q) residue, which was facing outward, the other three residues from the RFQV motif were faced inward and formed key interactions with the CCT domain (**Figure 1.11**). Interestingly, in addition to the primary pocket that acts as the docking site for the RFQV peptide, a second smaller pocket, termed the secondary pocket, was also observed through this groove, and it had no influence on the binding of the RFQV peptide (Villa et al., 2007, Vitari et al., 2006).

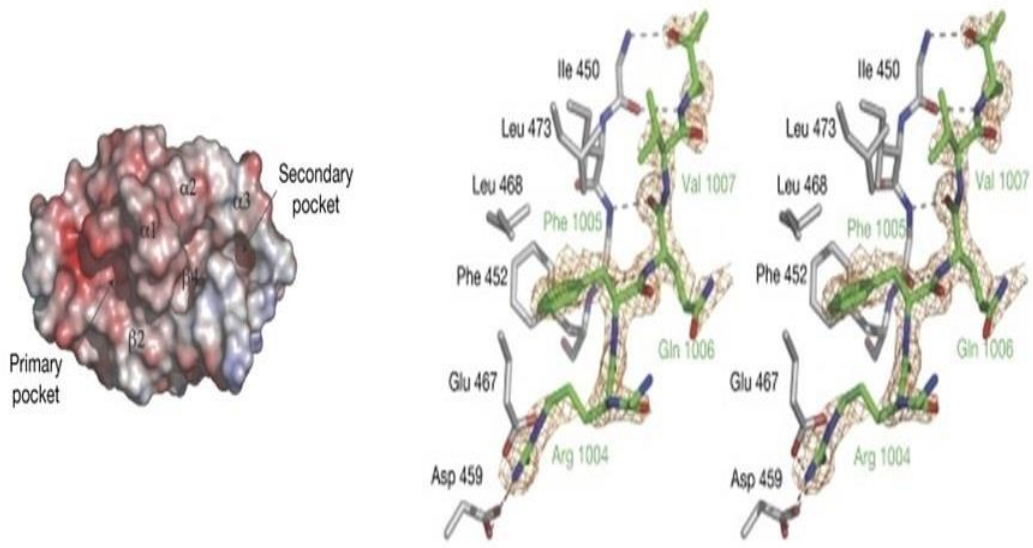

Figure 1.11: Structure of SPAK/OSR1 CCT-domains and their binding to the WNK4-derived RFQV-peptide. *Figure on the left shows the structural surface of OSR1 CCT, the residues in CCT domain are differentiated according the surface electrical charge in to positive (blue areas) and negative (red areas). The positions of primary and secondary pockets are also indicated. The middle and right figures show stick representation, showing the molecular interaction of RFQV-peptide (green) with residues in CCT domain (grey). Ile, isoleucine; Leu, leucine; Phe, phenylalanine; Glu, glutamine; Asp, aspartic acid; Val, valine; Gln, glutamine. Figure adapted from (Villa et al., 2007).*

Mutational analysis of OSR1 CCT binding to the WNK4-RFQV peptide indicated that mutations in the primary pocket either reduced or completely abolished the binding to the RFQV. The most prominent inhibition of the binding was observed when the OSR1 CCT domain residues Asp479 and Leu493 of SPAK and Asp459 and Leu473 of OSR1 were mutated (Vitari et al., 2006). A pulldown assay utilizing mutations of R, F or V to alanine of the RFQV peptide indicated that only the RFAV peptide binds the CCT domain of OSR1 with similar affinity to the RFQV peptide (Villa et al., 2007, Vitari et al., 2006). In contrast, individual point mutations in secondary pockets did not affect the binding of the CCT domain. Recently, mutations in this secondary pocket were found to affect the catalytic activity of the kinase suggesting that the secondary pocket could have a regulatory role of SPAK and OSR1 kinase activities (Villa et al., 2007, AlAmri et al., 2017a)

1.2.4 Activation of SPAK and OSR1 by WNK kinases:

As mentioned above, WNK kinases phosphorylate SPAK and OSR1 at the highly conserved threonine residues Thr233 and Thr185 respectively, which are located in their threonine-rich loops, termed the T-loops (Richardson and Alessi, 2008). Moreover, WNK kinases also phosphorylate Ser325 in OSR1 and Ser373 in SPAK, which are located in the S-motifs. Although the function of this phosphorylation site remains unclear*, in vitro* phosphorylation of SPAK and OSR1 kinases by WNK1 showed that the phosphorylation of S-motif was of higher stoichiometry than that of the T-loop (Vitari et al., 2005). Mutational analysis of these WNK-phosphorylation sites revealed that SPAK and OSR1 activity is only affected by T-loop phosphorylation and not the S-motif phosphorylation (Richardson and Alessi, 2008, Murthy et al., 2017). To support the WNK phosphorylation of SPAK and OSR1 by WNK1, knockdown of WNK1

led to reduce SPAK and OSR1 kinase activity, which was found to be a result of reduced SPAK and OSR1 phosphorylation of their T- loops and S-motifs (Anselmo et al., 2006, Moriguchi et al., 2005, Zagórska et al., 2007).

The phosphorylation of SPAK and OSR1 kinases by WNKs is now established as the first activation step. This is because the Alessi group discovered that the WNK-activated SPAK/OSR1 are further activated by binding the scaffolding protein MO25 (Alessi et al., 2014). Indeed, mouse protein 25 (MO25) of which there are two isoforms in humans (α and β), was found to bind SPAK and OSR1 kinases, leading to 70–100 fold increase in their catalytic activity *in vitro* (Filippi et al., 2011). The fully activated SPAK and OSR1 kinases then phosphorylate and activate CCCs (Murthy et al., 2017).

Knockout of MO25 in human embryonic cells (HEK293) cells did not lead to alterations in the phosphorylation of SPAK and OSR1 at the WNK-phosphorylation sites, but as expected a decrease in the phosphorylation and activation of NKCC1, the physiological substrate of SPAK and OSR1 kinases, was observed (Filippi et al., 2011). This observation indicated that the interaction of MO25 with SPAK and OSR1 kinases did not affect their activation by WNK kinases, but rather increases the activity pre-WNK-phosphorylated SPAK and OSR1 kinases. This finding was reinforced by a study examining the function of MO25 in *Drosophila* (dr). Malpighian tubular cells, in which Fray kinase (insect analogous of human Ste20 kinases) was incubated with dr-WNK and dr-MO25 in *in vitro* assays led to increased activity of Fray protein (Sun et al., 2018). In contrast, dr-MO25 knockout in Malpighian system reduced ions transport in stimulated epithelial cells (Sun et al., 2018). This study provided another evidence that MO25 enhances the catalytic activity of SPAK and OSR1 kinases.

The function of SPAK and OSR1 could also be affected by trans-autophosphorylation (Rodan and Jenny, 2017). Indeed, it was proposed that trans-autophosphorylation of OSR1 could be mediated by its homodimerization (Rodan and Jenny, 2017), which allows the swapping of identical elements of the T-loops between SPAK and OSR1 monomers without distorting the intramolecular interactions of each monomer (Rodan and Jenny, 2017, Lee et al., 2009, Villa et al., 2008, Taylor et al., 2015).

The function of MO25 on the dimerization of SPAK and OSR1 was investigated in *Xenopus* oocytes where the ability of a complex of monomers or dimers of wild type (WT) alone or with various mutant SPAK to phosphorylate NKCC1 in the presence or absence of MO25 was explored (Ponce-Coria et al., 2012). This showed that MO25 was required to increase the catalytic activity of WT-SPAK dimers, as indicated by NKCC1 phosphorylation in the presence or absence of MO25. Interestingly, in the co-expression of MO25 with SPAK concatemer, which was composed of functional WT-SPAK monomer and inactive mutant SPAK monomer, the activation of NKCC1 was also observed. It was hypothesised that the activation resulted by exchange of the activation loop between the two SPAK monomers, this could substitute mutant inactive SPAK monomer (Ponce-Coria et al., 2012). Moreover, it was shown that the overexpression of the OSR1-WT rescued the activity of the mutant SPAK, that further supporting the possibility of heterodimer formation (Ponce-Coria et al., 2012). Together, these observations emphasise the role of MO25 in SPAK and OSR1 activation by possible stabilisation of the active form of the kinases as well as the facilitation of their dimerization (Gagnon et al., 2011).

1.2.5 Role of WNK-SPAK/OSR1 in ion homeostasis:

Ion homeostasis is a vital process for maintaining cell volume and proper cellular function in all tissues (Kahle et al., 2010). The precise tuning of [Cl] was found to be the crucial mechanism in intracellular osmoregulation, and it is strictly regulated by a family of CCCs known as *SLC12A* co-transporters (Kahle et al., 2010). This family comprises NKCCs, NCC and KCCs which mediate Na-derived Cl influx and K-derived Cl outflux respectively. These proteins play an important role in renal physiology, regulating BP and neurotransmission (Alessi et al., 2014). CCCs have been extensively explored over the last two decades and some of the key findings was that these co-transporters are activated and deactivated by phosphorylation at serine and threonine residues in either *N*- or *C*-terminal domains (Bazúa-Valenti et al., 2016). WNK-enzymes along with their downstream substrates, SPAK/OSR1, and upstream regulators, CUL3/KLHL3 (**section 1.3.3**), all of which comprise the WNK-signalling cascade, regulate the function of the *SLC12A* co-transporters and therefore electrolytes homeostasis (Shekarabi et al., 2017). Despite the progress achieved, the role of phosphatases, which dephosphorylate proteins, in the function of these co-transporters is still not as well investigated as the role of protein kinases.

In humans, the *SLC12A* family contains nine members, (**Table 1.2**), two of which NKCC2 and NCC, are kidney specific (Richardson and Alessi, 2008). The rest of the co-transporters are widely distributed except KCC2, which is neuronal specific protein (Richardson and Alessi, 2008). Mutations in these co-transporters could lead to a series of diseases in humans. For instance, Gitelman's syndrome is now understood to result from malfunctioning of NCC (Simon et al., 1996b), while Bartter's type-1 is caused by a mutation in the NKCC2 gene (Simon et al., 1996a). Both syndromes are characterised by hypotension that is associated with electrolytes

disturbances and inherited metabolic alkalosis (Simon et al., 1996a, Simon et al., 1996b).

Member	Symbol	Ion co-transporter	Expression
SLAC12A1	NKCC2	$Na^+/K^+/2Cl^-$	Kidney (Thich ascending limb)
SLAC12A2	NKCC1	$Na^+/K^+/2Cl^-$	Ubiquitous
SLAC12A3	NCC	Na^+/Cl^-	Kidney (distal convoluted tubules)
SLAC12A4	KCC1	K^+/Cl^-	Ubiquitous
SLAC12A5	KCC2	K^+/Cl^-	Nerve
SLAC12A6	KCC3	K^+/Cl^-	Ubiquitous
SLAC12A7	KCC4	K^+/Cl^-	Ubiquitous
SLAC12A8	CCC9	Unknown	Ubiquitous
SLAC12A9	CIP	Unknown	Ubiquitous

Table 1.3: Co-transporter protein members of the SLC12A family. *Table adapted from (Richardson and Alessi, 2008).*

1.2.5.1 Regulation of NKCC1 by WNK-SPAK/OSR1:

NKCC1 was the first SPAK and OSR1 kinase substrate identified (Piechotta et al., 2003, Piechotta et al., 2002). Indeed, SPAK and OSR1 bind NKCC1 and phosphorylate it at a series of *N*-terminal threonine residues, Thr203, Thr207, Thr212 and Thr217 (**Figure 1.12**), leading to its activation. Interestingly, single point mutation of Thr217 or Thr212 into alanine inhibited NKCC1 activity (Dowd and Forbush, 2003, Gagnon et al., 2007a). It is ubiquitously expressed and possesses twelve transmembrane segments (TM) with cytoplasmic *N*- and *C*-termini (Markadieu and Delpire, 2014). It has an ability to dimerize though the monomers have also been

shown to be fully functional (Markadieu and Delpire, 2014). The NKCC1 co-transporter takes up Cl, which co-transported with Na, and counter-transport it with K, enabling the regulation of cell osmolarity and volume equilibrium with the extracellular environment (Flatman, 2007, Gerelsaikhan and Turner, 2000). Not long after the discovery of NKCC1, NKCC2 and KCC, were also found to bind SPAK and OSR1 kinases, which phosphorylate them following osmotic stress (Vitari et al., 2005).

At the molecular level, NKCC1 interacts with SPAK and OSR1 via the docking of RFxV stretch of NKCC1 into the CCT domain of SPAK and OSR1, akin to WNK kinases docking to these CCT domain motifs (Alessi et al., 2014). NKCC1 has two RFxV motifs in *N*-terminus (**Figure 1.12**). Mutations in these RFxV sequences prevented the binding to SPAK and OSR1, resulting in inhibition of NKCC1 activation (Vitari et al., 2006, Gagnon et al., 2007a). Interestingly, it has been found that the SPAK and OSR1 CCT domain could bind either WNK or NKCC1, which both contain multiple RFxV motifs. This indicated that the dissociation of WNK-activated SPAK and OSR1 from WNK kinases is essential for the subsequent binding to NKCC1 as the CCT domain could only accommodate one protein at a time. Zagoroska et al demonstrated that Ser1261 of WNK1, which is located immediately after the RFQV motif, was phosphorylated under osmotic stress in HEK293 cell line, suggesting that SPAK and OSR1 kinases dissociated from WNK kinases following this WNK1 Ser1261 phosphorylation (Zagórska et al., 2007).

This finding was supported by the failure to pulldown SPAK and OSR1 kinases using a WNK4-derived RFxV peptide phosphorylated at a threonine residue that falls immediately after the RFQV sequence (Villa et al., 2007). The kinase that phosphorylates these threonine residues that are located immediately after the RFQV motifs remains elusive. In 2012, the Alessi group found that WNK1 Ser1261 was not

phosphorylated by SPAK and OSR1 kinases since the phosphorylation of this residue by osmotic stress was completely unaffected by the loss of SPAK and OSR1 kinase activity (Thastrup et al., 2012). Thus, it was suggested that these threonine sites could be phosphorylated either by WNK isoforms themselves, in a trans-phosphorylation phenomenon, or by an unknown upstream kinase (Thastrup et al., 2012).

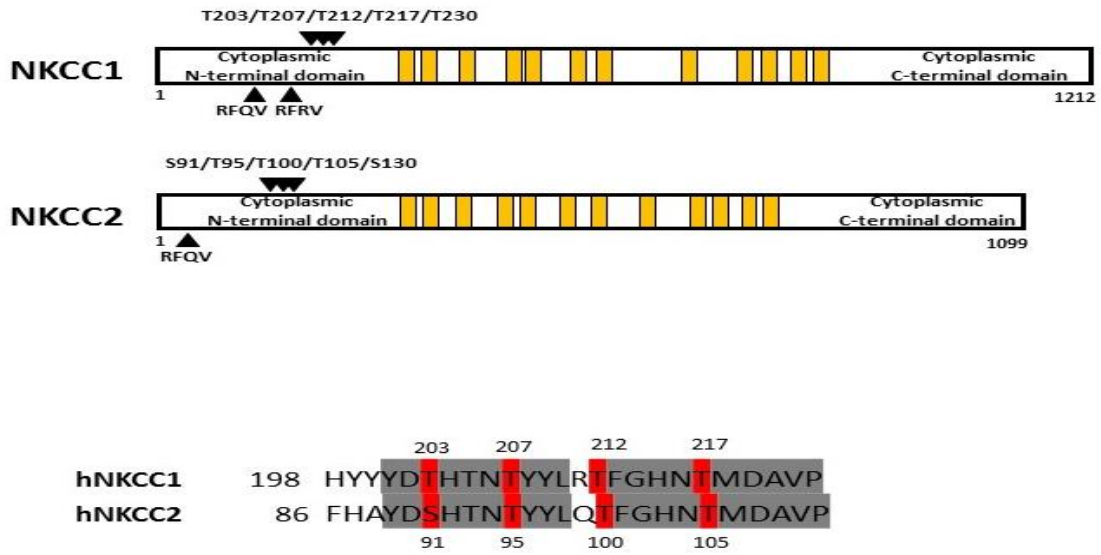

Figure 1.12: The structural domains of human the SLC12A transporters NKCC1 and NKCC2. *Schematic diagram of NKCC1 and NKCC2 showing the transmembrane domains (yellow), the key domains and phosphorylation sites in both the N-terminus as well as the SPAK/OSR1 binding regions. The bottom panel is sequence alignments of human NKCC1 and NKCC2 showing the conserved residues (grey) and SPAK/OSR1 phosphorylated sites (red) (Richardson and Alessi, 2008).*

1.2.5.2 WNK-SPAK/OSR1 regulation of NKCC2:

NKCC2 is a pivotal *SLC12A* member and it possesses 60 % sequence similarity to NKCC1 (Markadieu and Delpire, 2014). In contrast to NKCC1, NKCC2 is only expressed in renal TAL and it contributes to the reabsorption of 25 % of filtrated

glomerular salts. NKCC2 is the molecular target of the antihypertensive loop diuretics (Flatman, 2007). WNK-activated SPAK and OSR1 kinases interact with and phosphorylate NKCC2 at *N*-terminal serine and threonine residues, Ser91, Thr95, Thr100 and Thr105 (**Figure 1.12**). Phosphorylation analysis of NKCC2 *N*-terminus revealed that the SPAK/OSR1-phosphorylated residues are also conserved in NKCC1 and NCC (Richardson et al., 2011). Subsequent studies have shown that only three sites on NKCC2, Thr95, Thr100 and Thr105, are exclusively phosphorylated by the SPAK and OSR1 kinases.

Interestingly, under osmotic stress five of seven phosphorylation sites on the *N*-terminus of NKCC2 were identified, some of which were WNK-SPAK/OSR1-independent (Richardson et al., 2011). For example, Ser130 was found to be phosphorylated by AMPK (AMP-activated protein kinase) in response to hypotonic condition (Richardson et al., 2011). Out of the identified five phosphorylation sites, Thr105 and Ser130 were confirmed to play important roles in switching on and off the activity of NKCC2. Single point mutation of one of these residues reduced the NKCC2 activity by 30-40 %, while mutations of both led to complete abolition of the co-transporter function (Richardson et al., 2011). Notably, this finding contrasted NKCC1 regulation, where single point mutation of NKCC1 Thr217, which is equivalent to NKCC2 Thr105, was enough to abolish the function of NKCC1 (Richardson et al., 2011).

Beyond the direct effect of SPAK and OSR1 on the function of NKCC2, the SPAK and OSR1 phosphorylation of NKCC2 has been shown to have an effect on the co-transporter total protein levels. For instance, it was demonstrated that the expression and phosphorylation of NKCC2 were elevated in universal SPAK knockout mice (Yang et al., 2010). This was hypothesised to be a result of the compensatory

effect exerted by OSR1 in TAL (Grimm et al., 2012). Interestingly, viable transgenic mice with $SPAK^{T243A/T243A}$ mutation that could not be activated by WNK isoforms, they displayed Gitelman's like syndrome and the expression as well as the phosphorylation of all co-transporters including NKCC2 were diminished (Rafiqi et al., 2010). These data revealed that OSR1 is the predominant regulator of NKCC2 in TAL and SPAK is regulating NCC in renal DCT (Bazúa-Valenti et al., 2016). Although the protein phosphatases that regulate NKCC2 activity have not been fully defined, calcineurin, a serine/threonine protein phosphatase, had been shown to regulate the function of NKCC2 (Borschewski et al., 2016). The inhibition of calcineurin by cyclosporine, led to elevated levels of NKCC2 phosphorylation by SPAK and OSR1 (Borschewski et al., 2016).

As mentioned above, osmotic stress could lead to SPAK/OSR1-independent phosphorylation of NKCC2. This notion is supported by previous studies that NKCC2 could be phosphorylated by protein kinase A (PKA) signalling and increased levels of cyclic adenosine monophosphate (cAMP) in TAL (Gunaratne et al., 2010). Given the role of PKA is regulating the function of G protein coupling receptors (GPCR), this may link WNK-signalling to the function of GPCRs (Gunaratne et al., 2010, Bazúa-Valenti et al., 2016). Beyond PKA, various reagents that increase cAMP levels, e.g. vasopressin (VAP), β-adrenergic agonists (such norepinephrine and isoproterenol), glucagon, parathormone and calcitonin, are known to modulate Na and Cl reabsorption in TAL and thus they may produce these effects through the PKA-mediated phosphorylation of CCCs (Ares et al., 2011b). An example of this is VAP, which has been shown to induce phosphorylation of NKCC2 at Ser126 and Ser874 via PKA-signalling, which translates into increased activity of the NKCC2 co-transporter (Gunaratne et al., 2010).

1.2.6 Regulation of WNK-SPAK/OSR1-CCCs cascade:

1.2.6.1 Physiological regulators of WNK signalling:

Since the WNK-SPAK/OSR1 signalling pathway responds to intracellular ionic levels, it was hypothesised that the activity of this signalling cascade is adjusted by amount of salt intake (Uchida et al., 2014). Indeed, low intake of Na/Cl increased the phosphorylation of SPAK/OSR1 and NCC (Thr53, Thr58 and Ser71) in the kidneys (Vallon et al., 2009). The phosphorylation of SPAK/OSR1 and NCC was reduced with high salt diet and administration of spironolactone (Chiga et al., 2008). However, aldosterone administration reverses this phosphorylation reduction. This suggesting that the aldosterone effects could be mediated via the WNK-SPAK/OSR1 signalling cascade (Chiga et al., 2008). Similarly, dietary potassium (K) regulates this pathway, as high dietary K down regulated WNK-SPAK/OSR1-NCC cascade (Uchida et al., 2014). Whereas, low ingested K increases the levels of NCC expression and phosphorylation as consequence of raised activity of WNK4-SPAK signalling (Castañeda-Bueno et al., 2014, Sorensen et al., 2013, Vallon et al., 2009). With this in mind, it was not surprising to find that the kinase activity of WNK1 and OSR1 was stimulated when cells were treated with low K medium and inhibited by high K buffers (Naito et al., 2011).

Recent *in vivo* studies demonstrated that K- deficient diet triggers NCC activity, causes Na retention and increases BP even with the intake of high salt diet (Terker et al., 2015). This effect was found to be mediated by low plasma K, hypokalaemia, which causes membrane hyperpolarization of DCT cells that diminishes [Cl] (Terker et al., 2015). This Cl efflux though chloride channel consequently activates WNK kinases to limit the loss of K (Terker et al., 2015, Nomura et al., 2018). This explains how WNK kinases are activated in response to hypokalaemia.

In addition to the salt effect on WNK signalling, the body hormones are also involved in the regulation of WNK-SPAK/OSR1. Vasopressin (Vas) (Rieg et al., 2013, Saritas et al., 2013), angiotensin 2 (Ang2) (Castaneda-Bueno et al., 2012, van der Lubbe et al., 2011) have been shown to induce the activation of WNK-signalling. Moreover, insulin was shown to activate SPAK/OSR1 by reducing activity of WNK4 via the phosphatidylinositol 3 kinase/Akt signalling cascade (Takahashi et al., 2014, Chavez-Canales et al., 2013, Nishida et al., 2012). These findings could explain the elevated sensibility to the salt in patients with hyperinsulinemic metabolic syndromes (Uchida et al., 2014).

1.2.6.2 Drug regulation of WNK-SPAK/OSR1 cascade:

Since the discovery of the association of WNK kinases with HPT in 2001, this signalling cascade emerged as an attractive target for the discovery of new antihypertensive drugs. In 2013, the first small WNK-signalling inhibitors were reported (Mori et al., 2013). These compounds were designed to bind the highly conserved CCT domains of SPAK and OSR1 kinases and inhibit their binding to the upstream WNK kinases. Then, several other WNK-signalling inhibitors that targeted different components of the WNK-SPAK/OSR1 signalling pathway were discovered (AlAmri et al., 2017b, Cheng et al., 2017). The WNK-signalling inhibitors discovered to date were classified into four categories according to their mechanism of inhibition. The first were WNK kinases inhibitors, which were divided into competitive and non-competitive ATP inhibitors, e.g. WNK463 and WNK476, respectively. Secondly, inhibitors of WNK binding to SPAK and OSR1 kinases and these include STOCK1S-50699 and STOCK1S-26016. The third group composed of compounds that acted as direct SPAK and OSR1 kinase inhibitors, e.g. STOCK1S-14279, Closantel and Rafoxanide, all of

which are non-ATP-competitive inhibitors. Whereas, the fourth group is composed of molecules that inhibit the binding of SPAK and OSR1 kinases to MO25 (AlAmri et al., 2017b). To date, only one compound, HK01, has been discovered as an inhibitor of this interaction and it is an indirect inhibitor of SPAK and OSR1 kinases (Kadri et al., 2017, AlAmri et al., 2017b).

1.3 The beta 2-adrenergic receptor (β2AR)

1.3.1 β2AR overview:

The human guanosine triphosphate protein (GTP)-binding protein (G-protein) coupled receptors (GPCRs) are the largest superfamily of cell membrane receptors (Rasmussen et al., 2011b). GPCRs have been the targets of many drug discovery initiatives because their ability to respond to a variety of stimuli, hormones, peptides, ions, protons, small molecules and light, and their involvement in many human diseases such as pulmonary, cardiac diseases, cancer, metabolic and monogenic disorders (Shoichet and Kobilka, 2012). Human GPCRs are classified into four main classes; class A, B, C, and F based on their sequence homology and function (Fredriksson et al., 2003).

Historically, the adrenergic receptors (AR) belong to the aminergic group of Class-A non-rhodopsin GPCRs (Basith et al., 2018, Cherezov et al., 2007). They have been classified into two major subfamilies; α- and β-receptors, which is subdivided into β1-, β2- and β3-AR. Although, the β-subtypes share 60-70 % resemblance, they vary in tissue expression, function and in the pattern of agonist binding (Mutlu and Factor, 2008). The β1AR is found in the heart, brain, kidney and blood vessels. The β2AR is

expressed in the lung, heart, smooth and skeletal muscles, blood vessels, kidney and uterus. The β3 subtype is expressed mainly in adipose tissues, heart and vasculature (Mutlu and Factor, 2008). In terms of their function, the β1AR is primarily implicated in the elevation of heart rate and force of contraction. The β2AR is involved in the stimulation and relaxation of the smooth muscles whereas the β3AR has a significant role in obesity (Kurose, 2004).

The β2AR is a heptahelical transmembrane protein, interconnected with three intracellular loops (ICL) and three extracellular loops (ECL). Its *C*-terminus is cytoplasmic while the *N*-terminus is projected extracellularly (Kobilka, 1992). It conveys the signals into cytosolic proteins through predominantly triggering of its cognate heterotrimeric G-protein, however other G-protein-independent signalling transductions have also been reported, such as recruitment of β-arrestin (Lefkowitz, 2000, Cherezov et al., 2007).

Like other GPCRs, the β2AR has high ability to stimulate G_s protein even when it is not engaged to an agonist (Manglik and Kobilka, 2014).This phenomenon is known as 'basal activity', which could be reduced by inverse agonists and elevated by agonists (Manglik et al., 2015). GPCRs, including the β2AR, are highly dynamic and flexible which exist in multiple functional conformations with low energetic barriers (Deupi and Kobilka, 2010). Therefore, the term bimodal switch (inactive/active) could not be used with these GPCRs (Manglik and Kobilka, 2014). The receptor dynamics are influenced by various stimuli such as ligands, cytosolic protein binding, pH, lipids, ions and perhaps alteration in membrane potential (Latorraca et al., 2017). In addition to their structural flexibility, homo- and hetero-dimerization of these receptors also takes place and this could also be an issue for understanding the biological functions of these receptors in health and disease (Manglik and Kobilka, 2014). Most of GPCRs

exist in monomer-dimer equilibrium state, also the half-life of monomeric association is less than seconds, resulted in a failure of crystallization of multimeric forms of receptors that make several questions related to the role of dimerization have not been solved yet (Lambert, 2010). In addition, single activated monomer has ability to interact to and activates G-proteins (Gurevich and Gurevich, 2008) which make the understanding of the role of dimerization/oligomerization in receptor function is unclear (Manglik and Kobilka, 2014).

1.3.2 The crystal structure of the β2AR:

The human β2AR gene is about 1,200 base pairs and is located on chromosome 5, which encodes 413 amino acids of 46.5 kD (Mutlu et al., 2004b). Although, it was firstly discovered in the 1990s, the β2AR crystal structure had not been solved until 2007 in complex with the inverse agonist, Carazolol (Cz) (Cherezov et al., 2007).

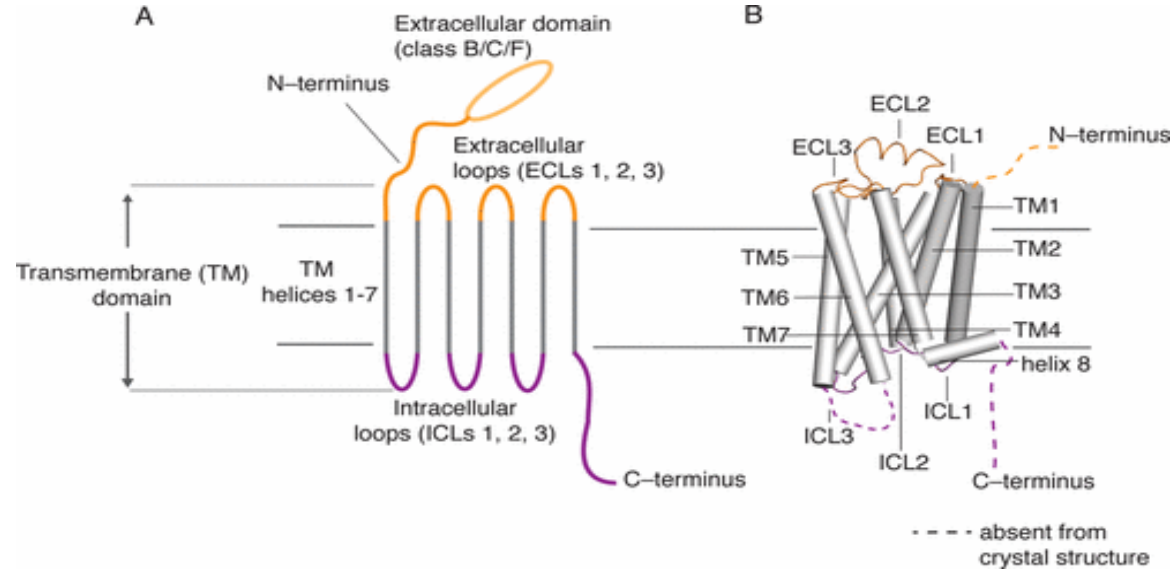

Figure 1.13: General topology of GPCRs and structure of the β2AR. *(A) The overall structure of GPCRs showing the seven transmembrane (TM) segments in grey, the N-terminus and ECL in orange, the ICL and the C-terminus end in purple. (B) Diagram showing the structure of the β2AR, highlighting the TM orientation, loops, N- and C-terminal ends. Figure adapted from (Latorraca et al., 2017).*

Unlike rhodopsin GPCRs, structural analysis of the β2AR revealed that it shows inherited conformational flexibility, and substantial basal activity, which could be observed in the absence of a ligand (Manglik et al., 2015). The β2AR possesses a long resilient ICL3, which is thought to make the crystallization of the receptor challenging (Bang and Choi, 2015). Thus, for its crystallisation, β2AR was complexed with Cz to reduce the receptor fluctuation and stabilize it in an inactive state. Additionally, to overcome the plasticity of the ICL3, stabilisation of receptor at cytoplasmic side is required, either by creating a complex of the ICL3 with a Fab, an antibody fragment against ICL3, or by replacing the ICL3 by T4-lysozyme, an engineered β2AR incorporated protein (Cherezov et al., 2007, Rosenbaum et al., 2007, Rasmussen et al., 2007).

These advanced techniques enabled a favourable packing interactions of the β2AR crystals in high resolution where the β2AR appeared to be monomeric although several biophysical and biochemical studies indicated that the β2AR existed in well organised oligomers in biological membranes (Bulenger et al., 2005). The crystal structures of the β2AR revealed that it possesses the GPCRs common spanning seven hydrophobic transmembrane (7TM) helices, which are intervened with intracellular and extracellular hydrophilic loops (**Figure 1.13**). Each TM domain consists of 20-25 amino acids, which harbour the highest conserved residues among the β2AR sequence (Strader et al., 1989). Also, it was noted that the β2AR has *N*-terminal glycosylation sites at Asn6, Asn15 and Asn187 which had been shown to be essential for receptor integration into plasma membranes and in agonist-mediated trafficking processes (Mialet-Perez et al., 2004).

Comparison of the β2AR to rhodopsin revealed that active rhodopsin has closer arrangement of TM helices than in the β2AR because of the presence of a conserved

[E/D]R[Y/W] sequences on TM3 (Bang and Choi, 2015). These sequences are involved in the formation of hydrogen bonds between Glu134 and Arg135 of [E/D]R[Y/W] on TM3 and Glu247 on TM6 (**Figure1.14A**), interactions that have been termed the ionic lock. Such interactions appear to be responsible for the structural stability of the receptor and it is thought to limit the receptor basal activity (Rasmussen et al., 2007). Since the β2AR also possesses the [E/D]R[Y/W] motif, similar function of these sequences were predicted and this was later shown to be the case as mutations within these sequences produced constitutively active β2AR (Ballesteros et al., 2001). Nevertheless, the β2AR appeared to have broader TM segments than that in rhodopsin because the distance between Arg131 on TM3 (Cz binding site) and Glu268 of TM6 was wider and thus disrupting the ionic lock (**Figure1.14A**). This structural arrangement of the β2AR TM regions could explain the receptor's basal activity in the absence of ligand binding (Rasmussen et al., 2007).

In addition, the other key residue that could be vital in minimizing the β2AR basal activity is Leu272 on TM6, which has been shown to participate in van der Waals interactions with Ile135 on TM3, Tyr141 of ICL2, Val222 and Tyr219 on TM5 residues (Rasmussen et al., 2007). This observation was supported by the mutation of Leu272 into Ala, which resulted in continuously active β2AR (Samama et al., 1993).

The T4-lysozyme replacement and lipid cubic phase crystallization technique provided a high-resolution structure of the β2AR ligand binding site (Bang and Choi, 2015). Among the key insights provided was that Cz formed hydrogen bonds with Asp113, Asn312 and Tyr316. Also, it formed hydrophobic interactions with Val114, Phe193 and Phe290 (Bang and Choi, 2015). In contrast to rhodopsin, the Cz docking site in the β2AR is not as deep, and ECL2 of the β2AR does not interact with the *N*-terminus. This makes the ligand binding site in the β2AR slightly open to the

surrounding solvent thus permitting Cz to simply diffuse in and out of the binding site (Bang and Choi, 2015).

Interestingly, other inactive conformations of the β2AR in complex with different ligands e.g., timolol, ICI118551 (inverse agonists) or alprenolol (antagonist) have been reported (Hanson et al., 2008, Wacker et al., 2010). These revealed that the general structure of the receptor was preserved, but only minor differences in the ligand binding site were identified (Wacker et al., 2010).

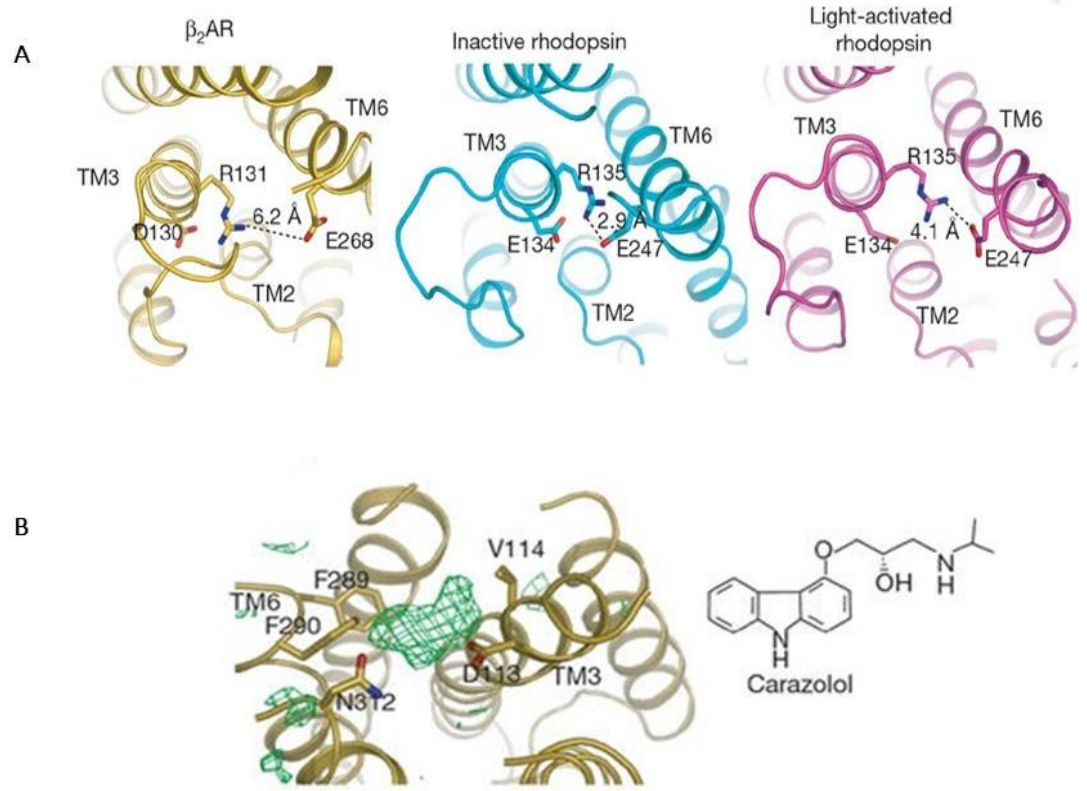

Figure 1.14: β2AR in comparison with rhodopsin. *(A) Topology of TM3 and TM6, showing the conserved E/DRY/W motif in TM3 of both β2AR and rhodopsin. (B) Carazolol chemical structure in right, and its binding site at β2AR between TM3 and TM6, the involved residues (Asp113, Val114, Phe290 and Phe289) are also illustrated. Figure and ligand adapted from (Rasmussen et al., 2007).*

β2AR were preserved, extra hydrogen bonds and hydrophobic interactions take place depending on the ligand's structure from these ligands and could be related to their strength (Bang and Choi, 2015).

1.3.3 Activation of the β2AR:

Following the first report of the β2AR structure in 2007, there were several attempts at obtaining the agonist-bound active form of the receptor. Due to the structural dynamics of the β2AR even in the unstimulated form where it is in equilibrium between different conformations, stabilizing receptor on one structural conformation that allows crystallisation was a challenge (Bang and Choi, 2015). To achieve this, the agonist FAUC50 was designed to covalently bind the mutant β2AR-H93C by forming a disulphide bond with Cys93 at the end of TM2. However, this showed that, unexpectedly, the binding of agonist alone to the β2AR was insufficient to achieve a steady active conformation (**Figure1.15A**) (Rosenbaum et al., 2011). Thus, to capture the β2AR active conformation, a combined use of high affinity agonist, BI-167107, and cytoplasmic stabilization approaches either by G-protein or antibody (nanobody 80) have been used (Rasmussen et al., 2011a, Rasmussen et al., 2011b).

By comparing the BI-167107-bound active and Cz-bound inactive β2AR structures, only little differences on the extracellular side of the receptor were noted and these were slight alterations in the agonist-binding pocket to accommodate the agonist. However, significant changes were observed in the cytoplasmic side (Bang and Choi, 2015). Indeed, once the full agonist BI-167107 bound the β2AR, it formed hydrogen bounds with Ser204 and Ser207 at TM5 attracting the upper segment of TM5 to TM6, which lead to the rearrangement of the hydrophobic connector region

that is made up of Pro211, Ile121 and Phe282. These interactions caused outward rotation and swaying of TM6 by about 14 Å (**Figure1.15B**) (Rasmussen et al., 2011a, Rasmussen et al., 2011b). This outer movement of TM6 was accompanied with a relative inward rearrangement of TM5 and TM7 that enabled the insertion of a G-protein or its mimetic (Manglik et al., 2015). The residues on TM3-7, referred to above as the connector region, are thought to serve as a central pivot that senses and rearranges the TM segments in response to agonist binding (Latorraca et al., 2017, Rasmussen et al., 2011a).

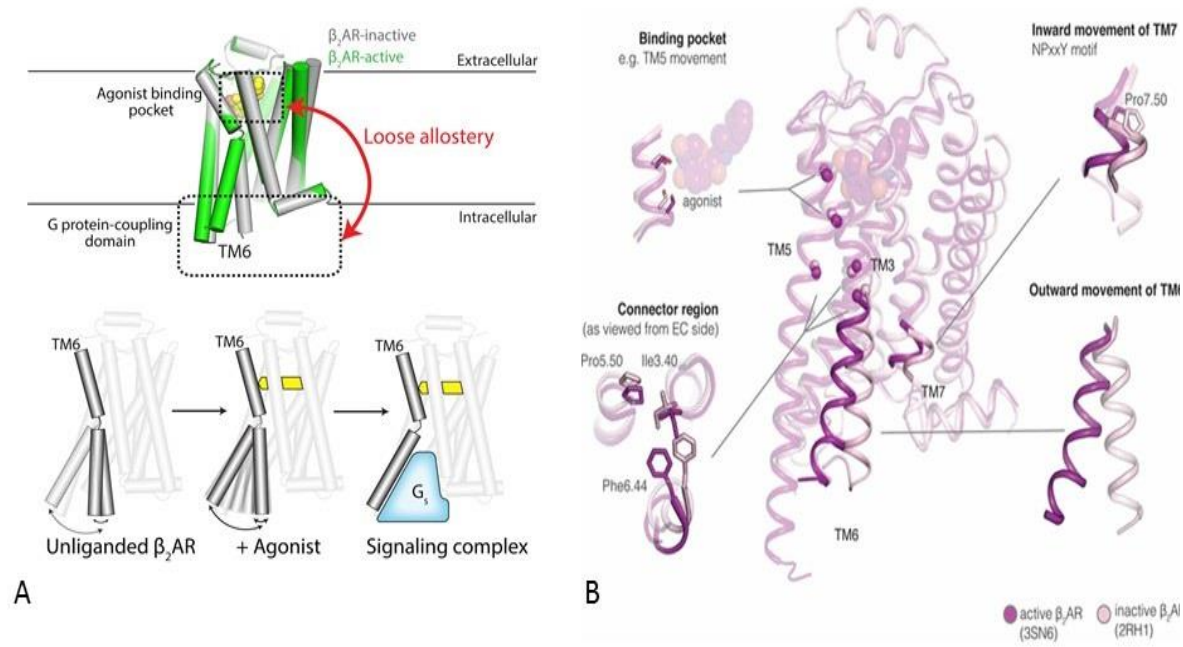

Figure 1.15: The β2AR dynamic activation and loose allosteric regulation. *(A) Schematic diagram of the β2AR showing loose allosteric regulation between the binding pocket and the cytoplasmic ends of the TM segments (Top). The role of the outward movement of TM6 in the β2AR activation (bottom) (Manglik et al., 2015). (B) Topology of the β2AR showing the ligand-binding pocket and rearrangement of the TM segment in the β2AR activation. The dark purple (active β2AR) and light purple (inactive β2AR). Figure adapted from (Latorraca et al., 2017).*

All of these structural insights must be understood in light of the fact that in each case, the β2AR was captured in a constant conformation, so the observations made are most likely specific to that conformation and the many β2AR conformations are undetected, that they take place during the activation process (Bang and Choi, 2015). Hence, to achieve better understanding of the molecular dynamics of the β2AR activation and the link between the agonist-binding pocket and the cytoplasmic G-protein incorporation site, double electron electron resonance (DEER) and nuclear magnetic resonance (NMR) spectroscopy have been used. To simplify the analysis, the β2AR was divided into three functional regions; the ligand binding pocket, the connector and the cytoplasmic domains (**Figure 1.16A**) (Latorraca et al., 2017).

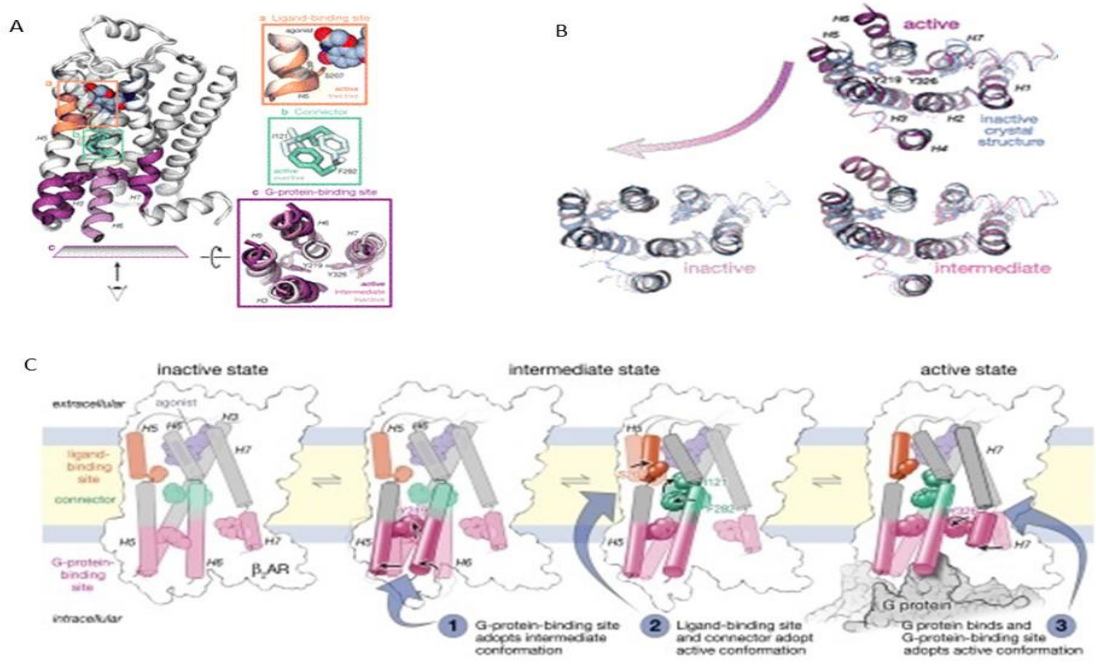

Figure 1.16: Activation mechanism of the β2AR. *(A)Diagram illustrating the three regions involved in the loose allosteric coupling of the active β2AR. Ligand binding pocket (orange), the connector region (green) and cytoplasmic binding domain (purple). (B) The dynamic changes of the cytoplasmic domains during the β2AR activation showing the intermediate state in a simulation model. (C) Schematic diagram of the β2AR activation steps. Figures adapted from (Dror et al., 2011).*

The spectroscopic findings agreed with the notion that binding of a high affinity agonist, e.g. BI167107 alone was not enough to stabilize the β2AR cytoplasmic domain in the active state (Nygaard et al., 2013). Although agonist binding leads to fluctuation of the cytoplasmic domain from inactive to active-like state, the full activation could only be detected after the incorporation of the G-protein and with gradual dissociation of agonist (Manglik et al., 2015). It was supposed that this G-protein binding enhances agonist binding affinity (endogenous allosteric regulation) (Latorraca et al., 2017). However, interestingly, the recent findings revealed that the association between the ligand-binding site and the cytoplasmic domains is loosely allosteric (**Figure 1.16**) (Manglik et al., 2015, Ring et al., 2013). This proposed hypothesis of loose allosteric regulation is delivered by unbiased simulation analysis of the β2AR molecular dynamic where agonist-conjugated β2AR was rapidly interconverting between active and inactive conformations (Dror et al., 2011). This showed that the three parts of the β2AR, agonist binding pocket, the connector and the cytoplasmic domain do not behave like an interconnected gear, but rather than each part interconverts independently between inactive, intermediate or active conformations, although the conformation of a region probably depended on the conformation of other regions (Latorraca et al., 2017). This notion of loose association between the three parts was also confirmed by NMR results (Manglik et al., 2015).

1.3.4 The β2AR-signalling:

The β2AR is a versatile receptor that could regulate multiple signalling pathways through different second messengers and mostly in response to particular ligand binding (Nygaard et al., 2013). The β2AR could be engaged by a rich variety of ligands, which are generally categorised according to their efficacy (ability to generate

cAMP). These categories are: 1) neutral antagonist that does not alter the basal activity, 2) a partial agonist that induces submaximal response, 3) full agonist that produces maximum response, 4) inverse agonist that reduces the receptor's basal activity (**Figure 1.17**) (Rosenbaum et al., 2009).

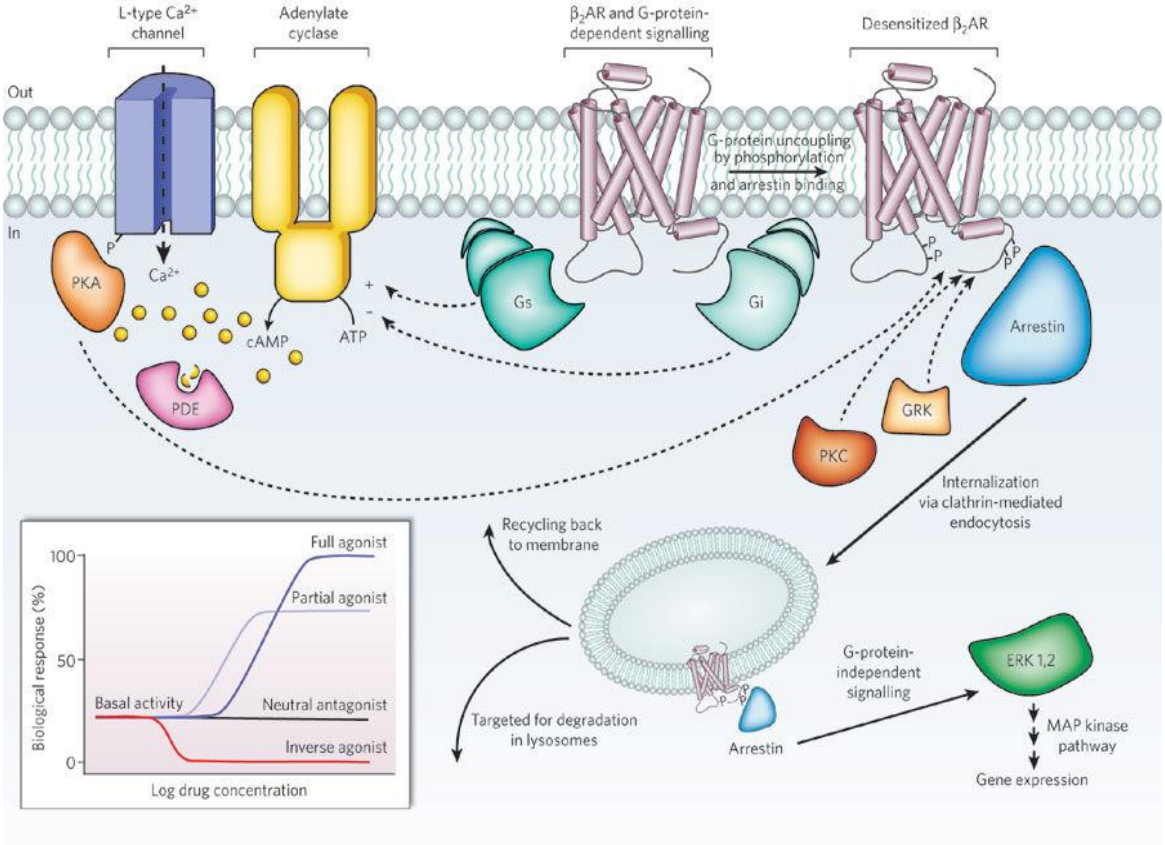

Figure 1.17: The β2AR signalling pathways, recycling and desensitization. *The β2AR modulates the activity of adenylate cyclase via activation of G-proteins (Gsα and Giα). Adenylate cyclase catalyses cAMP to trigger protein kinase A (PKA), Also, the activation of the β2AR results in the activation of G protein coupled receptor kinase (GRK) and arrestin (G-protein independent pathway), which phosphorylate and promote the receptor's internalization, respectively. Also, recruitment of arrestin stimulate gene expression through ERK1/2 MAP kinase pathway. Protein kinase C (PKC) also phosphorylates the β2AR and reduces its interaction with Gαs. Biological response to ligands (lower left corner), which are classified according to their efficacy on GPCRs including the β2AR. Figure adapted from (Rosenbaum et al., 2009).*

Full or partial agonist engagement to the β2AR triggers the canonical pathway Gsα protein by dissociating it from Gsβγ complex (Mutlu and Factor, 2008). This subsequently activates adenylate cyclase (AC) that catalyses cAMP formation, which in turn stimulates PKA (Mutlu and Factor, 2008). In cases where the binding of the inverse agonist or antagonist does not produce biological response, the Gs pathway is inactivated (Mutlu and Factor, 2008). The β2AR also couples to the Giα, which plays a vital role in cardiac pathophysiology by regulating the excitatory effect of the β1AR in the heart (Zhu et al., 2001). Over stimulation of the β2AR-G_iα could be involved in over relaxation of cardiac muscles and ultimately the development of dilated cardiomyopathy (McCloskey et al., 2008).

The β2AR interacts with protein kinases such as PKA, and the G-protein coupling receptor kinase 2 (GRK2). These phosphorylate the receptor leading to conformational alterations and hence converting the receptor towards inactive state (Lefkowitz and Shenoy, 2005). Moreover, the β2AR phosphorylation by GRK2 enables the binding of arrestin proteins resulting in the dissociation of the receptor from Gs, a process that initiates the endocytosis of the β2AR through a clathrin-mediated mechanism (**Figure 1.17**) (Lefkowitz and Shenoy, 2005).

Interacting proteins	*Effect*	*References*
Protein kinase A (PKA)	Phosphorylation of β2AR • ↓ coupling with Gs • ↑ coupling with Gi	(Okamoto et al., 1991)
Protein kinase C (PKC)	Phosphorylation of β2AR. • ↓ coupling with Gs	(Benovic et al., 1985).
Arrestin	• Regulates receptor ubiquitination. • ↑ Receptor internalization. • Interacts with GRK-activated receptor.	(DeFea et al., 2000, Miller and Lefkowitz, 2001).
G-protein coupling receptor kinase (GRK2)	Phosphorylation of agonist bound β2AR. • ↑ binding to arrestin. • ↓ coupling with Gs.	(Cong et al., 2001).
GRK5	Phosphorylation of agonist bound β2AR. • ↓ binding to PDZ motif proteins. • ↑ binding to arrestin.	(Cao et al., 1999).
Insulin receptor	Phosphorylation of β2AR at Tyr residues. • ↑ cAMP (Tyr350/354). • ↓ cAMP (Tyr141).	(Hadcock et al., 1992, Karoor et al., 1995).
Insulin like growthfactor-1	Phosphorylation of β2AR at Tyr residues. Activation of ERK1/2.	(Maudsley et al., 2000).
PDZ-motif containing proteins	• ↓ Activity of Na^+/H^+ exchanger. • ↑ Receptor recycling.	(Cao et al., 1999)
A-kinase anchoring proteins AKAP79 / AKAP250	• Tethering PKA with the receptor at C-terminus.	(Gardner et al., 2006, Tao et al., 2003)
Na/H exchanger regulatory factor1 (NHERF-1)	• Involved in activation of Na^+/H^+ exchanger	(Hall et al., 1998)

Table 1.4: *Summary of the proteins involved in the β2AR signalling pathway. Table adapted from (Mutlu and Factor, 2008, Ritter and Hall, 2009).*

1.3.5 Roles of the β2AR in ions homeostasis:

Stimulation of the β2AR modulates several key proteins through cAMP-dependent and -independent cascades (Mutlu and Factor, 2008). Examples of these proteins include the Na/K-*ATPase*, cystic fibrosis transmembrane conductor regulator (CFTR) and amiloride-sensitive epithelial Na-channels (eNaC), which are all required for ions and fluid homeostasis (Mutlu and Factor, 2008).

1.3.5.1 Stimulation of sodium channels:

Early investigations in the 1980s demonstrated that non-selective βAR-agonists induced influx of ions in monolayer alveolar cells that were isolated from rat lungs (Mutlu and Sznajder, 2004). Subsequent studies showed that catecholamines stimulated the βARs on alveolar fluid clearance (AFC) (Mutlu and Factor, 2008). Several non-selective β2AR agonists (e.g. isoproterenol, epinephrine and dobutamine) and selective β2AR agonists (e.g. procaterol, terbutaline and salmeterol) have been used and showed increase in AFC in many animal models such as rats (Jayr et al., 1994), mice (Fukuda et al., 2000, Icard and Saumon, 1999), dogs (Berthiaume et al., 1988), guinea pigs (Norlin et al., 1998), as well as in *ex vivo* human pulmonary cells (Sakuma et al., 1997). A β2AR knockout mice confirmed the role of the β2AR in AFC regulation (Mutlu et al., 2004a). Together, these revealed that the β2AR plays an important role in the adjustment of Na active transport probably through the Na/K-ATP*ase* pump (Mutlu et al., 2004a).

In an *in vitro* study, it was shown that non-selective cation channels, and selective Na channels e.g. eNaC and high selective-Na channels, could be stimulated by βAR-agonists (Chen et al., 2002, Mutlu and Factor, 2008). Additionally, terbutaline stimulated βARs in alveolar type-2 cells, where it accelerated Na flow in the apical

membrane by enhancing the eNaC abundance in plasma membrane and prolonging the channel's opening time (Yue et al., 1994). This up-regulatory mechanism was found to be mediated by the cAMP-PKA pathways, which phosphorylate cytoskeleton proteins that regulate membrane trafficking of Na channels (Berdiev et al., 1996). Furthermore, it was shown that the β2AR stimulation enhances Na/K-*ATPase* activity in pulmonary epithelium by increasing the assembly of the Na/K-pump and its exocytosis into the plasma membrane through the activation of PKA and Rho-associated kinase (Lecuona et al., 2003). The regulation of the Na/K-pump could also be prolonged by modulating the transcription of the α1-subunit via the activation of PKA and mitogen activated protein (MAP) kinases and the extracellular-signal regulatory kinase (ERK) (Pesce et al., 2003).

1.3.5.2 CFTR regulation:

In addition to Na regulation, the β2AR also regulates Cl movement through cystic fibrosis transmembrane conductor regulator (CFTR) (Mutlu and Factor, 2008, Nielsen et al., 1998). A number of studies revealed that Cl transport elevation was mediated by the β2AR-stimulated CFTR (Fang et al., 2002, Huang et al., 2001, Jiang et al., 2001, O'Grady et al., 2000). CFTR plays a vital role in prevention of pulmonary oedema (excess fluid in air spaces), but is not in the normal lung where the β2AR accelerates AFC (Mutlu and Factor, 2008). Additionally, CFTR overexpression in transgenic mice that lack the β2AR failed to accelerate the rate of AFC likewise in CFTR knockout mice (Mutlu et al., 2005, Mutlu and Factor, 2008). These findings indicated the critical roles of both the β2AR and CFTR in ions and fluid homeostasis in the pulmonary system.

1.3.5.3 Role of the β2AR in renal salts reabsorption:

BP can be elevated by increased salt intake due to an increase in the activity of the renal sympathetic system (SPS) supply, which causes salt retention (Campese et al., 1982, Fujita et al., 1980, Mu et al., 2011). Overactivity of the renal SPS could play a key role in developing salt-dependent HPT by rising Na reabsorption (Mu et al., 2011). Patients with salt-dependent HPT and who are on high salt diet have higher levels of norepinephrine in their blood than that in salt-resistant individuals. This indicates persistent overactivity of the adrenergic system in these patients (Fujita, 2014). Therefore, the kidneys have central roles in regulating BP and this has led to several attempts to treat salt-sensitive hypertensive patients with renal sympathetic denervation (Esler et al., 2010, Krum et al., 2009).

Interestingly, the β2AR mediates norepinephrine- and isoproterenol-induced HPT, as the salt-induced HPT was only developed in wild type and the β1AR knock out mice but did not in the β2AR knock out mice (Mu et al., 2011). The βARs have been shown to be expressed in the renal nephrons using combined labelling autoradiography with light microscopy (Summers et al., 1985). Immunofluorescence (IF) imaging in rat kidneys (Boivin et al., 2001) revealed that the β1AR is abundant and diffusely expressed in TAL, DCT and glomeruli. The β2AR comprises only about 37 % of the βARs expressed in the kidney and is predominantly expressed in the DCT and the collected ducts (CD) (Morla et al., 2016). Notably, the DCT has also been shown to contains several types of salt transporting carriers including NCC, eNaC, Na/H exchanger and Na/K *ATPase* (McCormick and Ellison, 2015).

In the literature, there has been some indirect links between the β2AR and NCC, the established physiological substrate of SPAK and OSR1 kinases. For instance, the total amount and activity of NCC was increased in salt-sensitive

hypertensive rat models though the underlining mechanism was not investigated (Li and Wang, 2007). In another study, stimulation of the βARs in mice by isoproterenol (Iso) indicated that the activation of the β2AR but not the β1AR is responsible for developing salt-sensitive HPT (Mu et al., 2011). This was hypothesised, as a result of decreased expression of WNK4 through a cAMP-PKA dependent mechanism with involvement of glucocorticoid receptors following β2AR stimulation (Mu et al., 2011). This suppression of WNK4 eventually led to increased expression and phosphorylation of NCC in the DCT. Glucocorticoid receptors are crucially required to this pathway because knocking out of this receptor abolished the Iso-mediated WNK4 downregulation. Additionally, the Iso effect on WNK4 was entirely blocked by ICI11851 (specific β2AR blocker) but not by metoprolol (specific β1AR blocker). This indicated that the β2AR-activated NCC stimulation mediates Na reabsorption in the DCT (Mu et al., 2011).

Similarly, to support this findings, a micro-puncture analysis of Na^+ reabsorption in the DCT showed increased Na uptake during stimulation with Iso (Greven and Heidenreich, 1975). However, a contrasting report by Terker and co-workers showed that the infusion of norepinephrine induced salt-sensitive HPT (Terker et al., 2014). Such increase was found to be a result of enhanced activity and abundance of NCC, a process that was mediated by the β1AR activation through OSR1 and not SPAK (Terker et al., 2014). Notably, however, patients with the β2AR polymorphism manifested salt-induced HPT, low renin levels and impaired renal Na excretion (Pojoga et al., 2006, Snyder et al., 2006).

As mentioned above, there is evidence that the WNK-SPAK/OSR1 signalling pathway can be regulated by hormones. For instance, angiotensin 2 (A2) induced the activation of NCC because it reduced the inhibitory effect of WNK4 on NCC through a

SPAK-mediated mechanism (Castaneda-Bueno et al., 2012). Also, acute aldosterone administration was shown to activate NCC via either a WNK4-SPAK-dependent pathway (Ko et al., 2013) or the WNK4 extracellular signalling regulated kinase 1/2 (ERK1 / 2) signalling cascade (Lai et al., 2012). Additionally, Iso-mediated stimulation of NCC and Iso-induced suppression of WNK4 transcription were A2 and aldosterone independent suggesting that the β2AR-WNK-NCC pathway could be a novel independent regulator of these phenomenons (Mutlu and Factor, 2008). Therefore, it would be interesting to find whether the β2AR stimulation induced salt-sensitive HPT could be mediated via WNK-SPAK/OSR1-NCC signalling in the DCT. **To date, there has not been any direct links between the β2AR and the WNK-SPAK/OSR1 kinases.** Intriguingly, analysis of the amino acid sequence of the human β2AR revealed that it has a SPAK/OSR1 consensus binding sequence, Arg239-Phe240-His241-Val242, located on ICL3 (**Figure 1.18**). This suggests that the human β2AR could bind SPAK and OSR1 kinases.

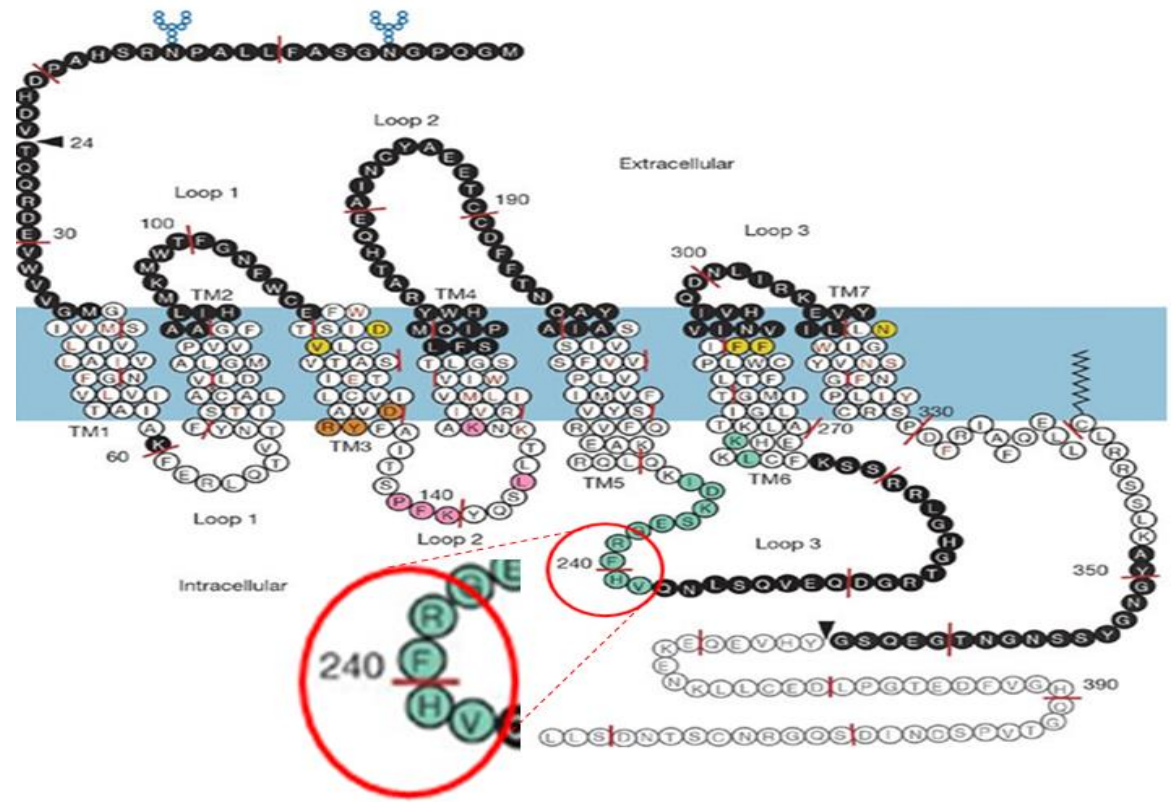

Figure 1.18: Structure and arrangement of the human β_2AR. *The diagram shows the 7TM structure of the β_2AR with extracellular T-terminus and intracellular C-terminus ends. Yellow residues indicate amino acids involved in ligand binding. The conserved DRY sequences are in orange. The green amino acids form the Fab antigen and it also contain the SPAK/OSR1 binding sequences (Arg239-Phe240-His241-Val242). The figure was adapted from (Rasmussen et al., 2007).*

1.4 Research aims and objectives:

I. Hypothesis

The intracellular β2AR RFHV tetrapeptide (amino acids. 239-242) may mediate the binding to SPAK and OSR1 kinases, which could modulate its function through a phosphorylation-(in) dependent mechanism.

II. Research aims:

The overall aim of this project is verifying the possible cross talk between SPAK/OSR1 kinases and the human β2AR. This goal to be achieved by addressing the following main points:

I. Verifying the binding of the SPAK/OSR1 kinases to the human β2AR.
II. Determining whether SPAK/OSR1 kinases phosphorylate the β2AR.
III. Exploring the role of SPAK/OSR1 activation and inhibition on the β2AR internalization.
IV. Establishing the effects of the β2AR binding on catalytic activity of SPAK/OSR1 kinases.
V. Determining the effects of the β2AR activation on endogenous SPAK/OSR1 kinase activity and expression.

III. Research objectives:

Aim I	**Objective 1:**	Use in silico modelling to examine the binding of the β2AR-RFHV peptide to OSR1.
	Objective 2:	Use affinity-pull down assays to determine the binding of SPAK and OSR1 kinases to the β2AR- RFHV peptide.
	Objective 3:	Use mass spec to determine whether SPAK/OSR1 kinases bind the β2AR.

Aim II	**Objective 4:**	Use *In vitro* kinase assays to determine if the β2AR is phosphorylated by OSR1.
Aim III	**Objective 5:**	Use membrane labelling, pulldown, ELISA and flow cytometry techniques to determine the effects of SPAK/OSR1 activation and inhibition on the β2AR internalization.
Aim IV	**Objective 6:**	*Use In vitro* kinase assays to establish the effects of the β2AR binding on the catalytic activity of OSR1.
Aim V	**Objective 7:**	Use Western blotting to examine the effects of the β2AR activation and inhibition on SPAK/OSR1 kinases activity and abundance.

Chapter 2 : Materials and Methods

2.1 Materials and reagents.

2.1.1 Chemicals and reagents:

STOCK1S-50699 was purchased from Vistas-M laboratory. Verteporfin (catalogue number: SML0534), isoproterenol hydrochloride (catalogue number: I6504), propranolol hydrochloride (catalogue number: P0884) were purchased from Sigma, Gillingham, UK. ICI118551 hydrochloride and PCG20712 (catalogue number: 1874 batch 6) were purchased from Tocris, Bristol, UK. ADP-Glo^{TM} kit was purchased from Promega, Southampton, UK. The biotinylated 18-mer RFQV containing peptide (biotin-C6-SEEGKPQLVGRFQVTSSK, catalogue number; 331938). AFQV containing peptide (biotin-C6-SEEGKPQLVGAFQVTSSK, catalogue number: 372447). RFHV containing peptide (biotin-C6-DKSEGRFHVQNLSQ, catalogue number: 372432), and AFHV containing peptide (biotin-C6-DKSEGAFHVQNLSQ, catalogue number: 372438) as well as CATCHtide (RRHYYYDTHTNTYYLR-TFGHNTRR) were purchased from GLS Peptide synthesis, Shanghai, China. Dulbecco's modified Eagle's media (DMEM) (catalogue number: D6429), 100 units/ml penicillin and 0.1 mg/ml streptomycin (Pen/Strep, catalogue number: P4333), Dulbecco's phosphate buffer saline (PBS), (catalogue number: D8662), dimethyl sulfoxide (DMSO), (catalogue number: D2650) were purchased from Sigma, Gillingham, UK. Fetal bovine serum (FBS), (catalogue number: 10270106) and Trypsin-EDTA 1x0.25 % (catalogue number: 25200056) were purchased from Gibco. Linear polyethylenimine (PEI) (catalogue number: 23966-1) was purchased from Polysceince Inc, Bergstrasse, Germany. Cell culture plasticware and pipettes were purchased from Corning.

2.1.2 Antibodies:

2.1.2.1 Antibodies used in Western blotting (WB) and immunoprecipitation (IP).

Primary antibody	*Molecular weight of targeted proteins (kDa)*	*Dilution*
Rabbit anti-GAPDH (D16H11, CST).	37	1:5,000
Rabbit anti-pan cadherin (4073, CST).	130-150	1:1,000
Sheep anti-OSR1 (S636B, Dundee)	58	10µg/mg (IP)
Sheep anti-SPAK (S551D, Dundee)	63	2µg/ml (WB) 10µg/mg (IP)
Sheep anti-SPAK- phospho-Ser373 (S670B, Dundee)	63	2µg/ml
Sheep anti-SPAK-phospho-Thr233 (S668B, Dundee)	63	2µg/ml
Sheep anti-NKCC1 (DU 6146, Dundee).	130-180	2µg/ml
Sheep anti-NKCC1-phospho-Thr203+Thr207+Thr212 (S763B, Dundee).	130-180	2µg/ml
Sheep anti-NKCC2-phospho Ser91 (S451C, Dundee).	/	2µg/ml
Sheep anti-NKCC2-phospho-Thr105 (S378C, Dundee).	/	2µg/ml
Sheep anti-NKCC2-phospho-Ser130 (S432C, Dundee).	/	2µg/ml
Rabbit anti-β-catenin (9582, CST).	92	1:1,000
Mouse anti-FLAG-HRP (ab2493, Abcam)	/	1:5,000
Mouse anti-FLAG (F1804, Sigma)	/	1:1,000
Mouse anti-FLAG monoclonal M2 (F3165, Sigma).	/	10µg/mg (IP)
Rabbit anti-LKB1 (3047, CST)	54	1:1,000
Rabbit anti-LKB1-phospho-Ser428 (3482, CST).	54	1:1,000
Rabbit anti-β_2AR (SAB4500577, Sigma)	46	1:500
Rabbit anti-GST (2622, CST)	/	1:1,000

Table 2.1: *Primary antibodies with dilutions for probing proteins by western blot (WB) and immunoprecipitation (IP) according to manufactural instructions and were also confirmed by my work. Antibody specificity has been determined si-RNA by the company as provided in data sheet.*

Secondary antibody	*Dilution*
Rabbit anti-mouse IgG HRP antibody (7076, CST).	1:2,000
Goat anti-rabbit IgG HRP antibody (7074, CST).	1:2,000
Rabbit anti-sheep IgG HRP antibody (ab97130, Abcam).	1:10,000

Table 2.2: *Secondary antibodies with dilutions for immunoblot.*

2.1.2.2 Antibodies used in enzyme linked immunosorbent assay (ELISA):

The primary antibody used was a mouse anti-FLAG monoclonal M2 (F3165, Sigma). It was used at 1:1,000 dilution while the secondary antibody was goat anti-mouse IgG Alkaline phosphatase linked (ab97020, Abcam). It was used at 1:10,000 dilution. Monoclonal mouse IgG (NCG01) (ab81032, Abcam) was used as an isotype control.

2.1.2.3 Antibodies used in flow cytometry:

The primary antibodies were the rabbit anti-β2AR (SAB4500577, Sigma), which was used at 1:500 dilution or the mouse anti-FLAG monoclonal M2 Ab (F3165, Sigma), which was used at 1:2,000 dilution. The secondary antibodies were the goat anti-rabbit-FITC 488 antibody (ab77050, Abcam), which was used at 1:1,000 dilution or the goat anti-mouse FITC 488 antibody (ab6785, Abcam), which was used at 1:1,000 dilution.

2.1.3 DNA plasmids.

All of cDNA plasmids were purchased from the MRC Reagents and Services (Dundee) except when stated otherwise. For the expression of proteins in mammalian cells the following constructs were used pCMV5-GST-EV (DU41864), pEBG-HA-SPAK (DU2923), pCMV5-FLAG-NKCC2-FL-WT (DU10098), pcDNA5-FRT/TO-FLAG-NKCC2-R20A (DU17023), pCMV-FLAG-NKCC2 (1-174)-WT (DU13857), pcDNA5-FRT/TO-FLAG-β2AR-WT (lot:390869S, Genscript), pCMV5-FLAG-β2AR-R239A (DU39345), pEBG-HA-OSR1T185E (DU6130), pEBG-HA-OSR1T185E+L473A (DU6699), pEBG-HA-OSR1-T185E+D459A (DU6696). For bacterial *E. coli* protein expression, the following cDNA clones were used; pGEX-NKCC2 (1-174) (DU13763), pGEX-OSR1-T185E full length (DU 6231) and pGEX-MO25α (DU2945).

2.2 Buffers and Medias

2.2.1 Mammalian cells lysis buffer:

Three different lysis buffers were used in this work. Lysis buffer 1 (LB1) was used for harvesting non-transfected cells, SPAK, OSR1 or NKCC2 transfected cells and mouse heart. It was made of 50 mM Tris/HCl (pH 7.5), 1 mM sodium orthovanadate, 1 mM EGTA, 1 mM EDTA, 50 mM sodium fluoride, 0.27 M sucrose, 5 mM sodium pyrophosphate, 1 % (w/v) Nonidet P40 plus protease inhibitors 0.1 mM phenylmethanesulfonylfluoride (PMSF), 1 mM benzamidine, and 0.1 % (v/v) 2-mercaptoethanol (de Los Heros et al., 2014). Lysis buffer 2 (LB2) was LB1 supplemented with 1 % (w/v) *n*-dodecyl β-D-maltoside (catalogue number; 89902, ThermoFisher). Lysis buffer 3 (LB3) was used to solubilize β2AR-transfected

mammalian cells and it contained 50 mM HEPES (pH 7.5), 0.5 % Nonidet P40, 145 mM sodium chloride, 2 mM EDTA, and 10 % (v/v) glycerol, 0.1 mM PMSF, 1 mM benzamidine, 0.1 % (v/v) 2-mercaptoethanol and 1 % (w/v) final concentration of *n*-dodecyl β-D-maltoside was freshly added before cell lysing (Han et al., 2012).

2.2.2 Hypotonic low Cl buffer (HLB):

This buffer was used for stimulating the WNK-SPAK/OSR1 signalling pathway and it contained 7.5 mM HEPES (pH7.5), 67.5 mM sodium gluconate, 0.25 mM $CaCl_2$, 2.5 mM potassium gluconate, 0.5 mM Na_2HPO_4, 0.25 mM $MgCl_2$ and 0.5 mM Na_2SO_4 (de Los Heros et al., 2014).

2.2.3 Preparation of PEI for cell transfection:

Polyethylenimine (PEI) was used for protein expression in mammalian cells and it was prepared as a solution of 1 mg/ml PEI in 25 mM HEPES pH 7.5 and 150 mM NaCl, which was filtrated through 0.45 µM and aliquoted to several tubes then were stored at -20 °C.

2.2.4 SDS sample buffer (4x):

This consisted of 240 mM Tris/HCl (pH6.8), 40 % glycerol, 8 % sodium dodecyl sulphate (SDS), 5 % 2-mercaptoethanol and 0.04 % bromophenol blue.

2.2.5 Buffer A:

This consisted of 50 mM Tris/HCl (pH7.5), 0.1 mM EGTA and 0.1 % (v/v) 2-mercaptoethanol (AlAmri et al., 2017a).

2.2.6 Western blotting running buffer:

This consisted of 25 mM Tris/base (pH7.5),1.92 M glycine and 34.6 mM SDS ,(AlAmri et al., 2017a, AlAmri et al., 2018)..

2.2.7 Western blotting transfer buffer:

This consisted of 48 mM Tris/base, 39 mM glycine supplemented with 20% (v/v) methanol immediately before use (AlAmri et al., 2017a, AlAmri et al., 2018).

2.2.8 TBST buffer:

This consisted of 50 mM Tris/HCl (pH7.5), 150 mM NaCl, 0.2 % (v/v) Tween-20 with the final buffer pH adjusted to 8.3 by adding concentrated HCl (AlAmri et al., 2017a, AlAmri et al., 2018).

2.2.9 Western blotting blocking buffer:

This consisted of 10 % (w/v) of dried skimmed milk dissolved in TBST buffer (AlAmri et al., 2017a, AlAmri et al., 2018).

2.2.10 Kinase reaction buffer:

This consisted of 10 mM $MgCl_2$, 50 mM Tris/HCl (pH 7.5), 0.1 % (v/v) 2-mercaptoethanol and 0.1 mM ATP (AlAmri et al., 2017a, AlAmri et al., 2018).

2.2.11 ELISA blocking buffer:

This consisted of serum free MDEM media supplemented with HEPES (pH 7.4) and 0.01 % BSA (Han et al., 2012).

2.2.12 Preparation of LB (Lennox) media:

LB Lennox (catalogue number; L7275-100TAB, Sigma, Gillingham UK) media for bacterial culture was prepared according manufactures manual; 1 tablet per 48 ml of dH_2O in pre-autoclaved bottle. The media was then autoclaved at 190 °C and stored in dry dark place.

2.2.13 Preparation of LB with agar:

LB with agar Lennox (catalogue number; L7025-100TAB, Sigma, Gillingham UK) media was prepared by dissolving 1 tablet per 48 ml of dH_2O in pre-autoclaved bottle after which the media was autoclaved at 190 °C. It was then kept in dry dark place and heated up and poured into 10-cm plates when needed.

2.2.14 Bacterial cells lysis buffer:

This consisted of 50 mM Tris/HCl (pH7.5), 150 mM NaCl, 1 mM EDTA, 1 mM EGTA, 0.27 M sucrose, 0.1 mM PMSF, 1 mM benzamidine, 2 mM dithiothreitol (DTT), 0.01 % 2mercaptoethanol, 0.5 mg/ml lysozyme and 0.3 mg/ml DNase (AlAmri et al., 2017a, AlAmri et al., 2018).

2.2.15 Normal buffer:

This was the same to the bacterial lysis buffer but missing the lysozyme and DNase, it was used for washing steps in protein isolation from bacteria (AlAmri et al., 2017a, AlAmri et al., 2018).

2.2.16 High salt buffer:

This was the same to the normal buffer, but it contained a final NaCl concentration of containing 500mM (AlAmri et al., 2017a, AlAmri et al., 2018)..

2.3 Methods.

2.3.1 Cell culture:

2.3.1.1 Maintenance of mammalian cell lines:

Mammalian cells, such as human embryonic kidney 293 (HEK293), at passage range 5 - 25, were cultured in T-75 flasks, 10-cm or 6-well plates. The cells were cultured in DMEM supplemented with 10 % (v/v) FBS and 1 % (v/v) Pen/Strep. Once they reached 80-90 % confluency (log phase), the cells were regularly passaged in 1:5 ratio every 2-3 days. The cells were washed once by 3-5 ml of PBS after the removal of the media. Then, they were detached with 2 ml trypsin. Typically, the cells were grown in 12-15 ml media in T75, 7 ml media in 10-cm dishes or 3 ml media in the 6-well plates. All of the flasks and plates were maintained at 5 % CO_2 humified incubator at 37 °C. For the ELISA assay, HEK293 cells were cultured and transfected in T-75 flasks. After 24 hrs, the cells were detached with 2 ml PBS and transferred into pre-coated 96-wells plates at 10,000 cells/well in 100 µl media.

2.3.1.2 Cells storage and recovery:

Cells were frozen for storage when they were 90 % confluent. The cells were washed and detached with 2 ml trypsin and incubated for 5 min. After adding 10 ml media, the cells were centrifuged at 1,500 *g* for 10 min at 4 °C. The cellular pellet of single T75 flask was resuspended in 1 ml of freezing medium, containing FBS with 10 % DMSO. The cells were then transferred into cryovials and kept within Mr Frosty at -80 °C for overnight. In the next day, the cryovials were stored at -80 °C.

For cell recovery, the cryovials were thawed and warmed up to room temperature or in a water bath at 37 °C. After completely defrosting, the contents were immediately transferred into a T75 flask containing 12-15 ml media. Next day the media was replaced, and the cells maintained in the incubator as above.

2.3.1.3 Mammalian cells transfections:

For protein expression in mammalian cells, HEK293 cells (passage ranged 5 - 25) were plated either in 6-well plates or 10-cm dishes. Once the cells reached 40-50 % confluency, they were transfected using the PEI method (Vitari et al., 2005). 1 µg of cDNA clones with 2 µl of 1 mg/ml PEI was mixed in a ratio of 1:2 in 200 µl FBS-free DMEM media per well of 6-well plates. 3 µg cDNA with 20 µl 1 mg/ml PEI in 1 ml FBS-free DMEM media for a single 10-cm dish. Then, the mixture was vortexed gently and left at room temperature for 25 min. This mixture was then added to the cells carefully to avoid their detachment and the cells were incubated at 37 °C. 36-48 hrs post-transfection, the cells were harvested, or undergone treatment as needed.

2.3.1.4 Preparation of cell samples:

A. Total cell lysate preparation:

In order to prepare samples for SDS-PAGE and Western blotting. The cells were seeded at 0.3 $X10^6$ or 2.2 $X\ 10^6$ in 6-well plates or 10-cm dishes respectively. Once were confluent, they were washed once with 1 ml or 2 ml of PBS respectively after removal of the media. 120 – 400 µl of Ice-cold lysis buffer was then added to each well. After detaching the cells by cell-scraper, the suspension was centrifuged at

12,000 *g* for 10 min at 4 °C. The total protein concentration was then measured by Bradford assay or alternatively stored at -80 °C until needed. After measuring the protein concentration, the samples were immediately prepared for the SDS-PAGE experiment by adding SDS 4x sample buffer and water to reach a 1x final concentration of SDS and 1 mg/ml total protein concentration. Then, the samples were mixed and heated on dry heater at 90 °C for 7 min. Finally, the samples were stored at -20 °C or used immediately in Western blotting.

B. Immunoprecipitation of FLAG-β2AR:

HEK293 cells were cultured and transiently transfected in 10-cm plates using PEI. 36-48 hrs post-transfection, the cells were washed once with 2 ml ice-cold PBS and detached by adding 400 µl/plate of ice cold LB3. Following cell detachment by scrappers, the suspension was vortexed and incubated on rotator shaker for 2 hrs or overnight at 4 °C (Han et al., 2012). The lysate was subsequently centrifuged at 12,000 *g* for 10 min at 4 °C. The supernatant was collected, and samples were prepared for SDS-PAGE to check receptor expression while the remaining lysate was stored at -80 °C.

In order to isolate FLAG-β2AR from cell lysate, pre-clearing of the cell lysate was first performed three times by incubating 1 mg cell lysate with 100 µl of 50 % slurry of protein-G-Sepharose beads (GE Health care life sciences, catalogue number: PG5-161501) on rotator shaker at 4 °C for 10 min. After this, the beads were collected by centrifuging at 1,000 *g* at 4 °C for 5 min. Anti-FLAG antibody (F3165, Sigma) conjugated to the protein-G Sepharose beads was added to the pre-cleared lysate at a ratio of 1:100, (10 µg conjugated-antibody: 1 mg cell lysate) (Vitari et al., 2005). After incubation for 1 hr on rotator shaker at 4 °C, the solid beads were collected by

centrifuging at 1,000 *g* for 5 min at 4 °C. The beads were then washed twice by resuspending in 1 ml of LB3, centrifuging at 1,000 *g* for 5 min at 4 °C. For preparing samples for kinase assay, beads were washed two more washes with LB3 contained 0.5M NaCl. After the last spin the beads were subsequently washed twice by resuspending in 1 ml buffer A and centrifuging at 1,000 *g* for 5 min at 4 °C. For Western blotting, proteins were eluted from the beads, by adding 60-80 µl of 1x SDS-sample buffer, mixed well by a bench vertex and heated in a dry heater at 90 °C for 10 min. Then samples were stored at -20 °C.

C. Bradford assay for protein concentration measurement:

The Bradford assay was used for measuring protein concentrations by computing the absorbance using BMG FLUOstar Omega 96-wells plate reader after adding the Bradford reagent (catalogue number: B6916, Sigma) to samples. As standards, known concentrations (0.125 mg/ml, 0.25 mg/ml, 0.5 mg/ml and 1 mg/ml) of the pure Bovine serum albumin (BSA) (catalogue number: A2153, Sigma) were used.

2 µl of the total cell lysates were placed into 96-wells plates in triplicates. 5 µl BSA of known concentrations, see above, were also added in triplicates. Then 280 µl of Bradford reagent was added for each well. The absorbance was read on a BMG FLUOstar Omega plate reader. Then the protein concentration was determined in relation to the known BSA concentrations.

2.3.1.5 Preparation of samples from mouse heart:

A. Total lysate:

Initially, the homogenizer and all of the equipment were sterilised as they were washed with deionized H_2O and 70 % ethanol. Then, the mouse heart was prepared as follows:

1- The heart was cut down in to small pieces.
2- The heart was homogenised in 1 ml of either LB1 or LB2.
3- The both lysates were incubated for 1 hr on rotator shaker at 4 °C.
4- Samples were centrifuged at 12,000 *g* at 4 °C for 20 min.
5- The supernatant was collected, and protein concentration was measured by the Bradford assay.
6- Then, the samples were either prepared for SDS-PAGE or snap frozen and stored at -80 °C.

B. Immunoprecipitation of endogenous OSR1/SPAK:

To immunoprecipitate endogenous SPAK and OSR1 kinases from the mouse heart, pre-clearing steps were carried out as before. Then, 50 µg of conjugated anti-OSR1 or anti-SPAK antibody was added to 5 mg of total protein lysate (Vitari et al., 2005). After incubation for 1 hr on rotator shaker at 4 °C, the beads were collected by centrifuging at 1,000 *g* for 5 min at 4 °C. The beads were washed twice by resuspending in 1 ml LB1, then centrifuging at 1,000 *g* for 5 min at 4 °C. After the last spin, the beads were washed twice by resuspending in 1 ml buffer A and centrifuging at 1,000 *g* for 5 min at 4 °C. Then, 60 µl of 1x SDS-sample buffer was added to the beads and mixed well by bench vertex. Subsequently, the samples were either prepared for SDS-PAGE as before or stored at -20 °C.

2.3.2 Conjugation of antibodies to protein-G Sepharose beads:

Overall, to enable protein elution and reduce antibody contamination, all of the antibodies used in immunoprecipitation experiments were covalently cross-linked to protein-G-Sepharose (catalogue number: PG5-161501, GE Healthcare) using dimethyl pimelimidate dihydrochloride (DMP), (catalogue number: D8388, Sigma) via the following procedure (Vitari et al., 2005).

1- The beads were washed three times with 1 ml PBS, centrifuged at 1,000 *g* for 5 min at 4 °C and collected.
2- The antibody was added to the beads at a 1:1 antibody, mixed well and incubated for 1 hr at 4 °C on rotator shaker.
3- The suspension was then centrifuged at 1,000 *g* for 5 min at 4 °C, the supernatant removed, and the beads were collected.
4- The antibody-beads conjugates were washed three times with 1 ml PBS and centrifuged at 1,000 *g* for 5 min at 4°C.
5- After removing the supernatant, the conjugates were resuspended and washed twice with 1 ml of 0.1 M sodium borate buffer (pH 9).
6- This was followed by resuspending the beads in in 1 ml DMP freshly-prepared buffer [20 mM DMP in 0.1 M sodium borate buffer, pH 9] and incubated on rotator shaker at 4 °C for 30 min.
7- The beads were then collected by centrifuging at 1,000 *g* for 5 min at 4 °C.
8- Steps 6 and 7 were repeated twice.
9- After that, the antibody-beads conjugate was washed twice by resuspending in 1 ml 50 mM glycine (pH 2.5) and centrifuging at 1,000 *g* for 5 min at 4°C.
10- Finally, after the last spin the antibody-beads conjugate was resuspended in 1 ml PBS, stored at 4 °C, and used within 24-48 hrs.

2.3.3 SDS-PAGE and Western blot:

All gels used in this study were resolving (10 % to 12 % acrylamide) and 4 % acrylamide stacking, and they were self-prepared following the recipe described in (**Table 2.3** and **Table 2.4**). Glass gel formers with space of 1.0-1.5 mm and 10- or 15-wells combs were used. All of the prepared gels were used either in the same day or stored at 4 °C for next day usage. The amount of total proteins loaded in each well was 20 µg/well for total cell lysate and 35 µg/well for samples from IP or pulled down samples. For each gel, 4-5 µl of molecular weight protein ladder (catalogue number: S6-0024, Genflow Ltd, Lichfield, UK) was used. Protein separation by electrophoresis was carried out at voltage ranged 160-185 mV for 50-70 min. Then, the proteins were transferred to nitrocellulose membranes 0.45 µM (catalogue number: 10600007, GE Healthcare) within a Western blot sandwich, which was soaked and assembled in transfer buffer containing 20 % methanol. The transfer was performed at 85 mV for 90 min at 4 °C. Protein transfer was confirmed by soaking the membranes in Ponceau stain after which they were washed three times with dH_2O.

Reagent	***10% (15ml)***	***12% (15ml)***
1.5 M Tris/HCl (pH8.8)	5ml	5 ml
30 % acrylamide	4ml	6 ml
Deionized H_2O	5.9ml	3.9 ml
20 % SDS	75µl	75 µl
10 % ammonium persulfate (APS)	75µl	75 µl
TEMED	25µl	25 µl

Table 2.3: *Recipe of both 10 % and 12 % of SDS-PAGE resolving gels.*

Reagent	*4% (5ml)*
0.5 M Tris/HCl (pH6.8)	0.62 ml
30 % acrylamide	0.833 ml
Deionized H_2O	3.82 ml
20 % SDS	25 µl
10 % APS	50 µl
TEMED	5 µl

Table 2.4: *Recipe of 4 % stacking gel of SDS-PAGE.*

The transferred membranes were loaded with the proteins were blocked in blocking buffer for 1 hr on a table shaker at room temperature. After washing the membranes by TBST buffer three timers at 5 min interval, they were incubated with a dilution of the relevant primary antibody [5 ml of 5 % non-fat skimmed milk for sheep raised antibodies or 5 % BSA in TBST for goat and rabbit raised antibodies] at room temperature for 1 hr or overnight at 4 °C on rotator shaker. After this primary antibody incubation, the membranes were washed with TBST three times and then incubated in 5 ml dilution of the relevant secondary antibody for 1 hr on rotator shaker at room temperature. This was followed by washing the membranes with TBST three times 5 min for each wash. The enhanced chemiluminescent (ECL) reagents A and B (catalogue number: 9770467, Amersham) were mixed (1:1) and added on the membranes. Then, the membranes were exposed to autoradiographic films (catalogue number: 28906839, Amersham). The films were then developed using automatic processor (SRX-101, Konica Minolta Medical) and finally the films were scanned on (PowerLook 1000, UMAX) and the figures were prepared using Microsoft PowerPoint.

2.3.4 Biotin-RFxV pulldown of SPAK and OSR1:

Once HEK293 cells cultured in 10-cm dishes were 80-90 % confluent, they were harvested and lysed. Then 1-5 mg of the total cell lysates was incubated with 3 µg of either the RFQV-peptide, the RFHV-peptide, the AFQV-peptide or the AFHV-peptide for 15 min at 4 °C on rotator shaker. After incubation, 40 µl of streptavidin 50 % slurry (which had been washed and equilibrated in lysis buffer) was added to each sample. The samples were then incubated on rotator shaker for 15 min at 4 °C. (Vitari et al., 2006). After that, the beads were collected by centrifuging at 1,000 *g* for 2 min at 4 °C. The beads were subsequently washed twice with 1 ml LB1 and washed again twice with 1 ml buffer A. Finally, the beads were prepared for SDS-PAGE as described above.

2.3.5 GST pull down:

Once cultured HEK293 cells in 10-cm dishes reached 50 % confluency, they were transfected with glutathione S-transferase (GST)-tagged proteins e.g. SPAK and OSR1 alone, or co-transfected with other FLAG-fusion proteins. 36 hrs post-transfections, the cells were harvested by adding 0.4 ml of suitable lysis buffer. Then, the cell suspensions were collected and clarified from cellular debris by centrifugation at 12,000 *g* for 10 min at 4 °C. The supernatants were collected, and protein concentration was measured by the Bradford assay and the samples were prepared for SDS-PAGE to assess protein expression while the remaining lysates were stored at -80 °C.

Pulldown of GST-tagged proteins was carried out by using glutathione Sepharose high performance (GST) beads (catalogue number: 17-527-01, GE Healthcare). GST beads were washed with 1 ml PBS three times by incubating with PBS and then centrifuging at 1,000 *g* at 4 °C for 5 min. After this, the collected GST-beads equilibrated in PBS at 50 % slurry. 0.5 mg of the cell lysates was incubated on rotator shaker in a 20 µl slurry of GST-beads either overnight at 4 °C or 1 hr at room temperature (Vitari et al., 2006). The beads were then collected by centrifugation at 1,000 *g* at 4 °C for 5 min. The collected beads were washed twice with 1 ml LB1 and twice with 1 ml buffer A. Finally, the beads were prepared for SDS-PAGE electrophoresis as described above.

2.3.6 Identification of proteins by mass spectrometry:

To identify OSR1 associated proteins in cardiac tissues, OSR1 was immunoprecipitated from mouse heart as described in **section 2.3.1.5 B**. 35 µl of control (empty beads) and OSR1-pulled down sample were loaded onto 10 % acrylamide gel. After subjecting the proteins to electrophoresis, the gel was stained by Colloidal Blue stain (catalogue number: LC6025, Invitrogen) according to manufactures instructions for 6 hrs. Then, the gel was washed by dH_2O for at least 12 hrs on bench shaker. On the following day, the protein bands were excised (**Figure 3.7**) and submitted to the Advanced Mass Spectrometry Facility in School of Biosciences at University of Birmingham. Following tryptic digestion of each band separately, protein identification by Orbitrap Elite mass spectrometer equipped with nano-flow liquid chromatographic (LC) system (LC-MS/MS) was performed. The raw files were analysed by Mascot (http://www.matrixscience.com) and the significant

probability of identified proteins was *P* > 95.0 % with at least two unique peptides were identified (Chung et al., 2013, Ohta et al., 2013).

2.3.7 ADP-Glo OSR1-T185E kinase in vitro assay:

The protein kinase OSR1-T185E, MO25α and NKCC2 (1-174) were expressed and purified from LB21 *E coli* **section 2.3.8.6** and FLAG-β2AR was immunoprecipitated from transfected HEK293 cells **section 2.3.1.4 B**. Cold ATP was used in this assay. The kinase reaction was performed in 1.5 ml tubes at a final volume of 25 µl/reaction in triplicate. Each reaction contained 0.4 µM OSR1-T185E with the presence or absence of 2 µM MO25α. The substrates were either 250 µM CATCHtide (RRHYYYDTHTNTYYLR-TFGHNTRR), 5 µM GST-cleaved NKCC2 (1-174) that were used as positive control, or 10 µg beads conjugated to immunoprecipitated β2AR. After all proteins were freshly prepared in kinase buffer which containing 10 mM MgCl, and 0.1 mM ATP (AlAmri et al., 2018). The samples were incubated on 30 °C for 40 min on gentle agitation. Then, the samples were transferred into a 96-wells plate and developed according manufacturer's instructions (ADP-Glo kit, Promega). This involved adding 25 µl of reagent-1 to each sample and incubation for 40 min at room temperature. Then, 50 µl of reagent-2 was added to each sample followed by incubation for 1 hr at room temperature (AlAmri et al., 2017a). The luminesce was subsequently measured by reading the plate on BMG FLUOStar Omega plate reader. The results were analysed by Graph Pad Prism and the data was presented as mean ± SD of three independent experiments.

2.3.8 Molecular biology:

2.3.8.1 Generation of competent bacterial cells:

DH5α strain of *E. Coli (E. coli)* was used for DNA cloning and amplification of cDNA for use in mammalian cells whereas LB21 *E. coli* strain cells were used for protein expression in bacteria. Both cells were stored at -80 °C. Once needed, they were thawed on ice and 10 µl of DH5α or BL21 cells were added into 10 ml of LB media in 50 ml falcon tube. The solution was incubated overnight at 37 °C/200 rpm. Next day, to set up the bacterial culture, 1 ml of overnight culture was re-cultured in 50 ml LB. Then, the new culture was left to grow at 37 °C/180 rpm for overnight. On the next day, the optical density (OD) was measured at 600 nm in cuvette spectrophotometer, when OD reached about 0.6, the bacterial cells were pelleted at 1500 *g* for 10 min at 4 °C. The supernatant was discarded, and the pellets were collected and resuspended in 5 ml ice-cold 0.1 M calcium chloride (CaCl). Then, they were incubated on ice for 1 hr. Then centrifugation of pellet at 2,000 *g* for 10 min at 4 °C. Then, the pellets were resuspended in 2 ml ice-cold 0.1 M CaCl and incubated in ice for 15 min. 1 ml of pre-autoclaved 80 % glycerol was added to 2 ml cell solution. Finally, cell suspensions were aliquoted and stored at -80 °C.

2.3.8.2 Transformation of E. coli:

All of the bacterial-related work which includes the media preparation and procedures of the transformation were performed under aseptic techniques. *E. coli* cells (DH5α or LB21) were thawed on ice, 50 µl of cells was taken in to pre-autoclaved Eppendorf tube. Then, 2-5 µl of the relevant cDNA was added. After gentle mixing, the cell suspension was incubated on ice for 10 min and the cells they were subjected to

heat shock at 42 °C for 90 seconds. Then, the cells were incubated on ice for 10 min. 50 µl of transformed *E. coli* were spread onto pre-warmed LB agar plate that contains 100 µg/ml ampicillin (catalogue number: A9518, Sigma). The plates were subsequently incubated, upside-down, at 37 °C for overnight. On the next day, a single colony from the plane was selected and transferred into 250 ml of LB media supplemented with100 µg/ml ampicillin. The bacterial culture was incubated at 37 °C overnight at 180 rpm. On the following day, for bacterial stock preparation, 500 µl of 80 % sterile glycerol was added and mixed with 500 µl of *E. coli* culture, then stocks were immediately stored at -80 °C. The remaining DH5α culture was used for DNA extraction while LB21 for protein expression. When the bacterial stock was required, a single drop of *E. coli* was transferred in to 50 ml LB media, which was then incubated at 37 °C for overnight at 180 rpm, on the next day 10 ml of overnight culture was transferred into 250 ml media and continue as mentioned below.

2.3.8.3 DNA extraction and purification:

For large scale extraction of plasmids, Qiagen Plasmid Maxi kit (catalogue number: 12163, Manchester, UK) was utilized. A 250 ml of overnight transformed DH5α culture was transferred to 300 ml centrifuge tube, then it was harvested by centrifugation at 6,000 *g* for 15 min at 4°C. After discarding the supernatant, the pelleted cells were resuspended in 10 ml of Buffer P1, which had been supplemented with RNase. Then, the flask content was transferred into 50 ml falcon tube and 10 ml of Buffer P2 (lysing buffer) was added and mixed thoroughly by inversion until a blue colour developed, which indicates full lysis. After this, the suspension was incubated at room temperature for 5 min. Subsequently, 10 ml pre-chilled P3 (neutralising buffer) was added followed by vigorous mixing until the blue colour turns to white. The

suspension was then incubated for 20 min on ice. Then, the suspension was centrifuged at 16,000 *g* for 30 min at 4°C to remove cell proteins, debris and precipitated genomic DNA. The provided extraction column was equilibrated and washed with the supplied buffer QBT. The purified supernatant was applied to column and allowed to flow through the column by gravity. Then, it was washed twice with 30 ml of buffer QC. The bound DNA plasmid was eluted by adding 15 ml of buffer QF (elution buffer) and 10.5 ml of isopropanol was subsequently added to the filtrate to precipitate the plasmid DNA. The solution was centrifuged at 16,000 *g* for 30 min at 4°C. After careful disposal of the supernatant, the pelleted DNA was washed with 5 ml of 70 % ethanol and it was then centrifuged at 16,000 *g* for 10 min at 4 °C. Ethanol was discarded and the pelleted plasmid DNA was left to dry for 5 min then resuspended in to 1 ml nuclease-free water (catalogue number: P1193PRO, Promega, Southampton, UK). The purified DNA was subsequently quantified as described below.

2.3.8.4 DNA quantification:

The concentration of the purified DNA was performed by using BMG LABTECH LVis plat (a low volume microplate). The microplate was cleaned and 2 µl of the samples were then loaded followed by 2 µl of nuclease-free water. The absorbance was determined by a BMG LABTECH PHERAStar plate reader. All of the samples were run in duplicates. The significant purity of DNA was determined as 260/280 1.8, and any DNA displayed less than that value was considered to be contaminated with proteins or debris and thus discarded. All of the purified DNAs were aliquoted to reduce the thawing/freezing cycle and stored at -20 °C.

2.3.8.5 DNA sequencing:

All of the purified plasmid DNAs were subjected to sequencing for identity confirmation. This was carried out by Functional Genomic Proteomic and Metabolic Facility of School of Bioscience at University of Birmingham. When the results were obtained, they were analysed by Chromas 2.1.1, Technelysium and the nucleotide sequences were aligned by BLAST versus nucleotide database.

2.3.8.6 Expression and purification of MO25α, OSR1-T185E and NKCC2(1-174):

Competent LB21 *E. coli* cells were transformed with MO25α, OSR1-T185E or NKCC2 (1-174) as described above. The cells were transferred to LB agar plates and after growth at 37 °C, a single colony was selected and transferred in to 200 ml LB supplemented with ampicillin (100 µg/ml). The culture was incubated at 37 °C for overnight at 180 rpm. On the next day, 50 ml of the overnight culture was transferred into 1 L of LB with ampicillin (100 µg/ml) and the flask was incubated at 37 °C with 180 rpm shaking. The OD of the incubated culture was measured every 30-40 min at 600 nm. When the OD reached 0.7, 250 µM of isopropyl β-D-1-thiogalactopyranoside (IPTG) was added and the cells were incubated for a further 16 hrs at 26 °C with 180 rpm shaking. On the following day, the cells were harvested by centrifugation at 3,500 *g* for 30 min at 4 °C. Each flask pellet was resuspended in 50 ml ice-cold bacterial lysis buffer and incubated for 30 min on ice. The bacterial cells were lysed by sonication; six cycles of 30 seconds each. Then to remove residual debris, the homogenised cells were centrifuged at 14,500 *g* for 30 min at 4 °C. Following the filtration of the supernatant though pre-washed 0.45 µM filters, the supernatant was incubated overnight on rotator shaker at 4 °C with pre-washed GST-beads (at ratio of 1.5 ml

beads per 1 L of bacterial culture). On the next day, the GST-beads were collected by centrifugation at 3,000 *g* for 2 min, then they were washed with normal buffer twice. The washing steps were repeated with high salt buffer then with buffer A. After the last wash, 1:1 ratio of buffer A was added to the beads. The GST-fused protein, which was attached to the beads, was incubated by PreScission protease (40 µg protease for 1 ml beads) for 30 min at room temperature followed by incubation for overnight at 4 °C. After that, to elute the proteins, the beads-protein suspension was transferred to column and washed three times with normal buffer under gravity. The collected filtrate was concentrated by centrifugation at 3,000 *g* at 4 °C to using columns with integrated 3 KDa molecular weight cut-off. The purity of the proteins was characterized by 15 % SDS-PAGE and their concentrations was determined by the Bradford assay. The proteins were stored at -80 °C.

2.3.9 Quantification of the β2AR by biotin cell membrane labelling:

Cell surface proteins could be quantified using Western blotting after being selectively isolated from whole cell lysates using a thiol-cleavable amine-reactive biotinylation reagent, EZ-Link^{TM} Sulfo-NHS-SS-Biotin (catalogue number: 21331, Thermo Fisher). For this purpose, HEK293 cells were firstly cultured in 6-well plates and once they reached 50 % confluency, they were transiently transfected with FLAG-β2AR. 36 hrs post-transfection, the cells were either left unstimulated or stimulated with the relevant conditions. After this, they were washed by 1 ml PBS and detached in 1 ml PBS by cell scraper. The cells from each well were subsequently transferred into 1.5 ml Eppendorf tubes and centrifuged at 400 *g* for 5 min at 4 °C. Then, the cells were resuspended in 1 ml ice-cold PBS and 80 µl of 10 mM the biotinylation reagent

was added to each tube to reach a final concentration of 0.8 mM (~ 0.48 mg/well) (Moore et al., 2004). The cells were then incubated on rotator shaker at room temperature for 30 min then pelleted by centrifugation at 400 *g* for 5 min at 4 °C. To quench the biotinylation reaction, the cells were washed twice with 1 ml 30 mM Tris (pH 8.0) by resuspension and centrifugation at 400 *g* for 5 min at 4 °C. The cells were homogenised in 120 µl of LB3 (supplemented with 1% (w/v) final concentration of *n*-dodecyl β-D-maltoside, but without the reducing agent 2-mercaptoethanol). Then, the suspension was vortexed and incubated on rotator shaker for 2 hrs at 4 °C. The lysate was clarified by centrifuging at 12,000 *g* for 10 min at 4 °C. To collect the biotinylated surface proteins, 80 µl of streptavidin slurry was added to each sample and then incubated for 4 hrs on rotator shaker at 4 °C. After that, the streptavidin beads were pelleted by centrifuging at 1,000 *g* for 2 min. The beads were subsequently washed twice with 1 ml of LB3 that lacks 2-mercaptoethanol and centrifuged at 1,000 *g* for 2 min. After two more washes in 1 ml of buffer A were performed, the disulphide bonds were cleaved off to release the biotinylated proteins from the streptavidin beads. For this, the final pelleted beads were resuspended in 80 1x SDS sample buffer (containing 5% 2-mercaptoethanol) then incubated at 90 °C for 10 min and centrifuged at 12,000 *g* (Moore et al., 2004). Then samples were stored at -20 °C. After the results have been obtained by immunoblotting, the protein bands were quantified using ImageJ and they were plotted by GraphPad prism v.5. Data presented as mean ± SD of two separate experiments.

2.3.10 Flow cytometric detection of surface the β2AR:

HEK293 cells were cultured in 6-well plates and when they were 50 % confluent, they were transiently transfected with FLAG-β2AR using the PEI method. 36 hrs post-transfection, the cells were treated by the appropriate drugs according to the experimental design and for the indicated times. Then, the cells were washed once by 1 ml PBS and were detached by adding 1 ml of 10 mM EDTA in PBS per well and incubated for 10 min at 4 °C. Subsequently, the cells were centrifuged at 400 *g* for 5 min at 4 °C. The pelleted cells were resuspended in 200 µl blocking buffer (0.5 % BSA in PBS) and 200 µl of 0.5 % BSA/PBS. Cell count was performed using hemocytometry and about 250,000 cells were transferred into fresh 1.5 ml tubes followed by centrifugation at 400 *g* for 5 min at 4 °C. After removal of the supernatant, the cells were resuspended in 100 µl primary anti-FLAG antibody (prepared in 0.5 % BSA/PBS) and the cells were incubated for 60 min at 4 °C. Then, they were washed three times with 200 µl of 0.5 % BSA/PBS followed by centrifugation at 400 *g* for 5 min at 4 °C. The cells were resuspended and incubated with 100 µl of the secondary FITC-tagged antibody (prepared in 0.5 % BSA/PBS) in dark for 1 hr at 4 °C. Subsequently, the cells were pelleted at 400 *g* for 5 min at 4 °C and washed three times with 200 µl of 0.5 % BSA/PBS. Finally, they were transferred into flow cytometry polypropylene tubes (final volume of 400 µl 0.5 % of BSA/PBS) and assed in same day using ADP Cyan flow cytometer (Beckman). The obtained data was analysed by FlowJo.V10.

2.3.11 Detection of surface β2AR by ELISA:

HEK293 cells were cultured and transfected with FLAG-β2AR using PEI. The cells were plated in pre-coated 96-well plates, labelled with antibodies and the

quantification of the receptors was performed by measuring the absorbance in a Bio-Rad plat reader.

2.3.11.1 Coating the plates with attachment factor:

Poly-D-lysine (PD-L) (catalogue number: P6407, Sigma) was used for plate coating. In a cell culture cabinet, 100 µl/well was added and incubated for 30 min. Then, the PD-L was aspirated, and plate was washed three times with 200 µl/well with sterile dH_2O. After the last wash, dH_2O was aspirated and the plate was left in the hood for 2 hrs until the water was completely evaporated. The plate was then stored at 4 °C.

2.3.11.2 Monitoring the internalization of the β2AR by ELISA:

HEK293 cells were plated in T75 flask and when they reached 50 % confluency, they were transfected with 7 µg of FLAG-β2AR using PEI. On the next day, the cells were detached with 2 ml PBS and transferred into a PD-L pre-coated 96-well plate and were seeded at 10,000 cells/well in 100 µl media. On the following day, the cells were pre-labelled with primary mouse anti-FLAG antibody (catalogue number: F3165, Sigma) at 1:1,000 dilution in ELISA blocking buffer. Simultaneously, some samples were also pre-incubated with either 10 µM St STOCK1S-50699 (St) or 1 µM propranolol (Pro) for 1 hr at 4 °C. After that, the cells were washed three times with 200 µl PBS, then either left unstimulated or treated by 1 µM Isoproterenol (Iso) and hypotonic low chloride buffer (HLB) for 1 hr at 37 °C. Subsequently, the cells were washed three times with 200 µl PBS and then labelled with secondary goat anti-mouse (alkaline phosphatase) antibody (1:5,000 dilution in ELISA blocking buffer) for 1 hr at 4 °C. After incubation, unbound antibodies were removed by washing three times with

200 µl PBS. To develop the colour, 100 µl of one-step *p*-nitrophenyl phosphate disodium salt (catalogue number: 37621, Thermo Fisher) was added. The plate was then gently mixed by agitation for 30 min until colour developed. After this, the reaction was stopped by adding 50 µl of 2N NaOH. Finally, the absorbance was measured at 405 nm on plate reader (Bio-Rad). The background control samples were transfected cells labelled with mouse-IgG isotype control. The plot of membrane β_2AR was generated by Graph Pad Prism 5 and the quantity of the surface receptors was normalised to untreated samples and presented in mean of single experiment.

2.3.12 Peptide docking by AutoDock:

Docking of the RFQV- and RFHV-peptides into OSR1-CCT domain was carried out using AutoDock Vina1.12 (AlAmri et al., 2017a). For this, the PDB file of the OSR1 CCT domain was prepared by AutoDock tool 1.5.6. Unbiased docking of the RFHV-peptide into OSR1-CCT (PDB ID: 2V3S) was performed and the interactions were confirmed by re-docking of RFQV-peptide as well in the same binding site (AlAmri et al., 2018).

2.3.13 Statistical analysis:

All of the plotted diagrams were generated using GraphPad Prism 5 and the data was presented as the average of a minimum of three independent replicates ± SD, unless indicated otherwise with the *n* value (number of replicates) shown in the figure's legends. To determine statistical significance, the samples were compared against the control, and *P* values were calculated using one-way ANOVA for more than two samples and Student T-test for two samples where $P < 0.05$ was considered to be significant.

Chapter 3 : Results and discussion

3.1 Characterization of the WNK and β2AR signalling pathways

Before getting into dissecting the relationship between the WNK and β2AR signalling cascades and exploring the effect of each protein on the other, the drugs, buffers and antibodies that will be used for such studies needed to be characterised.

3.1.1 Optimisation and characterization of WNK signalling.

Since WNK kinases are inactive under resting conditions and they became activated under osmotic stress or by changes in chloride concentration as mentioned in the introduction, we first had to establish and optimise the conditions of WNK-signalling activation. Endogenous WNK1 could be stimulated by either hyperosmotic agents such as sorbitol (Sor) or by hypotonic low chloride buffer (HLB) (Richardson and Alessi, 2008). This is known to induce phosphorylation of WNK1 at Ser382 and subsequent direct phosphorylation of Thr233 and Ser373 of SPAK and Thr185 and Ser325 of OSR1, which we could be used as the readout for WNK activation (Richardson and Alessi, 2008).

As Sor can stimulate other signalling pathways which are mediated by other kinases such as ERK1/2, JNK and p38, (Zagórska et al., 2007) and the underlying mechanism by which WNK kinase stimulation is not yet elucidated (Rodan and Jenny, 2017), HLB was used in this study to trigger WNK-signalling. To test the HLB activation of WNK-signalling, HEK293 cells were treated for 30 minutes (min) with HLB (**Figure 3.1**). To validate WNK1 signalling activation, STOCK1S-50699 (St) (a SPAK/OSR1 to WNK binding inhibitor) (Kikuchi et al., 2015) was added after exposure to HLB at 10

or 30 µM for 30 min (de Los Heros et al., 2014). As expected, the activation of WNK-signalling cascade was clearly observed following HLB treatment as judged by SPAK Ser373 phosphorylation (lane 2). This phosphorylation was inhibited completely by the addition of 10 or 30 µM St, (lane 3 and 4, **Figure 3.1**), as compared to the control (untreated cells) (lane 1, **Figure 3.1**).

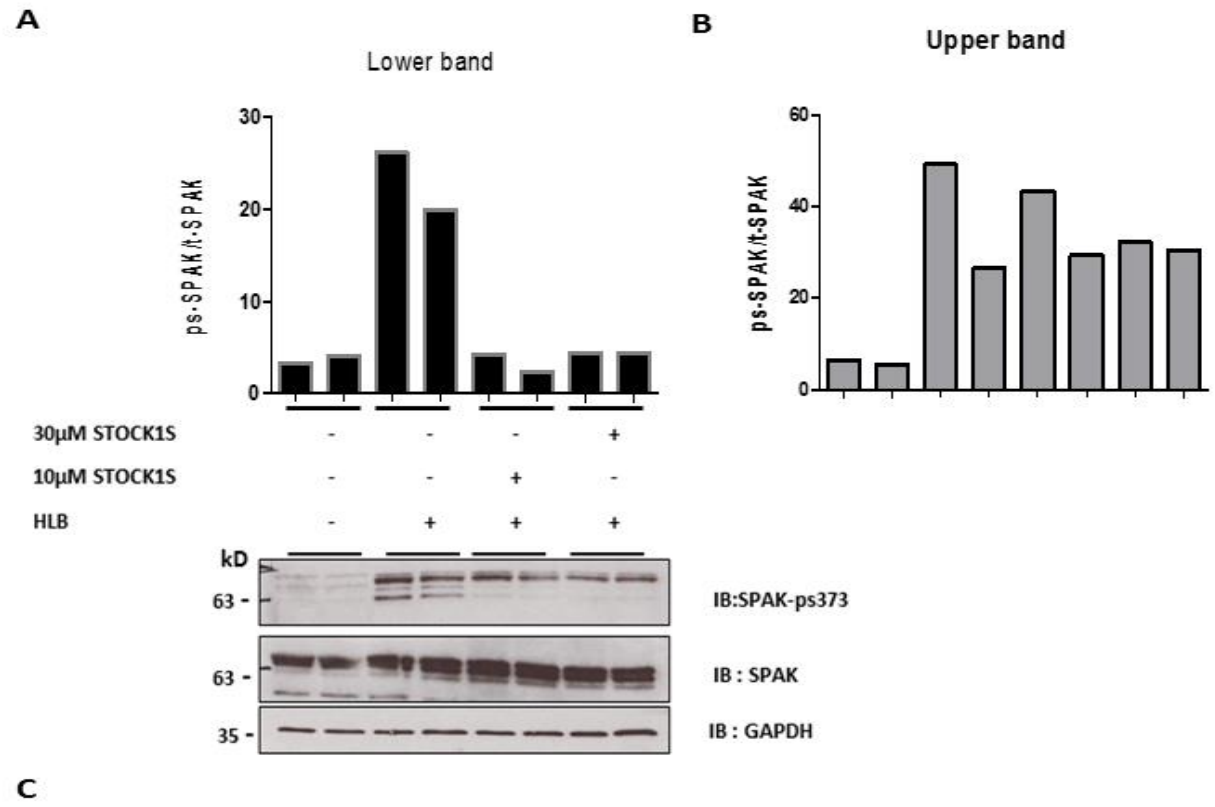

Figure 3.1: WNK signalling pathway stimulation by HLB and its inhibition by STOCK1S-50699. *(C) Immunoblot analysis of treated HEK-293 cells with HLB for 30 min which induced WNK signalling activation and SPAK phosphorylation at Ser373 residue (lane 2). Pre-treatment of cells with STOCK1S-50699 (St) for 30 min with the indicated concentrations 10 and 30 µM (lanes 3 and 4 respectively), blocked the WNK1-mediated activation of SPAK. Phosphorylation of SPAK in (C) was evaluated by densitometry (A) and (B) which it was normalized to total SPAK. (A) Phosphorylated SPAK in 63 kD was activated by HLB and was inhibited with addition of St, that indicating WNK-mediated SPAK Ser373 phosphorylation. (B) This SPAK phosphorylation also increased with HLB but however did not respond to St pre-treatment which unlikely to be a phosphorylated Ser373 residue (de Los Heros et al., 2014). The figure shows single experiment (n = 1). Glyceraldehyde 3-phosphate dehydrogenase (GAPDH) was used as a loading control, kD: kilo Dalton. GAPDH (1:5,000), SPAK (2 µg/ml) SPAK-pSer373 (2 µg/ml).*

To further validate the activation and inhibition of WNK-SPAK/OSR1 signalling, the specificity of WNK-signalling inhibitors (AlAmri et al., 2017b, Yamada et al., 2016) and antibodies that recognise phospho-proteins e.g. phospho-NKCC1, were assessed. The WNK ATP-competitive kinase inhibitor WNK463 (AlAmri et al., 2017b, Yamada et al., 2016) was added to HEK293 cells at the indicated doses for 30 min and St was used a as a positive control while the negative control was HLB-only treated cells (**Figure 3.2**). As demonstrated in previous report by Yamada et al, our results re-confirmed the fact that WNK463 is able to produce a significant WNKs inhibition in HEK293 cells (Yamada et al., 2016), which prevents the WNK-mediated NKCC1 phosphorylation and activation at approximately 5 µM as compared to 20 µM with St (lane 3). Moreover, the high level of WNK activation was noticed by exposing cells to HLB (lane 2) and this was reduced or completely prevented by addition of 3 µM and 5 µM WNK463 respectively.

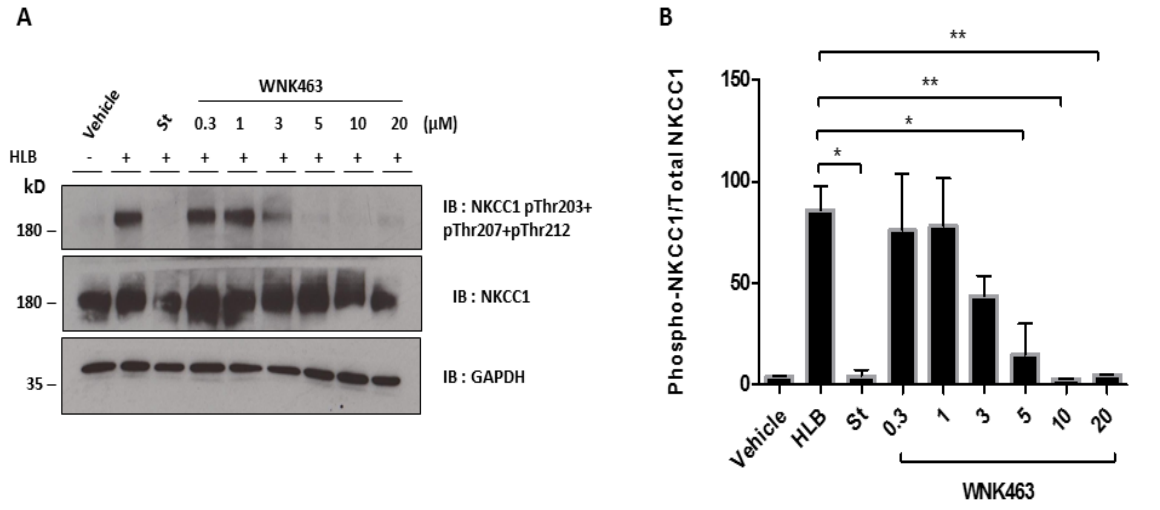

Figure 3.2: Optimisation of WNK kinases inhibition by WNK463.

*(A) Representative Western blot analysis of endogenous NKCC1 phosphorylation in extracts from HEK293 cells. The analysis includes unstimulated (vehicle was DMSO only treated cells), HLB treated cells or cells treated with WNK463 at the indicated doses. In comparison to 20 µM St, WNK463 induced WNK1 inhibition at 5 µM (lane 7), as it prevented NKCC1 phosphorylation by HLB. (B) Densitometric analysis of NKCC1 phosphorylation in (A), demonstrated a surge activation of NKCC1 with HLB and this stimulation was completely prevented with 20 µM St and 5 to 20 µM WNK463. Data represent mean ± SD of two independent experiments (n=2). ** P < 0.0025, *P < 0.05, (ANOVA with post-Bonferroni's test). GAPDH (1:5,000), NKCC1 (2 µg/ml), NKCC1-pT203+T207+T212 (2 µg/ml).*

3.1.2 Characterization of β2AR signalling pathway:

3.1.2.1 Optimization of the β2AR expression in mammalian cells:

Generally, most of the GPCRs including β2AR have very low abundance in native tissues (Maeda and Schertler, 2013). This makes studying the signalling and biological structures of these receptors a stern challenge. Therefore, establishing an effective protein expression system for these GPCRs is essential to obtain a suitable amount of the protein for biological analysis (Maeda and Schertler, 2013). Among these systems is GPCRs expression in mammalian cell lines, which has several advantages as it provides a natural environment for the requirement of membrane-protein expression e.g. lipid composition, post-translation modifications, and protein folding (Maeda and Schertler, 2013). A prime example of the expression of GPCRs in mammalian cells is that of rhodopsin, which could be expressed in HEK293S cells at ~ 10 mg/L, where these cells lacking *N*-acetylglucosaminyl transferase 1 (GnTI) and they have been developed in suspension, to be adapted to express a variety of mammalian receptors (Chaudhary et al., 2012).

In this work, HEK293 cells were predominantly used for exploring the link between WNK signalling pathway and β2AR. The endogenous expression of β2AR is extremely low approximately 0.02 pmol/mg in HEK293 cells (Han et al., 2012), a finding also confirmed during the optimization steps of the receptor expression in these cells (**Figure 3.3,** lane 1 and 2). Thus, overexpression of the β2AR was used for the purpose of the study. The choice of HEK293 cells for this work was also supported by the fact that these cells express endogenously all of the components of the WNK-signalling cascade; WNK1 and 4, SPAK, OSR1, MO25, Cul3, KLHL3 and the various ion co-transporters (e.g. NKCC1) (Vitari et al., 2006, Filippi et al., 2011, Ohta et al., 2013).

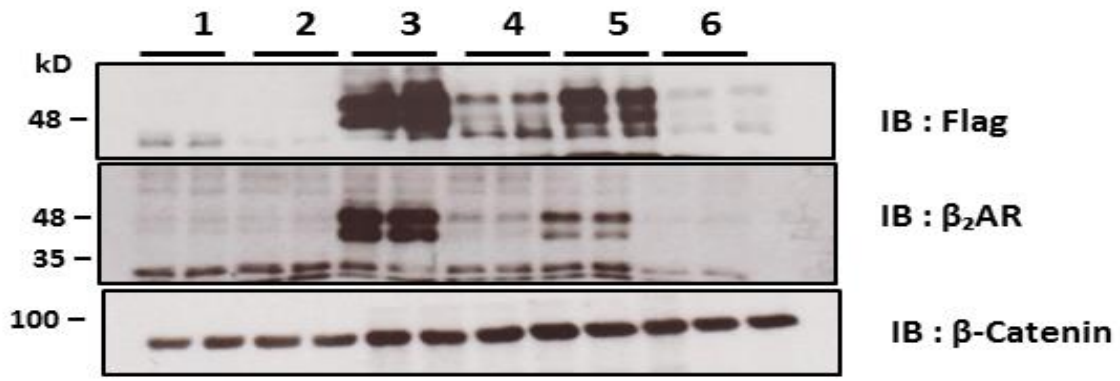

Figure 3.3: Optimization of FLAG-β2AR expression in HEK293 cells. *Immunoblot analysis of FLAG-β2AR expression in extracts from HEK293 cells. Untransfected cells (lane 1) and 12 µg PEI only (lane 2) did not show expression of the* β2AR*. Transfected cells using cDNA: PEI ratios of 1:2 and 1:4 showed the best expression ratio (lanes 3 and 5 respectively). The validation of β2AR expression was confirmed using both anti-FLAG and anti-β2AR antibodies.*

Please note that the result represents a single experiment (n=1) which was performed to determine the best cDNA: PEI ratio for HEK293 transfection.

1 Un-transfected cells.

2 PEI only treated cells (12 µg).

3 Transfected cells at ratio 1:2.

4 Transfected cells at ratio 1:3.

5 Transfected cells at ratio 1:4.

6 Transfected cells at ratio 1:5.

FLAG (1:1,000), β-catenin (1:1,000), β2AR (1:500).

The *N*-terminally FLAG-tagged β2AR was transiently expression in HEK293 cells using PEI (**Method Chapter**). To optimise the overexpression of the β2AR in HEK293 cells, the cells were first cultured in 6-well plates and then they were transfected with different ratios of β2AR cDNA clone and PEI (**Figure 3.3**). The cells were harvested by lysis buffer 2 (LB2), which contains 1 % NP40 and supplemented with 1 % (w/v) *n*-dodecyl β-D-maltoside (DDM). The cell lysates subsequently

underwent SDS-PAGE electrophoresis and the membranes were probed for the β2AR using anti-FLAG and anti-β2AR antibodies. This showed that the receptors were successfully overexpressed with a MW ~ 48 kD and these bands were not present in the untransfected cells (lanes 1 and 2, **Figure 3.3**). This experiment showed the cDNA: PEI ratios of 1:2 and 1:4 resulted in significant overexpression of the β2AR with the 1:2 ratio being the most efficient. Hence, going forward in this work, for the overexpression of the β2AR, a 1:2 ratio of cDNA: PEI was used.

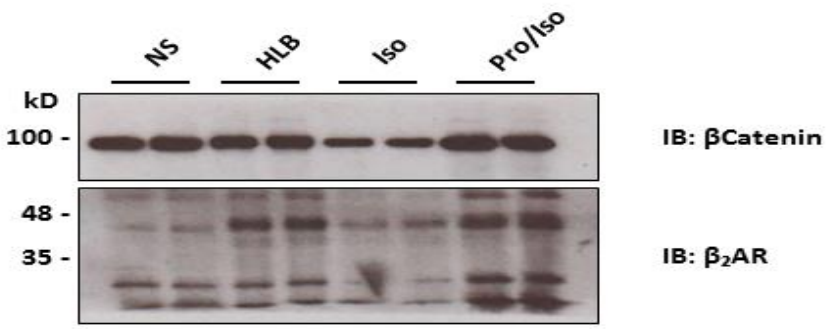

Figure 3.4: Poor solubilization and extraction of β2AR.

Immunoblot analysis of the β2AR solubilisation and extraction from HEK293 cells. Cells were transfected with FLAG-β2AR and then treated with HLB, isoproterenol (Iso), propranolol (Pro) or left unstimulated (NS). After that, they were lysed using LB2 and prepared for SDS-PAGE. The receptors were probed for using the anti-β2AR antibody. As shown, the unstimulated and Iso treated samples had low expression of the receptors that because of lysis buffer (LB2) was not efficient for receptor extraction and it needed to be optimized (n = 1). β-catenin (1:1,000), β2AR (1:500).

After the overexpression conditions of β2AR in HEK293 cells were optimized, the extraction of receptors from the cell lysates was occasionally poor and needed to be optimised (**Figure 3.4**). This is because GPCRs generally possess both amphipathic character; lipophilic surfaces which enable them to interact with lipid

membrane and hydrophilic areas that are directed towards to aqueous intracellular and extracellular environments (Loll, 2014) as well as inherent instability when not bound to membranes (Maeda and Schertler, 2013). These features affect the receptor's solubility and isolation from cell membranes (Loll, 2014).

To improve the extraction of the β2AR from cell membranes, there was a need to identify a suitable lysis buffer that not only facilitates the receptor extraction from membrane bilayer, but it also helps to maintain receptor solubility and stability in the aqueous solution by adsorption of receptor's lipophilic sides within the detergent micelles (le Maire et al., 2000). These complexes are highly dynamic molecules as the detergent monomers are in equilibrium between the free form state and aggregated in to the detergent-receptor complexes. Therefore, to overcome the receptor's hydrophobicity, the availability of free detergent monomers must be maintained in the aqueous solution (Loll, 2014). To reach this point, the detergent concentration in the solution should be kept higher than the critical micellar concentration (CMC) (Loll, 2014). However, extremely elevated concentrations of the detergent could induce receptor inactivation. This highlights the necessity of adjusting the detergent concentration. Moreover, the solubility of membrane receptors depends on the biophysical and biochemical properties of the detergent (Prince and Jia, 2013).

Finding of a suitable lysis buffer that has ability to extract the receptors from membranes and maintain both receptor folding and protein interactions is necessary. Previous reports indicated that supplementing lysis buffer 3 (LB3) with DDM and incubating samples for least 2 hrs was very effective in solubilizing the β2AR (Han et al., 2012). For the characterization of LB3, LB3 was initially tested versus LB2 and RIPA (**Figure 3.5**). LB3 produced a significant change in term of receptor solubilization

and isolation from biological membranes of HEK293 cells (**Figure 3.5**) and it gave the best receptor resolution over LB2 and RIPA in 10 % SDS-PAGE gels.

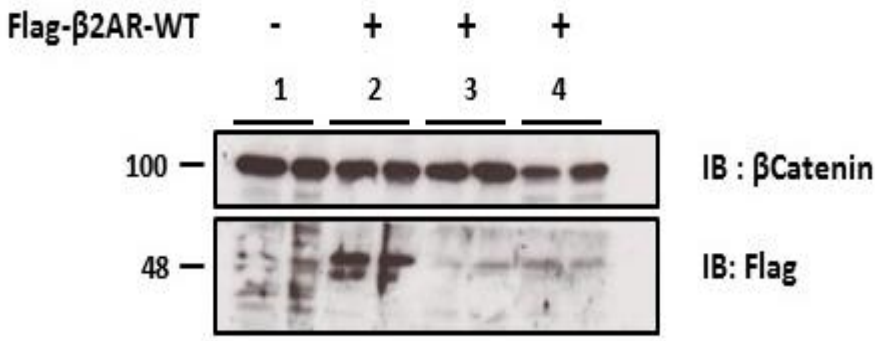

Figure 3.5: Western blot analysis of LB3 characterization for β2AR solubilisation in HEK293 cells. *HEK293 cells were either left untransfected (lane1) or transfected with FLAG-β2AR-WT (lanes 2-4). The cells were lysed by different lysis buffers: lanes 1 and 2 cells harvested with LB3, LB2 (lane 3) or RIPA (lane 4). β2AR was probed for by anti-FLAG antibody. The receptors were only detected in LB3 harvested cells with a MW at ~ 48kD reflecting the monomeric form of the receptor (n=1). FLAG (1:1,000), β-catenin (1:1,000).*

Subsequently, LB3 was mainly used and receptor expression was primarily assessed by the use of anti-FLAG antibody before continuing with the downstream procedures. The β2AR was identified by mouse anti-FLAG antibody which has negligible cross reactivity. Interestingly, the β2AR existed in two forms; higher migrating monomers and homodimers, which they have been observed at ~ 50 kD and ~ 100 kD respectively in 10 % SDS-PAGE (**Figure 3.6**) (Bulenger et al., 2005).

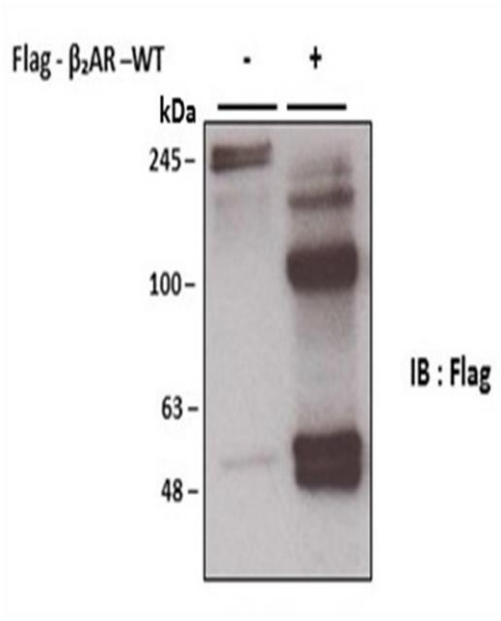

Figure 3.6: Western blot analysis of the FLAG-β2AR expression in HEK293 cells. *HEK293 were cultured in 10-cm plates and transiently transfected with the β2AR cDNA clone. After 48 hrs, the cells were lysed in ice cold LB3 and incubated for 2 hrs at 4 ˚C. Then, they were subjected for SDS-PAGE. β2AR was probed by anti-FLAG antibody. Monomeric β2AR was detected at 50 kD and bands around 100 kD indicated homodimer formation (n =1). FLAG (1:1,000).*

3.1.2.2 Characterization of the β2AR signalling cascade:

In addition to the assessment of receptor's expression, the compounds that have been used in this study to manipulate the β2AR had first to be characterised. These include Isoproterenol (Iso), a full βAR agonist, ICI118551(ICI), a high affinity β2AR inverse agonist and propranolol, a non-selective βAR antagonist. To determine an appropriate concentration of Iso for receptor stimulation, Iso was added to the β2AR transfected HEK293 cells at different concentrations (**Figure 3.7**). From then the 300 nM and 1 μM were chosen for β2AR stimulation and internalization respectively throughout the study. To identify the β2AR activation, probing for phosphorylated serine residues e.g. Ser345 and Ser346 have been performed by using specific antibodies against these residues (Gao et al., 2014). Unfortunately, phosphorylation at these sites was not detected (**Figure S1**). As agonist-stimulated β2AR elevates cAMP and activates PKA, which phosphorylates the liver kinase B1 (LKB1) at Ser428 (Sapkota et al., 2001, Zheng et al., 2009), we next probed for LKB1 pS428. We were

able to detect the phosphorylated LKB1 Ser428 through β2AR activation pathway. Thus, LKB1 was used for detection agonist-stimulated β2AR, and this phosphorylation was recognised by a highly specific rabbit anti-LKB1-pS428 antibody **(Figure 3.7**).

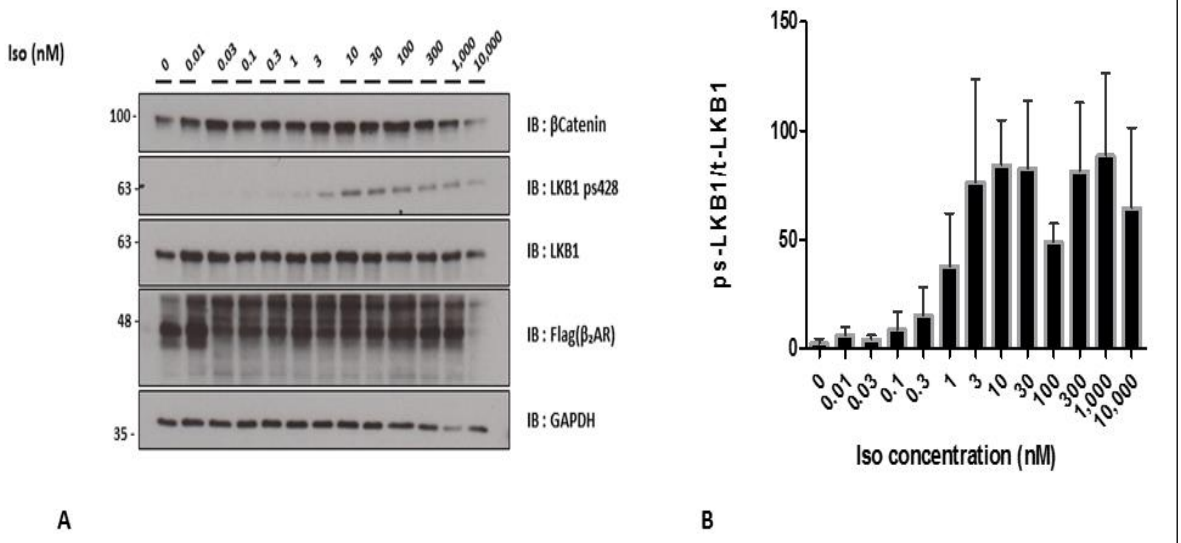

Figure 3.7: Isoproterenol dose-dependent stimulation of the β2AR.

(A) Representative Western blot of LKB1 phosphorylation in HEK293 cells. Cells were transfected with FLAG-β2AR-WT and 48 hrs post-transfection, they were treated with Isoproterenol (Iso) at the indicated concentrations for 30min. Phosphorylation of LKB1 at Ser428 was observed from 3 nM and gradually increased to reach 1 μM then reduced at 10 μM. GAPDH and β-catenin were used as housekeeping proteins (B) Densitometry analysis of LKB1 phosphorylation was carried out, where phospho-LKB1 was normalised to total LKB1, and data present in mean ± SD of three independent experiments (n=3). FLAG (1:1,000), β-catenin (1:1,000), LKB1 (1:1,000), pLKB1(1:1,000), GAPDH (1:5,000).

To obtain optimum inhibition of Iso-mediated activation of the β2AR, ICI was added to cells prior exposure to Iso at various concentrations 10 nM, 30 nM, 100 nM and finally 1 μM (**Figure 3.8**). This resulted in that 30 nM of ICI showed inhibition of

phosphorylation of LKB1 and thus the activation of the β2AR, a finding is in the agreement with previous reports (Kitagawa et al., 1995). Going forward, 1 μM of the ICI compound was used for the receptor inhibition studies.

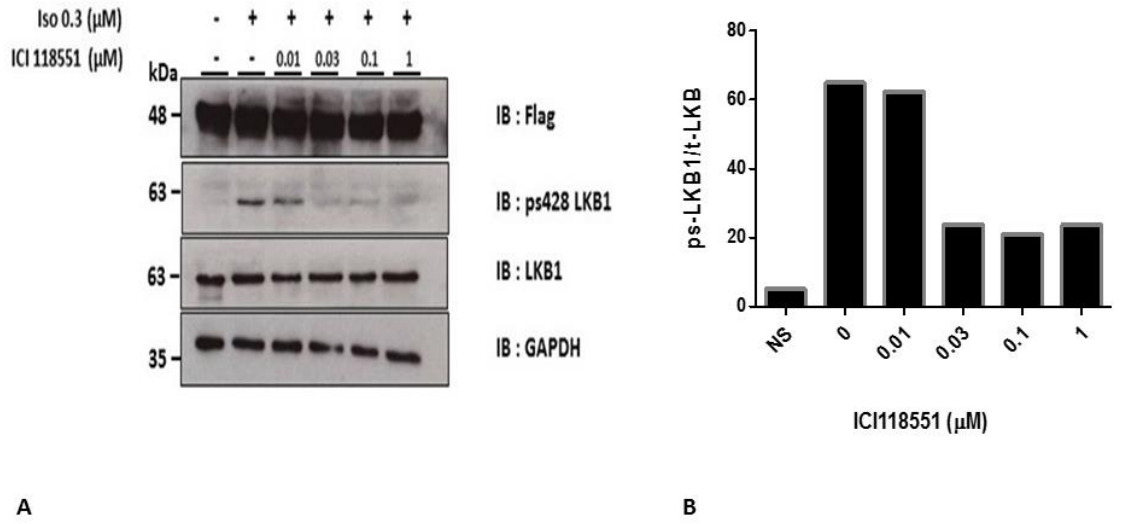

Figure 3.8: ICI118551 inhibition of Isoproterenol stimulation of β2AR.

(A)HEK 293 cells were transiently transfected with FLAG-β2AR-WT and after 48 hrs, the cells receptors were at first either left unstimulated or treated with ICI118551 (ICI) at indicated concentration for 60 min. These cells were then either left unstimulated or treated with 300 nM of Iso for 30 min. (B) ICI118551 blocked the effect of 300 nM Iso from 30 nM as judged by the inhibition of LKB1 phosphorylation at Ser428. Data represented a single experiment (n=1). FLAG (1:1,000), LKB1 (1:1,000), pLKB1 (1:1,000), GAPDH (1:5,000).

3.2 Molecular interaction of SPAK and OSR1 to β2AR:

3.2.1 Molecular docking of β2AR-derived RFHV into OSR1 CCT:

Human OSR1 and SPAK protein kinases share 68 % sequence homology and possess two high conserved regions; an *N*-terminal kinase domain and a CCT domain that has 79% sequence similarly between SPAK and OSR1 (Villa et al., 2007). The CCT domain enables SPAK and OSR1 to interact with RFxV tetrapeptide motifs from upstream activators, i.e. WNK isoforms, and of downstream substrates NKCC1, NKCC2 and NCC (Alessi et al., 2014). This interaction takes place in the primary pocket of the CCT domain (Richardson and Alessi, 2008). Truncation of the CCT in both kinases abolishes the binding of SPAK and OSR1 to their upstream and downstream proteins (Vitari et al., 2006).

Interestingly, the crystal structure of the β2AR revealed that the receptor possesses a single RFHV motif (239-242) at ICL3, which matches the SPAK and OSR1 RFxV tetrapeptide binding motif (Rasmussen et al., 2007). To investigate whether the β2AR's RFHV peptide interacts with the same residues of OSR1 CCT that bind to RFQV, we initially performed molecular docking of the RFHV tetrapeptide into the structure of OSR1 CCT domain (**Figure 3.9 A**). The docking results showed that the WNK kinases RFQV and the β2AR's RFHV peptides docked in the same primary pocket on OSR1 CCT domain. Like the RFQV tetrapeptide interactions, the Arg, Phe and Val of the β2AR's RFHV peptide were found to be important for forming interactions with the OSR1 CCT domain. This also showed that Asp459 and Lys473 of OSR1 CCT domain formed key interactions of the RFHV peptide of the β2AR (**Figure 3.9 B**). This is an interesting finding, as a single pointed mutation in these two residues was shown to abolish the binding of OSR1 to the RFxV motif of either NKCC1 or WNK1/4 (Vitari et al., 2006). These results indicated that the β2AR's RFHV

tetrapeptide is likely to bind OSR1 CCT domain akin to how the WNK RFxV peptides bind this domain.

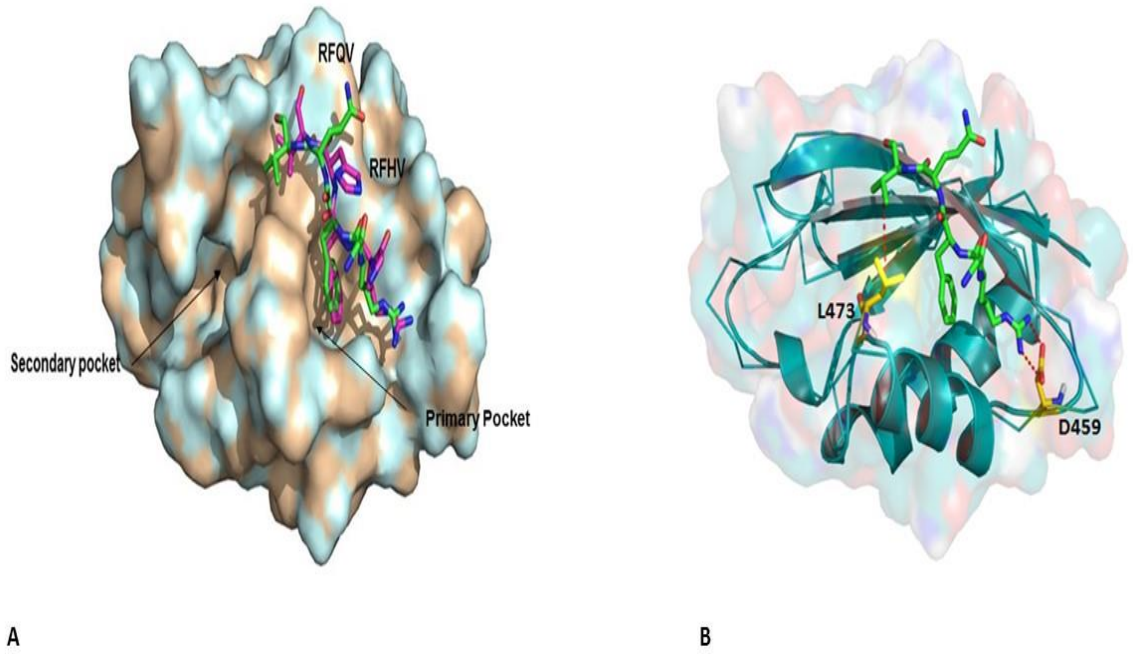

Figure 3.9: Molecular docking of β2AR-derived RFHV into OSR1-CCT domain. *The cartoon showing interaction of RFQV and RFHV with OSR1-WT (A) The protein surface of OSR1-CCTRFHV (pink) showed to have same binding site as RFQV (green) in OSR1(PDB code: 2V3S). Arg, Phe and Val of both peptides shared similar docking. While His of RFHV is protruded outward like Gln of RFQV. (B) Diagram illustrate the most crucial two residues, lys473 and Asp459 of CCT that are involved in the interaction with RFQV. Figures were generated by AutoDock Vina. This docking experiment was performed by Mubarak Alameri.*

3.2.2 Binding of the β2AR-derived RFHV peptide to endogenous SPAK

In order to examine the proposed interaction of the β2AR's RFHV peptide to SPAK/OSR1 CCT, we investigated the binding ability of *N*-terminally biotinylated wild type (WT) RFHV and its mutant AFHV peptides to endogenous SPAK in HEK293 cells. Initially, 1 mg of HEK293 cell lysate was incubated with 3 µg of the indicated peptide followed by biotin-streptavidin pulldown. This initial attempt showed that endogenous SPAK did bind the RFQV peptide as expected, but its binding to the RFHV was very low (**Figure S2**). To optimise this assay, SPAK was then pulled down by incubating 1-10 mg of total cell lysate with 3 µg of either the RFQV or the RFHV peptides. The peptides were pulled down by adding streptavidin beads and SPAK binding to the peptides was assessed by blotting for SPAK (**Figure 3.10**). As expected, endogenous SPAK bound the RFHV peptide at 1, 5 and 10 mg of total cell lysates while 5 mg of total cell lysate was the best concentration for both peptides binding to SPAK as RFQV appeared to have less binding ability to SPAK with less than 5 mg of total protein cell lysate in contrast to the previous finding.

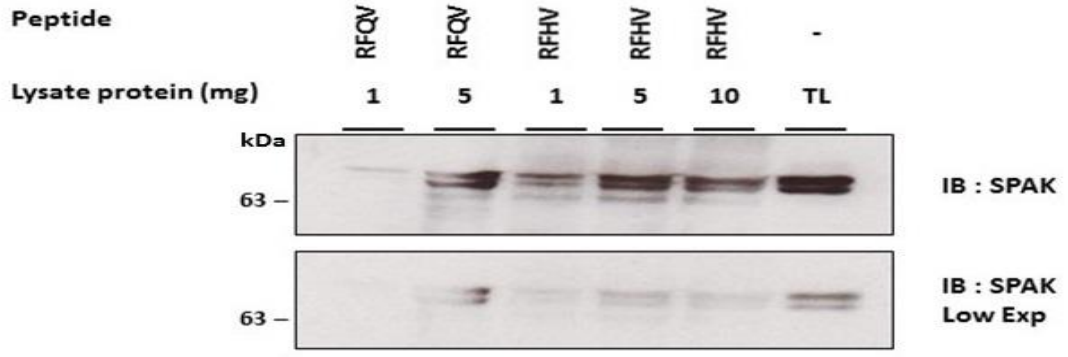

Figure 3.10: Optimization of the interaction of the RFHV peptide to endogenous SPAK in HEK293. *3 µg of indicated RFxV peptides was incubated with different concentrations of HEK293 cell lysate as indicated. This was followed by biotin-streptavidin pull down of the biotinylated peptide and blotting for endogenous SPAK. TL: Total lysate (n =1). SPAK (2 µg/ml).*

Next, to verify the binding of the β2AR's peptide to SPAK, 5 mg cell lysate was incubated with either WNK4-derived RFQV peptide (positive control), AFQV peptide (negative control), RFHV-peptide or AFHV-peptide. After pulling down the peptides with streptavidin beads, SPAK was probed for by immunoblotting. The results revealed that SPAK successfully bound to RFQV-peptide while AFQV failed to bind to SPAK. Similarly, the RFHV was also shown to bind endogenous SPAK similar to the RFQV while mutant AFHV did not (**Figure 3.11).** These findings validated our hypothesis that the β2AR's RFHV-peptide interacts with SPAK at cellular level. This is in agreement with previous studies that showed that RFxV tetrapeptides bind SPAK and OSR1 (Villa et al., 2007, Vitari et al., 2006).

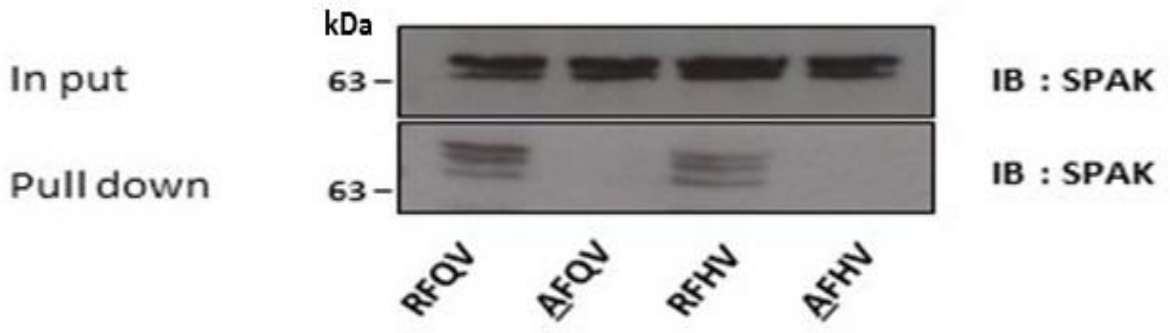

Figure 3.11: The biotinylated RFHV-peptide interacts with endogenous SPAK. *Representative IB analysis of SPAK binding to the RFHV peptide. 5 mg lysate from untransfected HEK293 cells was incubated with biotinylated RFQV, AFRV, RFHV or AFHV-peptides. This was followed by biotin-streptavidin pulldown and Western blot for endogenous SPAK. Results represented of three independent experiments (n=3).*

SPAK (2 µg/ml).

3.2.3 D459A and L473A mutations in OSR1 CCT inhibit the binding to the RFHV peptide

To further confirm the interaction between CCT OSR1 and the β2AR's RFHV peptide in more detail, we investigated the ability of RFHV-peptide interaction with full length GST-OSR1-T185E, or with two OSR1 CCT domain single point mutations namely GST-OSR1-T185E-D459A and GST-OSR1-T185E-L473A. The choice of these two OSR1 CCT domain mutants was due to their ability to abolish the binding to the RFQV peptide (AlAmri et al., 2017a, Villa et al., 2007). In our experiments, the WNK4 RFQV peptide was used as positive control. Following the overexpression of these proteins in HEK293 cells, the binding of these proteins to biotinylated RFQV or RFHV peptides was assessed using biotin-streptavidin. The results revealed that the β2AR-derived RFHV peptide binds only to OSR1-T185E and not those with the CCT domain mutants (**Figure 3.12**). This indicated that the β2AR's RFHV peptide docks into OSR1 CCT domain akin to how the WNK4 RFQV peptide does and such docking involves the interaction between the RFHV peptide to the OSR1 CCT domain D459 and L473 residues. This interaction is similar to how the WNK4 RFQV peptide binds the primary pocket of CCT-OSR1 as verified by numerous reports in the literature (Gagnon et al., 2007b, Piechotta et al., 2002). As the β2AR's RFHV peptide is located in the intracellular loop ICL3 of the receptor and SPAK and OSR1 kinases are cytoplasmic proteins, such binding is very plausible.

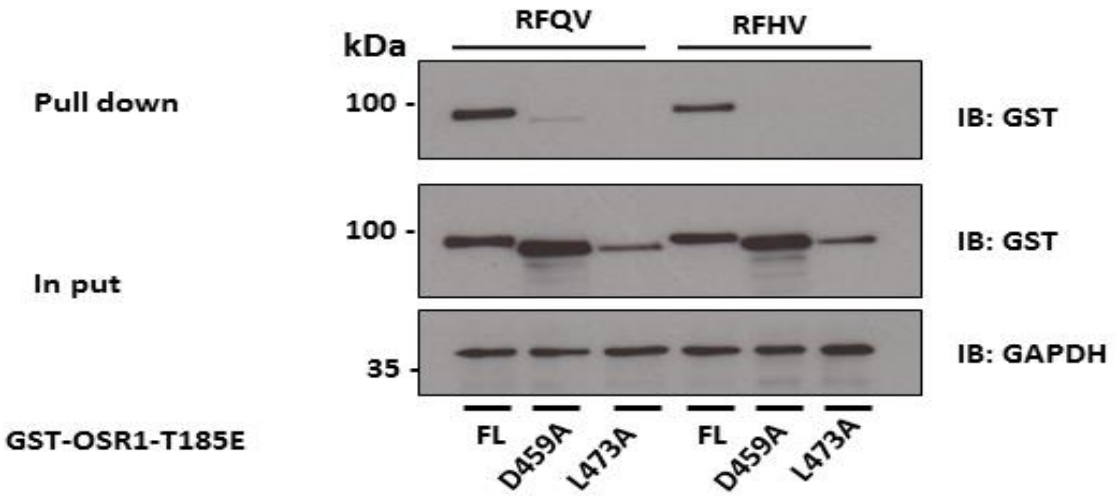

Figure 3.12: The RFHV-peptide binds to OSR1 but not OSR1 CCT domain mutations D459A or L473A. *HEK293 cells were transfected with GST-OSR1-T185E (FL), GST-OSR1-T185E+D459A or GST-OSR1-T185E+L473A. 48 hrs post transfection, the cells were lysed, and affinity purification was performed by biotin-streptavidin pulldown. The purified samples (pull down) were subjected to SDS-PAGE and OSR1 was probed by anti-GST antibody. The input indicates the cell lysates before pulldown. The same results have been obtained from three independent experiments (n=3). GAPDH (1:5,000), GST (1:1,1000).*

3.2.4 Identification of OSR1 associated proteins in the heart:

Encouraged by the possible β2AR binding to SPAK and OSR1 kinases from the data discussed above, we subsequently planned to explore such binding at the endogenous level. First, we performed immunoprecipitation (IP) of endogenous OSR1 from mouse (*Mus Musculus*) heart lysate, using a highly selective anti-OSR1 antibody that had been covalently conjugated to protein-G-Sepharose beads (**Methods Chapter**). The isolated proteins were stained by Colloidal blue stain after samples were separated by SDS-PAGE gel electrophoresis. Then, the gel was cut into twenty-

two pieces without gaps as shown in **Figure 3.13**. Lanes 1 to 11 were the empty beads (negative control), which was devoid of antibody, to identify proteins that may bind non-specifically to the beads while immunoprecipitated samples (OSR1-IP) were represented in lanes 12 to 22 (**Figure 3.13**). The samples were subsequently subjected to trypsin digestion and analysis by mass spectrometry (MS). To identify the proteins from which the peptide came from, the mass spec raw data were analysed by Mascot (Ohta et al., 2013).

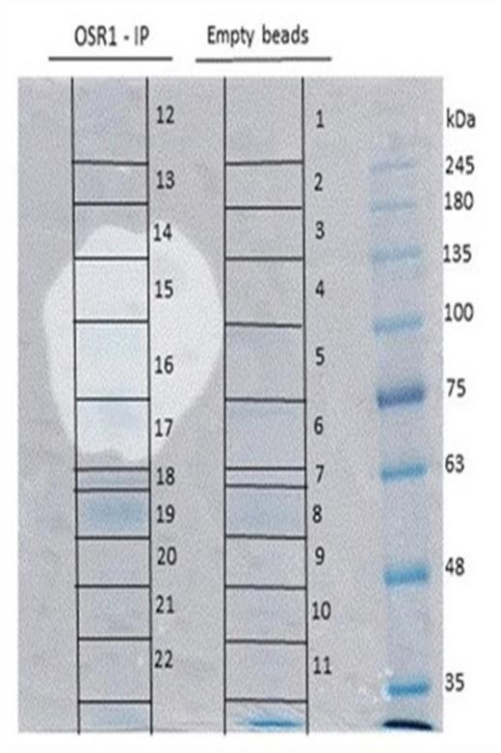

Figure 3.13: OSR1 immunoprecipitation from mouse heart lysates.

Mouse heart was harvested by LB2 and OSR1 was immunoprecipitated from 5 mg lysate, using anti-OSR1 antibodies covalently conjugated to Sepharose beads. Following the electrophoresis of samples, proteins were visualised by Colloid Blue staining. Molecular weight is on the right-side, empty beads (negative control) (lanes 1 to 11) while immunoprecipitated sample was OSR1-IP (lanes 12 to 22). Lysis buffer 2 (LB2). Results were obtained from single experiment (n =1).

Once the Mascot files were obtained, the proteins that were identified in the empty beads were extracted from the proteins in samples 12-22. Then, the amino acid sequences of the remaining proteins were analysed to identify whether they have RFxV/I motif (Delpire and Gagnon, 2007). This led to the identification of 27 proteins that contain such motif (**Table 3.1**), but only 17 of which have a significant mascot

score 67 ($P < 0.05$) with at least 2 peptides matched, a criteria often used in analysing such mass spec data (**Table 3.1**) (Ohta et al., 2013).

Encouragingly, we were able to identify the WNK isoforms with high mascot scores WNK1 (830), WNK2 (144), WNK3 (89) and WNK4 (97). Since WNK kinases are established and verified as SPAK and OSR1 kinases' binders, the results gave us confidence in the outputs of this OSR1 IP experiment. Analysing the other positive OSR1 binders from this IP showed that the β2AR protein was not present. Nevertheless, several proteins whose functions are associated with the β2AR signalling have been identified. Indeed, several novel proteins were identified as possible binders to OSR1, most of which are related to molecular transport. These include ryanodine receptors 1, 2, and 3 (RYR), which are protein channels mediating Calcium (Ca) release from sarcoplasmic reticulum to cytosol and promoting cardiac contractility. These proteins have multiple RFxV motifs and have high mascot scores ranging from 101 to 1321 **Table 3.1**. RYR form homo-tetramers that create large ion-channels. Notably, RYR2 is mostly expressed in heart and it is regulated by PKA and Ca/calmodulin-dependent kinase-2, which phosphorylate of RYR at Ser2808, Ser2814 and Ser2030 as a result of βAR activation and cAMP elevation (Denniss et al., 2018). However, studying these proteins represents technical challenges as they have large molecular weights, human RYR1 (570 kD), human RYR2 (569 kD) and human RYR3 (557 kD).

Among the other protein hits identified from the OSR1 IP experiment was the anion related protein carrier known as the voltage dependent anion -selective channel protein (VDAC1), which has a Mascot score of 441 and VDAC3 which had a lower score of 42 (**Table 3.1**). Both VDAC1 and 3 contain an RFGI-motif that could enable OSR1 binding. VDAC1 is located at outer membrane of mitochondria, and it regulates

Ca transport in and out of the mitochondria (Shoshan-Barmatz et al., 2017a). Moreover, it controls the movement of numerous metabolites like succinate, malate and pyruvate between the mitochondria and the cytoplasm (Shoshan-Barmatz et al., 2017a). VDAC1 is also involved in several signalling and metabolic pathways though interaction to many protein proteins as thoroughly reviewed by Shoshan (Shoshan-Barmatz et al., 2017b). Remarkably, VDAC1 was found to be associated with the β2AR in proteomic analysis (Chung et al., 2013). Thus, our mass spec link between VDAC1 and OSR1 could provide a molecular mechanism of the proposed VDAC1 and β2AR signalling interplay.

Interestingly, the Na/K pump β1-sbunit and glucose transporter member-4 (GLUT4) were also identified to have RFDV and RFLI motifs respectively from the OSR1 IP (**Table 3.1**). The Na/K pump consists of α- and β-subunits and could link OSR1 to other ions regulating pathways such the β2AR. Activation of the β2AR elevates the cellular activity of the Na/K pump through the cAMP-PKA pathway in alveolar cells, and this activation was mediated by increased assembly of Na/K pump α-subunit in plasma membrane (Bertorello et al., 1999, Mutlu and Factor, 2008). As the β-subunit of this pump is the one that contains a RFxV/I motif, this indicates that OSR1 could bind the β-subunit, which is required for a fully functional Na/K pump (Xie et al., 2013). Due to the versatility of GPCRs, this could propose that the signal may be transduced from β2AR to Na/K pump α-subunit and β-subunit via the activation of PKA and OSR1 respectively.

GLUT4 enhances glucose entrance into muscle cells and adipocytes in response to insulin, where insulin stimulates GLUT4 trafficking to the plasma membrane through involvement of several proteins such as sortilin, VAMP2, IRAP and LRP1 (Bogan, 2012). Intriguingly, as mentioned earlier (**Introduction Part**),

hyperinsulinemia, systemic insulin resistance, is associated with increase salt reabsorption in kidney due to elevated activity of the WNK-SPAK/OSR1-NCC cascade (Nishida et al., 2012). This metabolic syndrome is also manifested by the disruption of glucose absorption as a result of reduction of GLUT4 in addition to down regulation of the β2AR in patients with cardiac complications of diabetes (Mishra et al., 2010).

Moreover, OSR1 could be linked with many other proteins that involved in several metabolic pathway which could be associated with the β2AR, such as Succinyl-CoA ligase, NADH-dehydrogenase and Acetyl-Co-A carboxylase-2 (Chung et al., 2013). These enzymes were found to have RFxV motif (**Table 3.1**) and showed high Mascot scores. This reveals the importance of OSR1 in the cell metabolism beside ion homeostasis. Altogether, this exercise did not only highlight the novel role of OSR1 in cellular processes but also encouraged our pursuit of the possible association of WNK-SPAK/OSR1 to the β2AR signalling pathway.

As mentioned above, the β2AR was not detected in our MS results despite the high Mascot score of OSR1 (1504) and the fact that MS is the method of choice for the identification of protein-protein interactions (Daulat et al., 2009). MS as a technique, however, has some limitations in identification of GPCR protein partners because of the low expression levels of β2AR in the heart as it consists only 20 % of βAR and obstacles of working with such proteins. This difficulty is also related to the structural features of the β2AR, which has high hydrophobicity and inherited flexibility that makes the receptor poorly extractable from native tissue and less soluble or misfolded in the solution, which ultimately reduces the receptor's interactions with its protein partners (Helbig et al., 2010, Rabilloud, 2009).

	Gel lane	Protein name	MW (kDa)	Mascot Score	Peptide Matches	Sequences coverage %	RFxV/I
	18	**Serine/threonine kinase (OSR1)**	58.46	**1504**	117	33	**/**
1 *	12	**Ryanodine receptor 2 (RYR2)**	569.64	**1321**	114	99	**RF[R/A][I/V]**
2	12	**Serine/threonine-protein kinase WNK1**	251.8	**830**	46	38	**RF[I/Q/S]V**
3 *	19	**Succinyl-CoA ligase beta subunit (SUCB2)**	47	**569**	28	20	**RFFV**
4 *	21	**Gap junction alpha 1 (CXA1)**	43.49	**563**	29	11	**RFWV**
5 *	22	**Voltage dependent anion-selective channel protein (VDAC1)**	32.5	**441**	21	13	**RFGI**
6 *	22	**NADH dehydrogenase (NDUA9)**	42.61	**404**	22	14	**RFRV**
	17	**STE20/SPS1-related proline-alanine rich kinase (SPAK)**	60.79	**203**	10	8	
7 *	12	**Spectrin beta chain erythrocytic (SPTB1)**	245.89	**200**	18	18	**RF[Q/D]I**
8	12	**Serine/threonine-protein kinase WNK2**	228.9	**144**	12	11	**RF[K/S]V**
9 *	19	**Sodium/potassium transport ATPase beta1 subunit (AT1B1)**	35.57	**138**	11	8	**RFDV**
10*	12	**Ryanodine receptor 3 (RYR3)**	556.9	**134**	21	19	**RF[A/W][V/I]**
11 *	22	**Serine/threonine-protein phosphatase (PP1B)**	37.9	**131**	7	5	**RFNI**
12 *	12	**Ryanodine receptor 1 (RYR1)**	570.38	**101**	16	16	**RFAV**
13	12	**Serine/threonine-protein kinase WNK4**	133.3	**97**	7	7	**RF[Q/T][V/I]**
14 *	12	**Acetyl-CoA carboxylase 2 (ACACB)**	277.96	**93**	12	11	**RF[V/F][V/I]**
15	12	**Serine/threonine-protein kinase WNK3**	195.4	**89**	9	9	**RFQV**
16 *	21	**Facilitated glucose transporter member4 (GLUT4)**	54.94	**90**	5	5	**RFLI**
17 *	21	**Creatine kinase M-type (KCRM)**	43.2	**51**	4	4	**RFCV**
18 *	21	**Phosphorylase B kinase gamma catalytic chain (PHKG1)**	45.3	**50**	3	3	**RFLV**
19 *	13	**Serine/threonine-protein kinase MRCK beta (MRCKB)**	196.5	**46**	4	4	**RFYI**
20 *	22	**Voltage dependent anion-selective channel protein (VDAC3)**	31	**42**	2	2	**RFGI**
21 *	13	**1-phopshatidylinositol 4,5 bisphosphate phosphodiesterase (PLCH2)**	189.6	**29**	9	9	**RFLV**
22 *	12	**E3 ubiquitin protein ligase (HERC2)**	533.9	**24**	11	11	**RF[L/M/T]I/V]**
23 *	19	**Glycerol kinase (GLPK)**	62	**22**	3	3	**RFLV**
24 *	15	**Inositol hexakisphosphate diphosphoinositol-pentakisphosphate kinase**	128.4	**22**	5	5	**RF[F/H]V**
25 *	12	**Ubiquitin-like modifier-activating enzyme 1 (UBA1)**	119	**16**	2	2	**RFEV**
26 *	13	**E3 ubiquitin protein ligase**	227	**16**	8	7	**RFVV**
27 *	12	**M-phase inducer phosphatase 3 (MPIP3)**	50.68	**14**	3	2	**RFYI**

Table 3.1: Identification of OSR1-associated proteins in the heart by mass spectrometry. *The labelled lanes in (**Figure 3.13**) were excised, and proteins were defined by mass spectral peptide mass fingerprint. The identified proteins that have > 67 mascot score (P < 0.05) and peptide match > 2, were considered to be significant. Proteins arranged according to their mascot score. (*) refers to the novel proteins that have identified in this study. Molecular weight (MW), RFxV/I-peptide; OSR1/SPAK binding motif. Results had been obtained from a single experiment (n=1).*

To overcome such difficulties, Kobilka's group developed a new strategy for mimicking cell membranes, where receptors are integrated in lipid bilayer environment, by the reconstitution and preparation of the β2AR in high density lipoprotein (HDL) molecules (Chung et al., 2013). This allows the reconstituted β2AR to be in a folded form and stabilised by insertions into the lipid bilayer to mimic its conformation and stability in vivo. These molecules were then utilized as a bait to attract protein partners from the lysate of bovine heart (Chung et al., 2013). Among the many proteins identified by MS to bind the reconstituted β2AR, endogenous SPAK was identified as a possible binder (Chung et al., 2013). Notably, in the Kobilka study, they did not further verify the β2AR interaction with SPAK and OSR1. Still, this finding strengthened our hypothesis that the β2AR interacts directly with SPAK and OSR1 kinases.

3.2.5 Identification the interaction of β2AR to SPAK in the heart:

Since the direct interaction between the β2AR and SPAK/OSR1 kinases was not confirmed by MS, we then moved on to the use of Western blot. Indeed, to further verify the Kobilka finding discussed above, we performed the IP of endogenous SPAK from mouse hearts that had been homogenized using two different lysis buffers, LB1 or LB2 (**Method Chapter**). The samples were then separated by SDS-PAGE and the proteins were identified by immunoblotting for endogenous β2AR. Encouragingly, no β2AR were detected in the empty beads (EB) lanes (**Figure 3.14**). Notably, the β2AR was detected at approximately 48 kD in both SPAK IP samples (**Figure 3.14**). Furthermore, β2AR seems to be highly dissolved in LB2 as its abundance was more than that in LB1. This confirms the fact that the interaction between SPAK/OSR1 and the β2AR takes place in biological systems. This IP result emphasized the molecular docking and peptides pulldown experiments which revealed that like RFQV-motif, the RFHV-peptide in this case, has the same binding affinity to SPAK/OSR1 CCT domain. Moreover, this result also supports previous literatures that demonstrated SPAK/OSR1 binding to their protein partners, NKCC, NCC and WNK isoforms, was mediated by the RFxV motif (Piechotta et al., 2002, Richardson et al., 2008).

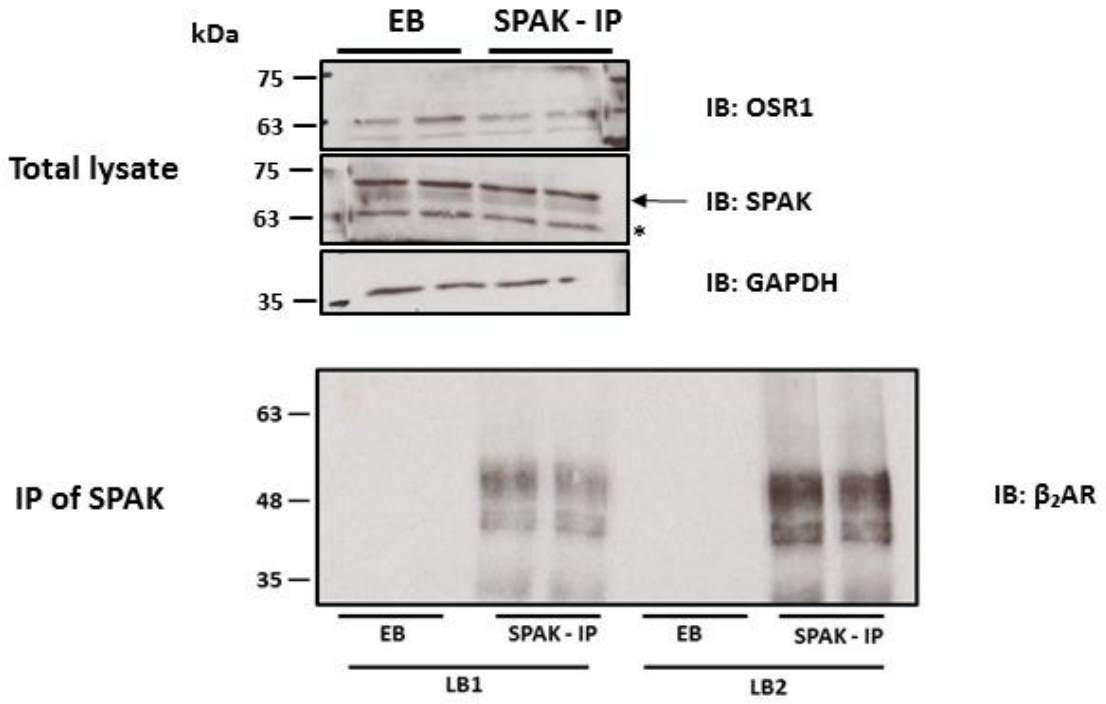

Figure 3.14: Western blot analysis of the β2AR binding to SPAK at endogenous level in mouse heart lysate. *To determine the solubility of receptors, mouse heart was harvested by two different lysis buffers, LB1 and LB2. Then SPAK protein was immunoprecipitated (SPAK-IP) by conjugated anti-SPAK antibody, samples were subjected to SDS-PAGE gel, and β2AR was probed by anti-β2AR antibodies. EB was negative control. Before IP was performed, the interested proteins were probed top blot, SPAK and OSR1 successfully identified, SPAK arrow indicated while (*) for non-specific bands most likely due to OSR1 cross reactivity. Please consider that mouse SPAK is ~ 10 kDa larger than human. GAPDH housekeeping protein. Abbreviations: Empty beads (EB). Lysis buffer1 and 2 (LB1) and Lysis buffer2 (LB2). The result was obtained from single experiment (n=1). GAPDH (1:5,000), SPAK (2 µg/ml), OSR1 (2 µg/ml), β2AR (1:500).*

3.2.6 The interaction of SPAK and the β2AR is mediated by RFHV-motif:

By inspecting the crystal structure of the human β2AR, it was noted that it contained a single RFxV-motif, (RFHV, residues 239 -242 at ICL3) (Rasmussen et al., 2007) which is a highly conserved sequence for binding SPAK/OSR1 kinases (Delpire and Gagnon, 2007, Villa et al., 2007). To validate the interaction of this GPCR with SPAK and provide evidence whether the interaction is mediated though the RFHV motif, FLAG-β2AR WT or FLAG-β2AR R239A were co-expressed with GST-SPAK full length in HEK293 cells. Furthermore, FLAG-NKCC2 WT full length, which contains the RFQV motif (RFQV, sequences 20-23) or NKCC2 R20A full length (where Arg20 was mutated to Ala) have been used as positive and negative controls respectively (**Figure 3.15**). To assess the interaction, overexpressed SPAK was isolated by GST-pull down and Western blotting with an anti-FLAG antibody was performed. The results showed that the β2AR-WT as well as NKCC2-WT did bind SPAK (**Figure 3.15**). However, this binding was abolished by single pointed mutation, β2AR R239A, although this mutation did not interfere with the receptor expression (**Figure 3.15**). Similarly, NKCC2 R20A reduced the binding as observed previously by others (Richardson et al., 2011). As noted, the β2AR monomers were around 48 kD while the top bands at about 100 kD could represent oligomeric and glycosylated forms of the receptor (**Figure 3.15**) (Ng et al., 2012, Mialet-Perez et al., 2004).

Depire's group have been demonstrated that SPAK/OSR1 interacted with NKCC1, NKCC2 and KCC3 through yeast 2 hybrid experiments, and the binding was confirmed by pulldown and co-immunoprecipitation assays which it took place through physiological docking of RFxV/I motifs of these co-transporters into CCT of SPAK/OSR1 (Piechotta et al., 2002, Villa et al., 2007, Vitari et al., 2006). And this docking was necessary for their phosphorylation and activation (Richardson et al.,

2011), and single pointed mutations within the motif not only abolished their binding, but also inhibited their subsequent phosphorylation (Gagnon et al., 2007b, Vitari et al., 2006). Herein, our pulldown revealed that the wild type of both NKCC2 and β2AR interacted with SPAK in biological system while a single point mutation of Arg20 and Arg239 of NKCC2 and β2AR respectively to Ala abolished their binding to SPAK and OSR1 kinases. This confirms the binding of SPAK to β2AR is principally mediated through docking of RFHV-motif in to the primary pocket of SPAK CCT.

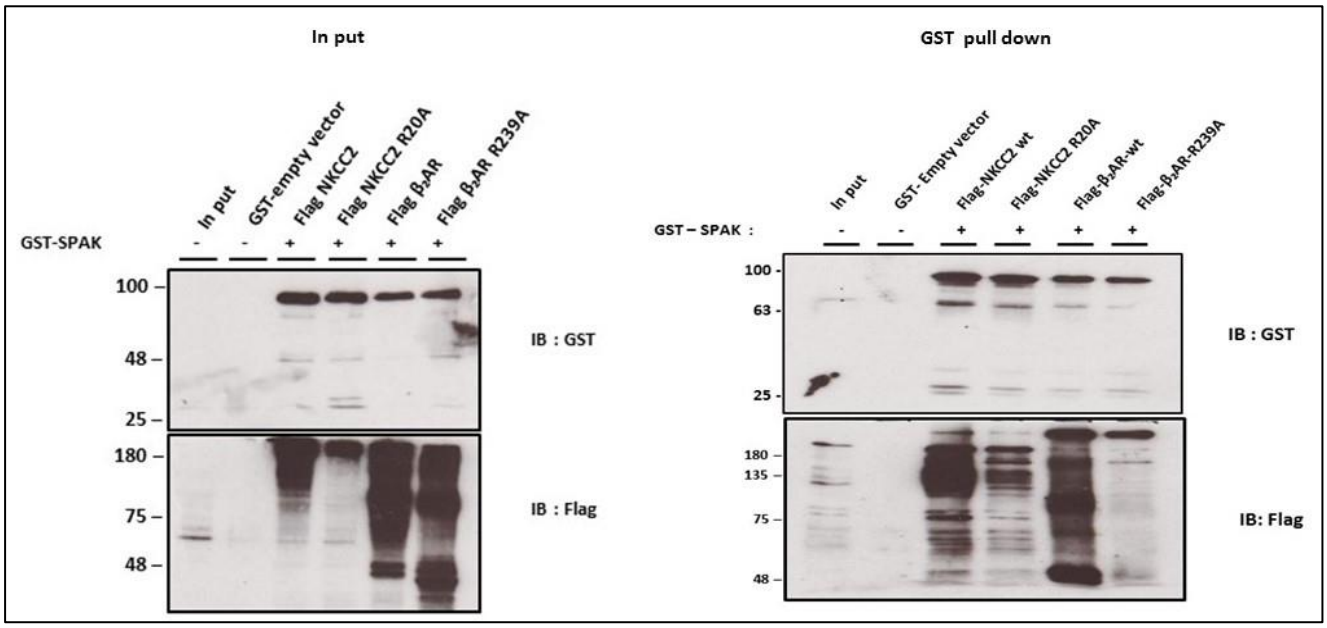

Figure 3.15: The molecular binding of SPAK to β2AR is mediated by RFHV-motif. *HEK293 cells were transiently co-transfected with GST-SPAK and either with FLAG-NKCC2-WT, FLAG-NKCC2-R20A, FLAG-β2AR-WT or FLAG-β2AR-R239A. 48 hrs post-transfection, cells were harvested by LB1 and LB3 (for β2AR solubilization), then collected lysates (input) were subjected to SDS-PAGE and IB where GST-tagged and FLAG-tagged proteins were probed by anti-GST and anti-Flag antibodies respectively for confirming their expression (left blot). (Right blot) shows GST-SPAK purification by GST pulldown assay, and FLAG-tagged proteins were detected by anti-FLAG antibody. FLAG-NKCC2-WT and FLAG-β2AR-WT bind to GST-SPAK (lanes 3 and 5), while mutation of R to A of RFxV-motif of both proteins reduces the interaction significantly (lanes 4 and 6). Lanes 1 and 2 were negative controls total cell lysate (input) and GST-empty vector (GST) respectively. Same results have obtained in three independent experiments (n=3). GST (1:1,1000), FLAG (1:1,000).*

3.2.7 Characterization of the β2AR interaction to SPAK CCT domain:

To explore the interaction of the β2AR to SPAK/OSR1 CCT domain in more details and to validate whether the docking of the β2AR's RFHV-motif takes place in the primary pocket of SPAK/OSR1 CCT domain. A competition experiment was conducted where HEK293 cell were co-transfected with FLAG-β2AR-WT and GST-SPAK and following cell lysis the lysates were cleared by incubation with empty GST beads. Then, RFQV-peptide or AFQV-peptide were added to compete the binding of overexpressed FLAG-β2AR to overexpressed GST-SPAK (**Method Chapter**). To assess the interaction, GST-SPAK was isolated by GST beads pulldown assay in the absence or presence of the peptides and pulled down material underwent Western blotting for the β2AR using ant-FLAG antibody. Untransfected and GST-empty vector transfected cells were used as negative controls. The results showed that FLAG-β2AR interacted with GST-SPAK further confirming our previous studies, while the addition of the RFQV peptide prevented such binding (**Figure 3.16).** The AFQV peptide, as anticipated, did not inhibit the binding of SPAK to the β2AR (**Figure 3.16).** This is in line with previous studied where such mutations was shown to make the peptide incompatible for binding to OSR1 and SPAK CCT domains (Vitari et al., 2006). In the same context, surface plasmon resonance (SPR) analysis and pulldown assays utilizing numerous single point mutations in RFQV peptide revealed that the RFQV and RFxV peptides have similar affinity to OSR1 CCT domain (Vitari et al., 2006). This further indicates that the β2AR's RFHV peptide is able to interact with SPAK/OSR1 and could be competed out by the WNK RFQV peptide. Moreover, it was demonstrated that SPAK/OSR1-binding peptides inhibited the binding of endogenous NKCC1 to those enzymes by a competition mechanism as NKCC1 contains two RFxV-motifs (Vitari et al., 2006, Villa et al., 2007). As the β2AR has a single RFHV sequence,

the RFQV peptide was sufficiently able to inhibit the binding. However, the RFHV binding to SPAK was also abolished by the AFQV peptide though why this occurred in this case remains unclear. Overall, this set of results further supports out hypothesis that the β2AR binds SPAK and OSR1 kinases by the docking of the receptors RFHV motif into SPAK and OSR1 kinases' CCT domains akin to how WNK kinases bind SPAK and OSR1 kinases (Vitari et al., 2006).

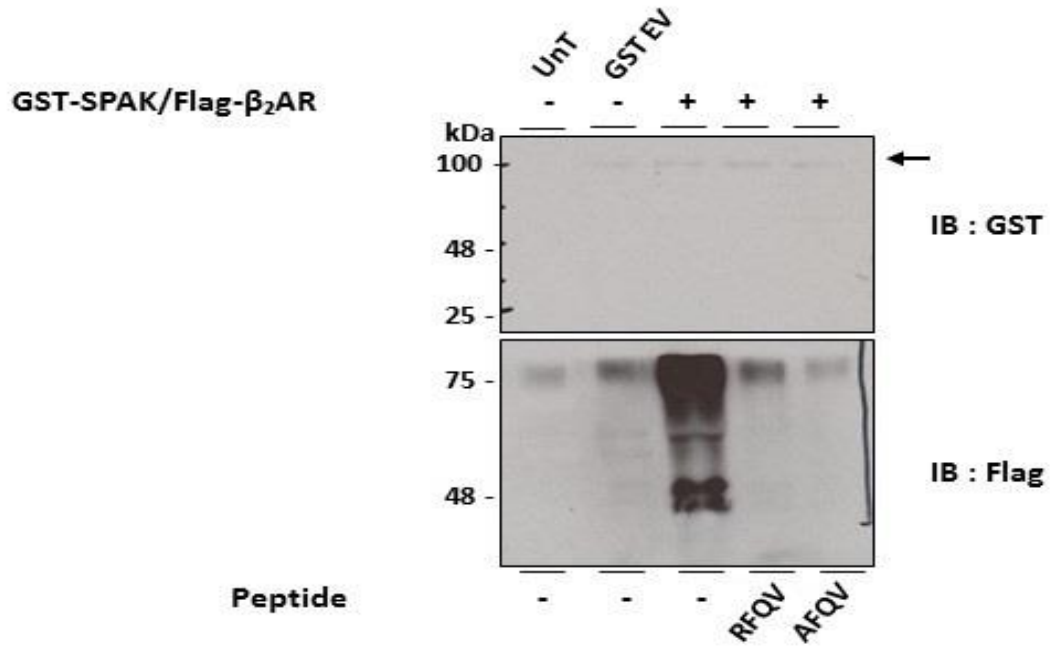

Figure 3.16: RFQV-peptide competes the binding of overexpressed FLAG-β2AR to GST-SPAK. *Representative IB demonstrates the effect of RFQV and AFQV-peptides on SPAK-β2AR interaction. HEK293 cells were co-transfected with GST-SPAK and FLAG-β2AR. 48 hrs post transfection cells were lysed, and 1 mM RFQV or AFQV were added to 500 µg cell lysate. GST pulldown assay was performed to assess the interaction between SPAK and β2AR. Anti-FLAG antibody was used to probe the receptor, FLAG-β2AR bound to GST-SPAK in absence of peptide (lane3), adding RFQV prevent the binding as well as adding AFQV which was unexpected. Experiment was done nine times (n=9). Arrow indicates GST-SPAK expression. Abbreviation: UnT, un-transfected cells. GST-EV, GST-empty vector. GST (1:1,1000), FLAG (1:1,000).*

3.3 OSR1 phosphorylates the β2AR in vitro:

SPAK and OSR1 kinases phosphorylate their substrates, e.g. NKCC1, NKCC2 and NCC, by docking the RFxV motifs of these ion co-transporters into SPAK and OSR1 CCT domains. After the interaction between SPAK/OSR1 and the β2AR has been established, we explored whether SPAK and OSR1 kinases phosphorylate the β2AR *in vitro*. To do this, we overexpress FLAG-β2AR WT and FLAG-β2AR R239A in HEK293 cells performed their pulldown using anti-FLAG antibody and used them in SPAK and OSR1 in vitro kinase assays.

After the conjugated antibody was added to 1 mg HEK293 cell lysate at the indicated concentrations (**Figure 3.17**), the samples were incubated and then washed and prepared for SDS-PAGE. Several controls were used, the negative controls were untransfected total lysate, IP from untransfected lysate and empty beads. The positive control was total lysate of β2AR WT transfected cells. The result indicated the successful immunoprecipitation of β2AR WT as the receptor was detected at ~ 50 kD in IP sample where the ratio of antibody: cell lysate with 30 µg: 1 mg ratio showing the least of the receptor quantity being pulled down as compared to 5,10 and 20 µg of antibody to 1 mg of cell lysate. Subsequently, 10 µg antibody to 1 mg of cell lysate was used.

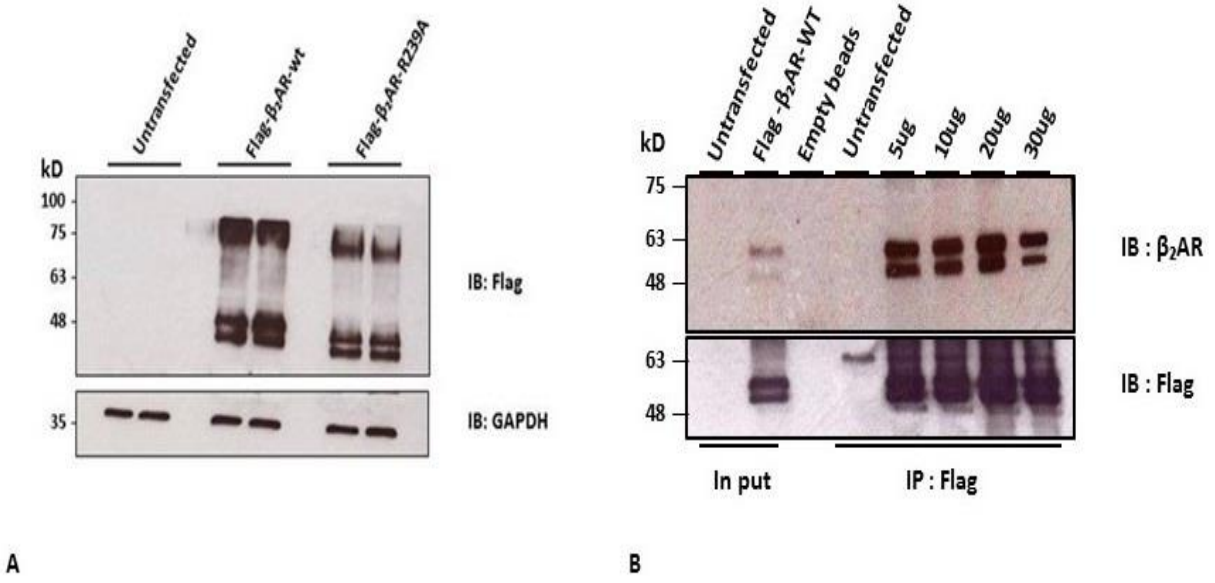

Figure 3.17: Western blot demonstrated the expression and immunoprecipitation of FLAG-β2AR in HEK293 cells. *(A) HEK293 cells were left un-transfected or either transiently transfected with FLAG-β2AR-WT or FLAG -β2AR-R239A. Then cells were harvested with LB3 and samples were subjected to SDS-PAGE and expressed proteins were probed by anti-FLAG antibody that shown a great specificity as no bands were observed on un-transfected cells (lane 1) and receptors were detected on wild type (WT) and mutant samples (lane 2 and 3) at MW 48 and 75 kD which represented monomeric and dimeric receptors respectively. (B) FLAG-β2AR-WT was immunoprecipitated with anti- FLAG antibody from 1 mg cell lysate. The ratio of antibody: cell lysate concentrations have been optimized, antibody concentration started with 5 µg to 30 µg while cell lysate was 1 mg (lane 5 to 8). Also, IP was done from un-transfected cells (lane 4) which was used as negative control beside the empty beads, that were utilised to identify non-specific bound proteins. Another, controls have been also used to determine antibody efficiency and specificity, for this purpose total cell lysates of un-transfected and transfected (input) have been used. The immunoprecipitated proteins were probed by both anti-β2AR (top blot) and anti-FLAG (bottom blot). This experiment was preformed once (n = 1), to determine the best concentration of anti-FLAG antibody to be used for IP of FLAG-β2AR. GAPDH (1:5,000), FLAG (1:1,000), β2AR (1:500).*

To explore whether the β2AR could be phosphorylated by SPAK/OSR1, an *in vitro* OSR1 ADP-Glo™ kinase assay (Zegzouti et al., 2009) was carried out where the immunoprecipitated WT and mutant β2AR were washed and prepared as substrates for the reaction. The constitutively active GST-OSR1 T185E, where threonine (T) 185 was mutated into glutamic acid (E) to mimic WNK1 phosphorylation, and the scaffolding protein MO25 were expressed and purified from *E. coli* (Filippi et al., 2011). Moreover, cation chloride co-transported peptide (CATCHtide), a stretch 198-217 of human NKCC1 (Vitari et al., 2006), was also used as positive SPAK and OSR1 peptide substrate.

As shown in **Figure 3.18 A**, OSR1 T185E phosphorylated β2AR WT with a similar phosphorylation efficiency the SPAK and OSR1 peptide substrate CATCHtide. Interestingly, a single pointed mutation of R239A in OSR1-binding motif of β2AR reduced significantly the phosphorylation of the receptor by about 45 % (**Figure 3.18**). This suggested that the docking of the β2AR RFHV-motif into OSR1-CCT domain is not only crucial for the binding to OSR1 but it also important for receptor phosphorylation.

Although OSR1-T185E has ability to phosphorylate CATCHtide which devoid of RFxV-motif, the integrity of binding motif is crucial in the phosphorylation of RFxV containing substrates (Vitari et al., 2006). It was previously reported in comparison analysis between CATCHtide and NKCC1(1-260), RFQV-motif containing protein, that OSR1-T185E truncated CCT-domain was able to efficiently phosphorylate CATCHtide while NKCC1(1-260) was poorly phosphorylated (Vitari et al., 2006). Moreover, the phosphorylation of NKCC1, NKCC2 as well as NCC by SPAK/OSR1 was dependent on RFxV/I motif docking into their CCT domains and the phosphorylation of these co-transporters had been strikingly reduced by mutation of the R to A at their RFxV/I-

motif. This highlighted the importance of the RFxV to both the binding and the phosphorylation of endogenous substrates (Moriguchi et al., 2005, Richardson and Alessi, 2008, Richardson et al., 2011, Vitari et al., 2006). In agreement with this, our results where OSR1 regulates the phosphorylation of human β2AR *in vitro*, and this phosphorylation is mediated by the β2AR's RFHV-motif binding to the OSR1 CCT-domain. Interestingly, we also demonstrated that a single individual mutation R239A in this motif results in a significant reduction in the phosphorylation of the receptor.

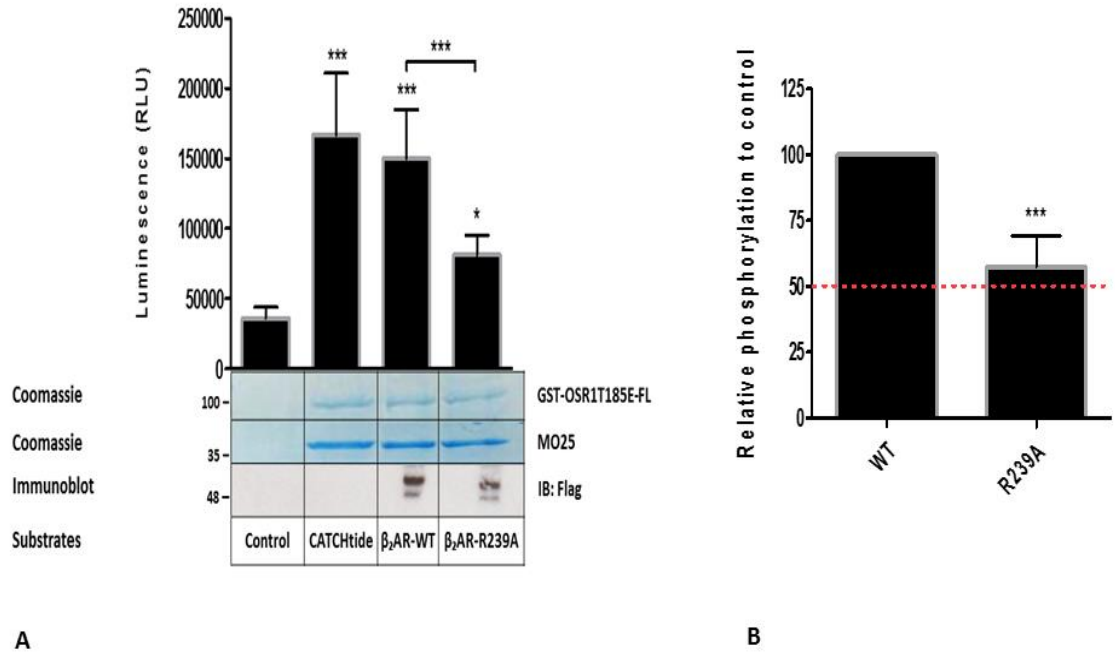

Figure 3.18: ORS1-T185E phosphorylates β2AR WT and R239A mutation reduces its phosphorylation in vitro. *Representative ADP-Glo™ kinase assay of 250 µM CATCHtide, 10 µg β2AR-WT and 10 µg β2AR-R239A. Substrates were incubated with OSR1T185E and MO25α for 30 min. Luminescence was detected by plate reader. (A) β2AR-WT (lane 3) was phosphorylated similarly to CATCHtide (lane 2) by OSR1-T185E. The control (lane 1) was CATCHtide in kinase buffer in absence of OSR1. B) Data of β2AR-R239A in (A) was normalized to β2AR-WT (WT), to stress the significant decrease of β2AR phosphorylation by R239A mutation. Results represent mean ± SD of triplicate samples from three independent experiments (n =3). P value was calculated by ANOVA with post-Bonferroni's test in (A) and Student's t-test in (B). P < 0.05 was determined as statistical significance. *** P value < 0.0001 and ** P value < 0.0025. Red dotted line in (B) indicates 50 % of maximum phosphorylation activity. FLAG (1:1,000).*

In order to further validate the phosphorylation of the β2AR is dependent on the catalytic activity of OSR1 T185E, we performed an in vitro kinase assay to which Verteporfin (VP), a SPAK and OSR1 kinase inhibitor, was added (AlAmri et al., 2018). VP is used clinically as a therapy of diabetic retinopathy and tumours (Scott and Goa, 2000). Firstly, we investigated the inhibitory effect of VP on OSR1-T185E activity using NKCC2 WT (1-174) as a substrate (**Figure 3.19**). The results revealed that NKCC2 (1-174) phosphorylation was inhibited by VP in a dose-dependent manner.

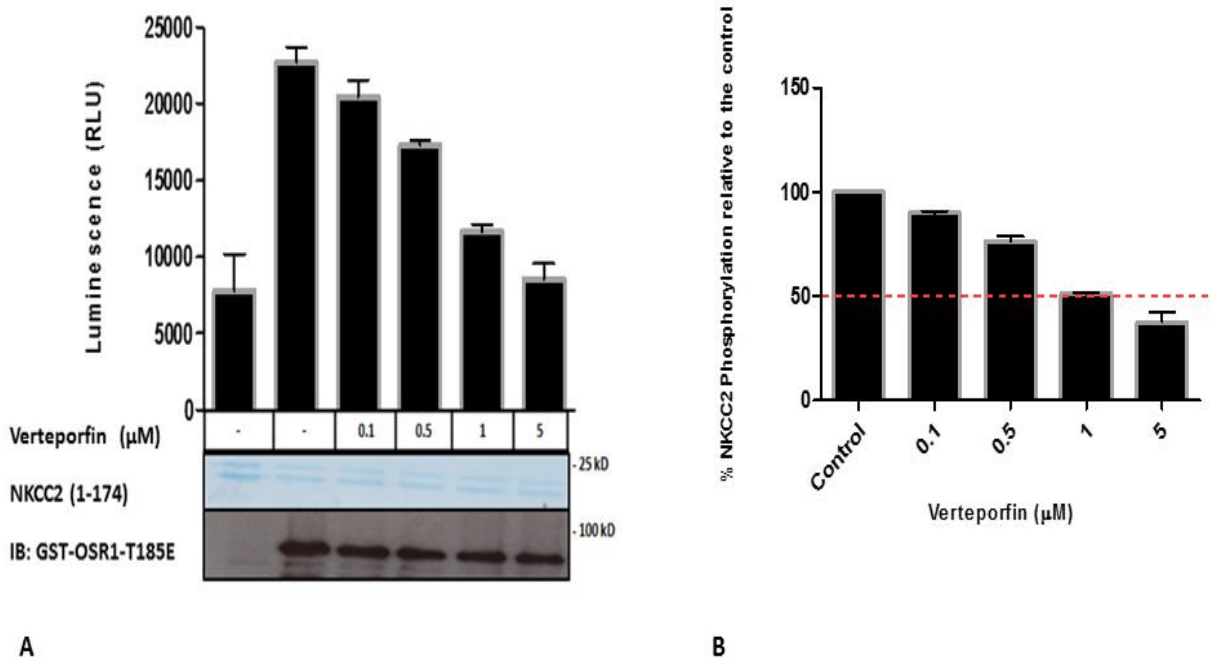

Figure 3.19: Verteporfin inhibition of OSR1-T184E In vitro kinase assay.

In vitro ADP-Glo™ kinase assay showing the inhibition effect of Verteporfin (VP). (A) 5 μM NKCC2 (1-174) was incubated either alone (lane 1) or with 0.4 μM GST-OSR1-T185E in absence of VP (lane 2) or in presence of the drug in indicated doses (lanes 3-6), which resulted in a dose dependent reduction of the catalytic activity of OSR1-T185E. B) Normalised data in (A) to the control (without VP, lane 2 in A). All data represent mean ± SD of triplicate samples from single experiment (n = 1). Arrow indicates NKCC1 (1-174) in Coomassie Blue stain. Red dotted line in (B) indicates 50% of maximum kinase activity. GST (1:1,000).

After validation of the VP inhibitory effects on OSR1 T185E kinase activity in vitro, we run the kinase assay of using the β2AR as a substrate and a parallel assay that employs NKCC2-(1-174) as control (**Figure 3.20**). Notably, the assay was run in the absence or presence of 5 µM VP. Interestingly, the results revealed a noticeable phosphorylation of both NKCC2 and β2AR and this phosphorylation was completely inhibited by the OSR1 kinase inhibitor VP. Even though the β2AR could be phosphorylated by several protein kinases such PKA and GRK (Rosenbaum et al., 2009), our results suggest that it could also be phosphorylated by OSR1 though this still needs to be confirmed in cells and *in vivo*.

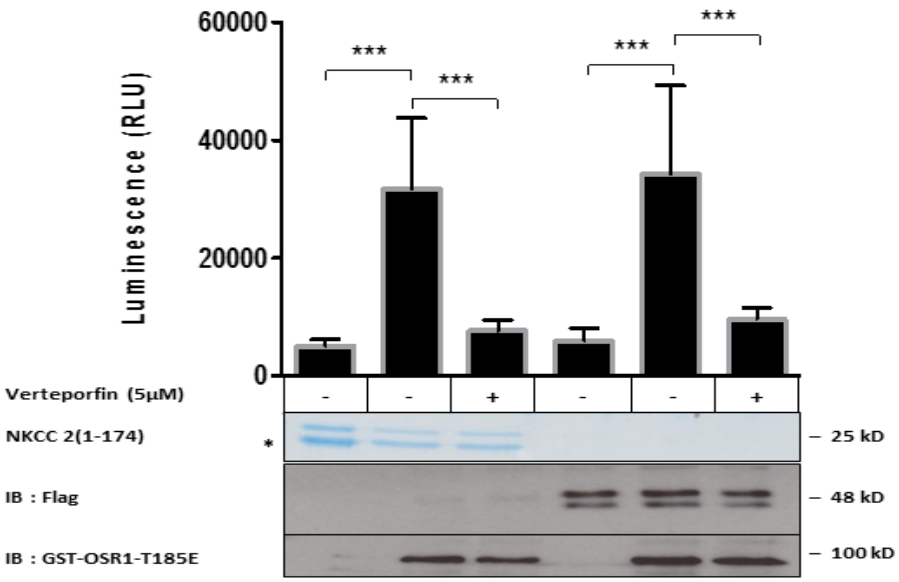

Figure 3.20: In vitro phosphorylation of β2AR by OSR1-T185E and inhibition by VP. *In vitro ADP-Glo™ kinase assay of NKCC2 (1-174) and FLAG-β2AR-WT were incubated with GST-OSR1-T185E without or with presence of 5 µM VP. Similar phosphorylation of NKCC2 (1-174) and β2AR-WT was observed with OSR1T185E, while 5 µM VP interestingly reduced the phosphorylation significantly. All data represented in mean ± SD of triplicate samples from three independent experiments (n=3). ANOVA with post-Bonferroni's test was performed for statistical analysis. ***P value<0.0001 and **P value<0.0025. Arrow in Coomassie Blue stain indicates NKCC2 (1-174). The dotted red line indicates 50 % of maximum kinase activity. FLAG (1:1,000), GST 1:1,000).*

3.4 Binding of the β2AR does not alter the catalytic activity of SPAK and OSR1 kinases:

In this section, the effect of the β2AR binding to OSR1 on its catalytic activity was examined. Specifically, a series of in vitro kinase assays were performed in the absence or presence of the β2AR's RFHV or AFHV peptides. The kinase assays employed bacterially expressed OSR1 T185E and the CATCHtide or NKCC2 (1-174) as substrates. The results demonstrated that the addition of the β2AR's RFHV peptide did not have any substantial effect on OSR1 T185E's ability to phosphorylate CATCHtide (**Figure 3.21 A** and **B**). A similar result was observed with the sample supplemented with the AFHV peptide instead of the RFHV peptide. This suggests that the docking of the β2AR's RFHV motif itself into the OSR1 CCT domain does not affect the catalytic activity of the enzyme though it is needed for their binding (**Figure 3.15**).

To further confirm that the RFHV peptide does not alter OSR1 kinase activity but rather it competes with binding of the substrate, a kinase assay that uses the NKCC2 (1-174), which contains an RFQV motif, was carried out. Surprisingly, similar results as to the ones observed with the CATCHtide were noted in this experiment as there was no variation between OSR1's ability to phosphorylate NKCC2 (1-174) either without or with RFHV peptide (**Figure 3.21 C** and **D**). Notably, this is contrary to what was observed when studying WNK and NKCC2 binding to SPAK and OSR1 kinases since the authors demonstrated that the RFQV and RFXV peptides reduce dramatically the phosphorylation of NKCC1 (1-260) while CATCHtide phosphorylation has not been affected (Vitari et al., 2006). We probably did not reach the same conclusion as previous work because we used *N*-terminally biotinylated peptides RFHV peptides and this may have lower binding affinity to OSR1 CCT as compared to the untagged peptide. Overall, these experiments showed that the β2AR's RFHV

motif binding to OSR1 does not regulate affect its kinase activity but may influence the binding of substrates that possess a RFXV-motif.

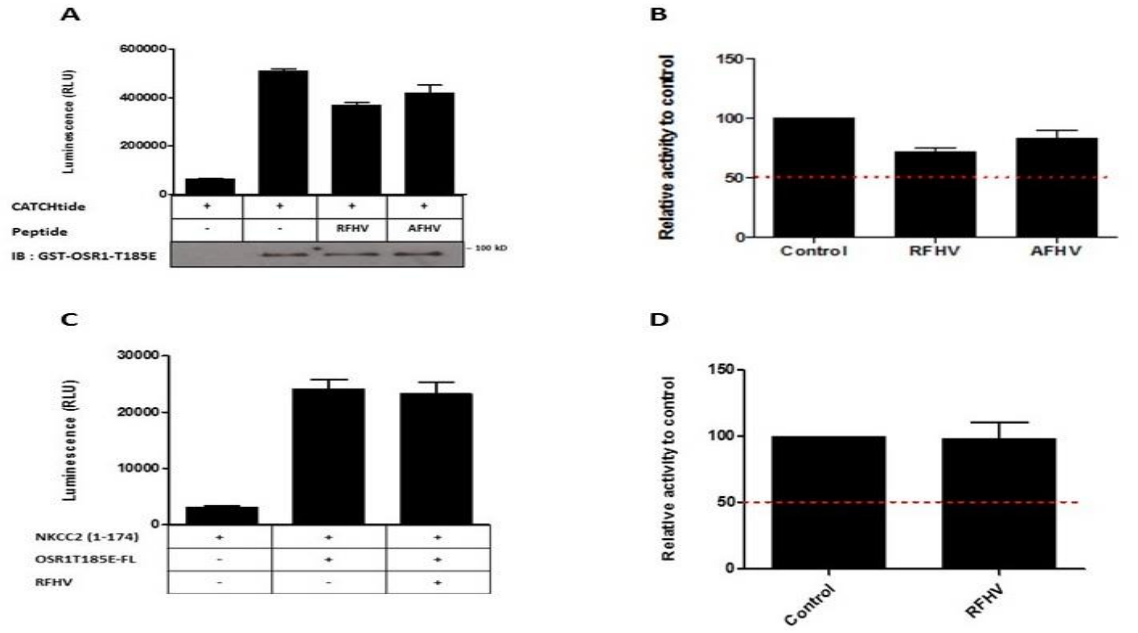

Figure 3.21: RFHV-peptide does not alter OSR1-T185E activity in vitro. *In vitro ADP-Glo™ kinase assay demonstrated the effect of RFHV-biotinylated peptide on OSR1 activity. (A) 250 μM CATCHtide and 0.4 μM GST-OSR1-T185E were incubated either with/without 1mM of indicated [R/A]FHV-peptide at 30˚C for 30 min. Then the phosphorylation was determined. The phosphorylation of CATCHtide has not been affected by either RFHV or AFHV-peptides which revealed that RFHV-derived β2AR peptide binding does not alter the catalytic activity of the kinase. (B) Data in (A) are presented as relative to control i.e. un-treated samples (lane 2). No significant reduction of OSR1 kinase activity was detected. (C) Same reaction in (A) however NKCC2(1-174) was used instead, no alteration of OSR1 activity was also observed with RFHV addition. (D) Normalized RFHV data to control. All results represented as mean ± SD for triplicate samples. Results shown have been obtained from single experiment (n=1). The red dotted line in (B) and (D) represented to 50 % enzymatic activity.*

3.5 SPAK/OSR1-independent internalization of β2AR in hypotonic stress:

Like most GPCRs, the β2AR has a typical feature of rapid deactivation and internalization following agonist binding (Han et al., 2012). This rapid attenuation is mediated by PKA, PKC and GRK phosphorylation of certain Ser/Thr residues in receptor's cytoplasmic domains. Phosphorylated β2ARs fully uncoupled from protein-G when and associate with β-arrestin which interact with clathrin to initiate the receptor's endocytosis (Iyer et al., 2006). At this stage, the β2AR trafficking is considerably regulated by post-endocytic ubiquitination or deubiquitination mechanisms that ultimately result in either its degradation or recycling respectively (Han et al., 2012).

As we have shown that OSR1 kinases phosphorylate the β2AR in vitro as discussed above, we studied the effect of SPAK and OSR1 activation in cells on the internalisation of the β2AR. For this, HEK293 were transfected with FLAG-β2AR WT and cell surface proteins were quantified by enzyme linked immunosorbent assay (ELISA) or flow cytometry while biotinylated proteins were probed by immunoblotting (Lam et al., 2013)

3.5.1 Identification by Western blotting:

To determine if HLB activated SPAK/OSR1 is involved in the internalization of the β2AR, HEK293 cells transfected with FLAG-β2AR WT were left untreated, as negative control, or treated with HLB, to activate WNK-SPAK/OSR1 signalling, or Iso to activate the β2AR signalling and lead to the receptor's internalisation. Also, STOCK1S-50699 (St), a SPAK/OSR1 kinase inhibitor, Propranolol (Pro), non-selective βAR antagonist or ICI (Nasrollahi-Shirazi et al., 2016, Kitagawa et al., 1995), were used. Cell surface proteins were labelled with biotin as reported (Cao et al.,

2005) and described in the **Method Chapter**). This was followed by lysis and streptavidin pulldown and Western blotting (**Figure 3.22**).

HLB triggers WNK-SPAK/OSR1-NKCC1 signalling cascade, as indicated by phosphorylation of endogenous NKCC1 at *N*-terminal regulatory residues Thr 203, Thr 207 and Thr 212, also SPAK/OSR1 phosphorylate another key residue Thr217 which it was not explored in this work. It was reported that Thr 212 and Thr217 are fundamental residues for NKCC1 function, because mutations of either of these two residues significantly inhibited the activation of the transporter by hyper- or hypotonic stress (Gagnon et al., 2007b, Richardson and Alessi, 2008). Notably, St is strongly able to prevent the phosphorylation of these NKCC1 residues by inhibition of WNK1-mediated SPAK/OSR1 activation (de Los Heros et al., 2014). As illustrated in below figure, Iso caused agonist-mediated receptor internalization approximately 55 % of total membrane β2AR ($P < 0.001$) (**Figure 3.22 A,** lane 4), which it was principally inhibited by Pro and ICI (lanes 5 and 6). The activation of β2AR signalling pathway was monitored by probing the phosphorylation of LKB1 at Ser428, which only was observed with addition of Iso alone.

Simultaneously, like Iso effect, HLB interestingly induced a significant reduction of surface β2AR ($P < 0.001$) (**Figure 3.22 A** lane 2). Interestingly, St failed to prevent the internalization of β2AR (lane 3), suggesting that this receptor downregulation by HLB is nether dependent on SPAK/OSR1 catalytic activity, nor related to the SPAK/OSR1-mediated receptor phosphorylation. Because St capable to inhibit both WNK-induced and self-intrinsic SPAK/OSR1 catalytic activity (AlAmri et al., 2017a), subsequently St blocked the phosphorylation of β2AR by these kinases.

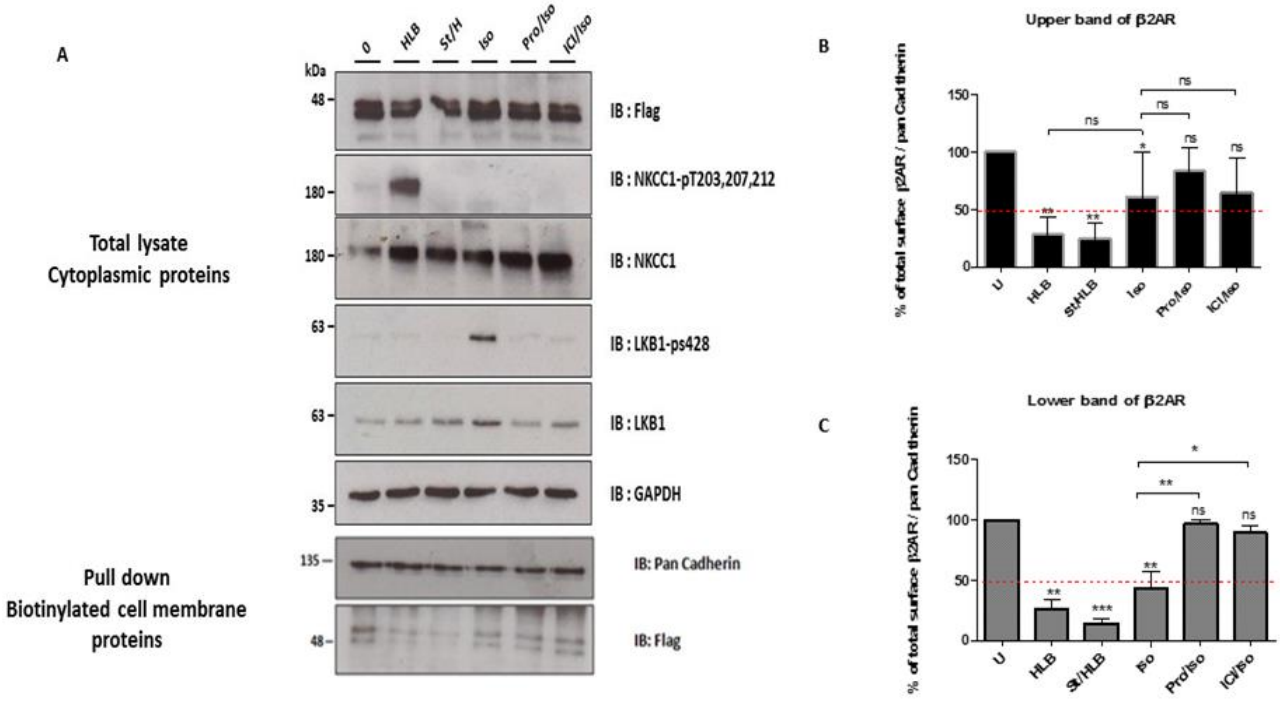

Figure 3.22: Internalization of β2AR by hypotonic low chloride buffer (HLB) independent of SPAK/OSR1 activity. *(A) HEK293 cells were transfected with FLAG-β2AR, 48hrs post-transfection, cells were left un-stimulated (U) or treated with HLB or 1μM Isoproterenol (Iso) alone or pre-treated with 10 μM STOCK1S-50699 (St), 1 μM Propranolol (Pro) or 1 μM ICI118551 (ICI). All pre-stimulation was for 1 hr and cells stimulation was for 1 hr. HLB activates WNK-SPAK/OSR1-NKCC1 signalling (lane 2) as denoted by phosphorylation of Thr203, Thr207 and Thr212 residues and it surprisingly internalizes β2AR. This down regulation is SPAK/OSR1 independent (lane 3) which it had don't been prevented by St. Iso produces phosphorylation of LKB1 at Ser428 and internalizes β2AR which inhibited by Pro and ICI. (B) and (C) are cumulative optical density (COD) data represented of cell membrane FLAG- β2AR which was normalised to Pan Cadherin. (B) COD data of top band of FLAG- β2AR while (C) was of lower band of FLAG- β2AR. Both bar graphs illustrating 70 % and 55 % reduction of surface β2AR with hypotonic stress and Iso respectively. Results represented as mean ± SD of two independent experiments (n = 2), and samples were normalized to untreated cells (U). Red line represented the 50 % of total cell membrane receptors. One-way ANOVA test was performed and ***P < 0.0001, **P < 0.001, *P < 0.05 and ns; no significant. FLAG (1:1,1000), NKCC1 (2μg/ 1ml), ps-NKCC1(2μg/ 1ml), LKB1 (1:1,000), LKB1pSer428 (1:1,000), GAPDH (1:5,000), Pan cadherin (1:1,000).*

As SPAK/OSR1 activity is involved in regulation of several membrane proteins (Rodan and Jenny, 2017), it was not surprising that the activated SPAK/OSR1 elevate the amount and activity of ion channels such CCC as well as potassium channels (KCNE1) (Elvira et al., 2015). However, on the other hand, this SPAK/OSR1 activity could be a negative regulator of other channel proteins such as Ca-stimulated K channels (Elvira et al., 2016), Cl channels (CLC-2) (Warsi et al., 2014), CFTR (Yang et al., 2011) and ROMK1 (Elvira et al., 2014). Intriguingly, the catalytic activity of protein kinases may not be essential for the internalisation of membrane proteins. For instance, it was reported that the role of WNK1 and WNK4 kinases in the internalization of ROMK1 was independent of their catalytic activity as they acted just as scaffolding proteins that bound both intersectin and ROMK1 to enable ROMK1 internalization by clathrin (He et al., 2007). Thus, the role of both SPAK and OSR1 kinases, and maybe WNK kinases, in the β2AR internalization by HLB maybe mediated by a scaffolding effect rather than their kinase activity.

Our finding that under hypotonic conditions, the β2AR gets internalised is in itself a novel finding that has not been previously reported in the literature. Saying this, it has been demonstrated that GPCRs are highly sensitive to mechanical disturbance or fluidity alteration of cell membrane, which lead to the receptor's conformational changes and subsequent agonist-independent activation (Chachisvilis et al., 2006). Due to the fact that the hypotonic shock does not only stimulate WNK-SPAK/OSR1 signalling, but it also induces influx of osmotic water into the cell and that causes cell swelling and increases the tension of plasma membrane therefore stimulation of GPRCs. Moreover, by assuming an agonist induces 100 % activation of GPCRs, various membrane disordered stimuli have been investigated and results revealed that hypotonicity, benzyl alcohol and shear stress cause GPCRs activation by 23 %, 9 %

and 14 % respectively (Chachisvilis et al., 2006). Thereby, the mechanical stimulation of the β2AR may also play a role in receptor internalization in addition to the direct effect of hypotonicity. In contrast to hypotonic stress, hypertonicity such as exposure to sucrose or hypertonic media stabilizes GPCRs, and these stimuli lead to drastic decrease of the formation of clathrin coated pit with a loss of lattice characteristic of clathrin (Heuser and Anderson, 1989). In contrast to this, hypotonicity may induces receptor down regulation by affecting on similar pathway that is involved in sucrose stabilization. These observations indicate that the β2AR internalization is affected by several factors other than phosphorylation including ions perturbations that make the internalisation mechanism so complicated.

Additionally, in this experiment NKCC1 phosphorylation by the β2AR stimulation could be addressed. It was reported that NKCC1 activity increased in response to stimuli other than osmotic stress such as norepinephrine, calyculin, phosphatase 1 and 2 inhibitors, or fluoride in a study assessing whether the co-transporter phosphorylation was mediated by a single kinase (Lytle, 1997). Phospho-mapping results demonstrated that the four mentioned stimuli promoted phosphorylation of similar serine/threonine residues at *N*-terminus, which led to the suggestion that NKCC1 was at least regulated by two different kinases (Lytle, 1997). A subsequent study by Darman and Forbush showed that three *N*-terminal Thr residues were phosphorylated by PKA after activation by forskolin, an adenylate cyclase activating drug (Darman and Forbush, 2002). Interestingly, these residues were Thr184, Thr189 and Thr202 in shark NKCC1 sequences, which are equivalent to Thr212, Thr217 and Thr230 in human NKCC1 sequences (Darman and Forbush, 2002, Richardson and Alessi, 2008). Based on this, there were two shared residues, Thr212 and Thr217, between the two different signalling pathways (WNK-SPAK/OSR1

and cAMP/PKA cascades) (Gagnon et al., 2007b, Richardson and Alessi, 2008), which could indicate that SPAK/OSR1 is a kinase that may be involved in the two signalling pathways (**Figure 3.22**).

Interestingly, our results revealed that Iso-activated β2AR did not induce phosphorylation of NKCC1, at least on the SPAK/OSR1-dependent sites, more specifically at the key Thr212 (**Figure 3.22 A**). Despite this Iso-mediated NKCC1 phosphorylation has been noted previously as NKCC1 phosphorylation and abundance were found to be elevated in Iso-perfused rat tissues such as parotid salivary gland, trachea and crypts cells of colon (Flemmer et al., 2002, Russell, 2000).

3.5.2 Quantification of the surface β2AR:

To further assess the internalization of the β2AR by HLB and whether it is SPAK/OSR1-dependent phenomenon, a quantification of the surface β2AR was performed. First, flow cytometric analysis was carried out where HEK293 cells were transiently transfected with FLAG-tagged β2AR. The cells were then stained with FITC-labelled antibodies. The non-specific fluorescence was determined by secondary only labelled cells as reported (Cao et al., 2005, Nasrollahi-Shirazi et al., 2016). The cells were then analysed by fluorescent activated cell sorting (FACS) flow cytometry and the data was analysed by FlowJo (Alvarez et al., 2010).

As an optimization step, the detection of receptor expression was first examined. Encouragingly, the receptors were identified with significant levels of expression ($P < 0.05$) (**Figure S3**) though some cells were poorly labelled. Then, several attempts of optimization steps were performed but there were insufficient cells labelling because of poor antibody FLAG-epitope interaction. Though the median

fluorescent intensity (MFI) showed a little reduction of surface β2AR with Iso and HLB treatment, which was SPAK/OSR1 independent, the histogram plot revealed insignificant reduction of surface receptors by the indicated compounds (**Figure S4**). Numerous repeats had been done on this experiment, but the same results were obtained because of poor cells labelling or unhealthy cells. Due to resources and time limitations, the progress with this FACS interrogation of the β2AR internalisation was not continued.

However, we alternatively pursued the β2AR internalisation with ELISA, which had to be developed and optimized. In this assay, the extracellular FLAG epitopes of *N*-terminus FLAG-β2AR WT was targeted. To evaluate the internalization of the receptor with and without WNK-SPAK/OSR1 activation, transfected HEK293 cells were cultured in 96-well plates. The cells were then left untreated (control), pre-incubated with St or Pro for 1 hr before stimulation with HLB or Iso for 1 hr. The subsequent absorbance reading revealed that HLB (**Figure 3.23**) induced a reduction in the surface β2AR and St, a SPAK/OSR1 inhibitor, appeared to have no effect on this internalization. This suggested that the β2AR internalisation process may be SPAK/OSR1-independent mechanism, which is in agreement with the Western blot data shown in **Figure 3.22**. Moreover, Iso as expected induced about 30 % reduction of the total surface β2AR (**Figure 3.23**) through the established clathrin- and dynamin-mediated endocytosis (Han et al., 2012). Pro completely blocked the Iso-induced internalization of the β2AR due to its antagonism of the receptor.

These results revealed a novel effect of HLB by producing β2AR stimulation and internalization in an agonist-independent mechanism, a process that appears to be independent of SPAK and OSR1 kinase activity though a non-enzymatic role of WNK kinases and SPAK/OSR1 could not be ruled out. The HLB-mediated

internalisation of the β2AR that we observed points towards an internalisation mechanism that is related to the internal milieu ions disturbance, which could lead to the stimulation of several signalling pathways that regulate receptors trafficking and recycling.

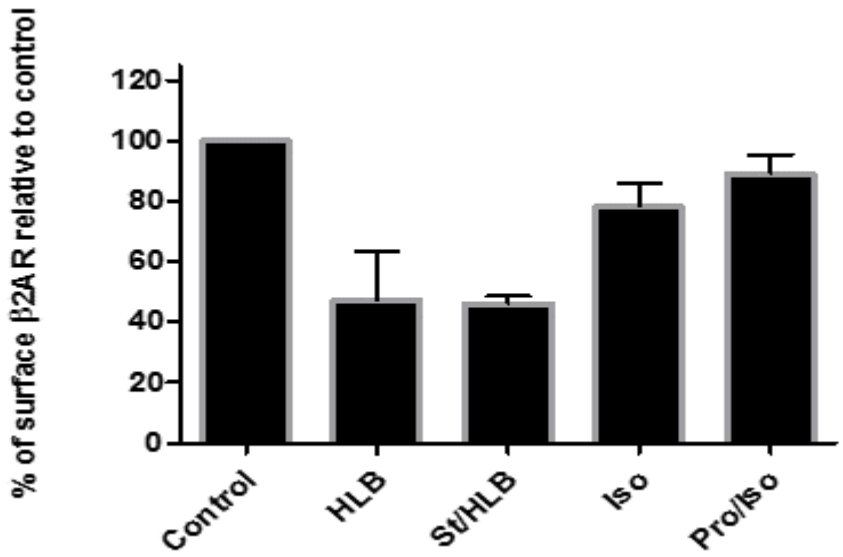

Figure 3.23: SPAK/OSR1-independent internalization of β2AR by hypotonic stress. *HEK293 cells were transfected with FLAG-β2AR-WT, then cells were plated in coated 96-well plate. Cells were labelled with mouse IgG1 anti-FLAG antibody, then they were either left rested (control) or pre-treated with 10 μM St or 1 μM Pro. Then cells were stimulated by HLB or 1 μM Iso for 1 hr. After Alkaline phosphatase (AP) conjugated anti-mouse antibody and p-nitrophenyl phosphate disodium (PNPP) substrate were added, then the absorbance was read by plate reader. HLB internalized β2AR via SPAK/OSR1 independent mechanism, as approved by addition of 10 μM St. Moreover, hypotonic stress is showing a stronger internalization effect than Iso. Data represented in mean ± SD of triplicate samples from a single experiment (n = 1).*

3.6 Stimulation of the β2AR does not phosphorylate SPAK Ser373:

Since the WNK-SPAK/OSR1 plays a vital role in salt homeostasis through regulation of ion co-transporters, the regulation of this signalling cascade has gained considerable attention. Beside the dietary salt modulation of WNK-SPAK/OSR1 signalling pathway, hormonal effects were also reported (Sohara and Uchida, 2016). Numerous hormones such as angiotensin-2 (Ang2), vasopressin (Vas), insulin and aldosterone have been found to activate this signalling cascade in the kidneys (Sohara and Uchida, 2016). Additionally, sympathetic system (SPS), which is significantly involved in regulation of renal salts reabsorption, has also been implicated in the regulation of WNK-SPAK/OSR1 signalling (DiBona, 2005). Moreover, it was found that norepinephrine and Iso infusion in mice induced HPT by reduction of renal Na excretion along the DCT (Greven and Heidenreich, 1975, Mu et al., 2011).

A subsequent study showed that this elevation of BP was mediated by upregulation of NCC via chronic stimulation of the β2AR, which reduced the suppression effect of WNK4 on SPAK/OSR1 by inhibiting WNK4 expression (Fujita, 2014, Mu et al., 2011). However, the direct link between β2AR stimulation and SPAK/OSR1 kinases has not been previously investigated. Thereby, in this part, the stimulatory effect of the β2AR by the epinephrine analogue (Iso) on SPAK has been explored.

In cultured HEK293 cells, SPAK is activated under osmotic stress by WNKs phosphorylation primarily at its T-loop Thr233 (Richardson and Alessi, 2008, Richardson et al., 2008). WNK kinases also phosphorylate SPAK at Ser373 and although this phosphorylation does not lead to the direct activation of the kinase, its often used as a readout of the kinase activity since the antibodies for pSer373 are much cleaner than those of pThr233 (Richardson and Alessi, 2008, Richardson et al.,

2008). Interestingly these two residues were found also to be phosphorylated by Ang2 through a WNK4 dependent pathway (Castaneda-Bueno et al., 2012). This observation was made after noting that the phosphorylation of these two sites was preluded by losartan, a competitive angiotensin receptor type 1 (AT1) blocker (San-Cristobal et al., 2009, Castañeda-Bueno et al., 2012). Accordingly, SPAK phosphorylation at Ser373 has been analysed following the activation of the β2AR by Iso. To do this, HEK293 cells were transfected with FLAG-β2AR. 48 hours post-transfection, the cells were treated with increasing doses of Iso, from 10 picomolar (pM) up to 10 micromolar (µM), for 60 minutes (min). The negative control in this case was the unstimulated cells (NS) (**Figure 3.24**). Surprisingly, the data revealed that β2AR stimulation may not phosphorylate SPAK Ser373 residue, even at 300 nanomolar (nM) or higher, however it could phosphorylate other sites than Ser373 (**Figure 3.24**). Also, there was not obvious alteration of total SPAK at the highest dose of Iso used, 10 µM in this case. Phosphorylation of LKB1 at Ser428 represented the activation of PKA as a result of triggering of the β2AR signalling pathway by Iso (**Figure 3.24**).

The phosphorylation of SPAK at Thr233 residue is crucial because this residue is the main on/off switch for the enzymatic activity in response to WNK activation (Vitari et al., 2005). As the phosphorylation of Thr233 and Ser373 residues is observed simultaneously in WNK mediated activation (San-Cristobal et al., 2009), using SPAK Ser373 phosphorylation as a single readout in this experiment is sufficient for WNK-induced SPAK activation. Nevertheless, several endeavours for optimizing anti-SPAK pT233 detection were performed, no success was achieved, and this is consistent with what is known in the field in term of the lack of a powerful anti-SPAK pT233 antibody (**Figure S5 A**).

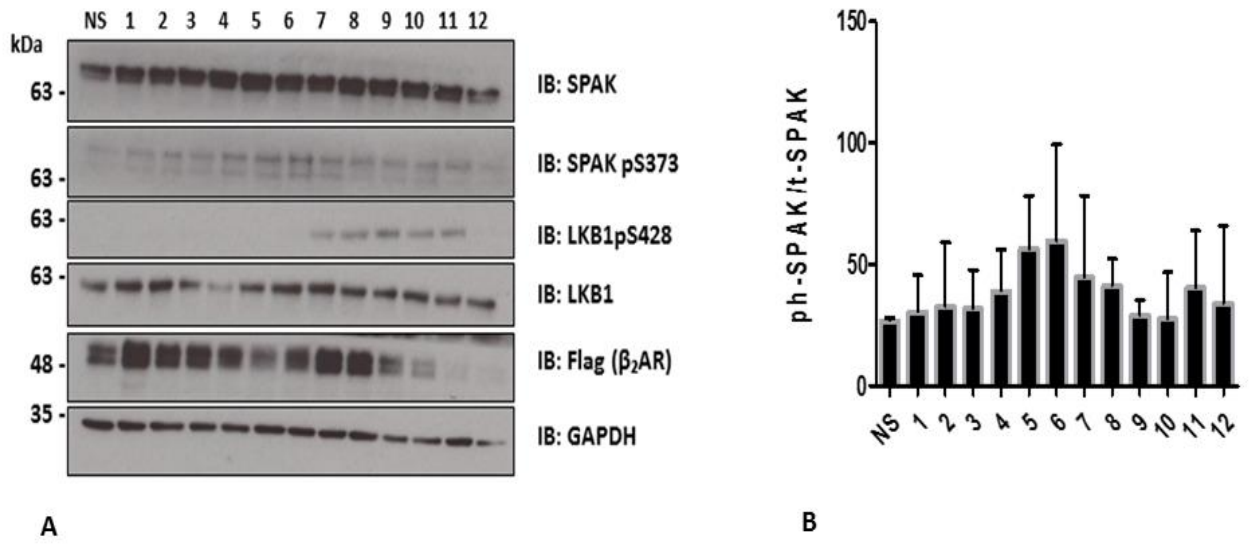

Figure 3.24: No effect of Isoproterenol stimulation of β2AR on SPAK-Sre373. *(A) Immunoblotting analysis of SPAK phosphorylation following β2AR activation in HEK293 cells. Cells were transfected with FLAG-β2AR-WT. 48 hrs post-transfection cells were left not-stimulated (NS) or stimulated with Iso in dose-dependent manner, started from 10 pM up to 10 μM for 1 hr. No changes have noticed either in SPAK phosphorylation at Ser373 or in its abundance. (B) Densitometry analysis of SPAK phosphorylation in (A), the quantification analysis also revealed that β2AR activation may not phosphorylate SPAK-Ser373. Results presented mean ± SD of two separate experiment (n = 2), P value was also calculated by ANOVA with post-Bonferroni's test (P value = 0.9249), it is not statistically significant, (significant P < 0.05). Abbreviations: (NS) not-stimulated. 1- 10 pM. 2- 30 pM. 3- 100 pM. 4- 300 pM. 5-1 nM. 6- 3 nM. 7- 10 nM. 8- 30 nM. 9- 100 nM. 10- 300 nM. 11- 1 μM. 12- 10 μM. SPAK (2 μg/ml) SPAK-pSer373 (2 μg/ml), LKB1-pSer428 (1:1,000), LKB1 (1:1,1000), FLAG (1:1,1000), GAPDH (1:1,000).*

Our results revealed that β2AR activation may not phosphorylate SPAK at Ser373 residue which may indicate that WNK kinases are not activated, although WNK-1 activated OSR1 phosphorylates β2AR *in vitro* (**Figure 3.18** and **3.20**). Nevertheless, this does not exclude the possibility of SPAK to be phosphorylated by a kinase other than WNKs during β2AR activation. For instance, Ganon and Delpire demonstrated that four protein kinase C isoforms possess SPAK/OSR1 binding motif and only two of which, PKCδ and PKCθ, have been experimentally explored and

verified to bind SPAK to date (Gagnon and Delpire, 2012). SPAK was found to be associated to PKCθ in naïve Jurkat T-lymphocytes and this association was increased by cells stimulation with anti-CD3/CD28 (Li et al., 2004). Moreover, PKCθ had the ability to phosphorylate mouse SPAK in an *in vitro* kinase assay at Ser321 and Ser335 (Gagnon and Delpire, 2012, Li et al., 2004), where the major phosphorylation residue Ser321 corresponds to Ser311 in the human sequence. Interestingly, this phosphorylation site is essential in receptor-induced SPAK activation to stimulate the transcription factor AP-1 in T-cells (Li et al., 2004).

In the same context, PKCδ mediates the regulation of NKCC1 through either hormonal or hyperosmotic stress in alveolar epithelium (Smith et al., 2008). Three independent studies showed that SPAK was as downstream kinase of PKCδ in the regulation of NKCC1 activation under hyperosmotic stress (Gagnon and Delpire, 2012). Although a subsequent study showed that SPAK phosphorylation by PKCδ was confirmed both *in vitro* and *in vivo*, the exact residues of SPAK that get phosphorylated by PKCδ have not been identified (Smith et al., 2008). Additionally, PKCα and PKA activate WNK4-SPAK/OSR1-NCC signalling pathway as response to activation by Ang2 and Vas (Gagnon and Delpire, 2012). That takes place by the phosphorylation of WNK4 directly at multiple Ser sites (Ser47, Ser64, Ser1169, Ser1180 and Ser1196). Notably, Ser64 and Ser1169 promoted the kinase catalytic activity, which subsequently led to phosphorylation and activation of both SPAK and NCC (Castañeda-Bueno et al., 2017). Furthermore, PKC induces the phosphorylation of KLHL3 at Ser433, which resulted in an inhibition of WNK4 interaction to and degradation by KLHL3 (Shibata et al., 2014). Thus, the levels of WNK4 and NCC were elevated (Shibata et al., 2014). Hence, several cellular mechanisms could control the total levels and activity of SPAK and OSR1 kinases.

Given that the previous study shown in **Figure 3.24** was performed at a single time point treatment of 1 hr, we performed the same study using different time points. The aim of this was to assess whether chronic stimulation of the β2AR may induce phosphorylation of SPAK at Ser373. The data shown in **Figure 3.25** revealed that short (5 min) and long (up to 72 hr) of persistent activation of the β2AR did not lead to phosphorylation of SPAK Ser373. This suggested that the Iso-stimulated β2AR may not lead to the phosphorylation of SPAK at Ser373. Therefore, the phosphorylation of SPAK Thr233 should be investigated. Moreover, it would be interesting if phospho-mapping of SPAK was carried out following Iso-stimulation to identify whether SPAK gets phosphorylated in any other residues. Because of various signalling events that take place following the activation of the β2AR, which include the activation of both PKA and PKC through the elevation of cAMP, it is likely that SPAK could be phosphorylated by either direct or indirect phosphorylation by WNK kinases or other protein kinases.

It is worth noting that when these experiments were being carried out, the cells appeared to be stressed as judged by the high expression levels of stress proteins including SPAK (**Figure S5 B**). The reasons for this were unclear. Hence, the alteration of SPAK/OSR1 via the β2AR activation was difficult to probe. Because of resources and time restrictions, some questions in this study remained unresolved, specifically, the effect of β2AR stimulation on SPAK/OSR1 activation and quantity. It would be interesting if this work had continued for in depth MS studies that could identify novel phosphorylation sites on both SPAK/OSR1 and β2AR after activation of either signalling pathway. Furthermore, another important experiment could be done that examines the effect of acute and chronic inhibition of the β2AR by Propranolol on SPAK/OSR1 abundance and phosphorylation.

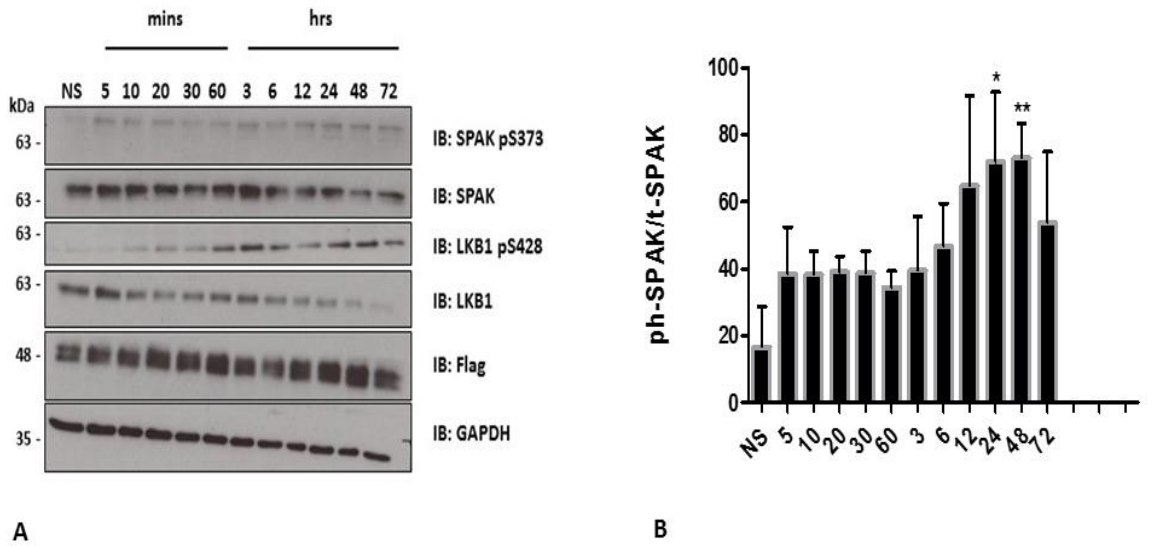

Figure 3.25: Chronic β2AR stimulation does not induce SPAK-Ser373 phosphorylation. *(A) Immunoblotting analysis of SPAK-Ser373 phosphorylation following β2AR activation in transfected HEK293 cells. Cells were treated with iso for indicated time course up to 3 days (72 hrs) and no SPAK-Ser373 phosphorylation has been detected however that does not exclude the possibility of SPAK phosphorylation by β2AR in other site than Ser-373 as demonstrated in densitometry analysis in (B). This phosphorylation may reach the maximum on 24 and 48 hrs. Results presented in mean SD from three independent experiments (n=3). ** P value < 0.0025, *P value < 0.05 was calculated by ANOVA with post-Bonferroni's test. SPAK (2 µg/ml), SPAK-pSer373 (2 µg/ml), LKB1-pSer428 (1:1,000), LKB1 (1:1,1000), FLAG (1:1,1000), GAPDH (1:5,000).*

3.7 Exploring the proposed β2AR-SPAK/OSR1-NKCC2 signalling pathway

SPAK and OSR1 mediate NKCC2 and NCC activation by GPCRs in TAL and DCT (Morla et al., 2016). For instance, vasopressin (Vas), a hormone secreted by hypothalamus, induces salt and water reabsorption in the kidneys through activation V2 receptors in TAL and DCT (Morla et al., 2016, Nonoguchi et al., 1995). The V2 receptors are coupled with G_s proteins that elevate cAMP, which in turn activates PKA (Morel et al., 1982). Through these signalling events Vas increases Na reabsorption by enhancing NKCC2 and NCC membrane trafficking in TAL and DCT respectively (Morla et al., 2016, Rieg et al., 2013). Interestingly, this Vas activation of NKCC2 and NCC is intermediated by SPAK/OSR1 activation and not by direct PKA phosphorylation (Ares et al., 2011a, Morla et al., 2016). Recent reports have demonstrated that Vas induces SPAK and OSR1 phosphorylation in both TAL and DCT (Saritas et al., 2013). Therefore, this indicates that SPAK/OSR1 could play a role as a second messenger of GPCRs activation in the regulation of NaCl homeostasis.

As such, exploring the effect of β2AR stimulation ion the activation of NKCC2 was required. To do this, HEK293 cells were transfected with FLAG-NKCC2 (1-174). 48 hrs post-transfection, they were pre-incubated first with 10 µM WNK463 (WNK kinases inhibitor), 10 µM St, 1 µM ICI for 1 hr, and then they were stimulated with HLB or Iso for another 1 hr. The results showed that HLB activation led to the phosphorylation of NKCC1 at Thr203, Thr207 and Thr212 by WNK-activated SPAK/OSR1, as expected, and this activation was inhibited by WNK463 and St (**Figure 3.26**). Interestingly, Iso treatment did not lead to the activation of NKCC1 but when combined with HLB it seemed to enhance the phosphorylation of NKCC1 (**Figure 3.26**). The phosphorylation of NKCC2, however, was only detected under Iso-treatments and not HLB alone. Intriguingly, this phosphorylation was not inhibited by

ICI or the WNK kinases inhibitor, WNK463. The inhibition of NKCC2 was only achieved by the treatment of the SPAK/OSK1 kinase inhibitor St. Furthermore, LKB1 S428 phosphorylation by PKA was inhibited by Pro and not by WNK463 and St. Together, this suggested that the observed NKCC2 phosphorylation was WNK- and PKA-independent but involved SPAK and OSR1 kinases.

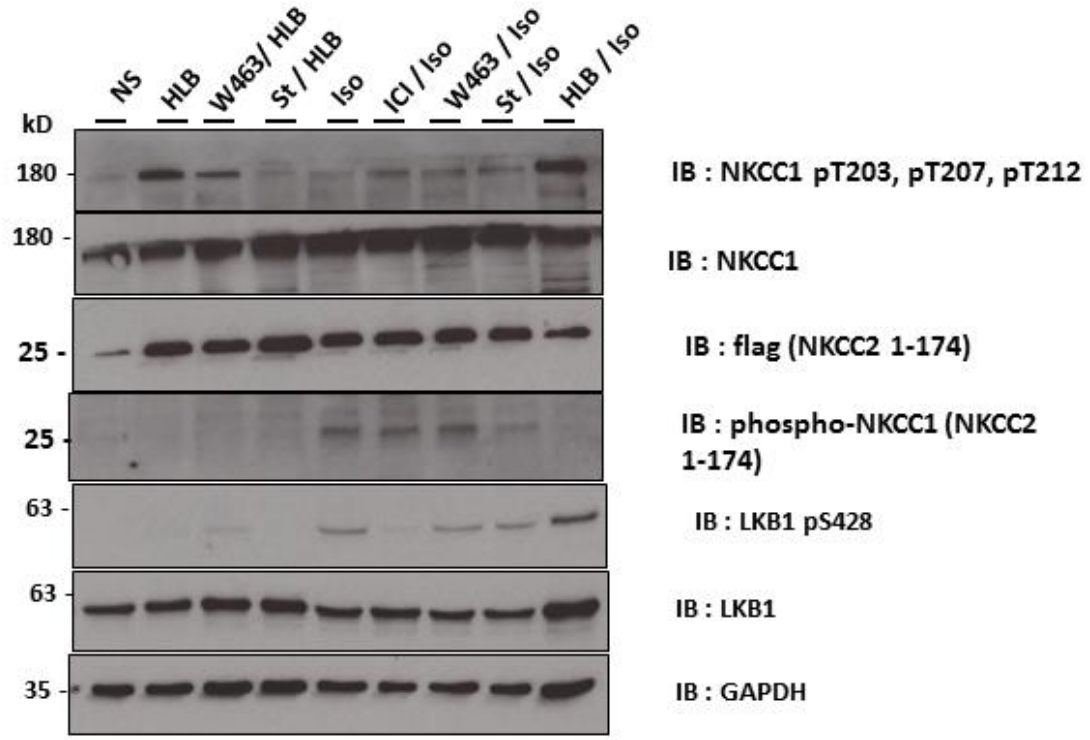

Figure 3.26: Immunoblotting analysis of NKCC2 phosphorylation during βAR activation. *HEK293 cell were transiently transfected with FLAG-NKCC2 (1-174). 48 hrs post-transfection cells were pre-incubated with 10 µM WNK463 (WNK kinases inhibitor), 10 µM St, 1 µM ICI for 1 hr, then cells were stimulated with HLB or Iso for another 1 hr. Weak phosphorylation of NKCC2 was observed, as detected by anti-NKCC1-phophoThr antibodies which recognised with Iso treated cells and did not either respond to ICI blocking or WNK463 but it responding to St pre-treatment. The result represents single experiment (n=1). NKCC1-pT (2 µg/ml) NKCC1 (2 µg/ml), LKB1-pSer428 (1:1,000), LKB1 (1:1,1000), FLAG (1:1,1000), GAPDH (1:5,000).*

For more elucidation and to verify the signalling pathway that stimulates these Thr residues of NKCC2 (1-174), which are known to be stimulated by SPAK/OSR1, several efforts were performed using co-transfected HEK293 cells with FLAG-NKCC2 (1-174) and FLAG-β2AR. Following transfection, the cells were pre-treated with WNK463 (W), St, ICI, Pro, or CGP-20712 (a selective β1AR blocker) (CGP) for 1 hr. Subsequently, the cells were stimulated with either Iso or HLB (**Figure 3.27**). The results showed that the only phosphorylation that was detected was that of LKB1 and in this case it was in most of the samples with overexpressed FLAG-β2AR. Such phosphorylation may be an artificial effect as it is known that overexpression of some GPCRs could cause activation of protein kinases, PKA in this case, which phosphorylated LKB1 at S428. The probing of phosphorylation of NKCC2 at Ser92, Thr 105 and Ser130 was carried out beside NKCC1 phosphorylation, but because of either poor protein transfer during Western blot or antibody issues, the results varied significantly and were not consistent to support drawing of any conclusions. Moreover, the detection of the over-expressed β2AR was difficult in all samples because of an antibody artefact. Several attempts of optimization and characterization of phospho-NKCC-2 antibodies were conducted, but these were not successful within the timeframe of this work.

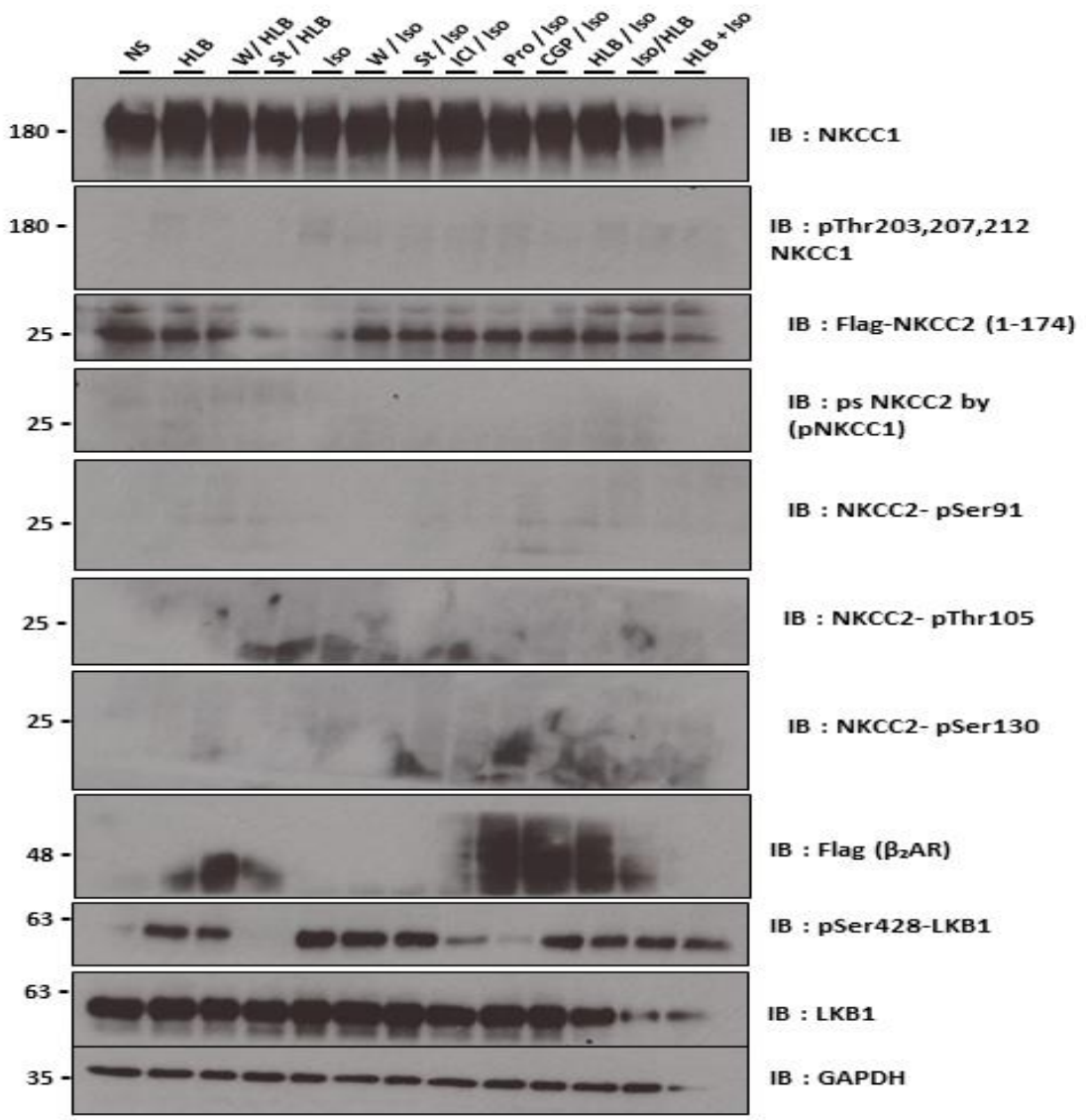

Figure 3.27: Immunoblotting analysis of NKCC2 phosphorylation during β2AR stimulation. *HEK293 cells were co-transfected with flag-NKCC2 (1-174) and FLAG-β2AR. After transfection, they were pre-treated with 10 μM WNK463 (W), 10 μM St, 1 μM ICI, 1 μM iso, 1 μM Pro or 1 μM CGP20712 for 1 hr, then they were stimulated with HLB or Iso for 1 hr. No NKCC2 or NKCC1 phosphorylation were detected. The only detectable phosphorylation was LKB1 which was unexpectedly stimulated by HLB, the figure obtained from single experiment (n=1). Please note that this experiment has been repeated at least four times to detect NKCC2 phosphorylation at Ser91, Thr105, and Ser130 but without success. NKCC1-pT (2 μg/ml) NKCC1 (2 μg/ml), LKB1-pSer428 (1:1,000), LKB1 (1:1,1000), FLAG (1:1,1000), GAPDH (1:5,000). NKCC2 pSer91 (2 μg/ml), NKCC2 pT105 (2 μg/ml), NKCC2 pSer130 (2 μg/ml).*

Chapter 4 : Final conclusions and future work

Since discovering the genetic link between WNK kinases and hypertension in the early 2000s, great advances have been made in dissecting the WNK-signalling pathway. Among the key discoveries was the identification of SPAK and OSR1 kinases as the physiological substrates of WNKs and the subsequent finding that these regulate the function of cation chloride co-transporters (CCCs). To date, almost all of the studies relating to WNK-signalling have focused on its ability to modulate the function of CCCs.

At the molecular level, WNK kinases binding to SPAK and OSR1 kinases was found to be mediated by the binding of the highly conserved SPAK and OSR1 CCT domains to RFxV/I tetrapeptide sequences that are present in the human WNK isoforms. Indeed, such interaction was also noted as being responsible for the binding of SPAK and OSR1 kinases to the CCCs, which also possess RFxV/I tetrapeptide sequences. Equipped with this information, we discovered that the human β2-adrenergic receptors (β2AR) contains an RFHV tetrapeptide sequence (aa. 239-242). This indicated that the β2AR may also bind SPAK and OSR1 kinases. Thus, in this work, we sought to verify and confirm the binding of SPAK and OSR1 kinases to the β2AR as well as determine the effects of such binding on the WNK- and β2AR-signalling.

In the present work, we successfully showed that the β2AR-derived RFHV peptide binds to the endogenous SPAK in HEK293 cell lines, an observation that was made following the use of peptide pulldown assays. Additionally, the binding of overexpressed SPAK and OSR1 kinases to overexpressed β2AR in HEK293 cells was

confirmed by GST-tagged protein pull down and by competition assays where adding the WNK's RFQV peptide competed out the β2AR's RFHV binding to SPAK and OSR1 kinases. Furthermore, we also showed that SPAK and OSR1 binding to the β2AR was inhibited by mutating the arginine residue on the β2AR's RFHV motif to AFHV or by single point mutations on SPAK and OSR1 CCT domains. Together, these experiments provided the first evidence of SPAK and OSR1 direct binding to the human β2AR.

Subsequently, we showed that the constitutively active OSR1 was able to phosphorylate the human β2AR in vitro, and this phosphorylation was significantly reduced when the mutant the β2AR R239A was used as a substrate instead of the β2AR wild-type. Additionally, the phosphorylation of the β2AR was inhibited in vitro by OSR1 kinase inhibitors in a dose-dependent manner. Although our work provided the first evidence of OSR1 and perhaps its homologous, SPAK, phosphorylate the β2AR, the exact phosphorylation sites on this receptor remain unidentified. Thus, as part of the future work for this project, it is critical that phosphor-mapping in performed to identify the SPAK and OSR1 phosphorylation sites on the β2AR.

In term of investigating the effect of the β2AR modulation on SPAK and OSR1 kinase activity, isoproterenol stimulated β2AR was used in β2AR-tranfected HEK293 cells, and this showed that the β2AR stimulation did not induce WNK-mediated SPAK and OSR1 activation following short- and long-term β2AR stimulation. Admittedly, this study focused on monitoring only SPAK S373, which is a WNK phosphorylation site, because it has robust phosphor-antibodies. Therefore, the possibility of the β2AR-activation leading to the phosphorylation of SPAK on residues other than Ser373 can not be excluded. This could be investigated in the future using initially pan-phosphoserine, phosphor-threonine and phospho-tyrosine antibodies and if they show

phosphorylation exact phosphor-mapping could be carried out to identify these phosphorylation sites. In cells, the activation of the WNK-SPAK/OSR1-signalling cascade by hypotonic buffer led to the internalisation of the β2AR. Although the use of a SPAK/OSR1 kinase inhibitor named STOCK-1S50699 did not prevent such internalisation, the involvement of WNK-kinases could not be ruled out. This is because this inhibitor is rather promiscuous and recently Novartis developed specific WNK kinase inhibitors, which should be used in the future to investigate the β2AR internalisation. Critically, SPAK and OSR1 kinases may also regulate the β2AR through a scaffolding mechanism and this should also be investigated in the future. Intriguingly, our work showed that the CCC, NKCC2, a known SPAK and OSR1 substrate, was phosphorylated as a response to the β2AR and this phosphorylation was supressed by the inhibition of SPAK and OSR1 kinases, but not by the inhibition of WNK kinases. This suggested that the Iso-mediated phosphorylation of NKCC2 is WNK kinases independent, but involves SPAK and OSR1 kinases, and hence these latter kinases maybe regulated by other upstream kinases other than WNKs following Iso-stimulation.

Work limitations and future experiments

In this study the RFxV peptides have shown to be bound to endogenous SPAK only in HEK293 cell lines which is it could be a limiting factor, so it would be interesting to determine the binding of β2AR derived RFHV-tetrapeptide to the kinase in other cell lines. Although this work provides the first evidence of binding SPAK kinase to β2AR which could link the adrenergic system to WNK-signalling pathway and could explain the increase of BP by sympathetic activation, this finding was only validated by over-

expression of both proteins in HEK293 cells, that could enhance the binding ability of two proteins i.e. non-physiological conditions. Although, SPAK binding to β2AR in immune-precipitated samples from mouse heart have been identified, further verifying the interaction under normal physiological state in human native tissues e.g. lung, muscles, kidneys, blood vessels or uterus is also required.

Some analysis in this study has primarily relayed on Western blot (WB) which has some restrictions such as antibody specificity and cross reactivity and poor protein transfer from SDS gels to nitrocellulose membranes. These factors could affect the data interpretation. For instance, β2AR expression in HEK293 cells was evaluated by WB either in total cell crude or membranous fraction, thus other methods for determining receptor expression could be used such as flow cytometry, immunohistochemistry (IHC) or by si-RNA. Also, there were some issues in using WB to determine few phosphorylated proteins such as SPAK phosphorylation at Thr233 and NKCC2 phosphorylation.

In present work, our data revealed that OSR1 phosphorylates β2AR *in vitro,* and this phosphorylation was reduced by introducing mutant R239A β2AR or by inhibiting OSR1 catalytic activity, while *in vivo* phosphorylation of the receptor by SPAK or OSR1 is needed to be investigated and the sites of phosphorylation are required to be identified by phosphor-mapping. Moreover, the effect of this phosphorylation on β2AR function had not assessed, it would be interesting examining the effect of R239A mutation in receptor function by performing cAMP assay. Also, it has noticed that β2AR was internalized by HLB, this internalisation mechanism requires more investigations, to confirm whether the scaffolding role SPAK/OSR1 mediates this mechanism. IHC and fluorescent activated cell sorting (FACS) could be used to assess mutant R293A β2AR (non-SPAK and OSR1 binder) function.

In conclusion, this work provides the first evidence of the direct interaction between SPAK and OSR1 kinases with the human β2AR. Given the important role the β2AR plays in the pathogenesis of many human diseases such as heart failure, asthma and COPD, our discovery adds a new dimension to the pathogenesis of these diseases. Critically, this may eventually highlight the repurposing of WNK-signalling inhibitors in the management and treatment of β2AR-diseases.

Chapter 5 : Appendix

1- Table S1: Row data of densitometry analysis of SPAK-Ser373 phosphorylation

SPAK phosphorylation at Ser373 mediated by HLB-activated WNK1 (**Figure 3.1 C**). This phosphorylation has been analysed by densitometry. The results revealed that the lower bands are more likely to be Ser373 phosphorylation sites than the upper ones which could be phosphorylated residues by kinases other than WNK1/4. Data obtained from single experiment (n=1).

Upper band	*6.44*	*5.53*	*49.29*	*26.57*	*43.43*	*29.32*	*32.26*	*30.56*
Lower band	3.33	4.12	26.15	19.94	4.22	2.38	4.39	4.42

Table S.1: *Row data of densitometry analysis of SPAK-Ser373 phosphorylation.*

2- Table S2: Row data of densitometry analysis of NKCC1 phosphorylation.

This work has been carried to optimise the concentration of WNK463 inhibitor in HEK293 cells (**Figure 3.2**). Data represented two independent experiments (n=2).

Samples	***Experiment 1 Ps-NKCC1/NKCC1***	***Experiment 2 Ps-NKCC1/NKCC1***	***Mean***	***± SD***
Vehicle	4.54	4.16	4.353	0.186
HLB	77.15	94.25	85.700	8.550
St	2.20	6.39	4.307	2.091
WNK463 0.3 µM	95.65	56.32	77.331	18.011
WNK463 1 µM	94.65	61.36	78.512	17.145
WNK463 3 µM	36.78	50.76	43.773	6.9869
WNK463 5 µM	3.95	25.66	14.812	10.856
WNK463 10 µM	2.62	2.99	2.810	0.1808
WNK463 20 µM	5.01	4.51	4.763	0.2533

Table S.2: *Row data of densitometry analysis of NKCC1 phosphorylation.*

3- Table S3: Row data of densitometry of LKB1 phosphorylation by Iso stimulation.

Quantification data of phosphorylation of LKB1 after stimulation of Isoproterenol dose dependent course for 30 min in HEK293 cells (**Figure 3.7**). Data obtained from three experiments (n=3).

Samples Isoproterenol concentration in (nM)	***Experiment 1 psLKB1/LKB1***	***Experiment 2 psLKB1/LKB1***	***Experiment 3 psLKB1/LKB1***	***Mean***	***± SD***
0	0.8846294	4.96329	0.803703	2.217209	1.942056
0.01	2.1902989	5.29745	10.19936	5.895703	3.296937
0.03	2.1790347	4.05029	6.173719	4.134351	1.631905
0.1	3.5696058	18.0996	3.912698	8.527301	6.770086
0.3	6.8330296	30.23403	8.289744	15.11893	10.70452
1	11.337408	41.84822	59.72763	37.63775	19.97831
3	28.406838	78.72484	122.2946	76.47543	38.3625
10	60.184907	94.86625	79.17605	78.07574	14.17996
30	65.468709	63.73934	118.5999	82.60264	25.46368
100	49.842921	39.85731	56.68536	48.7952	6.90985
300	45.172886	99.86604	99.23594	81.42495	25.63537
1,000	44.774294	113.1005	107.744	88.53957	31.02389
3,000	33.524751	105.2303	54.50973	64.42161	30.10102

Table S.3: *Row data of densitometry of LKB1 phosphorylation by Iso.*

4- Table S4: Row data of densitometry of ICI inhibitory effect.

Quantification data of ps-LKB1/LKB1 to assess the inhibitory effect of ICI118551 (ICI) in transfected HEK293 cells (**Figure 3.8**). It was obtained from single experiment (n=1).

Samples	**NS**	**Iso**	**0.01 ICI**	**0.03 ICI**	**0.1 ICI**	**1 ICI**
psLKB1/LKB1	5.1047	62.9902	64.2716	23.8081	21.0131	23.7114

Table S.4: *Row data of densitometry of ICI effect.*

5- Figure S1: Immunoblot analysis of Identify β2AR phosphorylation.

This experiment aimed to determine β2AR phosphorylation at Ser345 and Ser346 after HLB and isoproterenol stimulation. The top panel showed β2AR expression after transfection in all samples but its phosphorylation at these Ser residues was not seen (bottom blot).

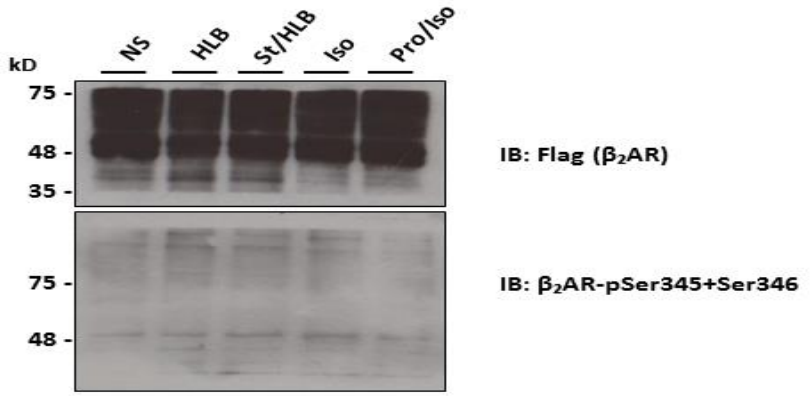

Figure S.1: *Immunoblot for identification of β2AR Ser345 and Ser346 phosphorylation after HLB and 300nM Isoproterenol (Iso) stimulation in transfected HEK293 cells.*

6- Figure S2: Immunoblot analysis attempted to identify the interaction of SPAK to RFxV peptides where SPAK was isolated with RFQV but did not with RFHV.

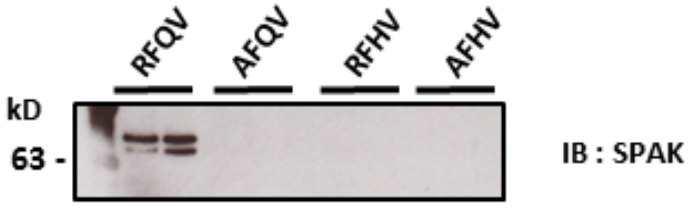

Figure S.2: *RFxV binding to endogenous SPAK.*

Figure obtained from single experiment.

7- **Table S5:** Row data of in vitro ADP-Glo™ kinase assay of phosphorylation of β2AR by OSR1-T185E, the below table showed data in mean ± SD of three independent samples (n = 3). **(Figure 3.18 A and B).**

Lanes	***Luminescence (RLU)***		***% Luminescence (RLU) relative to control***	
	Mean	± SD	*Mean*	± SD
1-Control	43429	7132.357	////	
2-CATCHtide+OSR1	145589	10953.05	////	
3-β2AR-WT+OSR1	135244	5559.018	100	
4-β2AR-R239A+OSR1	86783	11237.489	61.031	4.7324

***Table S.5* :** *Row data of in vitro OSR1 kinase assay of β2AR phosphorylation.*

8- **Table S6:** Row data of in vitro ADP-Glo™ kinase assay of the inhibitory effect of Verteporfin (VP) on OSR1-T185E activity (**Figure 3.19A and B**). Data were obtained from single experiment in triplicate (n=1).

Lanes	***Luminescence (RLU)***	***% Luminescence (RLU) relative to control***
NKCC2(1-174)	7793	////
NKCC2(1-174) + OSR1-T185E	22707	100
0.1 µM VP	20451	90.04391
0.5 µM VP	17311	76.30306
1 µM VP	11629	51.21696
5 µM VP	8544	37.67089

Table S.6: *Row data of OSR1 in vitro kinase assay of Verteporfin inhibition of NKCC2 phosphorylation.*

9- **Table S7**: Row data of in vitro ADP-Glo™ kinase assay of β2AR.

β2AR phosphorylation by OSR1-T185E and with the inhibitor 5 µM VP, to verify receptor phosphorylation is dependent on the kinase activity of OSR1T185E (**Figure 3.20**). Data were obtained from three independent experiments (n=3).

Lanes	*Luminescence (RLU)*	*Mean*	*± SD*
1-NKCC2(1-174)	4743 4093 6585.5	5140.5	1055.665
2-NKCC2(1-174) + OSR1-T185E	27562 48784.5 20672	32339.5	11963.74
3-NKCC2(1-174) + OSR1-T185E+ 5µM VP	6694 6664.5 10127.5	7828.667	1625.565
4- β2AR	4452 5264.5 8866	6194.167	1918.169
5- β2AR+ OSR1-T185E	26909 55902.5 23289.5	35367	14595.78
6- β2AR+ OSR1-T185E+ 5µM VP	9073 7672 12180	9641.667	1883.8

Table S.7: *Row data of In vitro OSR1 kinase assay of β2AR phosphorylation and its inhibition by Verteporfin.*

10-Table S8: Row data of in vitro ADP-Glo™ kinase assay of CATCHtide phosphorylation by OSR1-T185E and the effect of [A/R]FHV-peptides on OSR1 activity (**Figure 3.21 A** and **B**).

Lanes	*Luminescence (RLU)*	*% Luminescence (RLU) relative to control*
1-CATCHtide	58785 64876 67158	////
2-CATCHtide + OSR1-T185E	516510 516764 504523	100 100 100
3-CATCHtide + OSR1-T185E+ RFHV	357110 380760 368951	69.139 73.681 73.128
4-CATCHtide + OSR1-T185E+ AFHV	400495 408425 456775	77.53 79.035 90.369

Table S.8**:** *Row data of OSR1 in vitro kinase assay of A/RFHV effect on the enzyme activity.*

11-Table S9: Row data of in vitro ADP-Glo™ kinase assay of NKCC2(1-174) phosphorylation by OSR1-T185E and the effect of [A/R]FHV-peptides on OSR1 activity (**Figure 3.21 C**).

Lanes	***Luminescence (RLU)***
1-NKCC2(1-174)	3256 3259 2933
2-NKCC2(1-174) + OSR1-T185E	26183 25222 20816
3-NKCC2(1-174) + OSR1-T185E+ RFHV-peptide	22129 22082 25572

Table S.9: *Row data of OSR1 in vitro kinase assay of the effect of RFHV on NKCC2 phosphorylation.*

12-Table S10 and S11: Row data of western blot quantification of membrane β_2AR bands intensity of (**Figure 3.22 B and C**).

Samples	***1st Experiment***	***2nd Experiment***	***Mean***	***± SD***
U	*100*	*100*	*100*	*0*
HLB	*17.17*	*38.77*	*27.97*	*15.2*
St/HLB	*15.06*	*33.85*	*24.45*	*13.3*
Iso	*33.93*	*88.33*	*61.13*	*12.5*
Pro/Iso	*69.23*	*97.76*	*83.49*	*15.2*
ICI/Iso	*42.63*	*85.57*	*64.10*	*7.36*

Table S.10**:** *Row densitometry data of β2AR upper bands.*

Samples	***1st Experiment***	***2nd Experiment***	***Mean***	***± SD***
U	*100*	*100*	*100*	*0*
HLB	*21.28*	*32.36*	*26.82*	*7.831*
St/HLB	*17.60*	*11.47*	*14.53*	*4.329*
Iso	*33.52*	*53.67*	*43.60*	*14,251*
Pro/Iso	*99.27*	*95.15*	*97.21*	*2.913*
ICI/Iso	*93.86*	*84.72*	*89.29*	*6.464*

Table S.11**:***Row densitometry data of β2AR lower band.*

13-Figure S.3: Identification of FLAG-β2AR expression by flow cytometry.

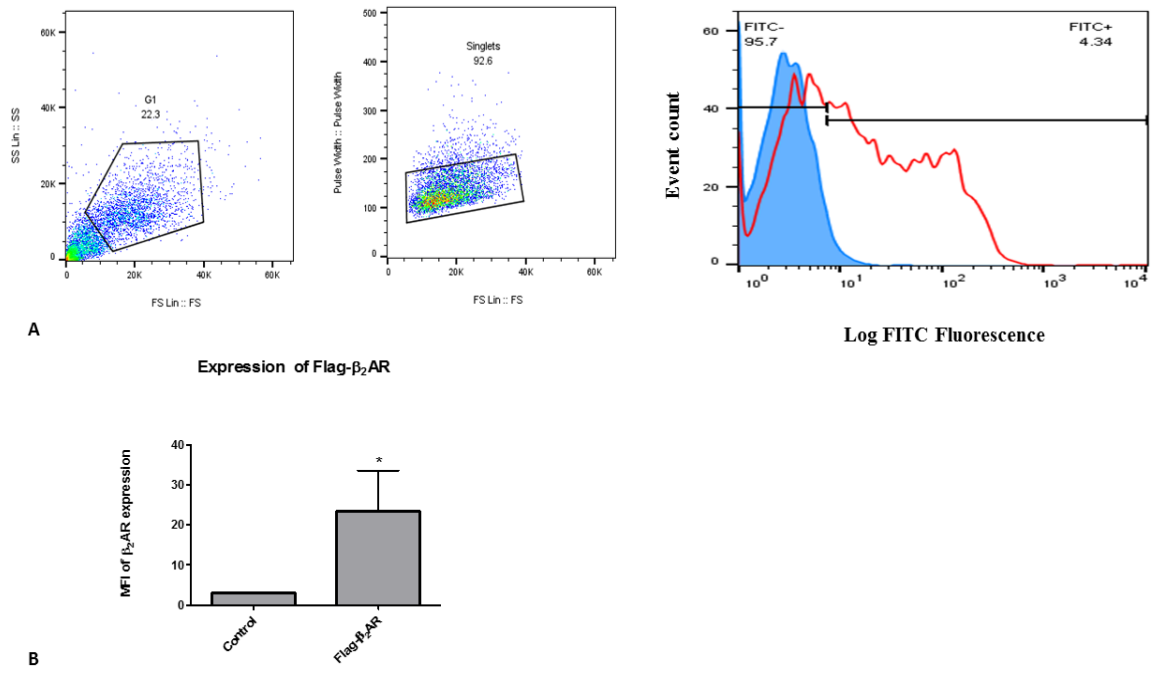

Figure S.3: Detection the expression of β2AR and gating strategy.

Illustrative flow cytometry plots of transiently transfected HEK293 cells with N-terminus FLAG-β2AR. 48 hrs post-transfection Cells were prepared for and analysed by Cyan ADP of fluorescence activated cell sorting (FACS) and FlowJo v 10. Primary mouse anti-FLAG antibody and FITC-488 anti-mouse secondary antibody had been used in the study. (A) Cells were analysed based on their size/intracellular granularity by forward scatter (FSS)/side scatter (SSC) respectively (left dot plot). More than one cells (cell aggregation or doublet) were excluded on pulse width/ FSS plot (middle dot plot). The interested subsets were then analysed by measuring the fluorescence of FITC labelled specific antibody on log scale versus cell number (red histogram), while non-specific signal was determined by secondary only labelled cells (blue area). (B) Median Fluorescent intensity (MFI) was calculated from histogram plot in (A) of three independent experiments (n=3). Data represented in mean ± SD and receptors expression were proved by Student t-test.

14-Figure S.4: Detection of SPAK/OSR1 independent internalization of β2AR by FACS.

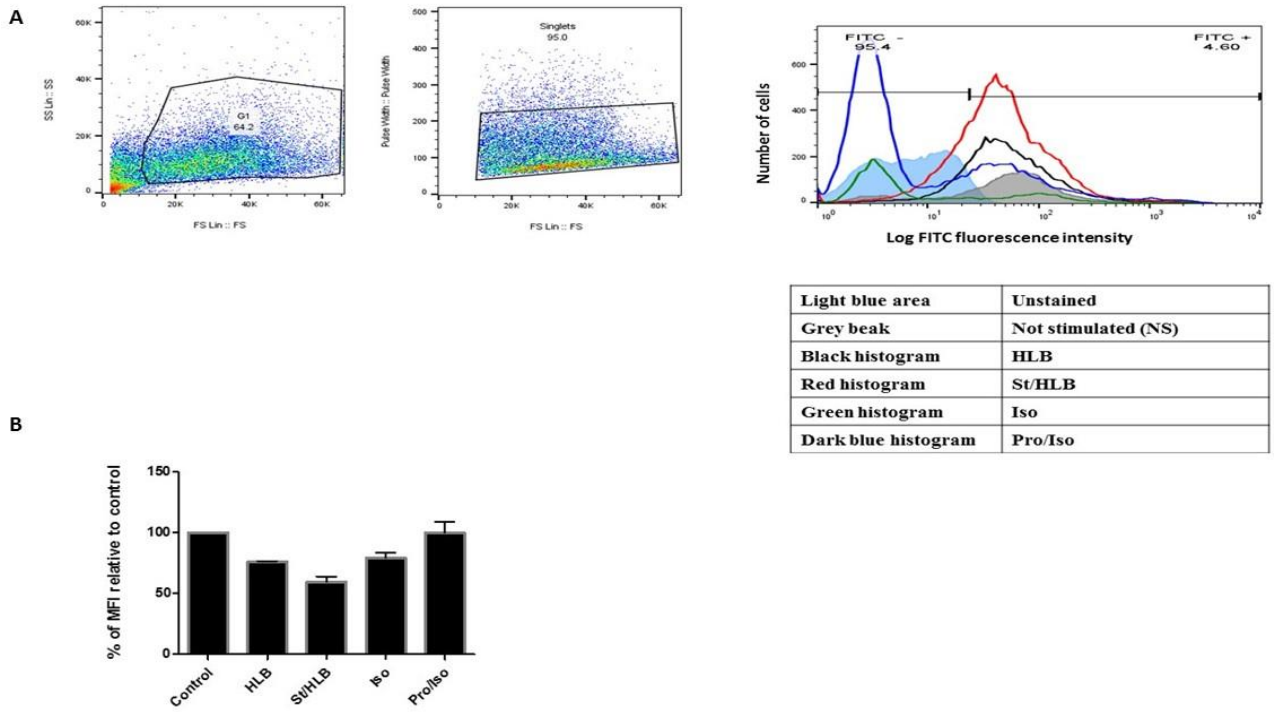

Light blue area	Unstained
Grey beak	Not stimulated (NS)
Black histogram	HLB
Red histogram	St/HLB
Green histogram	Iso
Dark blue histogram	Pro/Iso

Figure S.4: SPAK/OSR1 independent internalization of β2AR.

Flow cytometry plots of FLAG-β2AR transfected HEK293. 48 hrs post-transfection cells were left not-stimulated (NS), or pre-incubated with 10 µM St or 1 µM Pro for 1 hr, then cells were stimulated either with HLB or 1 µM Iso for 1 hr. Cells were analysed as previous figure. (A) Singlet cells were gated, fluorescence analysed on log scale of FITC-labelled antibody (right plot). (B)MFI was computed from histogram in (A) and Kruskal-Wallis followed by Dunn's multiple comparison test revealed non-significant difference between samples mean. Data presented in mean ± SD of two separate experiments (n=2). Although % of MFI relative to NS showed SPAK/OSR1 independent reduction of surface β2AR, and less internalization with Iso. However, little effect of treatment against NS (grey area) was observed and most of samples showed unequal cells number. Moreover, there was an overlap between samples and unstained which indicated less cells labelling particularly in Pro/Iso (dark blue) and Iso (green).

15-Table S12: Row data of ELISA assay of quantification of membrane surface β2AR-WT of (**Figure 3.23**). Data were obtained from single experiment (n=1).

Lanes	***% of Relative absorbance to control***
	Mean
1-Untreated cells (control)	100
2-HLB	78.15055
3-St/HLB	89.1177
4- Iso	44.43416
5- Pro/Iso	46.06071

Table S.12**:** *Row data of ELISA quantification of surface β2AR*.

16- Table S13: Row data of densitometry analysis of SPAK phosphorylation by Isoproterenol.

Densitometry data of SPAK phosphorylation by Iso stimulation, in dose dependent manner (Figure 3.24). Data have been obtained from two separate experiments (n=2).

Samples	***Mean***	***± SD***
NS	26.74196	0.878377
1	30.27842	10.70634
2	32.82276	18.4529
3	31.67429	11.23902
4	38.86027	12.1326
5	56.24615	15.59387
6	59.72523	27.96903
7	44.70796	23.7453
8	41.04777	7.91969
9	29.01706	4.295555
10	27.3344	13.6714
11	40.23147	16.63579
12	33.82606	22.67147

Table S.13: *Row data of densitometry analysis of SPAK phosphorylation by Isoproterenol in dose dependent manner.*

17- Table S14: Row data of densitometry of SPAK phosphorylation by Iso stimulation in time-dependent manner.

HEK293 cells were treated by 300nM Iso in time dependent manner, after 72hrs cells were treated and data were obtained. Data represented three independent experiments (n = 3).

Samples	***Mean***	***± SD***
NS	16.67695	9.92783
5 min	38.5055	11.38549
10 min	38.26748	5.880695
20 min	39.08742	3.764485
30 min	38.82006	5.271327
60 min	34.42249	4.033594
3 hrs	39.55901	13.07957
6 hrs	46.76407	10.45891
12 hrs	64.83308	21.79991
24 hrs	71.83936	17.20266
48 hrs	73.08802	8.504269
72 hrs	53.82733	17.32385

Table S.14: *Row data of densitometry of SPAK phosphorylation by Iso stimulation in time-dependent manner.*

18- Stimulation of β2AR did not phosphorylate SPAK Ser373 and difficulty to detect of SPAK-Thr233 phosphorylation.

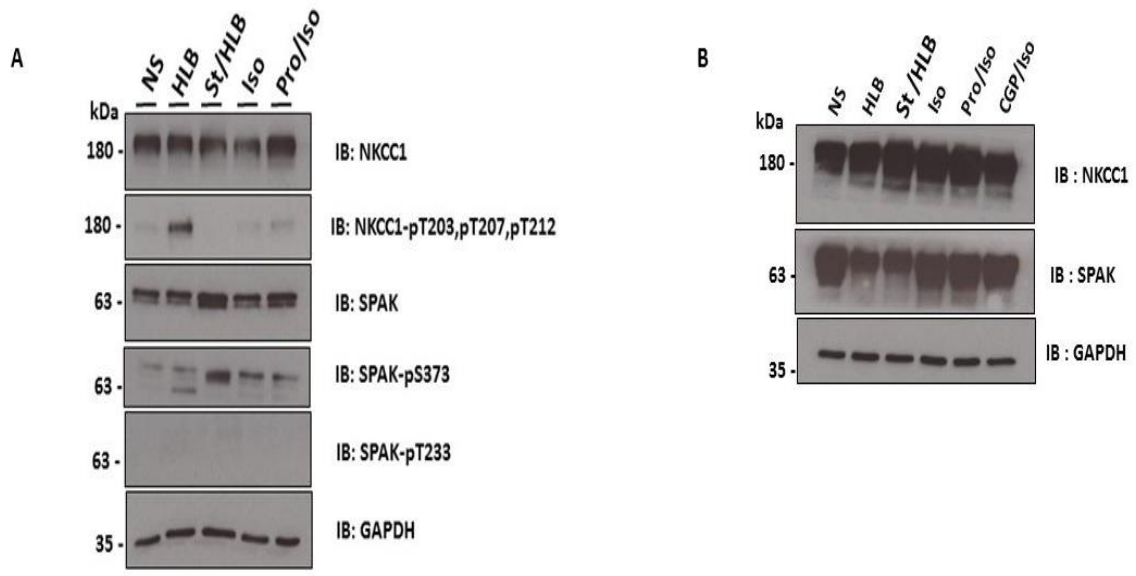

Figure S5: Iso-stimulated β2AR did not phosphorylate Ser373 of SPAK.

(A) HEK293 cells were transfected with Flag-β2AR, 48 hrs post-transfection cells were left untreated (NS) or pre-stimulated with 10 μM St or 1 μM Pro for 60 mins. Then cells were stimulated with HLB or 300 nM Iso for 60 mins. No activation had been observed in SPAK phosphorylation at Ser373 or change in protein abundance. NKCC phosphorylation for identification of SPAK activation. Also, detection of phosphorylation T233 was challenging to be obtained. (B) IB analysis demonstrates hyperexpression of endogenous SPAK in HEK293 cells. Please note the increased levels of SPAK abundance in (B) over than in (A) which is the normal expression level.

References

ALAMRI, M. A., KADRI, H., ALDERWICK, L. J., SIMPKINS, N. S. & MEHELLOU, Y. 2017a. Rafoxanide and Closantel Inhibit SPAK and OSR1 Kinases by Binding to a Highly Conserved Allosteric Site on Their C-terminal Domains. *ChemMedChem,* 12**,** 639-645.

ALAMRI, M. A., KADRI, H., DHIANI, B. A., MAHMOOD, S., ELZWAWI, A. & MEHELLOU, Y. 2017b. WNK Signaling Inhibitors as Potential Antihypertensive Drugs. *ChemMedChem,* 12**,** 1677-1686.

ALAMRI, M. A., KADRI, H., JEEVES, M., ALDERWICK, L. J. & MEHELLOU, Y. 2018. The Photosensitizing Clinical Agent Verteporfin is an Inhibitor of SPAK and OSR1 Kinases. *ChemBioChem,* 0.

ALESSI, D. R., ZHANG, J., KHANNA, A., HOCHDORFER, T., SHANG, Y. & KAHLE, K. T. 2014. The WNK-SPAK/OSR1 pathway: master regulator of cation-chloride cotransporters. *Sci Signal,* 7**,** re3.

ALVAREZ, D. F., HELM, K., DEGREGORI, J., ROEDERER, M. & MAJKA, S. 2010. Publishing flow cytometry data. *Am J Physiol Lung Cell Mol Physiol,* 298**,** L127-30.

ANSELMO, A. N., EARNEST, S., CHEN, W., JUANG, Y. C., KIM, S. C., ZHAO, Y. & COBB, M. H. 2006. WNK1 and OSR1 regulate the Na+, K+, 2Cl- cotransporter in HeLa cells. *Proc Natl Acad Sci U S A,* 103**,** 10883-8.

ARES, G. R., CACERES, P. S. & ORTIZ, P. A. 2011a. Molecular regulation of NKCC2 in the thick ascending limb. *Am J Physiol Renal Physiol,* 301**,** F1143-59.

ARES, G. R., CACERES, P. S. & ORTIZ, P. A. 2011b. Molecular regulation of NKCC2 in the thick ascending limb. *American Journal of Physiology-Renal Physiology,* 301**,** F1143-F1159.

BALLESTEROS, J. A., JENSEN, A. D., LIAPAKIS, G., RASMUSSEN, S. G. F., SHI, L., GETHER, U. & JAVITCH, J. A. 2001. Activation of the β2-Adrenergic Receptor Involves Disruption of an Ionic Lock between the Cytoplasmic Ends of Transmembrane Segments 3 and 6. *Journal of Biological Chemistry,* 276**,** 29171-29177.

BANG, I. & CHOI, H. J. 2015. Structural features of beta2 adrenergic receptor: crystal structures and beyond. *Mol Cells,* 38**,** 105-11.

BASITH, S., CUI, M., MACALINO, S. J. Y., PARK, J., CLAVIO, N. A. B., KANG, S. & CHOI, S. 2018. Exploring G Protein-Coupled Receptors (GPCRs) Ligand Space via Cheminformatics Approaches: Impact on Rational Drug Design. *Frontiers in Pharmacology,* 9.

BAZÚA-VALENTI, S., CASTAÑEDA-BUENO, M. & GAMBA, G. 2016. Physiological role of SLC12 family members in the kidney. *American Journal of Physiology-Renal Physiology,* 311**,** F131-F144.

BAZÚA-VALENTI, S., CHÁVEZ-CANALES, M., ROJAS-VEGA, L., GONZÁLEZ-RODRÍGUEZ, X., VÁZQUEZ, N., RODRÍGUEZ-GAMA, A., ARGAIZ, E. R., MELO, Z., PLATA, C., ELLISON, D. H., GARCÍA-VALDÉS, J., HADCHOUEL, J. & GAMBA, G. 2015. The Effect of WNK4 on the Na+–Cl− Cotransporter Is Modulated by Intracellular Chloride. *Journal of the American Society of Nephrology,* 26**,** 1781-1786.

BENOVIC, J. L., PIKE, L. J., CERIONE, R. A., STANISZEWSKI, C., YOSHIMASA, T., CODINA, J., CARON, M. G. & LEFKOWITZ, R. J. 1985. Phosphorylation

of the mammalian beta-adrenergic receptor by cyclic AMP-dependent protein kinase. Regulation of the rate of receptor phosphorylation and dephosphorylation by agonist occupancy and effects on coupling of the receptor to the stimulatory guanine nucleotide regulatory protein. *J Biol Chem,* 260**,** 7094-101.

BERDIEV, B. K., PRAT, A. G., CANTIELLO, H. F., AUSIELLO, D. A., FULLER, C. M., JOVOV, B., BENOS, D. J. & ISMAILOV, II 1996. Regulation of epithelial sodium channels by short actin filaments. *J Biol Chem,* 271**,** 17704-10.

BERTHIAUME, Y., BROADDUS, V. C., GROPPER, M. A., TANITA, T. & MATTHAY, M. A. 1988. Alveolar liquid and protein clearance from normal dog lungs. *J Appl Physiol (1985),* 65**,** 585-93.

BERTORELLO, A. M., RIDGE, K. M., CHIBALIN, A. V., KATZ, A. I. & SZNAJDER, J. I. 1999. Isoproterenol increases Na+-K+-ATPase activity by membrane insertion of alpha-subunits in lung alveolar cells. *Am J Physiol,* 276**,** L20-7.

BOGAN, J. S. 2012. Regulation of glucose transporter translocation in health and diabetes. *Annu Rev Biochem,* 81**,** 507-32.

BOIVIN, V., JAHNS, R., GAMBARYAN, S., NESS, W., BOEGE, F. & LOHSE, M. J. 2001. Immunofluorescent imaging of beta 1- and beta 2-adrenergic receptors in rat kidney. *Kidney Int,* 59**,** 515-31.

BORSCHEWSKI, A., HIMMERKUS, N., BOLDT, C., BLANKENSTEIN, K. I., MCCORMICK, J. A., LAZELLE, R., WILLNOW, T. E., JANKOWSKI, V., PLAIN, A., BLEICH, M., ELLISON, D. H., BACHMANN, S. & MUTIG, K. 2016. Calcineurin and Sorting-Related Receptor with A-Type Repeats Interact to Regulate the Renal Na+-K+-2Cl− Cotransporter. *Journal of the American Society of Nephrology,* 27**,** 107-119.

BOYCE, K. J. & ANDRIANOPOULOS, A. 2011. Ste20-related kinases: effectors of signaling and morphogenesis in fungi. *Trends Microbiol,* 19**,** 400-10.

BOYDEN, L. M., CHOI, M., CHOATE, K. A., NELSON-WILLIAMS, C. J., FARHI, A., TOKA, H. R., TIKHONOVA, I. R., BJORNSON, R., MANE, S. M., COLUSSI, G., LEBEL, M., GORDON, R. D., SEMMEKROT, B. A., POUJOL, A., VALIMAKI, M. J., DE FERRARI, M. E., SANJAD, S. A., GUTKIN, M., KARET, F. E., TUCCI, J. R., STOCKIGT, J. R., KEPPLER-NOREUIL, K. M., PORTER, C. C., ANAND, S. K., WHITEFORD, M. L., DAVIS, I. D., DEWAR, S. B., BETTINELLI, A., FADROWSKI, J. J., BELSHA, C. W., HUNLEY, T. E., NELSON, R. D., TRACHTMAN, H., COLE, T. R., PINSK, M., BOCKENHAUER, D., SHENOY, M., VAIDYANATHAN, P., FOREMAN, J. W., RASOULPOUR, M., THAMEEM, F., AL-SHAHROURI, H. Z., RADHAKRISHNAN, J., GHARAVI, A. G., GOILAV, B. & LIFTON, R. P. 2012. Mutations in kelch-like 3 and cullin 3 cause hypertension and electrolyte abnormalities. *Nature,* 482**,** 98-102.

BULENGER, S., MARULLO, S. & BOUVIER, M. 2005. Emerging role of homo- and heterodimerization in G-protein-coupled receptor biosynthesis and maturation. *Trends Pharmacol Sci,* 26**,** 131-7.

CAMPESE, V. M., ROMOFF, M. S., LEVITAN, D., SAGLIKES, Y., FRIEDLER, R. M. & MASSRY, S. G. 1982. Abnormal relationship between sodium intake and sympathetic nervous system activity in salt-sensitive patients with essential hypertension. *Kidney Int,* 21**,** 371-8.

CAO, T. T., BRELOT, A. & VON ZASTROW, M. 2005. The Composition of the β-2 Adrenergic Receptor Oligomer Affects Its Membrane Trafficking after Ligand-Induced Endocytosis. *Molecular Pharmacology,* 67**,** 288-297.

CAO, T. T., DEACON, H. W., RECZEK, D., BRETSCHER, A. & VON ZASTROW, M. 1999. A kinase-regulated PDZ-domain interaction controls endocytic sorting of the beta2-adrenergic receptor. *Nature,* 401**,** 286-90.

CASTAÑEDA-BUENO, M., ARROYO, J. P., ZHANG, J., PUTHUMANA, J., YARBOROUGH, O., SHIBATA, S., ROJAS-VEGA, L., GAMBA, G., RINEHART, J. & LIFTON, R. P. 2017. Phosphorylation by PKC and PKA regulate the kinase activity and downstream signaling of WNK4. *Proceedings of the National Academy of Sciences of the United States of America,* 114**,** E879-E886.

CASTAÑEDA-BUENO, M., CERVANTES-PEREZ, L. G., ROJAS-VEGA, L., ARROYO-GARZA, I., VÁZQUEZ, N., MORENO, E. & GAMBA, G. 2014. Modulation of NCC activity by low and high K(+) intake: insights into the signaling pathways involved. *American Journal of Physiology - Renal Physiology,* 306**,** F1507-F1519.

CASTANEDA-BUENO, M., CERVANTES-PEREZ, L. G., VAZQUEZ, N., URIBE, N., KANTESARIA, S., MORLA, L., BOBADILLA, N. A., DOUCET, A., ALESSI, D. R. & GAMBA, G. 2012. Activation of the renal Na+:Cl- cotransporter by angiotensin II is a WNK4-dependent process. *Proc Natl Acad Sci U S A,* 109**,** 7929-34.

CASTAÑEDA-BUENO, M., CERVANTES-PÉREZ, L. G., VÁZQUEZ, N., URIBE, N., KANTESARIA, S., MORLA, L., BOBADILLA, N. A., DOUCET, A., ALESSI, D. R. & GAMBA, G. 2012. Activation of the renal Na(+):Cl(−) cotransporter by angiotensin II is a WNK4-dependent process. *Proceedings of the National Academy of Sciences of the United States of America,* 109**,** 7929-7934.

CHACHISVILIS, M., ZHANG, Y. L. & FRANGOS, J. A. 2006. G protein-coupled receptors sense fluid shear stress in endothelial cells. *Proc Natl Acad Sci U S A,* 103**,** 15463-8.

CHAUDHARY, S., PAK, J. E., GRUSWITZ, F., SHARMA, V. & STROUD, R. M. 2012. Overexpressing human membrane proteins in stably transfected and clonal human embryonic kidney 293S cells. *Nature Protocols,* 7**,** 453.

CHAVEZ-CANALES, M., ARROYO, J. P., KO, B., VAZQUEZ, N., BAUTISTA, R., CASTANEDA-BUENO, M., BOBADILLA, N. A., HOOVER, R. S. & GAMBA, G. 2013. Insulin increases the functional activity of the renal NaCl cotransporter. *J Hypertens,* 31**,** 303-11.

CHEN, W., YAZICIOGLU, M. & COBB, M. H. 2004. Characterization of OSR1, a member of the mammalian Ste20p/germinal center kinase subfamily. *J Biol Chem,* 279**,** 11129-36.

CHEN, X. J., EATON, D. C. & JAIN, L. 2002. Beta-adrenergic regulation of amiloride-sensitive lung sodium channels. *Am J Physiol Lung Cell Mol Physiol,* 282**,** L609-20.

CHENG, C. J., RODAN, A. R. & HUANG, C. L. 2017. Emerging Targets of Diuretic Therapy. *Clin Pharmacol Ther,* 102**,** 420-435.

CHEREZOV, V., ROSENBAUM, D. M., HANSON, M. A., RASMUSSEN, S. G. F., THIAN, F. S., KOBILKA, T. S., CHOI, H.-J., KUHN, P., WEIS, W. I., KOBILKA, B. K. & STEVENS, R. C. 2007. High-Resolution Crystal Structure of an Engineered Human β₂-Adrenergic G Protein–Coupled Receptor. *Science,* 318**,** 1258-1265.

CHIGA, M., RAI, T., YANG, S. S., OHTA, A., TAKIZAWA, T., SASAKI, S. & UCHIDA, S. 2008. Dietary salt regulates the phosphorylation of OSR1/SPAK kinases

and the sodium chloride cotransporter through aldosterone. *Kidney Int,* 74**,** 1403-9.

CHUNG, K. Y., DAY, P. W., VÉLEZ-RUIZ, G., SUNAHARA, R. K. & KOBILKA, B. K. 2013. Identification of GPCR-Interacting Cytosolic Proteins Using HDL Particles and Mass Spectrometry-Based Proteomic Approach. *PLOS ONE,* 8**,** e54942.

CONG, M., PERRY, S. J., LIN, F. T., FRASER, I. D., HU, L. A., CHEN, W., PITCHER, J. A., SCOTT, J. D. & LEFKOWITZ, R. J. 2001. Regulation of membrane targeting of the G protein-coupled receptor kinase 2 by protein kinase A and its anchoring protein AKAP79. *J Biol Chem,* 276**,** 15192-9.

COPE, G., GOLBANG, A. & O'SHAUGHNESSY, K. M. 2005. WNK kinases and the control of blood pressure. *Pharmacology & Therapeutics,* 106**,** 221-231.

DAN, I., WATANABE, N. M. & KUSUMI, A. 2001. The Ste20 group kinases as regulators of MAP kinase cascades. *Trends Cell Biol,* 11**,** 220-30.

DARMAN, R. B. & FORBUSH, B. 2002. A Regulatory Locus of Phosphorylation in the N Terminus of the Na-K-Cl Cotransporter, NKCC1. *Journal of Biological Chemistry,* 277**,** 37542-37550.

DAULAT, A. M., MAURICE, P. & JOCKERS, R. 2009. Recent methodological advances in the discovery of GPCR-associated protein complexes. *Trends Pharmacol Sci,* 30**,** 72-8.

DBOUK, H. A., HUANG, C.-L. & COBB, M. H. 2016. Hypertension: the missing WNKs. *American Journal of Physiology - Renal Physiology,* 311**,** F16-F27.

DE LOS HEROS, P., ALESSI, D. R., GOURLAY, R., CAMPBELL, D. G., DEAK, M., MACARTNEY, T. J., KAHLE, K. T. & ZHANG, J. 2014. The WNK-regulated

SPAK/OSR1 kinases directly phosphorylate and inhibit the K+-Cl- co-transporters. *Biochem J,* 458**,** 559-73.

DEFEA, K. A., ZALEVSKY, J., THOMA, M. S., DERY, O., MULLINS, R. D. & BUNNETT, N. W. 2000. beta-arrestin-dependent endocytosis of proteinase-activated receptor 2 is required for intracellular targeting of activated ERK1/2. *J Cell Biol,* 148**,** 1267-81.

DELALOY, C., LU, J., HOUOT, A.-M., DISSE-NICODEME, S., GASC, J.-M., CORVOL, P. & JEUNEMAITRE, X. 2003. Multiple Promoters in the WNK1 Gene: One Controls Expression of a Kidney-Specific Kinase-Defective Isoform. *Molecular and Cellular Biology,* 23**,** 9208-9221.

DELPIRE, E. & GAGNON, K. B. 2007. Genome-wide analysis of SPAK/OSR1 binding motifs. *Physiol Genomics,* 28**,** 223-31.

DELPIRE, E. & GAGNON, K. B. 2008. SPAK and OSR1: STE20 kinases involved in the regulation of ion homoeostasis and volume control in mammalian cells. *Biochem J,* 409**,** 321-31.

DENNISS, A., DULHUNTY, A. F. & BEARD, N. A. 2018. Ryanodine receptor Ca2+ release channel post-translational modification: Central player in cardiac and skeletal muscle disease. *The International Journal of Biochemistry & Cell Biology,* 101**,** 49-53.

DEUPI, X. & KOBILKA, B. K. 2010. Energy Landscapes as a Tool to Integrate GPCR Structure, Dynamics, and Function. *Physiology,* 25**,** 293-303.

DHANOA, B. S., COGLIATI, T., SATISH, A. G., BRUFORD, E. A. & FRIEDMAN, J. S. 2013. Update on the Kelch-like (KLHL) gene family. *Hum Genomics,* 7**,** 13.

DIBONA, G. F. 2005. Physiology in perspective: The Wisdom of the Body. Neural control of the kidney. *Am J Physiol Regul Integr Comp Physiol,* 289**,** R633-41.

DOWD, B. F. X. & FORBUSH, B. 2003. PASK (Proline-Alanine-rich STE20-related Kinase), a Regulatory Kinase of the Na-K-Cl Cotransporter (NKCC1). *Journal of Biological Chemistry,* 278**,** 27347-27353.

DROR, R. O., ARLOW, D. H., MARAGAKIS, P., MILDORF, T. J., PAN, A. C., XU, H., BORHANI, D. W. & SHAW, D. E. 2011. Activation mechanism of the beta2-adrenergic receptor. *Proc Natl Acad Sci U S A,* 108**,** 18684-9.

DUTZLER, R., CAMPBELL, E. B., CADENE, M., CHAIT, B. T. & MACKINNON, R. 2002. X-ray structure of a ClC chloride channel at 3.0 A reveals the molecular basis of anion selectivity. *Nature,* 415**,** 287-94.

ELVIRA, B., MUNOZ, C., BORRAS, J., CHEN, H., WARSI, J., AJAY, S. S., SHUMILINA, E. & LANG, F. 2014. SPAK and OSR1 Dependent Down-Regulation of Murine Renal Outer Medullary K⁺ Channel ROMK1. *Kidney and Blood Pressure Research,* 39**,** 353-360.

ELVIRA, B., SINGH, Y., WARSI, J., MUNOZ, C. & LANG, F. 2016. OSR1 and SPAK Sensitivity of Large-Conductance Ca2+ Activated K+ Channel. *Cellular Physiology and Biochemistry,* 38**,** 1652-1662.

ELVIRA, B., WARSI, J., FEZAI, M., MUNOZ, C. & LANG, F. 2015. SPAK and OSR1 Sensitive Cell Membrane Protein Abundance and Activity of KCNQ1/E1 K⁺ Channels. *Cellular Physiology and Biochemistry,* 37**,** 2032-2042.

ESLER, M. D., KRUM, H., SOBOTKA, P. A., SCHLAICH, M. P., SCHMIEDER, R. E. & BOHM, M. 2010. Renal sympathetic denervation in patients with treatment-resistant hypertension (The Symplicity HTN-2 Trial): a randomised controlled trial. *Lancet,* 376**,** 1903-9.

FANG, X., FUKUDA, N., BARBRY, P., SARTORI, C., VERKMAN, A. S. & MATTHAY, M. A. 2002. Novel role for CFTR in fluid absorption from the distal airspaces of the lung. *J Gen Physiol,* 119**,** 199-207.

FERDAUS, M. Z. & MCCORMICK, J. A. 2016. The CUL3/KLHL3-WNK-SPAK/OSR1 pathway as a target for antihypertensive therapy. *American Journal of Physiology - Renal Physiology,* 310**,** F1389-F1396.

FILIPPI, B. M., DE LOS HEROS, P., MEHELLOU, Y., NAVRATILOVA, I., GOURLAY, R., DEAK, M., PLATER, L., TOTH, R., ZEQIRAJ, E. & ALESSI, D. R. 2011. MO25 is a master regulator of SPAK/OSR1 and MST3/MST4/YSK1 protein kinases. *The EMBO Journal,* 30**,** 1730-1741.

FLATMAN, P. W. 2007. Cotransporters, WNKs and hypertension: important leads from the study of monogenetic disorders of blood pressure regulation. *Clin Sci (Lond),* 112**,** 203-16.

FLEMMER, A. W., GIMÉNEZ, I., DOWD, B. F. X., DARMAN, R. B. & FORBUSH, B. 2002. Activation of the Na-K-Cl Cotransporter NKCC1 Detected with a Phospho-specific Antibody. *Journal of Biological Chemistry,* 277**,** 37551-37558.

FREDRIKSSON, R., LAGERSTRÖM, M. C., LUNDIN, L.-G. & SCHIÖTH, H. B. 2003. The G-Protein-Coupled Receptors in the Human Genome Form Five Main Families. Phylogenetic Analysis, Paralogon Groups, and Fingerprints. *Molecular Pharmacology,* 63**,** 1256-1272.

FUJITA, T. 2014. Mechanism of Salt-Sensitive Hypertension: Focus on Adrenal and Sympathetic Nervous Systems. *Journal of the American Society of Nephrology,* 25**,** 1148-1155.

FUJITA, T., HENRY, W. L., BARTTER, F. C., LAKE, C. R. & DELEA, C. S. 1980. Factors influencing blood pressure in salt-sensitive patients with hypertension. *Am J Med,* 69**,** 334-44.

FUKUDA, N., FOLKESSON, H. G. & MATTHAY, M. A. 2000. Relationship of interstitial fluid volume to alveolar fluid clearance in mice: ventilated vs. in situ studies. *J Appl Physiol (1985),* 89**,** 672-9.

GAGNON, K. B. & DELPIRE, E. 2012. Molecular Physiology of SPAK and OSR1: Two Ste20-Related Protein Kinases Regulating Ion Transport. *Physiological reviews,* 92**,** 1577-1617.

GAGNON, K. B., ENGLAND, R. & DELPIRE, E. 2007a. A single binding motif is required for SPAK activation of the Na-K-2Cl cotransporter. *Cell Physiol Biochem,* 20**,** 131-42.

GAGNON, K. B., RIOS, K. & DELPIRE, E. 2011. Functional Insights into the Activation Mechanism of Ste20-related Kinases. *Cellular Physiology and Biochemistry,* 28**,** 1219-1230.

GAGNON, K. B. E., ENGLAND, R. & DELPIRE, E. 2007b. A Single Binding Motif is Required for SPAK Activation of the Na-K-2Cl Cotransporter. *Cellular Physiology and Biochemistry,* 20**,** 131-142.

GAMBA, G. 2005. Molecular physiology and pathophysiology of electroneutral cation-chloride cotransporters. *Physiol Rev,* 85**,** 423-93.

GAO, S., MALBON, C. & WANG, H.-Y. 2014. Probing the stoichiometry of β2-adrenergic receptor phosphorylation by targeted mass spectrometry. *Journal of Molecular Signaling,* 9**,** 3.

GARDNER, L. A., TAVALIN, S. J., GOEHRING, A. S., SCOTT, J. D. & BAHOUTH, S. W. 2006. AKAP79-mediated targeting of the cyclic AMP-dependent protein

kinase to the beta1-adrenergic receptor promotes recycling and functional resensitization of the receptor. *J Biol Chem,* 281**,** 33537-53.

GENSCHIK, P., SUMARA, I. & LECHNER, E. 2013. The emerging family of CULLIN3-RING ubiquitin ligases (CRL3s): cellular functions and disease implications. *EMBO J,* 32**,** 2307-20.

GERELSAIKHAN, T. & TURNER, R. J. 2000. Transmembrane Topology of the Secretory Na+-K+-2Cl− Cotransporter NKCC1 Studied by in Vitro Translation. *Journal of Biological Chemistry,* 275**,** 40471-40477.

GOLBANG, A. P., MURTHY, M., HAMAD, A., LIU, C. H., COPE, G., VAN'T HOFF, W., CUTHBERT, A. & O'SHAUGHNESSY, K. M. 2005. A new kindred with pseudohypoaldosteronism type II and a novel mutation (564D>H) in the acidic motif of the WNK4 gene. *Hypertension,* 46**,** 295-300.

GONG, H., TANG, Z., YANG, Y., SUN, L., ZHANG, W., WANG, W., CUI, B. & NING, G. 2008. A patient with pseudohypoaldosteronism type II caused by a novel mutation in WNK4 gene. *Endocrine,* 33**,** 230-4.

GORDON, R. D. 1986. Syndrome of hypertension and hyperkalemia with normal glomerular filtration rate. *Hypertension,* 8**,** 93-102.

GREVEN, J. & HEIDENREICH, O. 1975. A micropuncture study of the effect of isoprenaline on renal tubular fluid and electrolyte transport in the rat. *Naunyn Schmiedebergs Arch Pharmacol,* 287**,** 117-28.

GRIMM, P. R., TANEJA, T. K., LIU, J., COLEMAN, R., CHEN, Y.-Y., DELPIRE, E., WADE, J. B. & WELLING, P. A. 2012. SPAK Isoforms and OSR1 Regulate Sodium-Chloride Co-transporters in a Nephron-specific Manner. *Journal of Biological Chemistry,* 287**,** 37673-37690.

GUNARATNE, R., BRAUCHT, D. W. W., RINSCHEN, M. M., CHOU, C.-L., HOFFERT, J. D., PISITKUN, T. & KNEPPER, M. A. 2010. Quantitative phosphoproteomic analysis reveals cAMP/vasopressin-dependent signaling pathways in native renal thick ascending limb cells. *Proceedings of the National Academy of Sciences,* 107**,** 15653-15658.

GUREVICH, V. V. & GUREVICH, E. V. 2008. How and why do GPCRs dimerize? *Trends in pharmacological sciences,* 29**,** 234-240.

GUYTON, A. C. 1991. Blood pressure control--special role of the kidneys and body fluids. *Science,* 252**,** 1813-6.

HADCOCK, J. R., PORT, J. D., GELMAN, M. S. & MALBON, C. C. 1992. Cross-talk between tyrosine kinase and G-protein-linked receptors. Phosphorylation of beta 2-adrenergic receptors in response to insulin. *J Biol Chem,* 267**,** 26017-22.

HALL, R. A., PREMONT, R. T., CHOW, C. W., BLITZER, J. T., PITCHER, J. A., CLAING, A., STOFFEL, R. H., BARAK, L. S., SHENOLIKAR, S., WEINMAN, E. J., GRINSTEIN, S. & LEFKOWITZ, R. J. 1998. The beta2-adrenergic receptor interacts with the Na+/H+-exchanger regulatory factor to control Na+/H+ exchange. *Nature,* 392**,** 626-30.

HAN, S. O., XIAO, K., KIM, J., WU, J. H., WISLER, J. W., NAKAMURA, N., FREEDMAN, N. J. & SHENOY, S. K. 2012. MARCH2 promotes endocytosis and lysosomal sorting of carvedilol-bound beta(2)-adrenergic receptors. *J Cell Biol,* 199**,** 817-30.

HANKS, S., QUINN, A. & HUNTER, T. 1988. The protein kinase family: conserved features and deduced phylogeny of the catalytic domains. *Science,* 241**,** 42-52.

HANSON, M. A., CHEREZOV, V., GRIFFITH, M. T., ROTH, C. B., JAAKOLA, V. P., CHIEN, E. Y., VELASQUEZ, J., KUHN, P. & STEVENS, R. C. 2008. A specific cholesterol binding site is established by the 2.8 A structure of the human beta2-adrenergic receptor. *Structure,* 16**,** 897-905.

HE, G., WANG, H.-R., HUANG, S.-K. & HUANG, C.-L. 2007. Intersectin links WNK kinases to endocytosis of ROMK1. *Journal of Clinical Investigation,* 117**,** 1078-1087.

HELBIG, A. O., HECK, A. J. & SLIJPER, M. 2010. Exploring the membrane proteome--challenges and analytical strategies. *J Proteomics,* 73**,** 868-78.

HERSHKO, A. & CIECHANOVER, A. 1998. The ubiquitin system. *Annu Rev Biochem,* 67**,** 425-79.

HEUSER, J. E. & ANDERSON, R. G. 1989. Hypertonic media inhibit receptor-mediated endocytosis by blocking clathrin-coated pit formation. *J Cell Biol,* 108**,** 389-400.

HOFFMAN, G. R. & CERIONE, R. A. 2000. Flipping the switch: the structural basis for signaling through the CRIB motif. *Cell,* 102**,** 403-6.

HOLDEN, S., COX, J. & RAYMOND, F. L. 2004. Cloning, genomic organization, alternative splicing and expression analysis of the human gene WNK3 (PRKWNK3). *Gene,* 335**,** 109-19.

HUANG, P., LAZAROWSKI, E. R., TARRAN, R., MILGRAM, S. L., BOUCHER, R. C. & STUTTS, M. J. 2001. Compartmentalized autocrine signaling to cystic fibrosis transmembrane conductance regulator at the apical membrane of airway epithelial cells. *Proc Natl Acad Sci U S A,* 98**,** 14120-5.

ICARD, P. & SAUMON, G. 1999. Alveolar sodium and liquid transport in mice. *Am J Physiol,* 277**,** L1232-8.

IYER, V., TRAN, T. M., FOSTER, E., DAI, W., CLARK, R. B. & KNOLL, B. J. 2006. Differential phosphorylation and dephosphorylation of beta2-adrenoceptor sites Ser262 and Ser355,356. *Br J Pharmacol,* 147**,** 249-59.

JACKSON, R. E. & BELLAMY, M. C. 2015. Antihypertensive drugs. *BJA Education,* 15**,** 280-285.

JAYR, C., GARAT, C., MEIGNAN, M., PITTET, J. F., ZELTER, M. & MATTHAY, M. A. 1994. Alveolar liquid and protein clearance in anesthetized ventilated rats. *J Appl Physiol (1985),* 76**,** 2636-42.

JIANG, X., INGBAR, D. H. & O'GRADY, S. M. 2001. Adrenergic regulation of ion transport across adult alveolar epithelial cells: effects on Cl- channel activation and transport function in cultures with an apical air interface. *J Membr Biol,* 181**,** 195-204.

JOHNSTON, A. M., NASELLI, G., GONEZ, L. J., MARTIN, R. M., HARRISON, L. C. & DEAIZPURUA, H. J. 2000. SPAK, a STE20/SPS1-related kinase that activates the p38 pathway. *Oncogene,* 19**,** 4290-7.

KADRI, H., ALAMRI, M. A., NAVRATILOVA, I. H., ALDERWICK, L. J., SIMPKINS, N. S. & MEHELLOU, Y. 2017. Towards the Development of Small-Molecule MO25 Binders as Potential Indirect SPAK/OSR1 Kinase Inhibitors. *ChemBioChem,* 18**,** 460-465.

KAHLE, K. T., GIMENEZ, I., HASSAN, H., WILSON, F. H., WONG, R. D., FORBUSH, B., ARONSON, P. S. & LIFTON, R. P. 2004. WNK4 regulates apical and basolateral Cl(–) flux in extrarenal epithelia. *Proceedings of the National Academy of Sciences of the United States of America,* 101**,** 2064-2069.

KAHLE, K. T., RINEHART, J. & LIFTON, R. P. 2010. Phosphoregulation of the Na–K–2Cl and K–Cl cotransporters by the WNK kinases. *Biochimica et Biophysica Acta (BBA) - Molecular Basis of Disease,* 1802**,** 1150-1158.

KAROOR, V., BALTENSPERGER, K., PAUL, H., CZECH, M. P. & MALBON, C. C. 1995. Phosphorylation of tyrosyl residues 350/354 of the beta-adrenergic receptor is obligatory for counterregulatory effects of insulin. *J Biol Chem,* 270**,** 25305-8.

KHAN, J. M. & BEEVERS, D. G. 2005. Management of hypertension in ethnic minorities. *Heart,* 91**,** 1105-9.

KIKUCHI, E., MORI, T., ZENIYA, M., ISOBE, K., ISHIGAMI-YUASA, M., FUJII, S., KAGECHIKA, H., ISHIHARA, T., MIZUSHIMA, T., SASAKI, S., SOHARA, E., RAI, T. & UCHIDA, S. 2015. Discovery of Novel SPAK Inhibitors That Block WNK Kinase Signaling to Cation Chloride Transporters. *Journal of the American Society of Nephrology,* 26**,** 1525-1536.

KITAGAWA, Y., ADACHI-AKAHANE, S. & NAGAO, T. 1995. Determination of beta-adrenoceptor subtype on rat isolated ventricular myocytes by use of highly selective beta-antagonists. *Br J Pharmacol,* 116**,** 1635-43.

KO, B., MISTRY, A. C., HANSON, L., MALLICK, R., WYNNE, B. M., THAI, T. L., BAILEY, J. L., KLEIN, J. D. & HOOVER, R. S. 2013. Aldosterone acutely stimulates NCC activity via a SPAK-mediated pathway. *Am J Physiol Renal Physiol,* 305**,** F645-52.

KOBILKA, B. 1992. Adrenergic Receptors as Models for G Protein-Coupled Receptors. *Annual Review of Neuroscience,* 15**,** 87-114.

KREBS, E. G., GRAVES, D. J. & FISCHER, E. H. 1959. Factors Affecting the Activity of Muscle Phosphorylase b Kinase. *Journal of Biological Chemistry,* 234**,** 2867-2873.

KRUM, H., SCHLAICH, M., WHITBOURN, R., SOBOTKA, P. A., SADOWSKI, J., BARTUS, K., KAPELAK, B., WALTON, A., SIEVERT, H., THAMBAR, S., ABRAHAM, W. T. & ESLER, M. 2009. Catheter-based renal sympathetic denervation for resistant hypertension: a multicentre safety and proof-of-principle cohort study. *Lancet,* 373**,** 1275-81.

KUROSE, H. 2004. β2-Adrenergic receptors: Structure, regulation and signaling by partial and full agonists. *Allergology International,* 53**,** 321-330.

LAI, L., FENG, X., LIU, D., CHEN, J., ZHANG, Y., NIU, B., GU, Y. & CAI, H. 2012. Dietary salt modulates the sodium chloride cotransporter expression likely through an aldosterone-mediated WNK4-ERK1/2 signaling pathway. *Pflugers Arch,* 463**,** 477-85.

LAM, V. M., BEEREPOOT, P., ANGERS, S. & SALAHPOUR, A. 2013. A novel assay for measurement of membrane-protein surface expression using a beta-lactamase. *Traffic,* 14**,** 778-84.

LAMBERT, N. A. 2010. GPCR dimers fall apart. *Science signaling,* 3**,** pe12-pe12.

LATORRACA, N. R., VENKATAKRISHNAN, A. J. & DROR, R. O. 2017. GPCR Dynamics: Structures in Motion. *Chem Rev,* 117**,** 139-155.

LE MAIRE, M., CHAMPEIL, P. & MOLLER, J. V. 2000. Interaction of membrane proteins and lipids with solubilizing detergents. *Biochim Biophys Acta,* 1508**,** 86-111.

LECUONA, E., RIDGE, K., PESCE, L., BATLLE, D. & SZNAJDER, J. I. 2003. The GTP-binding protein RhoA mediates Na,K-ATPase exocytosis in alveolar epithelial cells. *Mol Biol Cell,* 14**,** 3888-97.

LEE, S. J., COBB, M. H. & GOLDSMITH, E. J. 2009. Crystal structure of domain-swapped STE20 OSR1 kinase domain. *Protein Sci,* 18**,** 304-13.

LEFKOWITZ, R. J. 2000. The superfamily of heptahelical receptors. *Nat Cell Biol,* 2**,** E133-6.

LEFKOWITZ, R. J. & SHENOY, S. K. 2005. Transduction of receptor signals by beta-arrestins. *Science,* 308**,** 512-7.

LENERTZ, L. Y., LEE, B.-H., MIN, X., XU, B.-E., WEDIN, K., EARNEST, S., GOLDSMITH, E. J. & COBB, M. H. 2005. Properties of WNK1 and Implications for Other Family Members. *Journal of Biological Chemistry,* 280**,** 26653-26658.

LI, J. & WANG, D. H. 2007. Function and regulation of epithelial sodium transporters in the kidney of a salt-sensitive hypertensive rat model. *J Hypertens,* 25**,** 1065-72.

LI, Y., HU, J., VITA, R., SUN, B., TABATA, H. & ALTMAN, A. 2004. SPAK kinase is a substrate and target of PKCtheta in T-cell receptor-induced AP-1 activation pathway. *Embo j,* 23**,** 1112-22.

LIN, S.-H., YU, I. S., JIANG, S.-T., LIN, S.-W., CHU, P., CHEN, A., SYTWU, H.-K., SOHARA, E., UCHIDA, S., SASAKI, S. & YANG, S.-S. 2011. Impaired phosphorylation of Na(+)-K(+)-2Cl(−) cotransporter by oxidative stress-responsive kinase-1 deficiency manifests hypotension and Bartter-like syndrome. *Proceedings of the National Academy of Sciences of the United States of America,* 108**,** 17538-17543.

LOLL, P. J. 2014. Membrane proteins, detergents and crystals: what is the state of the art? *Acta Crystallogr F Struct Biol Commun,* 70**,** 1576-83.

LOUIS-DIT-PICARD, H., BARC, J., TRUJILLANO, D., MISEREY-LENKEI, S., BOUATIA-NAJI, N., PYLYPENKO, O., BEAURAIN, G., BONNEFOND, A., SAND, O., SIMIAN, C., VIDAL-PETIOT, E., SOUKASEUM, C., MANDET, C., BROUX, F., CHABRE, O., DELAHOUSSE, M., ESNAULT, V., FIQUET, B., HOUILLIER, P., BAGNIS, C. I., KOENIG, J., KONRAD, M., LANDAIS, P., MOURANI, C., NIAUDET, P., PROBST, V., THAUVIN, C., UNWIN, R. J., SOROKA, S. D., EHRET, G., OSSOWSKI, S., CAULFIELD, M., INTERNATIONAL CONSORTIUM FOR BLOOD, P., BRUNEVAL, P., ESTIVILL, X., FROGUEL, P., HADCHOUEL, J., SCHOTT, J. J. & JEUNEMAITRE, X. 2012. KLHL3 mutations cause familial hyperkalemic hypertension by impairing ion transport in the distal nephron. *Nat Genet,* 44**,** 456-60, S1-3.

LYTLE, C. 1997. Activation of the Avian Erythrocyte Na-K-Cl Cotransport Protein by Cell Shrinkage, cAMP, Fluoride, and Calyculin-A Involves Phosphorylation at Common Sites. *Journal of Biological Chemistry,* 272**,** 15069-15077.

LYTLE, C. & FORBUSH, B., 3RD 1996. Regulatory phosphorylation of the secretory Na-K-Cl cotransporter: modulation by cytoplasmic Cl. *Am J Physiol,* 270**,** C437-48.

MAEDA, S. & SCHERTLER, G. F. 2013. Production of GPCR and GPCR complexes for structure determination. *Curr Opin Struct Biol,* 23**,** 381-92.

MANGLIK, A., KIM, T. H., MASUREEL, M., ALTENBACH, C., YANG, Z., HILGER, D., LERCH, M. T., KOBILKA, T. S., THIAN, F. S., HUBBELL, W. L., PROSSER, R. S. & KOBILKA, B. K. 2015. Structural Insights into the

Dynamic Process of beta2-Adrenergic Receptor Signaling. *Cell,* 161**,** 1101-1111.

MANGLIK, A. & KOBILKA, B. 2014. The role of protein dynamics in GPCR function: insights from the beta2AR and rhodopsin. *Curr Opin Cell Biol,* 27**,** 136-43.

MANNING, G., WHYTE, D. B., MARTINEZ, R., HUNTER, T. & SUDARSANAM, S. 2002. The protein kinase complement of the human genome. *Science,* 298**,** 1912-34.

MARKADIEU, N. & DELPIRE, E. 2014. Physiology and pathophysiology of SLC12A1/2 transporters. *Pflugers Arch,* 466**,** 91-105.

MAUDSLEY, S., PIERCE, K. L., ZAMAH, A. M., MILLER, W. E., AHN, S., DAAKA, Y., LEFKOWITZ, R. J. & LUTTRELL, L. M. 2000. The beta(2)-adrenergic receptor mediates extracellular signal-regulated kinase activation via assembly of a multi-receptor complex with the epidermal growth factor receptor. *J Biol Chem,* 275**,** 9572-80.

MCCLOSKEY, D. T., TURCATO, S., WANG, G. Y., TURNBULL, L., ZHU, B. Q., BAMBINO, T., NGUYEN, A. P., LOVETT, D. H., NISSENSON, R. A., KARLINER, J. S. & BAKER, A. J. 2008. Expression of a Gi-coupled receptor in the heart causes impaired Ca2+ handling, myofilament injury, and dilated cardiomyopathy. *Am J Physiol Heart Circ Physiol,* 294**,** H205-12.

MCCORMICK, J. A. & ELLISON, D. H. 2011. The WNKs: atypical protein kinases with pleiotropic actions. *Physiological reviews,* 91**,** 177-219.

MCCORMICK, J. A. & ELLISON, D. H. 2015. The Distal Convoluted Tubule. *Compr Physiol,* 5**,** 45-98.

MCCORMICK, J. A., MUTIG, K., NELSON, J. H., SARITAS, T., HOORN, E. J., YANG, C.-L., ROGERS, S., CURRY, J., DELPIRE, E., BACHMANN, S. &

ELLISON, D. H. 2011. A SPAK isoform switch modulates renal salt transport and blood pressure. *Cell metabolism,* 14**,** 352-364.

MCCORMICK, J. A., YANG, C. L., ZHANG, C., DAVIDGE, B., BLANKENSTEIN, K. I., TERKER, A. S., YARBROUGH, B., MEERMEIER, N. P., PARK, H. J., MCCULLY, B., WEST, M., BORSCHEWSKI, A., HIMMERKUS, N., BLEICH, M., BACHMANN, S., MUTIG, K., ARGAIZ, E. R., GAMBA, G., SINGER, J. D. & ELLISON, D. H. 2014. Hyperkalemic hypertension-associated cullin 3 promotes WNK signaling by degrading KLHL3. *J Clin Invest,* 124**,** 4723-36.

MIALET-PEREZ, J., GREEN, S. A., MILLER, W. E. & LIGGETT, S. B. 2004. A primate-dominant third glycosylation site of the beta2-adrenergic receptor routes receptors to degradation during agonist regulation. *J Biol Chem,* 279**,** 38603-7.

MILLER, W. E. & LEFKOWITZ, R. J. 2001. Expanding roles for beta-arrestins as scaffolds and adapters in GPCR signaling and trafficking. *Curr Opin Cell Biol,* 13**,** 139-45.

MIN, X., LEE, B. H., COBB, M. H. & GOLDSMITH, E. J. 2004. Crystal structure of the kinase domain of WNK1, a kinase that causes a hereditary form of hypertension. *Structure,* 12**,** 1303-11.

MISHRA, P. K., GIVVIMANI, S., METREVELI, N. & TYAGI, S. C. 2010. Attenuation of beta 2-adrenergic receptors and homocysteine metabolic enzymes cause diabetic cardiomyopathy. *Biochemical and biophysical research communications,* 401**,** 175-181.

MONIZ, S., MATOS, P. & JORDAN, P. 2008. WNK2 modulates MEK1 activity through the Rho GTPase pathway. *Cell Signal,* 20**,** 1762-8.

MOORE, R. H., MILLMAN, E. E., ALPIZAR-FOSTER, E., DAI, W. & KNOLL, B. J. 2004. Rab11 regulates the recycling and lysosome targeting of beta2-adrenergic receptors. *J Cell Sci,* 117**,** 3107-17.

MOREL, F., CHABARDES, D., IMBERT-TEBOUL, M., LE BOUFFANT, F., HUS-CITHAREL, A. & MONTEGUT, M. 1982. Multiple hormonal control of adenylate cyclase in distal segments of the rat kidney. *Kidney Int Suppl,* 11**,** S55-62.

MORI, T., KIKUCHI, E., WATANABE, Y., FUJII, S., ISHIGAMI-YUASA, M., KAGECHIKA, H., SOHARA, E., RAI, T., SASAKI, S. & UCHIDA, S. 2013. Chemical library screening for WNK signalling inhibitors using fluorescence correlation spectroscopy. *Biochemical Journal,* 455**,** 339-345.

MORIGUCHI, T., URUSHIYAMA, S., HISAMOTO, N., IEMURA, S.-I., UCHIDA, S., NATSUME, T., MATSUMOTO, K. & SHIBUYA, H. 2005. WNK1 Regulates Phosphorylation of Cation-Chloride-coupled Cotransporters via the STE20-related Kinases, SPAK and OSR1. *Journal of Biological Chemistry,* 280**,** 42685-42693.

MORLA, L., EDWARDS, A. & CRAMBERT, G. 2016. New insights into sodium transport regulation in the distal nephron: Role of G-protein coupled receptors. *World J Biol Chem,* 7**,** 44-63.

MU, S., SHIMOSAWA, T., OGURA, S., WANG, H., UETAKE, Y., KAWAKAMI-MORI, F., MARUMO, T., YATOMI, Y., GELLER, D. S., TANAKA, H. & FUJITA, T. 2011. Epigenetic modulation of the renal beta-adrenergic-WNK4 pathway in salt-sensitive hypertension. *Nat Med,* 17**,** 573-80.

MURTHY, M., KURZ, T. & O'SHAUGHNESSY, K. M. 2017. WNK signalling pathways in blood pressure regulation. *Cell Mol Life Sci,* 74**,** 1261-1280.

MUTLU, G. M., ADIR, Y., JAMEEL, M., AKHMEDOV, A. T., WELCH, L., DUMASIUS, V., MENG, F. J., ZABNER, J., KOENIG, C., LEWIS, E. R., BALAGANI, R., TRAVER, G., SZNAJDER, J. I. & FACTOR, P. 2005. Interdependency of beta-adrenergic receptors and CFTR in regulation of alveolar active Na+ transport. *Circ Res,* 96**,** 999-1005.

MUTLU, G. M., DUMASIUS, V., BURHOP, J., MCSHANE, P. J., MENG, F. J., WELCH, L., DUMASIUS, A., MOHEBAHMADI, N., THAKURIA, G., HARDIMAN, K., MATALON, S., HOLLENBERG, S. & FACTOR, P. 2004a. Upregulation of alveolar epithelial active Na+ transport is dependent on beta2-adrenergic receptor signaling. *Circ Res,* 94**,** 1091-100.

MUTLU, G. M. & FACTOR, P. 2008. Alveolar epithelial beta2-adrenergic receptors. *Am J Respir Cell Mol Biol,* 38**,** 127-34.

MUTLU, G. M., KOCH, W. J. & FACTOR, P. 2004b. Alveolar Epithelial β2-Adrenergic Receptors. *American Journal of Respiratory and Critical Care Medicine,* 170**,** 1270-1275.

MUTLU, G. M. & SZNAJDER, J. I. 2004. beta(2)-Agonists for treatment of pulmonary edema: ready for clinical studies? *Crit Care Med,* 32**,** 1607-8.

NAITO, S., OHTA, A., SOHARA, E., OHTA, E., RAI, T., SASAKI, S. & UCHIDA, S. 2011. Regulation of WNK1 kinase by extracellular potassium. *Clinical and Experimental Nephrology,* 15**,** 195-202.

NAKAMICHI, N., MURAKAMI-KOJIMA, M., SATO, E., KISHI, Y., YAMASHINO, T. & MIZUNO, T. 2002. Compilation and characterization of a novel WNK family of protein kinases in Arabiodpsis thaliana with reference to circadian rhythms. *Biosci Biotechnol Biochem,* 66**,** 2429-36.

NASROLLAHI-SHIRAZI, S., SUCIC, S., YANG, Q., FREISSMUTH, M. & NANOFF, C. 2016. Comparison of the β-Adrenergic Receptor Antagonists Landiolol and Esmolol: Receptor Selectivity, Partial Agonism, and Pharmacochaperoning Actions. *Journal of Pharmacology and Experimental Therapeutics,* 359**,** 73-81.

NG, S. Y. L., LEE, L. T. O. & CHOW, B. K. C. 2012. Receptor oligomerization: from early evidence to current understanding in class B GPCRs. *Frontiers in Endocrinology,* 3**,** 175.

NIELSEN, V. G., DUVALL, M. D., BAIRD, M. S. & MATALON, S. 1998. cAMP activation of chloride and fluid secretion across the rabbit alveolar epithelium. *Am J Physiol,* 275**,** L1127-33.

NISHIDA, H., SOHARA, E., NOMURA, N., CHIGA, M., ALESSI, D. R., RAI, T., SASAKI, S. & UCHIDA, S. 2012. Phosphatidylinositol 3-kinase/Akt signaling pathway activates the WNK-OSR1/SPAK-NCC phosphorylation cascade in hyperinsulinemic db/db mice. *Hypertension,* 60**,** 981-90.

NOMURA, N., SHODA, W., WANG, Y., MANDAI, S., FURUSHO, T., TAKAHASHI, D., ZENIYA, M., SOHARA, E., RAI, T. & UCHIDA, S. 2018. Role of ClC-K and barttin in low potassium-induced sodium chloride cotransporter activation and hypertension in mouse kidney. *Bioscience Reports,* 38.

NONOGUCHI, H., OWADA, A., KOBAYASHI, N., TAKAYAMA, M., TERADA, Y., KOIKE, J., UJIIE, K., MARUMO, F., SAKAI, T. & TOMITA, K. 1995. Immunohistochemical localization of V2 vasopressin receptor along the nephron and functional role of luminal V2 receptor in terminal inner medullary collecting ducts. *J Clin Invest,* 96**,** 1768-78.

NORLIN, A., FINLEY, N., ABEDINPOUR, P. & FOLKESSON, H. G. 1998. Alveolar liquid clearance in the anesthetized ventilated guinea pig. *Am J Physiol,* 274**,** L235-43.

NYGAARD, R., ZOU, Y., DROR, R. O., MILDORF, T. J., ARLOW, D. H., MANGLIK, A., PAN, A. C., LIU, C. W., FUNG, J. J., BOKOCH, M. P., THIAN, F. S., KOBILKA, T. S., SHAW, D. E., MUELLER, L., PROSSER, R. S. & KOBILKA, B. K. 2013. The dynamic process of β(2)-adrenergic receptor activation. *Cell,* 152**,** 532-42.

O'GRADY, S. M., JIANG, X. & INGBAR, D. H. 2000. Cl-channel activation is necessary for stimulation of Na transport in adult alveolar epithelial cells. *Am J Physiol Lung Cell Mol Physiol,* 278**,** L239-44.

O'REILLY, M., MARSHALL, E., SPEIRS, H. J. & BROWN, R. W. 2003. WNK1, a gene within a novel blood pressure control pathway, tissue-specifically generates radically different isoforms with and without a kinase domain. *J Am Soc Nephrol,* 14**,** 2447-56.

O'SHAUGHNESSY, K. M. & KARET, F. E. 2006. Salt Handling and Hypertension. *Annual Review of Nutrition,* 26**,** 343-365.

OHTA, A., SCHUMACHER, F. R., MEHELLOU, Y., JOHNSON, C., KNEBEL, A., MACARTNEY, T. J., WOOD, N. T., ALESSI, D. R. & KURZ, T. 2013. The CUL3-KLHL3 E3 ligase complex mutated in Gordon's hypertension syndrome interacts with and ubiquitylates WNK isoforms: disease-causing mutations in KLHL3 and WNK4 disrupt interaction. *Biochem J,* 451**,** 111-22.

OKAMOTO, T., MURAYAMA, Y., HAYASHI, Y., INAGAKI, M., OGATA, E. & NISHIMOTO, I. 1991. Identification of a Gs activator region of the beta 2-

adrenergic receptor that is autoregulated via protein kinase A-dependent phosphorylation. *Cell,* 67**,** 723-30.

PESCE, L., COMELLAS, A. & SZNAJDER, J. I. 2003. Beta-adrenergic agonists regulate Na-K-ATPase via p70S6k. *Am J Physiol Lung Cell Mol Physiol,* 285**,** L802-7.

PIALA, A. T., MOON, T. M., AKELLA, R., HE, H., COBB, M. H. & GOLDSMITH, E. J. 2014. Chloride sensing by WNK1 kinase involves inhibition of autophosphorylation. *Science signaling,* 7**,** ra41-ra41.

PIECHOTTA, K., GARBARINI, N., ENGLAND, R. & DELPIRE, E. 2003. Characterization of the interaction of the stress kinase SPAK with the Na+-K+-2Cl- cotransporter in the nervous system: evidence for a scaffolding role of the kinase. *J Biol Chem,* 278**,** 52848-56.

PIECHOTTA, K., LU, J. & DELPIRE, E. 2002. Cation chloride cotransporters interact with the stress-related kinases Ste20-related proline-alanine-rich kinase (SPAK) and oxidative stress response 1 (OSR1). *J Biol Chem,* 277**,** 50812-9.

PLOWMAN, G. D., SUDARSANAM, S., BINGHAM, J., WHYTE, D. & HUNTER, T. 1999. The protein kinases of Caenorhabditis elegans: A model for signal transduction in multicellular organisms. *Proceedings of the National Academy of Sciences,* 96**,** 13603-13610.

POJOGA, L., KOLATKAR, N. S., WILLIAMS, J. S., PERLSTEIN, T. S., JEUNEMAITRE, X., BROWN, N. J., HOPKINS, P. N., RABY, B. A. & WILLIAMS, G. H. 2006. Beta-2 adrenergic receptor diplotype defines a subset of salt-sensitive hypertension. *Hypertension,* 48**,** 892-900.

POKHREL, R., MCCONNELL, I. L. & BRUDVIG, G. W. 2011. Chloride regulation of enzyme turnover: application to the role of chloride in photosystem II. *Biochemistry,* 50**,** 2725-34.

PONCE-CORIA, J., GAGNON, K. B. & DELPIRE, E. 2012. Calcium-binding protein 39 facilitates molecular interaction between Ste20p proline alanine-rich kinase and oxidative stress response 1 monomers. *Am J Physiol Cell Physiol,* 303**,** C1198-205.

PRINCE, C. C. & JIA, Z. 2013. Detergent quantification in membrane protein samples and its application to crystallization experiments. *Amino Acids,* 45**,** 1293-302.

RABILLOUD, T. 2009. Membrane proteins and proteomics: love is possible, but so difficult. *Electrophoresis,* 30 Suppl 1**,** S174-80.

RAFIQI, F. H., ZUBER, A. M., GLOVER, M., RICHARDSON, C., FLEMING, S., JOVANOVIĆ, S., JOVANOVIĆ, A., O'SHAUGHNESSY, K. M. & ALESSI, D. R. 2010. Role of the WNK-activated SPAK kinase in regulating blood pressure. *EMBO Molecular Medicine,* 2**,** 63-75.

RASMUSSEN, S. G., CHOI, H. J., FUNG, J. J., PARDON, E., CASAROSA, P., CHAE, P. S., DEVREE, B. T., ROSENBAUM, D. M., THIAN, F. S., KOBILKA, T. S., SCHNAPP, A., KONETZKI, I., SUNAHARA, R. K., GELLMAN, S. H., PAUTSCH, A., STEYAERT, J., WEIS, W. I. & KOBILKA, B. K. 2011a. Structure of a nanobody-stabilized active state of the beta(2) adrenoceptor. *Nature,* 469**,** 175-80.

RASMUSSEN, S. G., CHOI, H. J., ROSENBAUM, D. M., KOBILKA, T. S., THIAN, F. S., EDWARDS, P. C., BURGHAMMER, M., RATNALA, V. R., SANISHVILI, R., FISCHETTI, R. F., SCHERTLER, G. F., WEIS, W. I. & KOBILKA, B. K.

2007. Crystal structure of the human beta2 adrenergic G-protein-coupled receptor. *Nature,* 450**,** 383-7.

RASMUSSEN, S. G., DEVREE, B. T., ZOU, Y., KRUSE, A. C., CHUNG, K. Y., KOBILKA, T. S., THIAN, F. S., CHAE, P. S., PARDON, E., CALINSKI, D., MATHIESEN, J. M., SHAH, S. T., LYONS, J. A., CAFFREY, M., GELLMAN, S. H., STEYAERT, J., SKINIOTIS, G., WEIS, W. I., SUNAHARA, R. K. & KOBILKA, B. K. 2011b. Crystal structure of the beta2 adrenergic receptor-Gs protein complex. *Nature,* 477**,** 549-55.

RICHARDSON, C. & ALESSI, D. R. 2008. The regulation of salt transport and blood pressure by the WNK-SPAK/OSR1 signalling pathway. *J Cell Sci,* 121**,** 3293-304.

RICHARDSON, C., RAFIQI, F. H., KARLSSON, H. K., MOLELEKI, N., VANDEWALLE, A., CAMPBELL, D. G., MORRICE, N. A. & ALESSI, D. R. 2008. Activation of the thiazide-sensitive Na+-Cl- cotransporter by the WNK-regulated kinases SPAK and OSR1. *J Cell Sci,* 121**,** 675-84.

RICHARDSON, C., SAKAMOTO, K., DE LOS HEROS, P., DEAK, M., CAMPBELL, D. G., PRESCOTT, A. R. & ALESSI, D. R. 2011. Regulation of the NKCC2 ion cotransporter by SPAK-OSR1-dependent and -independent pathways. *Journal of Cell Science,* 124**,** 789-800.

RIEG, T., TANG, T., UCHIDA, S., HAMMOND, H. K., FENTON, R. A. & VALLON, V. 2013. Adenylyl cyclase 6 enhances NKCC2 expression and mediates vasopressin-induced phosphorylation of NKCC2 and NCC. *Am J Pathol,* 182**,** 96-106.

RING, A. M., MANGLIK, A., KRUSE, A. C., ENOS, M. D., WEIS, W. I., GARCIA, K. C. & KOBILKA, B. K. 2013. Adrenaline-activated structure of beta2-adrenoceptor stabilized by an engineered nanobody. *Nature,* 502**,** 575-579.

RITTER, S. L. & HALL, R. A. 2009. Fine-tuning of GPCR activity by receptor-interacting proteins. *Nat Rev Mol Cell Biol,* 10**,** 819-30.

RODAN, A. R. & JENNY, A. 2017. WNK kinases in development and disease. *Current topics in developmental biology,* 123**,** 1-47.

ROSENBAUM, D. M., CHEREZOV, V., HANSON, M. A., RASMUSSEN, S. G. F., THIAN, F. S., KOBILKA, T. S., CHOI, H.-J., YAO, X.-J., WEIS, W. I., STEVENS, R. C. & KOBILKA, B. K. 2007. GPCR Engineering Yields High-Resolution Structural Insights into β₂-Adrenergic Receptor Function. *Science,* 318**,** 1266-1273.

ROSENBAUM, D. M., RASMUSSEN, S. G. & KOBILKA, B. K. 2009. The structure and function of G-protein-coupled receptors. *Nature,* 459**,** 356-63.

ROSENBAUM, D. M., ZHANG, C., LYONS, J. A., HOLL, R., ARAGAO, D., ARLOW, D. H., RASMUSSEN, S. G., CHOI, H. J., DEVREE, B. T., SUNAHARA, R. K., CHAE, P. S., GELLMAN, S. H., DROR, R. O., SHAW, D. E., WEIS, W. I., CAFFREY, M., GMEINER, P. & KOBILKA, B. K. 2011. Structure and function of an irreversible agonist-beta(2) adrenoceptor complex. *Nature,* 469**,** 236-40.

RUSSELL, J. M. 2000. Sodium-potassium-chloride cotransport. *Physiol Rev,* 80**,** 211-76.

SAKUMA, T., FOLKESSON, H. G., SUZUKI, S., OKANIWA, G., FUJIMURA, S. & MATTHAY, M. A. 1997. Beta-adrenergic agonist stimulated alveolar fluid clearance in ex vivo human and rat lungs. *Am J Respir Crit Care Med,* 155**,** 506-12.

SALOMONSSON, M., GONZALEZ, E., WESTERLUND, P. & PERSSON, A. E. 1991. Chloride concentration in macula densa and cortical thick ascending limb cells. *Kidney Int Suppl,* 32**,** S51-4.

SAMAMA, P., COTECCHIA, S., COSTA, T. & LEFKOWITZ, R. J. 1993. A mutation-induced activated state of the beta 2-adrenergic receptor. Extending the ternary complex model. *Journal of Biological Chemistry,* 268**,** 4625-4636.

SAN-CRISTOBAL, P., PACHECO-ALVAREZ, D., RICHARDSON, C., RING, A. M., VAZQUEZ, N., RAFIQI, F. H., CHARI, D., KAHLE, K. T., LENG, Q., BOBADILLA, N. A., HEBERT, S. C., ALESSI, D. R., LIFTON, R. P. & GAMBA, G. 2009. Angiotensin II signaling increases activity of the renal Na-Cl cotransporter through a WNK4-SPAK-dependent pathway. *Proceedings of the National Academy of Sciences of the United States of America,* 106**,** 4384-4389.

SAPKOTA, G. P., KIELOCH, A., LIZCANO, J. M., LAIN, S., ARTHUR, J. S., WILLIAMS, M. R., MORRICE, N., DEAK, M. & ALESSI, D. R. 2001. Phosphorylation of the protein kinase mutated in Peutz-Jeghers cancer syndrome, LKB1/STK11, at Ser431 by p90(RSK) and cAMP-dependent protein kinase, but not its farnesylation at Cys(433), is essential for LKB1 to suppress cell vrowth. *J Biol Chem,* 276**,** 19469-82.

SARITAS, T., BORSCHEWSKI, A., MCCORMICK, J. A., PALIEGE, A., DATHE, C., UCHIDA, S., TERKER, A., HIMMERKUS, N., BLEICH, M., DEMARETZ, S., LAGHMANI, K., DELPIRE, E., ELLISON, D. H., BACHMANN, S. & MUTIG, K. 2013. SPAK differentially mediates vasopressin effects on sodium cotransporters. *J Am Soc Nephrol,* 24**,** 407-18.

SCOTT, L. J. & GOA, K. L. 2000. Verteporfin. *Drugs Aging,* 16**,** 139-46; discussion 147-8.

SHEKARABI, M., ZHANG, J., KHANNA, A. R., ELLISON, D. H., DELPIRE, E. & KAHLE, K. T. 2017. WNK Kinase Signaling in Ion Homeostasis and Human Disease. *Cell Metab,* 25**,** 285-299.

SHIBATA, S., ARROYO, J. P., CASTAÑEDA-BUENO, M., PUTHUMANA, J., ZHANG, J., UCHIDA, S., STONE, K. L., LAM, T. T. & LIFTON, R. P. 2014. Angiotensin II signaling via protein kinase C phosphorylates Kelch-like 3, preventing WNK4 degradation. *Proceedings of the National Academy of Sciences of the United States of America,* 111**,** 15556-15561.

SHIBATA, S., ZHANG, J., PUTHUMANA, J., STONE, K. L. & LIFTON, R. P. 2013. Kelch-like 3 and Cullin 3 regulate electrolyte homeostasis via ubiquitination and degradation of WNK4. *Proc Natl Acad Sci U S A,* 110**,** 7838-43.

SHOICHET, B. K. & KOBILKA, B. K. 2012. Structure-based drug screening for G-protein-coupled receptors. *Trends Pharmacol Sci,* 33**,** 268-72.

SHOSHAN-BARMATZ, V., DE, S. & MEIR, A. 2017a. The Mitochondrial Voltage-Dependent Anion Channel 1, Ca(2+) Transport, Apoptosis, and Their Regulation. *Frontiers in Oncology,* 7**,** 60.

SHOSHAN-BARMATZ, V., KRELIN, Y., SHTEINFER-KUZMINE, A. & ARIF, T. 2017b. Voltage-Dependent Anion Channel 1 As an Emerging Drug Target for Novel Anti-Cancer Therapeutics. *Front Oncol,* 7**,** 154.

SIMON, D. B., KARET, F. E., HAMDAN, J. M., DIPIETRO, A., SANJAD, S. A. & LIFTON, R. P. 1996a. Bartter's syndrome, hypokalaemic alkalosis with hypercalciuria, is caused by mutations in the Na-K-2Cl cotransporter NKCC2. *Nat Genet,* 13**,** 183-8.

SIMON, D. B., NELSON-WILLIAMS, C., BIA, M. J., ELLISON, D., KARET, F. E., MOLINA, A. M., VAARA, I., IWATA, F., CUSHNER, H. M., KOOLEN, M., GAINZA, F. J., GITLEMAN, H. J. & LIFTON, R. P. 1996b. Gitelman's variant of Bartter's syndrome, inherited hypokalaemic alkalosis, is caused by mutations in the thiazide-sensitive Na-Cl cotransporter. *Nat Genet,* 12**,** 24-30.

SMITH, L., SMALLWOOD, N., ALTMAN, A. & LIEDTKE, C. M. 2008. PKCδ Acts Upstream of SPAK in the Activation of NKCC1 by Hyperosmotic Stress in Human Airway Epithelial Cells. *The Journal of Biological Chemistry,* 283**,** 22147-22156.

SNYDER, E. M., TURNER, S. T., JOYNER, M. J., EISENACH, J. H. & JOHNSON, B. D. 2006. The Arg16Gly polymorphism of the beta2-adrenergic receptor and the natriuretic response to rapid saline infusion in humans. *J Physiol,* 574**,** 947-54.

SOHARA, E. & UCHIDA, S. 2016. Kelch-like 3/Cullin 3 ubiquitin ligase complex and WNK signaling in salt-sensitive hypertension and electrolyte disorder. *Nephrology Dialysis Transplantation,* 31**,** 1417-1424.

SORENSEN, M. V., GROSSMANN, S., ROESINGER, M., GRESKO, N., TODKAR, A. P., BARMETTLER, G., ZIEGLER, U., ODERMATT, A., LOFFING-CUENI, D. & LOFFING, J. 2013. Rapid dephosphorylation of the renal sodium chloride cotransporter in response to oral potassium intake in mice. *Kidney Int,* 83**,** 811-24.

STRADER, C. D., SIGAL, I. S. & DIXON, R. A. 1989. Structural basis of beta-adrenergic receptor function. *The FASEB Journal,* 3**,** 1825-1832.

SUBRAMANYA, A. R., YANG, C. L., ZHU, X. & ELLISON, D. H. 2006. Dominant-negative regulation of WNK1 by its kidney-specific kinase-defective isoform. *Am J Physiol Renal Physiol,* 290**,** F619-24.

SUMMERS, R. J., STEPHENSON, J. A. & KUHAR, M. J. 1985. Localization of beta adrenoceptor subtypes in rat kidney by light microscopic autoradiography. *Journal of Pharmacology and Experimental Therapeutics,* 232**,** 561-569.

SUN, Q., WU, Y., JONUSAITE, S., PLEINIS, J. M., HUMPHREYS, J. M., HE, H., SCHELLINGER, J. N., AKELLA, R., STENESEN, D., KRAMER, H., GOLDSMITH, E. J. & RODAN, A. R. 2018. Intracellular Chloride and Scaffold Protein Mo25 Cooperatively Regulate Transepithelial Ion Transport through WNK Signaling in the Malpighian Tubule. *J Am Soc Nephrol*.

TAKAHASHI, D., MORI, T., NOMURA, N., KHAN, M. Z. H., ARAKI, Y., ZENIYA, M., SOHARA, E., RAI, T., SASAKI, S. & UCHIDA, S. 2014. WNK4 is the major WNK positively regulating NCC in the mouse kidney. *Bioscience Reports,* 34.

TAMARI, M., DAIGO, Y. & NAKAMURA, Y. 1999. Isolation and characterization of a novel serine threonine kinase gene on chromosome 3p22-21.3. *J Hum Genet,* 44**,** 116-20.

TAO, J., WANG, H. Y. & MALBON, C. C. 2003. Protein kinase A regulates AKAP250 (gravin) scaffold binding to the beta2-adrenergic receptor. *Embo j,* 22**,** 6419-29.

TAVOULARI, S., RIZWAN, A. N., FORREST, L. R. & RUDNICK, G. 2011. Reconstructing a chloride-binding site in a bacterial neurotransmitter transporter homologue. *J Biol Chem,* 286**,** 2834-42.

TAYLOR, C. A., JUANG, Y.-C., EARNEST, S., SENGUPTA, S., GOLDSMITH, E. J. & COBB, M. H. 2015. The domain-swapping switch point in Ste20 protein kinase SPAK. *Biochemistry,* 54**,** 5063-5071.

TAYLOR, S. S., KESHWANI, M. M., STEICHEN, J. M. & KORNEV, A. P. 2012. Evolution of the eukaryotic protein kinases as dynamic molecular switches. *Philosophical Transactions of the Royal Society B: Biological Sciences,* 367**,** 2517-2528.

TERKER, A. S., YANG, C. L., MCCORMICK, J. A., MEERMEIER, N. P., ROGERS, S. L., GROSSMANN, S., TROMPF, K., DELPIRE, E., LOFFING, J. & ELLISON, D. H. 2014. Sympathetic stimulation of thiazide-sensitive sodium chloride cotransport in the generation of salt-sensitive hypertension. *Hypertension,* 64**,** 178-84.

TERKER, A. S., ZHANG, C., ERSPAMER, K. J., GAMBA, G., YANG, C.-L. & ELLISON, D. H. 2016. Unique chloride-sensing properties of WNK4 permit the distal nephron to modulate potassium homeostasis. *Kidney international,* 89**,** 127-134.

TERKER, A. S., ZHANG, C., MCCORMICK, J. A., LAZELLE, R. A., ZHANG, C., MEERMEIER, N. P., SILER, D. A., PARK, H. J., FU, Y., COHEN, D. M., WEINSTEIN, A. M., WANG, W. H., YANG, C. L. & ELLISON, D. H. 2015. Potassium modulates electrolyte balance and blood pressure through effects on distal cell voltage and chloride. *Cell Metab,* 21**,** 39-50.

THASTRUP, JACOB O., RAFIQI, FATEMA H., VITARI, ALBERTO C., POZO-GUISADO, E., DEAK, M., MEHELLOU, Y. & ALESSI, DARIO R. 2012. SPAK/OSR1 regulate NKCC1 and WNK activity: analysis of WNK isoform

interactions and activation by T-loop trans-autophosphorylation. *Biochemical Journal,* 441**,** 325-337.

TZAKOS, A. G., GALANIS, A. S., SPYROULIAS, G. A., CORDOPATIS, P., MANESSI-ZOUPA, E. & GEROTHANASSIS, I. P. 2003. Structure-function discrimination of the N- and C- catalytic domains of human angiotensin-converting enzyme: implications for Cl- activation and peptide hydrolysis mechanisms. *Protein Eng,* 16**,** 993-1003.

UCHIDA, S., SOHARA, E., RAI, T. & SASAKI, S. 2014. Regulation of with-no-lysine kinase signaling by Kelch-like proteins. *Biol Cell,* 106**,** 45-56.

USHIRO, H., TSUTSUMI, T., SUZUKI, K., KAYAHARA, T. & NAKANO, K. 1998. Molecular cloning and characterization of a novel Ste20-related protein kinase enriched in neurons and transporting epithelia. *Arch Biochem Biophys,* 355**,** 233-40.

VALLON, V., SCHROTH, J., LANG, F., KUHL, D. & UCHIDA, S. 2009. Expression and phosphorylation of the Na+-Cl− cotransporter NCC in vivo is regulated by dietary salt, potassium, and SGK1. *American Journal of Physiology-Renal Physiology,* 297**,** F704-F712.

VAN DER LUBBE, N., LIM, C. H., FENTON, R. A., MEIMA, M. E., JAN DANSER, A. H., ZIETSE, R. & HOORN, E. J. 2011. Angiotensin II induces phosphorylation of the thiazide-sensitive sodium chloride cotransporter independent of aldosterone. *Kidney Int,* 79**,** 66-76.

VERISSIMO, F. & JORDAN, P. 2001. WNK kinases, a novel protein kinase subfamily in multi-cellular organisms. *Oncogene,* 20**,** 5562-9.

VIDAL-PETIOT, E., ELVIRA-MATELOT, E., MUTIG, K., SOUKASEUM, C., BAUDRIE, V., WU, S., CHEVAL, L., HUC, E., CAMBILLAU, M., BACHMANN,

S., DOUCET, A., JEUNEMAITRE, X. & HADCHOUEL, J. 2013. WNK1-related Familial Hyperkalemic Hypertension results from an increased expression of L-WNK1 specifically in the distal nephron. *Proc Natl Acad Sci U S A,* 110**,** 14366-71.

VILLA, F., DEAK, M., ALESSI, D. R. & VAN AALTEN, D. M. 2008. Structure of the OSR1 kinase, a hypertension drug target. *Proteins,* 73**,** 1082-7.

VILLA, F., GOEBEL, J., RAFIQI, F. H., DEAK, M., THASTRUP, J., ALESSI, D. R. & VAN AALTEN, D. M. 2007. Structural insights into the recognition of substrates and activators by the OSR1 kinase. *EMBO Rep,* 8**,** 839-45.

VITARI, A. C., DEAK, M., MORRICE, N. A. & ALESSI, D. R. 2005. The WNK1 and WNK4 protein kinases that are mutated in Gordon's hypertension syndrome phosphorylate and activate SPAK and OSR1 protein kinases. *Biochem J,* 391**,** 17-24.

VITARI, ALBERTO C., THASTRUP, J., RAFIQI, FATEMA H., DEAK, M., MORRICE, NICK A., KARLSSON, HÅKAN K. R. & ALESSI, DARIO R. 2006. Functional interactions of the SPAK/OSR1 kinases with their upstream activator WNK1 and downstream substrate NKCC1. *Biochemical Journal,* 397**,** 223-231.

WACKER, D., FENALTI, G., BROWN, M. A., KATRITCH, V., ABAGYAN, R., CHEREZOV, V. & STEVENS, R. C. 2010. Conserved binding mode of human beta2 adrenergic receptor inverse agonists and antagonist revealed by X-ray crystallography. *J Am Chem Soc,* 132**,** 11443-5.

WAKABAYASHI, M., MORI, T., ISOBE, K., SOHARA, E., SUSA, K., ARAKI, Y., CHIGA, M., KIKUCHI, E., NOMURA, N., MORI, Y., MATSUO, H., MURATA, T., NOMURA, S., ASANO, T., KAWAGUCHI, H., NONOYAMA, S., RAI, T.,

SASAKI, S. & UCHIDA, S. 2013. Impaired KLHL3-mediated ubiquitination of WNK4 causes human hypertension. *Cell Rep,* 3**,** 858-68.

WARSI, J., HOSSEINZADEH, Z., ELVIRA, B., BISSINGER, R., SHUMILINA, E. & LANG, F. 2014. Regulation of ClC-2 Activity by SPAK and OSR1. *Kidney and Blood Pressure Research,* 39**,** 378-387.

WILSON, F. H., DISSE-NICODÈME, S., CHOATE, K. A., ISHIKAWA, K., NELSON-WILLIAMS, C., DESITTER, I., GUNEL, M., MILFORD, D. V., LIPKIN, G. W., ACHARD, J.-M., FEELY, M. P., DUSSOL, B., BERLAND, Y., UNWIN, R. J., MAYAN, H., SIMON, D. B., FARFEL, Z., JEUNEMAITRE, X. & LIFTON, R. P. 2001. Human Hypertension Caused by Mutations in WNK Kinases. *Science,* 293**,** 1107-1112.

WU, G. & PENG, J. B. 2013. Disease-causing mutations in KLHL3 impair its effect on WNK4 degradation. *FEBS Lett,* 587**,** 1717-22.

XIE, J. X., LI, X. & XIE, Z. 2013. Regulation of Renal Function and Structure by the Signaling Na/K-ATPase. *IUBMB Life,* 65**,** 991-8.

XU, B.-E., ENGLISH, J. M., WILSBACHER, J. L., STIPPEC, S., GOLDSMITH, E. J. & COBB, M. H. 2000. WNK1, a Novel Mammalian Serine/Threonine Protein Kinase Lacking the Catalytic Lysine in Subdomain II. *Journal of Biological Chemistry,* 275**,** 16795-16801.

XU, B.-E., MIN, X., STIPPEC, S., LEE, B.-H., GOLDSMITH, E. J. & COBB, M. H. 2002. Regulation of WNK1 by an Autoinhibitory Domain and Autophosphorylation. *Journal of Biological Chemistry,* 277**,** 48456-48462.

YAMADA, K., PARK, H. M., RIGEL, D. F., DIPETRILLO, K., WHALEN, E. J., ANISOWICZ, A., BEIL, M., BERSTLER, J., BROCKLEHURST, C. E., BURDICK, D. A., CAPLAN, S. L., CAPPARELLI, M. P., CHEN, G., CHEN, W.,

DALE, B., DENG, L., FU, F., HAMAMATSU, N., HARASAKI, K., HERR, T., HOFFMANN, P., HU, Q. Y., HUANG, W. J., IDAMAKANTI, N., IMASE, H., IWAKI, Y., JAIN, M., JEYASEELAN, J., KATO, M., KAUSHIK, V. K., KOHLS, D., KUNJATHOOR, V., LASALA, D., LEE, J., LIU, J., LUO, Y., MA, F., MO, R., MOWBRAY, S., MOGI, M., OSSOLA, F., PANDEY, P., PATEL, S. J., RAGHAVAN, S., SALEM, B., SHANADO, Y. H., TRAKSHEL, G. M., TURNER, G., WAKAI, H., WANG, C., WELDON, S., WIELICKI, J. B., XIE, X., XU, L., YAGI, Y. I., YASOSHIMA, K., YIN, J., YOWE, D., ZHANG, J. H., ZHENG, G. & MONOVICH, L. 2016. Small-molecule WNK inhibition regulates cardiovascular and renal function. *Nat Chem Biol,* 12**,** 896-898.

YANG, D., LI, Q., SO, I., HUANG, C. L., ANDO, H., MIZUTANI, A., SEKI, G., MIKOSHIBA, K., THOMAS, P. J. & MUALLEM, S. 2011. IRBIT governs epithelial secretion in mice by antagonizing the WNK/SPAK kinase pathway. *J Clin Invest,* 121**,** 956-65.

YANG, S.-S., LO, Y.-F., WU, C.-C., LIN, S.-W., YEH, C.-J., CHU, P., SYTWU, H.-K., UCHIDA, S., SASAKI, S. & LIN, S.-H. 2010. SPAK-Knockout Mice Manifest Gitelman Syndrome and Impaired Vasoconstriction. *Journal of the American Society of Nephrology,* 21**,** 1868-1877.

YUE, G., SHOEMAKER, R. L. & MATALON, S. 1994. Regulation of low-amiloride-affinity sodium channels in alveolar type II cells. *Am J Physiol,* 267**,** L94-100.

ZAGÓRSKA, A., POZO-GUISADO, E., BOUDEAU, J., VITARI, A. C., RAFIQI, F. H., THASTRUP, J., DEAK, M., CAMPBELL, D. G., MORRICE, N. A., PRESCOTT, A. R. & ALESSI, D. R. 2007. Regulation of activity and localization of the WNK1 protein kinase by hyperosmotic stress. *The Journal of Cell Biology,* 176**,** 89-100.

ZEGZOUTI, H., ZDANOVSKAIA, M., HSIAO, K. & GOUELI, S. A. 2009. ADP-Glo: A Bioluminescent and homogeneous ADP monitoring assay for kinases. *Assay Drug Dev Technol,* 7**,** 560-72.

ZHENG, B., JEONG, J. H., ASARA, J. M., YUAN, Y.-Y., GRANTER, S. R., CHIN, L. & CANTLEY, L. C. 2009. Oncogenic B-RAF Negatively Regulates the Tumor Suppressor LKB1 to Promote Melanoma Cell Proliferation. *Molecular cell,* 33**,** 237-247.

ZHU, W. Z., ZHENG, M., KOCH, W. J., LEFKOWITZ, R. J., KOBILKA, B. K. & XIAO, R. P. 2001. Dual modulation of cell survival and cell death by beta(2)-adrenergic signaling in adult mouse cardiac myocytes. *Proc Natl Acad Sci U S A,* 98**,** 1607-12.